Ingeniería e Investigación
Journal

Abbreviated Journal Title: **Ing. Investig.**

Editor-in-chief
Sonia C. Mangones, PhD

Associate Editor
Andrés Pavas, PhD MSc.

Technical Editor
Lenin Alexander Bulla Cruz, Ph.D. MSc.

Editorial Assistants
Julian Arcila-Forero, M.Sc., B.Sc.
Ingri Gisela Camacho, B.Sc.

Frequency
Quarterly, three issues per year
April, August, and December

Cover Layout
Carlos Andres Ortiz Valle

Proofreader
José Daniel Gutiérrez-Mendoza

Layout Artist
David Mauricio Valero

For additional information contact
revii_bog@unal.edu.co
Bogotá - Colombia
2023

Table of Contents

Papers published in *Ingeniería e Investigación* are abstracted/indexed in

- Science Citation Index Expanded
- (SciSearch®), Clarivate Analytics
- Scopus - Elsevier
- Scientific Electronic Library Online - SciELO, Colombia
- Chemical Abstract
- Índice de Revistas Latinoamericanas
- en Ciencias Periódica
- Dialnet
- Sistema Regional de Información en Línea para
- Revistas Científicas de América Latina, el Caribe, España y Portugal - Latindex
- Ebsco Publishing
- DOAJ - Directory of Open Access Journals
- Redib - Red Iberoamericana de Innovación y Conocimiento Científico

The journal *Ingeniería e Investigación* was created in 1981. It is an entity in charge of spreading the teaching, Scientific, and technical research conducted at Universidad Nacional de Colombia's Department of Engineering and other national and international institutions. *Ingeniería e Investigación* deals with original, unedited scientific research and technological developments in the various disciplines related to engineering. *Ingeniería e Investigación* contributes the development of knowledge, generating a global impact on academia, industry, and society at large through an exchange of knowledge and ideas while maintaining a set of serious and recognized quality standards.

Ingeniería e Investigación publications are developed for the academic community who is interested in research and engineering knowledge development. We invite readers to be part of this Journal and participate either as authors, peer reviewers, or subscribers.

For additional information contact:
www.revistas.unal.edu.co/index.php/ingeinv
E-mail: revii_bog@unal.edu.co
Tel: 57(1) 3 16 5000 Ext. 13674

Tabla de Contenido

Research Article/Agricultural Engineering https://doi.org/10.15446/ing.investig.94777

An Initial Approximation to the Simulation of Soil CO_2 Emissions Using the IPCC Methodology in Agricultural Systems of Villavicencio

Una aproximación inicial a la simulación de emisiones de CO_2 del suelo usando la metodología del IPCC en sistemas agropecuarios de Villavicencio

Amanda Silva-Parra[1], Dayra Y. García-Ramirez[2], and Cristóbal Lugo-López[3]

ABSTRACT

At a global level, the agricultural sector has represented the largest source of greenhouse gas (GHG) emissions. Our research hypothesizes whether it is possible to faithfully define the effect of soil management factors on modeling soil carbon organic (SOC) sequestration and reducing soil CO_2 emissions in different agricultural systems across three zones of Villavicencio (Colombia) by applying the Tier-1 IPCC process-based model. Agroforestry systems (AFS) are typically found in zone 1, and intensive croplands (CL) in zones 3 and 4. Soil CO_2 emissions rates are calculated according to the current IPCC guidelines for national GHG inventories. Root-mean square error (RMSE, RMSE/n), R^2, and Nash-Sutcliffe efficiency (NSE) are measured to assess model performance. In zone 1, 7-year coffee-based agroforestry stored higher SOC, neutralizing -10,83t CO_2 eq ha^{-1} $year^{-1}$ than 25-year soybean/corn crop rotation in zone 3, with emissions of 2,56t CO_2 eq ha^{-1} $year^{-1}$. The agricultural systems of zones 3 and 4 turned out to be greater emitters, with 7 223 and 3 889t CO_2 eq $year^{-1}$, respectively, which could increase if CL continues to adopt agricultural practices that encourage full tillage. The beneficial effects of AFS on stored SOC are identified via field observations and correctly reproduced by RMSE evaluation.

Keywords: climate change, carbon sinks, land use, tillage

RESUMEN

A nivel mundial, el sector agropecuario ha representado la mayor fuente de emisiones de gases de efecto invernadero (GEI). Nuestra investigación hipotetiza si es posible definir fielmente el efecto de los factores de manejo del suelo en el modelado del secuestro de carbono orgánico del suelo (COS) y la reducción de las emisiones de CO_2 del suelo en diferentes sistemas agropecuarios para tres zonas de Villavicencio (Colombia) aplicando el modelo basado en procesos de nivel 1 del IPPC. Los sistemas agroforestales (AFS) se encuentran típicamente en la zona 1, y los sistemas intensivos de tierras de cultivo (CL) en las zonas 3 y 4. Las tasas de emisiones de CO_2 del suelo se calculan de acuerdo con las directrices actuales del IPCC para los inventarios nacionales de GEI. Se evalúan el error cuadrático medio (RMSE, RMSE/n), el R^2 y la eficiencia de Nash-Sutcliffe (NSE). En la zona 1, el sistema agroforestal de café de 7 años almacenó más COS, neutralizando -10,83t CO_2 eq ha^{-1} $año^{-1}$ que el cultivo de soya/maíz en rotación de 25 años de la zona 3, con emisiones de 2,56t CO_2eq ha^{-1} $año^{-1}$. Los sistemas agropecuarios de las zonas 3 y 4 resultaron ser más emisoras, con 7 223 y 3 889t CO_2 eq $año^{-1}$ respectivamente, lo cual puede aumentar si el CL continúa adoptando prácticas agrícolas que incentiven la labranza convencional. Los efectos benéficos de los AFS sobre el COS almacenado se identifican mediante observaciones de campo y se reproducen correctamente mediante la evaluación del RMSE.

Palabras clave: cambio climático, sumidero de carbono, uso del suelo, labranza

Received: April 07th, 2021
Accepted: February 09th, 2023

Introduction

Globally, agricultural-use land occupies about 40-50% of the land surface and generates about 10-12% of the total global anthropogenic emissions, *i.e.*, 5,1-6,1G t CO_2-eq per year (IPCC, 2006). Land uses in the study area (Villavicencio) are characterized mainly by conversion from grassland to continuous croplands, which causes a large degradation of soil organic matter (SOM) (Silva, 2018; Silva and Orozco, 2018), mainly due to conventional tillage (García *et al.*, 2018). Greenhouse gas emissions are influenced by the type of land used, especially by the types of crops and/or pastures in diverse environments (Mangalassery *et al.*,

[1] Agricultural Engineer, PhD in Agronomy, UNESP, Brazil. Affiliation: Full professor, Department of Agricultural Science and Natural Resources, ISAF Research Group, Universidad de los Llanos, Colombia. Email: asilvap@unillanos.edu.co
[2] Agricultural Engineer, MSc in Sustainable Tropical Production, Universidad de los Llanos, Colombia. Affiliation: Professor, Department of Agricultural Science and Natural Resources, Precision Agriculture Research Group, Universidad de los Llanos, Colombia. Email: dgarcia@unillanos.edu.co
[3] Agricultural Engineer, MSc in Agricultural Science, Universidad Nacional de Colombia, Colombia. Affiliation: Full professor, Department of Agricultural Science and Natural Resources, Precision Agriculture Research Group, Universidad de los Llanos, Colombia. Email: cristoballugolopez7@unillanos.edu.co

How to cite: Silva-Parra, A., García-Ramirez, D., and Lugo-López, C. (2023). An Initial Approximation to the Simulation of Soil CO2 Emissions Using the IPCC Methodology in Agricultural Systems of Villavicencio. *Ingeniería e Investigación, 43*(2), e94777. https://doi.org/10.15446/ing.investig.94777

2014; Chambers *et al*., 2016; Lal, 2018). The effects of land use on the emission of CO_2 are dominated by the type of tillage and/or pasture management (IPCC, 2006; Haddaway *et al*., 2017; Behnke *et al*., 2018; FAO, 2018). Land use may have direct and indirect effects on soil carbon stocks, and these changes may be conditioned to meet the social needs of farmers, such as the production of food, energy and fossil fuel, water supply, and crop residues management, in order to achieve higher productions in the short term (Popp *et al*., 2017; Nyambo *et al*., 2020). Several studies applying IPCC models to different extents corroborate that different soil management practices and types of tillage increase soil CO_2 emissions (IPCC, 2006; Cardinael *et al*., 2018; Lal, 2018; Parra *et al*., 2019). As an option for reducing soil CO_2 emissions, conservation practices have increased in many parts of the world, aiming to also increase production and sustainable development (Ogle *et al*., 2019). Agroforestry systems with trees and crops in interactive and simultaneous cultivation have been regarded as a key cropping practice for improving the productivity of agroecosystems and reducing soil CO_2 emissions (Nair, 2012; Feliciano *et al*., 2018). This can be seen in Figure 1.

Figure 1. (a) Cocoa-based agroforestry including *Acacia mangium* trees; (b) silvopastoral system of *B. decumbens* pasture with *Acacia mangium* in the study area (Villavicencio, Colombia). The capacity of soils and biomass in agroforestry systems to store C depends on several factors, including local edaphic and climatic conditions, previous land use, tree density and species, harvesting and pruning practices, and management activities (Nair, 2012).
Source: Authors

In general, the transition from cropland to an agroforestry system is beneficial to soil organic carbon (SOC) (Cardinael *et al*., 2018). The accumulation of SOC due to the sequestration of carbon in the soil is certainly one of the major benefits of agricultural systems, as it is effective in helping to mitigate the increase in atmospheric CO_2 concentrations (Lal, 2018). For example, in the southeastern USA, conservation tillage, combined with intensive crop rotations that include cover crops, can sequester an average of 1 700 lb of CO_2 each year, *i.e.*, 464 lb of C per acre (Franzluebbers, 2015). There are various methods to estimate soil CO_2 emissions from agriculture, ranging from simple Tier 1 methods (IPCC, 2006; Ogle, 2004; Parra *et al*., 2019) to complex process-based models that simulate the changes in soil carbon with some detail (Tiers 2 and 3) (FAO, 2018), although this relation is even more complex under the influence of climate change in tropical zones. Cardinael *et al*., (2018), applying a Tier 1 IPCC methodology, validated that the mean SOC storage rate (± confidence intervals) for croplands converted to agroforestry systems was 0,75±0,19 t C ha^{-1} yr^{-1}, while the mean SOC loss rate for forests converted to agroforestry systems was -1,15±1,02 t C ha^{-1} yr^{-1}, in all regions, climates, and agroforestry systems taken together. The mean SOC change rates for the conversion from grasslands to agroforestry systems were not significantly different from zero (0,23±0,25 t C ha^{-1} yr^{-1}). In this sense, by employing soil management practices, agricultural lands can both sequester soil carbon and reduce GHG emissions (IPCC, 2006). Nemo *et al*., (2017) showed a variant of Tier 1 testing with the 2 RothC model (IPCC, 2006), which is used to simulate the interaction between GHG emissions, growth, and grazing in managed grasslands, where the C-input was adjusted so the equilibrium C matched the measured total SOC at the end of the spin-up period. This variant is useful for grassland systems in which the plant-derived carbon input is the most uncertain parameter, as well as the one to which the model is most sensitive (Poeplau, 2011). These types of approaches have been used to estimate C sequestration potentials in grasslands, as well as the potential effects of pasture management on SOC and stock changes on global, national, and regional scales (Henderson *et al*., 2015; Chambers *et al*., 2016; Novaes *et al*., 2017; FAO, 2018; Parra *et al*., 2019). Our specific objectives were the following: (1) to test the performance of the IPCC Tier 1 ensemble approach to simulate soil CO_2 emissions; (2) to quantify differences in soil CO_2 emissions between agricultural systems and zones across the Villavicencio area by modeling and measuring SOC according to the effect of soil management practices as a first approximation to national inventories; and (3) to assess the performance of the IPCC Tier 1 approach with parameters such as the RMSE, the Nash-Sutcliffe efficiency (NSE), and R^2.

Material and methods

The Tier 1 IPCC model

The Tier 1 IPCC model is designed to simulate change in SOC stocks by assigning a reference SOC stock value, which varies depending on climate and soil management factors. To run the simulation, the Tier 1 model requires input parameters regarding the soil management factors (inputs). In this regard, (i) FLU is related to land use (long-term cultivated, paddy rice, perennial/tree crop, set aside); (ii) FMG characterizes the tillage regime (full, reduced, no tillage) for croplands, as well as different pasture management types for grasslands; and (iii) FI describes the carbon input level (low, medium, high without manure, high with manure). These factors come with individual error ranges (between ±5 and ±50%) and must be defined according to climatic conditions (IPCC, 2006). The main parameters (inputs) for modeling SOC changes (outputs) are presented in Figure 2.

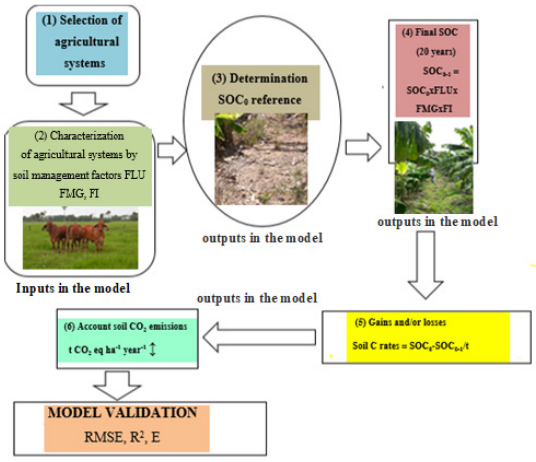

Figure 2. Methodological steps to simulate soil CO_2 emissions with the Tier 1 IPCC methodological approach (input and outputs) in the model
Source: Authors

Study site and empirical data

To parameterize the IPCC model, empirical data on local agricultural systems of Villavicencio were used. This area is located in the Meta Piedmont in Eastern Colombia, 4°8′31,2′′N and 73°37′35,9′′E, and it covers an area of ~1 328 km² within the sectoral soil analysis (Alcaldía de Villavicencio, 2012). In this study, three zones of agricultural vocation were selected (Figure 3, Table 1).

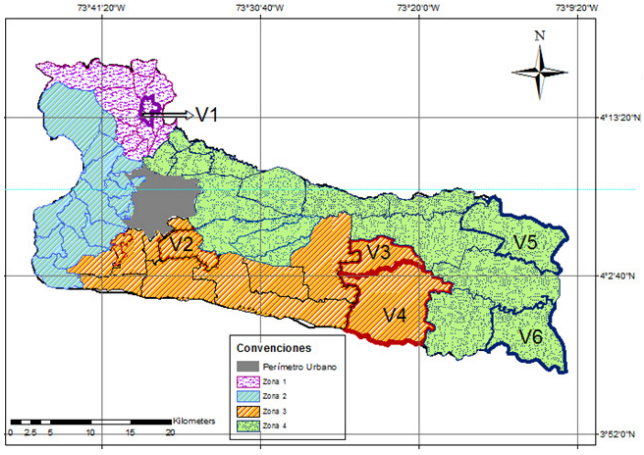

Figure 3. Map of the location of the sampling sites in the Villavicencio area: zone 1 includes Puente Abadía locality (V1); zone 3 comprises three localities: Barcelona (V2), Pompeya Alto (V3), and Pompeya Bajo (V4); and zone 4 has two localities: Indostant (V5) and Porvenir (V6).
Source: Authors

Soils are predominantly acid (Department of Agriculture, 1996). The criterion for the agricultural systems' (land uses) selection was area representativeness. Six agroforestry systems (AFS) were selected in zone 1, 23 in zone 3, and 21 in zone 4. These comprised AFS, croplands (CL), pasture types in different states of degradation, non-degraded pastures (NDP), and moderately degraded pastures (MDP), with different times of use. More information about the collected agricultural systems in each zone is provided in Table 2.

Table 1. Agro-ecological characteristics of the sampling localities, Villavicencio (Colombia).

Zones	Locality	Latitude Longitude	Meters above sea level, Climatic condition, mean annual rainfall (mm), mean temperature (°C)
Zone 1	Puente Abadía	4 ° 1 0 ′ 4 2 ′ ′ , 4°17′33′′ N. 73°36′24′′ 73°46′21′′E	800-2 000 Tropical humid 3856 20
Zone 3	Barcelona Pompeya Alto Pompeya Bajo	3° 56′ 15″ 4° 11′ 5″ N. 73° 10′ 00″ 73° 46′00″ E	500-220 Tropical humid 2 850 24
Zone 4	Indostat Porvenir	4 ° 0 1 ′ 0 4 ′ ′ 4°10′00′′ N. 7 3 ° 1 3 ′ 5 5 ′ ′ 73°37′10′′ E	400-225 Tropical humid 2 850 24

Adapted from Alcaldía de Villavicencio (2012). Typical hapludox (Department of Agriculture, 1996).
Source: Authors

The criteria for the characterization of agricultural systems were evaluated *in situ* by monitoring soil management factors (IPCC, 2006). For this stage, site information was employed, where land use transitions included information from five years before the implementation of the current agricultural system, which were often reported to have been assessed via the IPCC Tier 1 methodology (Table 3).

The identified soil management factors identified contrasted with the default values in Chapters 5 and 3 (*Cropland* and *Grasslands*, Tables 5.5 and 3.4.5) of the IPCC document (2006), which were used as input data for the model. Default values for FLU, FMG, and FI higher than 1,0 correspond to SOC storage, while those lower than 1,0 correspond to SOC loss.

Field measurements for model parameterization

To allow for a standardized analysis compatible with the IPCC guidelines, soil samples were collected (n=150) from the upper 0-30 cm layer (IPCC, 2006). Soil sampling was carried out for four months between January and April 2018 in the study area. The sieved soils were further milled to 0,25 mm in order to measure the initial physical-chemical soil analysis. Bulk density was determined from a core sample (Department of Agriculture, 1996).

The soil organic carbon content before (SOCinitial) in the soil samples was determined according to Walkley and Black (Department of Agriculture, 1996). Initial SOC stocks (SOC_0) were determined via Equation (1), as follows:

$$SOC_0\ (t\ C\ ha^{-1}) = SOC\ (\%)*(\rho b\ *100)*d\ (m) \quad (1)$$

where SOC_0 is the mean of initial soil C stocks (t C ha^{-1}); ρb is the bulk density (g cm^{-3}); and d denotes a depth of 0,30 m. In the model parameterization, the dynamics of SOC were projected to 20 years, in sufficient agreement with empirical

Table 2. Basic information on agricultural systems and the area in the data collection site, Villavicencio (Colombia)

Land use categories	Agricultural system definition	Author
Agroforestry systems, zone 1 (n = 1 115 ha), zone 3 (n = 1 115 ha), zone 4 (n = 1 317 ha)		
Shadow systems (SS), zone 1	Coffee and/or cocoa shrubs with multi-purpose shade species.	Nair (1985)
Agrisilvicultural systems (AS), zone 1	Simultaneously growing crops of coffee and cocoa involve trees, cover on the same piece of land, mainly leguminous.	Nair (1985)
Homegarden (HG), zones 3, 4	Perennial crops of citrus and livestock –all managed in the same piece of land.	Huai and Hamilton (2009)
Improved fallow (IF), zones 3, 4	Continuous cropping of fruits such as papaya and banana with limited or no fertilizer application to enrich the soil within a shorter time, in comparison with natural fallow.	Nair (1985)
Pasture types, zone 3 (n = 32,244 ha), zone 4 (n = 2,725 ha)		
Improved pasture	Grassland sustainably managed with moderate grazing pressure and receiving at least one improvement (*e.g.*, fertilization, species improvement, irrigation, mainly applied as SP).	IPCC (2006)
Non-degraded pasture, zone 3	Non-degraded and sustainably managed grassland, but without significant management improvements.	
Moderately degraded pasture zone 4.	Overgrazed or moderately degraded grassland, with somewhat reduced productivity (relative to the native or nominally managed grassland) and receiving no management inputs.	
Silvopastoral systems, zone 4 (n = 2,906 ha), zone 4 (n = 136 ha)		
Silvopastoral system (SP), zones 3, 4	Improved pasture of Brachiaria associated mainly with *A. mangium*, including agroforestry practice that integrates livestock, forage production, and forestry in the same land management unit.	Nair (1985)
Cropland, zone 3 (n = 15,109 ha), zone 4 (n = 4,607 ha)		
Cropland (CL), zone 3, 4	Area that has been continuously managed, mainly with rice and crop rotation (CR). Long term cultivated land between corn, soybean, and rice.	IPCC (2006)

Source: Authors

SOC measurements regarding observed and default values (FLU, FMG, FI) in each field plot (50 selected agricultural systems x 3 replicates = 150 samples). The model inputs required a total of three default values per agricultural system characterized, for a total of 450 parameters in the model, from which a mean was taken for each agricultural system, for a total of 150 data.

Model validation

To evaluate the accuracy of our model parameterization, the model performance was evaluated with four widely used quantitative methods, *i.e.*, the R^2 (squared correlation coefficient), which is described in Equation (2); the RMSE (root mean squared error) (Equation (3)) and RMSE/n (Moriasi *et al*., 2007), a measurement of accuracy calculated as the differences between model-predicted and measured SOC values; and the (E) (model performance efficiency) (Nash-Sutcliffe, 1970), which evaluates the degree of closeness between modeled and observed data (Ludwig *et al*., 2011) (Equation (4)). These indicators were analyzed with $P < 0{,}005$. The statistical analysis was performed using Infostat v. 17.0 for Windows.

$$R^2 = 1 - SS/res/SStot \quad (2)$$

where: SSres= sum $(Oi - Pi)^2$ and SStot = sum $(Oi - Omean)^2$; Oi = observed values (known results); Pi = expected values or unknown results.

$$RMSE = \text{Square root of } \sum (Oi-Pi)^2/n \quad (3)$$

The RMSE ranges from 0 to 100. At an ideal fit, the RMSE is equal to zero. A lower RMSE is better.

The Nash-Sutcliffe model efficiency coefficient E was calculated as follows:

$$E = 1 - \sum (Oi-Pi)^2 / \sum (Oi-\bar{O})^2 \quad (4)$$

where $\bar{O}$ is the observation mean. A higher E is better, and it can be expressed as a percentage when multiplied by 100 (Smith and Smith, 2007). A linear regression of the simulated SOC (yPi) and observed SOC (xOi) time-series data was performed (Equation (5)):

$$YPi = IPi + spi \cdot xOi \quad (5)$$

which resulted in a slope sPi, an intercept IPi, and the coefficient of determination R^2. In this sense, only the agricultural systems with the best fit in the model were graphed.

Model application to simulate soil CO_2 emissions

After validation, the Tier 1 IPCC model was used to simulate the current SOC initial stock changes in order to assess the effect of soil management factors on SOC final stocks (Equation (6)).

$$SOC_{0\text{-}1}\,[tC\ ha^{-1}] = SOC_0 * FLU * FMG * FI \quad (6)$$

Table 3. Characterization of agricultural systems five years before land use transitions and current land uses with soil management factors related to each zone studied, Villavicencio (Colombia)

Land use 5 years before/F_{MG}					Land use change/F_{MG}/F_I level/ID (F_{LU}_F_{LU}time)	
6	5	4	3	2	1	**Agricultural systems, zone 1**

Coffee crop / HG fruit trees/chicken /			DP Brachiaria/NT			AS coffee/MT/L/ASCf_1
----------Agrisilvicultural coffee/NT----------						SS of coffee/NT/H/ AFCf_7, SSCf_5
						SS of cocoa/NT/H/ SSCc_5
----------Cocoa crop/NT----------IP *Brachiaria*/FT						AS cocoa/MT/H/ ASCc_2
----------Cocoa crop/NT----------IP/FT----						AS cocoa/NT/H/ ASCc_4
Agricultural systems, zone 3						
--SP (*Brachiaria dictyoneura* pasture + *Acacia mangium*) /IP-						SP (*B. decumbens* and *A. mangium*+kudzu *P. phaseloides*) /IP/H/ Sp_8
-SP (*B. dictyoneura* + *A. mangium*) /IP-/ -----Brachiaria/NDP-						SP (*B. decumbens* + *A. mangium*) /IP/M/ Sp_3
----------SP/IP----------/ -----Brachiaria/NDP--						SP (*B. decumbens* + *A. mangium*) /IP/M/ Sp_1
----------IP *B. dictyoneura*/NDP----------						*B. decumbens*/ND/H/ NDP_26
------- *B. dictyoneura*/NDP/ -------*B. dictyoneura*/MDP-----						*B. decumbens*/ND/H/ NDP_15
-IF banana/NT-/ banana/MT-/ rice/MT-/ ----rice crop/FT-------						IF banana/MT/M/ IFB1_2
						IF banana/MT/M/ IFB_2
---IF banana/NT--/ ---------corn/soybean/NT----------						IF banana/FT/L/ IFB_1
----------IF citrus/NT----------						IF citrus/FT/L/ IFCi_7
--------IF citrus/NT----------/ ----------rice crop/FT----------						HG citrus/NT/M/ HGCi_2
----citrus crop/NT-/ ----------rice crop/FT----------						HG citrus/MT/M/ HGCi_1
-IF citrus/NT--/ ----------rice crop/FT----------						IFCitrus crop/MT/M/ IFCi_1, IFCi1_2
----------Citrus crop/FT----------						HG citrus/NT/M/ HGCi_5
----------Agrisilvicultural cocoa/NT----------						SS of cocoa/NT/H/ SSCc_6
----------papaya crop/FT---/ ----------corn/soybean/MT---------						IF papaya/NT/M/ IFP_3
--papaya/FT---/ ----------rice/soybean/MT----------						IF papaya/NT/M/ IFP_1
----------Continuous rice crop/MT----------						Continuous rice crop/FT/L/ CLR_29
----------Rice/corn/MT----------						Rice/corn/FT/M/ CRR/C_27
----------Rice crop/FT----------						Rice crop/FT/L/ CLR_23
----------CR rice/soybean/MT----------						CR rice/soybean/FT/L/CRR/S_25
rice/soybean/FT/ ----------rice/soybean/MT----------						CR rice/soybean/FT/L/ CRR/S_28
----------soybean/corn/FT----------						CR soybean/corn/FT/L/ CRS/C_25
Agricultural systems, zone 4						
----------Papaya crop/MT----------						IF papaya/MT/M/IFP_6
--papaya--/MT----------/ Brachiaria/MDP----------						IF papaya//NT/H/IFP_3
--HG citrus/NT-----/ ----------Brachiaria/MDP----------						HG citrus with herb/MT/HGCi_2
----------Citrus crop/NT----------						HG citrus with herb/NT/H CLC_20, HGCi_15
						HG citrus with legume/NT/HGCi_6, HGCi_10
----------HG citrus/NT----------						AS citrus/NT/H/ASCi_26
----------Pasture *B. decumbens*/NDP--------						SP *B. decumbens*+*A. mangium*/IP/H/SP_1
----------Pasture *B. dictyoneura*/MDP----------						Pasture *B. decumbens*/MD/M/MDP1_16, MDP_29
----------Pasture *B. decumbens*/MD----------						Pasture *B. dictyoneura*/MD/M/MDP_16
-------Banana crop/MT----------Brachiaria/MDP-						IF banana crop/MT/M/IFB1_3
-----IF banana crop/NT----------/ ---*B. decumbens*/MDP-						IFBanana crop/MT/M/IFB_3
--banana crop/MT--/ -------*B. decumbens*/MDP----------						IFBanana crop/FT/L/IFB_1
--rice/MT--/ ----------crop rice/FT----------						Continuous crop rice/FT/L/CLR_32
----------Crop rice/FT----------						Continuous crop rice/FT/L/CLR_18, CLR_25, CLR_20
----------Crop rice/MT----------						Continuous crop rice/MT/M/CLR_14
-----Crop rice/MT----------Crop rice/FT---						Continuous crop rice/MT/M/CLR_24

Legend: NT No tillage: Direct seeding without primary tillage, with only minimal soil disturbance in the seeding zone. FT Full tillage: Substantial soil disturbance with full inversion and/or frequent tillage operations (within year). MT Minimum tillage: Including primary and/or secondary tillage, but with reduced soil disturbance (usually shallow and without full soil inversion). AFS: Agroforestry system; SS: Shade system; AS: Agrosilvicultural system; SP: Silvopastoral system; NDP: Non-degraded pasture; MDP: Moderately degraded pasture; CL: Continuous and/or Intensive Cropland; L: Low input; M: Medium input; H: High input.
Source: Authors

where SOC_{0-1} is the mean of the final soil C stocks (t ha-1) over the next 20 years, (SOC_0) = SOCinitial Stock (t ha^{-1}); and FLU, FMG, and FI are the default values for soil management (IPCC, 2006). SOC stock changes in the top soil (0-30 cm) over a period of 20 years were calculated as follows (Equation (7)):

$$\Delta SOC\ [t\ C\ ha^{-1}\ year^{-1}] = (SOCfinal - SOCinitial)/T \quad (7)$$

where: ΔSOC = losses and/or gains in SOC rates, T = default time for transition between equilibrium SOC values (20 years). ΔSOC can be converted to atmospheric CO_2 stored in or emitted from the soil by multiplying the tons of C by 44/12 (the ratio of molecular weight for CO_2 and C) (IPCC, 2006).

Results and discussion

Rates of gains/losses of soil C and soil CO_2 emissions for each agricultural system

A significant limitation for model validation was that the change in SOC stock was equated with CO_2 emissions, as only input variables had an assigned probability distribution within each default value, depending on the soil management factor identified, without considering other input factors. The observed SOC storage rates regarding the conversion from pasture for coffee-based agroforestry (AFCf_7) in zone 1 were higher than those of the conversion of rice/corn crop rotation for improved banana fallow (IFB_2) of zone 3 (Table

Table 4. Simulated gains and losses of SOC rate data (outputs in the model) considering IPCC default values for soil management factors (inputs in the model) in agricultural systems, Villavicencio (Colombia)

Land use_ time use	Default values $F_{LU}xF_{MG}xF_I$ (inputs in the model)	Gains/losses of SOC rates t C ha^{-1} yr^{-1} (outputs in the model)	Land use_time use	Default values $F_{LU}xF_{MG}xF_I$ (inputs in the model)	Gains/losses of SOC rates t C ha^{-1} yr^{-1} (outputs in the model)
Zone 1			Zone 3		
ASCf_1	1,12	+0,91	CRR/C_27	0,55	-0,40
SSCf_7, SSCf_5	1,35	+2,96 +0,92	CLR_23	0,44	-0,57
SSCc_5	1,35	+0,70	CRR/S_25, CRR/S_28	0,50 0,44	-0,49 -0.63
ASCc_2	1,35	+1,05	CRS/C_25	0,44	-0,70
ASCc_4	1,35	+1,43	Zone 4		
Zone 3			IFP_6	1,15	+0,73
Sp_8	1,29	+0,92	IFP_3	1,35	+0,63
Sp_3	1,16	+0,15	HGCi_2	1,22	+0,58
Sp_1	1,17	+0,11	HGCi_20, HGCi_15	1,12 1,12	+0,36 +0,24
NDP_26	1,10	+0,10	HCic_6, HGCi_10	1,35 1,35	+1,15 +1,51
NDP_15	1,10	+0,12	ASCi_26	1,35	+1,17
IFB1_2	1,21	+0,43	SSP_1	1,29	+0,92
IFB_2	1,22	+0,08	MDP1_16, MDP_29	0,96 0,96	-0,02 -0,03
IFB_1	0,92	-0,06	MDP_16	0,97	-0,04
IFCi_7	1,12	+0,33	IFB1_3	1,15	+0,21
HGCi_2, HGCi1_1	1,26 1,22	+0,43 +0,26	IFB_3	1,22	+0,31
IFCi_1, IFCi1_2	1,21 1,22	+0,26 +0,26	IFB_1	0,92	-0,12
HGCi_5	1,21	+0,30	CLR_32	0,55	-0,18
SSCc_6	1,35	+0,41	CLR_18, CLR_25, CLR_20	0,44 0,44 0,44	-0,59 -0,62 -0,07
IFP_3, IFP_1	1,21 1,22	+0,30 +0,20	CLR_14	0,55	-0,55
CLR_29	0,50	-0,46	CLR_24	0,55	-0,47

Legend: AS: Agrisilvicultural system; SS: Shade system; SP: Silvopastoral system; NDP: Non-degraded pasture; IF: Improved fallow; HG: Homegarden system; MDP: Moderately degraded system; CL: Cropland; CR: Crop rotation; Cf: Coffee; Cc: Cocoa; B: Banana; Ci: Citrus; P: Papaya; R: Rice; S: Soybean; C: Corn; F_{LU}: land use factor; F_{MG}: pasture management and/or tillage regime in cropland (full, reduced, no tillage); F_I:carbon input level (low, medium, high without manure, high with manure).
Source: Authors

4) –levels: ΔSOC = AFCf_7 = 2,96 t C ha^{-1} $year^{-1}$ and IFB_2 = 0,08 t C ha^{-1} yr^{-1}, accounting for a neutralization of -10,83t CO_2eq ha^{-1} $year^{-1}$ in AFCf_7, which was due to default values FLU, FMG, and FI in the simulations that demonstrated potential mitigation.

The mean stock change factor (default value, ± confidence intervals) was 1,19±0,10 for grassland converted to agroforestry (Cardinael *et al*., 2018). Poeplau *et al*., (2011) demonstrated that conversion from grasslands to agroforestry systems did not improve SOC stocks. However, this work agrees that the returns of organic material (leaf litter) in coffee-based agroforestry systems is higher than in the monoculture of coffee as, demonstrated by Zaro *et al*., (2020). In general, the transition from cropland to an agroforestry system is beneficial to SOC (Lu *et al*., 2015), as demonstrated in the simulated IFB_2. The results in Table 4 also show that the effect of pasture management on gains/losses of soil C rates varied substantially between NDP_15 compared to the MDP1_16 of zones 3 and 4 (Table 4) –levels: ΔSOC = NDP_15 = 0,12 t C ha^{-1} $year^{-1}$ and MDP1_16 = -0,02 t C ha^{-1} $year^{-1}$. These values are in line with those reported by Silva and Orozco (2018) in degraded pastures of Ariari, Meta, Colombia. Typically, in the model-integrated soil management factors, NDP demonstrated better pasture management than MDP. Several previous studies also showed that many pasture techniques have been applied to mitigate GHG emissions from agriculture (Jadan *et al*., 2015; Parra *et al*., 2019). A plausible adoption rate of 30% for improved deep-rooted legumes associated to Brachiaria pastures in Cerrado, Brazil, represented a mitigation potential of -29,8 t CO_2-eq yr^{-1} to the atmosphere (Thornton and Herrero, 2010). However, belowground C-inputs from exudation and root sloughing from C4 grasses are high in Brachiaria pastures, forming the base for soil organic matter buildup in these systems (Anderson-Teixeira *et al*., 2016). Moreover, elements from agricultural systems (the impact of pasture management and grazing on growth and yield) need to be included in the modeling in order to allow predicting future food security (Van *et al*., 2018). The responses of our predictions showed that the adoption of silvopastoral systems SP_1 and SP_8 stemming from pastures by farmers of zone 3 resulted in a significant absorption of soil CO_2 emissions (Table 4) –levels: -3,37 and -3,39 t CO_2 eq ha^{-1} $year^{-1}$, respectively. In the tropical zone of Colombia, Parra *et al*. (2019), using the Tier 1 IPCC approach (2006), showed that a silvopastoral system had the highest potential for offset GHG emissions (-4,8 t CO_2eq ha^{-1} $year^{-1}$) due to soil C accumulation plus biomass C fixation in Acacia trees. Soil C sequestration by the world's grasslands could offset up to 4% of global GHG emissions (IPCC, 2006). This research showed that 34% of the agricultural systems evaluated (7 and 10 out of the 23 and 21 agricultural systems of zones 3 and 4) turned out to be CO_2eq emitters, mainly due to CL and MDP (Table 4). Default emission factors used in the Tier 1 IPCC model can be further sources of uncertainty, as they may not be representative of SOC changes and, in many cases, they can under- or overestimate soil CO_2 emissions and/or absorptions (FAO, 2018; Silva and Orozco, 2018). Soil C losses rates differ considerably between continuous the crop rotation of soybean/corn CRS/C_25 including FT of zone 3 and the MDP *B. decumbens* MDP1_16 with MT of zone 4 (Table 4) –levels: ΔSOC = CRS/C_25 = -0,70 and MDP1_16 = -0,02 t C ha^{-1} yr^{-1}. In fact, easily decomposable materials are fully or partially depleted, and the microbial population and decomposition rate of litter materials decline due to full tillage (Lal, 2018). Reduced tillage and 'no till', residue incorporation, improving soil biodiversity, and mulching enhance the sequestration of carbon in the soil. NRCS conservation practices can be expected to sequester approximately 0,07 to 0,96 t C ha^{-1} yr^{-1} due to improved soil management in croplands (Chamber *et al*., 2016).

Representativeness of soil CO_2 emissions by each category of land use and each zone across the Villavicencio area

The simulated total of contributions regarding emission and/or neutralization of soil CO_2 across the Villavicencio area, zone 1 (comprising AFS), account for -5 416 t CO_2eq yr^{-1} (Figure 4, Table 5) (-4,86 t CO_2eq ha^{-1} yr^{-1} * 1 115 ha), which is possibly due to a high SOC initial state (Table 5) and a higher default value used in the simulation. This is shown in Table 4.

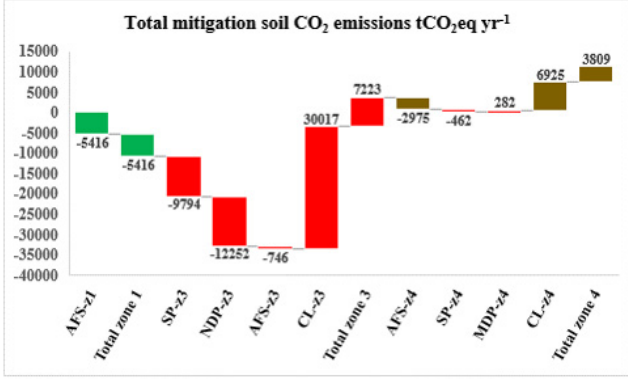

Figure 4. Contribution of soil CO_2eq emissions and sinks in each land use category and zone across the Villavicencio area, which was computed (SOC rates tC ha^{-1} yr^{-1} x area (#ha) x 3,65) based on the changes in SOC storage reported in Table 4. Soil CO_2 emissions are negative in the face of stored SOC and positive with released SOC. Legend: AFS: agroforestry systems; SP: silvopastoral systems; NDP: non-degraded pastures; CL: cropland; MDP: moderately degraded pasture; z: zone.
Source: Authors

Silva (2018) found that the SOC initial state has the greatest impact on emissions dynamics. Numerous studies across the globe demonstrate that the use of integrated practices such as AFS can increase soil C gains by 10-60%, thus reducing the carbon emissions associated with the residue inputs by 20-50% (Nair, 2012). For example, a cocoa AFS has the capacity to sequester about 3 t C ha^{-1} $year^{-1}$, with a reduction of 11 t CO_2eq ha^{-1} $year^{-1}$ (Jadan *et al*., 2015). On the other hand, zone 3 showed the highest soil CO_2 emissions across the Villavicencio area, followed by zone 4, due to the contributions of CL (Figure 4), *i.e.*, 7 223 t CO_2eq yr^{-1}, and 3 809 t CO_2eq yr^{-1}, respectively. As shown

in Table 5, the lowest initial SOC stocks mostly appear in the continuous CL of zones 3 and 4, where there is no land use transition between rice crops and crop rotation and soils are frequently disturbed by full tillage. Soil conservation practices such as crop rotation can fix a large amount of soil organic C and achieve a balance in C storage as long as full tillage is not performed (IPCC, 2006). Efforts for the mitigation of soil CO_2 should focus mainly on zones 3 and 4, adopting more sustainable soil management practices. In a study by Silva (2018), conversion from rice monoculture or crop rotation would increase the soil C stock by about of 12,3 t C ha^{-1} in 20 years, equivalent to 0,61 t C ha^{-1} yr^{-1}, which would reduce emissions by 2,27 t CO_2eq ha^{-1} $year^{-1}$. In zone 3, the contribution of NDP to the mitigation of emissions (-12 252 t CO_2eq yr^{-1}) (Figure 4) is more influenced by the area planted (ha) than by the rates of soil C gains per year (Table 5). However, the time reference of the NDP does not usually pose a challenge. This change is usually fast –soon after the introduction of the new practice– and eventually stabilizes when a new equilibrium is close by (FAO, 2018). The silvopastoral systems of zone 3 and 4 stemming from the conversion of NDP showed an apparent SOC storage (Table 4) and neutralizations of -9 794 and -462 t CO_2 eq yr^{-1}, respectively (Figure 4). MDP contributed with 7,40% of the total emissions of zone 3 (Figure 4). Converting degraded grassland to silvopastures could increase SOC stocks ((Mangalassery *et al*., 2014). Silvopastoral systems are agricultural strategies that can act positively for the potential mitigation of soil CO_2 emissions (Parra *et al*., 2019). As pointed out by the FAO (2018), there is a significant lack of rigorous data on C sequestration in silvopastoral systems, since a large amount of the root inputs (FI) of trees can be incorporated into these systems.

Model validation analysis

Among all zones, zone 3 was the best reproduced by the model (Table 5) –levels: RMSE = 3,96 t C ha^{-1}, RMSE/n = 0,05 t C ha^{-1}, Nash-Sutcliffe E= 0,33. The levels for zone 4 were (Table 5): RMSE = 10,95 t C ha^{-1}; RMSE/n = 0,17. In the agricultural systems of zone 1, a clear assessment of the source of deviations between the simulated and measured SOC data was difficult (Table 5) –levels: RMSE = 29, RMSE/n = 1,61 (Figure 5a). The modeled SOC accounted for 111,66 t C ha^{-1} over the entire measurement (86,47 t C ha^{-1}) (Table 5), which implies an overestimation of 29,13% by the model.

This is possibly related to several factors, mainly the high input factor (FI) due to manure application in these systems. Many controversies continue to arise as to the fact that conversion from pasture to AFS does not improve SOC stocks (Poeplau *et al*., 2011; Cardinael *et al*., 2018). Fujisaki *et al*. (2015) found slightly higher SOC stocks in grasslands than in forests. In this sense, more precise simulation

Table 5. Representativeness of soil CO_2 emissions by category of land use in each zone across the Villavicencio area and relationships of observed and simulated SOC data with statistical analysis R2, RMSE, RMSE/n, and model efficiency E.

Current land used by each zone	Area (ha)	SOC_0 Obs. t C ha^{-1}	SOC_{0-1} Sim. t C ha^{-1}	R^2	E	RMSE t C ha^{-1} (n=150)	RMSE/n t C ha^{-1}	SOC Rates t C ha^{-1} yr^{-1}
Agricultural systems, zone 1								
AFS	1 115	86,47	111,66	0,90	0,21	29,0 (n=18)	1,61	+1,32
Total, zone 1	1 115	86,47	111,66	0,90	0,21	29,0 (n=18)	1,61	
Agricultural systems, zone 3								
SP	2 906	29,18	36,65	0,85	0,21	10,28 (n=9)	1,14	+0,39
NDP	32 244	19,42	21,55	0,73	0,10	12,14 (n=6)	2,02	+0,11
AFS	757	25,47	30,58	0,96	0,51	5,73 (n=36)	0,15	+0,26
CL	15 109	19,73	9,43	0,95	0,31	10,48(n=18)	0,58	-0,54
Total, zone 3	51 016	23,45	24,55	0,94	0,33	3,96(n=69)	0,05	
Agricultural systems, zone 4								
AFS	1 317	50,60	62,31	0,98	0,22	14,69(n=33)	0,44	+0,61
SP	136	58,80	76,36	0,96	0,16	9,52 (n=3)	3,17	+0,92
MDP	2 725	17,90	17,36	0,74	0,13	10,58 (n=9)	1,17	-0,02
CL	4 607	15,71	7,87	0,95	0,41	9,64 (n=18)	0,53	-0,41
Total, zone 4	8 785	35,75	40,97	0,96	0,26	10,95(n=63)	0,17	

Legend: The *RMSE* unit is the amount of t C ha^{-1} standard deviations of the residuals (prediction errors). *E* is the Nash-Sutcliffe model efficiency. *AFS*: Agroforestry system; *SP*: Silvopastoral system; *ND*: Non-degraded pasture; *MDP*: Moderately degraded pasture; *CL*: Cropland.
Source: Authors

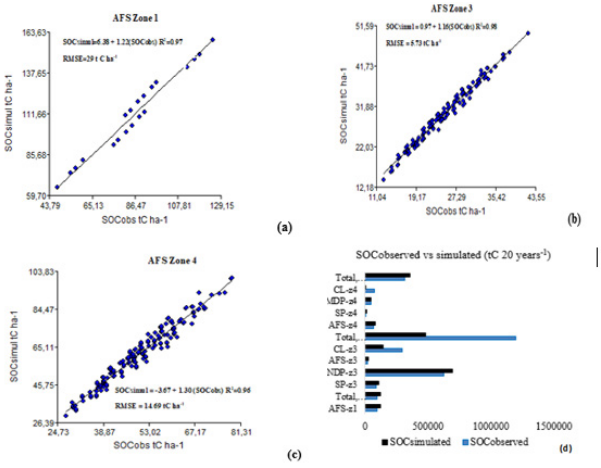

Figure 5. a) Relationship between observed and simulated SOC for AFS, zone 1; b) relationship between observed and simulated SOC for AFS, zone 3; (c) relationship between observed and simulated SOC for AFS, zone 4; d) relationship between observed and simulated SOC (tC 20 years^{-1}) for the agricultural systems in Table 5 (total ha). Legend: AFS: agroforestry systems; SP: silvopastoral systems; NDP: non-degraded pastures; CL: cropland, MDP: moderately degraded pasture; z: zone. **Source:** Authors

models must be elaborated which consider the monitoring of soil C stocks from previous systems. The main difficulty to properly assess SOC changes in agroforestry systems compared to other land uses is spatial heterogeneity (Cardinael *et al*., 2018). However, there were stronger and more significant R^2 between the SOC_0 and SOC_{0-1} for all of the AFS than for the NDP and MDP in zones 3 and 4 (Table 5). In global Tier 1 IPCC models for simulating grasslands, the model ensemble is highly uncertain, partly due to the difficulty in characterizing diverse grassland systems (Ogle *et al*., 2004). The linear regression of the simulated and observed SOC data shows a better fit for the AFS of zone 3 (Figure 5b) –levels: R^2 = 0,94, SOCsimulated = 0,97+1,16, SOCobserved, P < 0,005– that for those in zones 1 and 4 (Figures 5a, 5b, and 5c). An adjustment of these parameters with local data may be required to improve estimations (Figure 5d), as supported by FAO (2018). AFS management options targeting increases in leaf litter inputs could be a promising strategy to increase the SOC content. The SP of zones 3 and 4 differ considerably in terms of RMSE and RMSE/n (Table 5) **–**levels; RMSE = 9,52t C ha^{-1} and RMSE = 10t C ha^{-1}, respectively–, but the RMSE/n was higher in zone 4 due to a lower number of samples (Table 5). One significant limitation in assessing the suitability of process-based models can be the small number of datasets used. The livestock farmers of zone 3 and 4 can influence root biomass and thus SOC inputs by grazing management, as well as the plant species composition (Henderson *et al*., 2015). The Nash-Sutcliffe efficiency (E) coefficients supported the results of the statistical analysis conducted for the RMSE values. The mean values of said coefficients for the AFS of zone 3 was equal to 51% (Table 5). The continuous cropland system (CL) also demonstrated a better match between the modeled and measured SOC contents (Figure 5d), especially in zone 3, where the value of the positive Nash-Sutcliffe E coefficient reached 31% (Table 5). However, the NDP of zone 3 showed a low model E in predicting SOC changes, as well as a higher deviation in the observed and measured SOC (Table 5) –levels: E = 10%, RMSE/n = 2,02 t C ha^{-1}–, probably because the pastures exhibited a greater degree of SOC degradation variability. The uncertainty of SOC models for grazed grassland will likely be large, probably larger than that for models applied to croplands (FAO, 2018). Certainly, in all possible combinations of the observed FLU, FMG, and FI default values in the calibration, the inclusion of AFS in zones 3 and 4 yielded the best results.

Conclusions

As climate change research becomes more and more relevant, agroforestry system (AFS) models can play a major role in understanding the interplay between environmental change, SOC, and the functioning of these systems. In this sense, GHG simulations across Villavicencio zones showed that the highest removals took place in the AFS of zone 1 (-5 416 t CO_2 eq yr^{-1}). However, the better matches for AFS (between observations and simulations) were obtained in zones 3 and 4 in comparison with zone 1 (RMSE/n = 0,05, 0,17, and 1,61 t C ha^{-1}). In zone 1, there may be an overestimation of the modeled SOC in AFS. Our simulation analyses clearly indicate that a pathway for the reduction of soil CO_2 emissions is possible through a wide-scale adoption of different types of AFS that can optimize soil management factors for increased SOC. Silvopastoral systems (SP) have gained large attention during the last decades due to their SOC accumulation and should be considered to improve Moderately Degraded Pastures (MDP). In zones 3 and 4, the potentially significant negative impacts on soil CO_2 emissions (7 223 and 3 809 t CO_2 eq yr^{-1}, respectively) are due to SOC losses in Intensive Cropland (CL), which account for 30 017 and 6 925 t CO_2 eq yr^{-1}. In this sense, in CL, the reduction of soil CO_2 emissions can generate a large portion of the needed mitigation through the adoption of cropping rotation and soil management practices such as minimal tillage and higher above-crop residues. AFS are important Factor Land Use (FLU) to incentive low-carbon footprint agriculture, as a plan by the Colombian Government to reach its GHG emission reduction targets.

Acknowledgements

This project ID: C01-F01-006-2022 was financed by Direccion General de Investigaciones (DGI) Universidad de los Llanos. The authors would like to thank the Universidad de los Llanos and the Pontificia Universidad Javeriana de Cali. This work has been funded by the Program *ÓMICAS: In-silico Multiscale Optimization of Sustainable Agricultural Crops* (*Infraestructure and Validation in Rice and Sugarcane*), sponsored within the Colombia Scientific Ecosystem, formed by the World Bank, Ministry of Science, Technology, and Innovation (Minciencias), Icetex, The Ministry of Education and The Ministry of Industry and Tourism, Project ID: FP44842-217-2018.

Author contributions

D. Y. G. R., conceived the idea, did the background research, collected the data, developed the workflow, and performed the assessment. *C. L. L.,* and *A. S. P.,* supervised the research and provided critical feedback. *D. Y. G. R.* and *A. S. P.,* led the drafting process and wrote the main part of the manuscript, to which all authors contributed.

Conflicts of interest

The authors declare any type of conflict of interest.

References

Alcaldía de Villavicencio (2012). *Diagnóstico sectorial de suelos*. Alcaldía de Villavicencio, Gobernación del Meta, Villavicencio. https://es.slideshare.net/Skepper63/diagnostico-sectorialsuelo-villavicencio

Anderson-Teixeira, K. J., Wang M. M. H., McGarvey J. C., and LeBauer, D. S. (2016). Carbon dynamics of mature and re-growth tropical forests derived from a pantropical database (TropForC-db). *Global Change Biology, 22*(5), 1690-709. https://doi.org/10.1111/gcb.13226

Behnke, G. D., Zuber, S. M., Pittelkow, C. M., Nafziger, E. D., and Villamil, M. B. (2018). Long-term crop rotation and tillage effects on soil greenhouse gas emissions and crop production in Illinois, USA. *Agricultural Ecosystems and Environment, 261,* 62-70. https://doi.org/10.1016/j.agee.2018.03.007

Cardinael, R., Umulisa, V., Toudert, A., Olivier, A., Bockerl, L., and Bernoux, M. (2018). Revisiting IPCC Tier 1 coefficients for soil organic and biomass carbon storage in agroforestry systems. *Environmental Research Letters, 13,* 124020. https://doi.org/10.1088/1748-9326/aaeb5f

Chambers, A., Lal, R., and Paustian, K. (2016). Soil carbon sequestration potential of US croplands and grasslands: Implementing the 4 per Thousand Initiative. *Journal of Soil and Water Conservation, 71*(3), 68A-74A. https://doi.org/10.2489/jswc.71.3.68A

Department of Agriculture (1996). *Laboratory methods manual, soil survey investigations report No. 42, version 3.0, January 1996*. Department of Agriculture.

FAO (2018). *Measuring and modelling soil carbon stocks and stock changes in livestock production systems – Guidelines for assessment* (*Draft for public review*). Livestock Environmental Assessment and Performance (LEAP) Partnership, FAO.

Feliciano, D., Ledo, A., Hillier, J., and Nayak, D. R. (2018). Which agroforestry options give the greatest soil and above ground car-bon benefits in different world regions?. *Agricultural Ecosystems and Environment, 254*, 117-29. https://doi.org/10.1016/j.agee.2017.11.032

Franzluebbers, A. J. (2005). Soil organic carbon sequestration and agricultural greenhouse gas emissions in the southeastern USA. *Soil Tillage Research, 83*, 120-147. https://doi.org/10.1016/j.still.2005.02.012

Fujisaki, K., Perrin, A. S., Desjardins, T., Bernoux, M., Balbino, L. C. and Brossard, M. (2015). From forest to cropland and pasture systems: a critical review of soil organic carbon stocks changes in Amazonia. *Globlal Change Biology, 21*, 2773-2786. https://doi.org/10.1111/gcb.12906

García, D. Y., Cárdenas, J. F., and Parra, A. (2018). Evaluación de sistemas de labranza sobre propiedades fisicoquímicas y microbiológicas en un Inceptisol. *Revista de Ciencias Agrícolas, 35*(1), 16-25. https://doi.org/0000-0002-2501-4842

Haddaway, N. R., Hedlund, K., Jackson, L. E., Kätterer, T., Lugato, E., Thomsen, I. K., Jørgensen, H. B., and Isber, P.-E. (2017). How does tillage intensity affect soil organic carbon? A systematic review. *Environmental Evidence, 6*, 30. https://doi.org/10.1186/s13750-017-0108-9

Henderson, B. B., Gerber, P. J., Hilinski, T.E., Falcucci, A., Ojima, D.S., Salvatore, M., and Conant, R. T. (2015). Greenhouse gas mitigation potential of the world's grazing lands: modeling soil carbon and nitrogen fluxes of mitigation practices. *Agricultural Ecosystems and Environment, 207*, 91-100. https://doi.org/10.1016/j.agee.2015.03.029

Huai, H., and Hamilton, A. (2009). Characteristics and functions of traditional homegardens: A review. *Frontiers in Biology, 4*, 151-157. https://doi.org/10.1007/s11515-008-0103-1

IPCC (2006). *2006 IPCC guidelines for national greenhouse gas inventories* (*vol. 4: Agriculture, Forestry and Other Land Use*). InterGovernmental Panel on Climate Change.

Jadán, O., Cifuentes, M., Torres, B., Selesi, D., Veintimilla, D., and Günter, S. (2015). Influence of tree cover on diversity, carbon se-questration and productivity of cocoa systems in the Ecuatorian Amazon. *Bois Forestry and Tropic, 325*, 35-47. https://doi.org/10.19182/bft2015.325.a31271

Lal, R. (2018). Digging deeper: A holistic perspective of factors affecting soil organic carbon sequestration in agroecosystems. *Global Change Biology, 24*, 3285-3301. https://doi.org/10.1111/gcb.14054.

Lu, S., Meng, P., Zhang, J., Yin, C., and Sun, S. (2015). Changes in soil organic carbon and total nitrogen in croplands converted to walnut based agroforestry systems and orchards in southeastern Loess Plateau of China. *Environmental Monitoring and Assessment*, 187, 688. https://doi.org/10.1007/s10661-014-4131-9

Ludwig, B., Bergstermann, A., Priesack, E., and Flessa, H. (2011). Modelling of crop yields and N_2O emissions from silty arable soils with different tillage in two long-term experiments. *Soil Tillage Research, 112*, 114-121. https://doi.org/10.1016/j.still.2010.12.005

Mangalassery, S., Dayal, D., Meena, S. L., and Ram, B. (2014). Carbon sequestration in agroforestry and pasture systems in arid northwestern India. *Current Science, 107*, 1290-1293. http://www.jstor.org/stable/24107170

Moriasi, D., Arnold, J., Liew, M. W. V., Bingner, R., Harmel, R., and Veith, T. (2007). Model evaluation guidelines for systematic quantification of accuracy in watershed simulations. *ASABE, 50*, 885-899. https://swat.tamu.edu/media/1312/moriasimodeleval.pdf

Nair, P. K. R. (1985). Classification of agroforestry systems. *Agroforestry Systems, 3*, 97-128. https://doi.org/10.1007/BF00122638

Nair, P. K. R. (2012). Carbon sequestration studies in agroforestry systems: A reality-check. *Agroforestry Systems, 86*, 243-53. https://doi.org/10.1007/s10457-011-9434-z

Nash, J. E., and Sutcliffe, J. V. (1970). River flow forecasting through conceptual models – Part I: A discussion of principles. *Journal of Hydrology, 10*, 282-290. https://doi.org/10.1016/0022-1694(70)90255-6

Nemo, Klumpp, K., Coleman, K., Dondini, M., Goulding, K., Hastings, A., Jones, M.B., Leifeld, J., Osborne, B., Saunders, M., Scott, T., The, Y. A., and Smith, P. 2017. Soil organic carbon (SOC) equilibrium and model initialisation methods: An application to the Rothamsted carbon (RothC) model. *Environmental Modeling and Assessment, 22*, 215-229. https://doi.org/10.1007/s10666-016-9536-0

Novaes, R. M., Pazianotto, R. A., Brandão, M., Alves, B.J., May, A., and Folegatti-Matsuura, M. I. (2017). Estimating 20-year land-use change and derived CO2 emissions associated with crops, pasture and forestry in Brazil and each of its 27 states. *Global Change Biology, 23*(9), 3716-3728. https://doi.org/10.1111/gcb.13708

Nyambo, P., Chiduza, C., and Araya, T. (2020). Carbon input and maize productivity as influenced by tillage, crop rotation, resi-due management and biochar in a semiarid region in South Af-rica. *Agronomy, 10*, 705. https://doi.org/10.3390/agronomy10050705

Ogle, S. M., Conant, R. T., and Paustian, K. (2004). Deriving grass-land management factors for a carbon accounting method developed by the intergovernmental panel on climate change. *Environmental Management, 33*(4), 474-484. https://doi.org/10.1007/s00267-003-9105-6

Ogle, S., Alsaker, C., Baldock, J., Bernoux, M., Breidt F, and McConkey, B. G. *et al*. (2019). Climate and soil characteristics determine where No-Till management can store carbon in soils and mitigate greenhouse gas emissions. *Scientific Reports, 9*, 11665. https://doi.org/10.1038/s41598-019-47861-7

Parra, A. S., De Figueiredo, E. B., and De Bordonal, R. O., Moitinho, M. R., De Bortoli Texeira, D., and La Scala Jr., N. (2019). Greenhouse gas emissions in conversion from extensive pasture to other agricultural systems in the Andean region of Colombia. *Environment, Development and Sustainability, 21*, 249-262. https://doi.org/10.1007/s10668-017-0034-6

Poeplau, C., Don, A., Vesterdal, L., Leifeld, J., Van Wesemael, B., Schumacher, J., and Gensior, A. (2011). Temporal dynamics of soil organic carbon after land-use change in the temperate zone — carbon response functions as a model approach. *Global Change Biology, 17*, 2415-2427. https://doi.org/10.1111/j.1365-2486.2011.02408.x

Popp, A., Calvin, K., Fujimori, S., Havlik, P., Humpenöder, F., Stehfest, E., Bodirsky, B. L., Dietrich J. P., Doelmann, J. C., Gusti, M., Hasegawa, T., Kyle, P., Obersteiner, M., Tabeau, A., Takahashi, K., Valin, H., Waldhoff, S., Weindl, I., Wise, M. ... van Wuuren, D. P. (2017). Land-use futures in the shared socioeconomic pathways. *Global Environmental Change, 42*(1), 331-345. https://doi.org/10.1016/j.gloenvcha.2016.10.002

Silva, A. (2018). Modelación de los stocks de carbono del suelo y las emisiones de dióxido de carbono (GEI) en sistemas productivos de la Altillanura Plana. *Orinoquia, 22*, 158-271. https://doi.org/10.22579/20112629.525

Silva, A., and Orozco, D. (2018). Evaluación de tasas de pérdidas y ganancias de C asociadas a las emisiones y absorciones de CO_2 en sistemas productivos del Ariari. *Bistua: Facultad de Ciencias Básicas, 16*, 124-128. https://doi.org/10.24054/01204211.v1.n1.2018.587

Smith, P., and Smith, J. (2007). *Introduction to environmental modelling*. Oxford University Press. https://assets.cambridge.org/97811075/71693/frontmatter/9781107571693_frontmatter.pdf

Thornton, P., and Herrero, M. (2010). Potential for reduced methane and carbon dioxide emissions from livestock and pasture management in the tropics. *Proceedings of the National Academy of Sciences of the United States of America, 107*, 19667-19672. https://doi.org/10.1073/pnas.0912890107

Van Oijen, M., Bellocchi, G., and Höglind, M. (2018). Effects of climate change on grassland biodiversity and productivity: The need for a diversity of models. *Agronomy, 8*(2), 14. https://doi.org/10.3390/agronomy8020014

Zaro, G. C., Caramori, P. H., Yada Junior, G. M., Sanquetta, C. R., Androcioli Filho, A., Nunes, A. L. P., Prete, C. E. C., Voroney, P. (2020). Carbon sequestration in an agroforestry system of coffee with rubber trees compared to open-grown coffee in southern Brazil. *Agroforestry Systems, 94*, 799-809. https://doi.org/10.1007/s10457-019-00450-z

Research Article/Agricultural Engineering

http://doi.org/10.15446/ing.investig.98945

Modeling Biometric Attributes from Tree Height Using Unmanned Aerial Vehicles (UAV) in Natural Forest Stands

Modelación de atributos biométricos a partir de la altura del árbol usando vehículos aéreos no tripulados (VANT) en rodales de bosques naturales

Gerónimo Quiñonez-Barrazal[1], Marín Pompa-García[2], Eduardo D. Vivar-Vivar[3], José L. Gallardo-Salazar[4], Francisco J. Hernández[5], Felipa de J. Rodríguez-Flores[6], Raúl Solís-Moreno[7], Javier L. Bretado-Velázquez[8] Ricardo D. Valdez-Cepeda[9], and José C. Hernández-Díaz[10]

ABSTRACT

This study estimated biometric attributes of individual trees from the automated measurement of tree height (THUV) by using images from unmanned aerial vehicles (UAVs). An experiment was carried out in a natural forest stand in the north of Mexico by using a DJI P4 multispectral equipment and regression analysis. The results show that total tree height (TH) is successfully estimated from UAV images, as the automated estimation of total height (THUV) reaches a $R^2 = 0,95$ and a RMSE = 0,36 m. Consequently, THUV was statistically reliable to generate allometric equations ($R^2 > 0,57$) regarding the canopy height model (CH), diameter at breast height (DBH), basal diameter (BD), above-ground biomass (AGB), volume (V), and carbon contents (C). It is concluded that the estimation of total height with UAVs is a viable option to improve efficiency in forest inventories. However, increased efforts towards the configuration of modern technologies and statistical algorithms are needed; future research challenges remain, particularly in the densest forests areas.

Keywords: allometric relationships, individual tree variables, unmanned aerial vehicle, DJI Phantom 4 Multispectral

RESUMEN

Este estudio estimó los atributos biométricos de árboles individuales a partir de la altura total estimada automáticamente mediante el uso de imágenes de vehículos aéreos no tripulados (VANT). Se llevó a cabo un experimento en un rodal de bosque natural en el norte de México utilizando un equipo multiespectral DJI P4 y análisis de regresión. Los resultados muestran que la altura total del árbol (TH) se estima con éxito a partir de imágenes de VANT, ya que la estimación automática de la altura total (THUV) alcanza un $R^2 = 0,95$ y un RMSE = 0,36 m. En consecuencia, el THUV fue estadísticamente confiable para generar ecuaciones alométricas ($R^2 > 0,57$) con respecto al modelo de altura del dosel (CH), el diámetro a la altura del pecho (DAP), el diámetro basal (BD), la biomasa superficial (AGB), el volumen (V) y el contenido de carbono (C). Lo que se concluye es que la estimación de altura total con VANT es una opción viable para mejorar la eficiencia en los inventarios forestales. Sin embargo, se requieren más esfuerzos orientados a la configuración de tecnologías modernas y algoritmos estadísticos; persisten los desafíos de la investigación futura, particularmente en las áreas boscosas más densas.

Palabras clave: relaciones alométricas, variables de árboles individuales, vehículos aéreos no tripulados, DJI Phantom 4 Multiespectral

Received: October 10th, 2021
Accepted: May 25th, 2022

[1] PhD in Forest Sciences, Colegio de Postgraduados, México. Affiliation: Researcher in Forest Management and Environmental Services Research Program, Campo Experimental Valle del Guadiana, Instituto Nacional de Investigaciones Forestales, Agrícolas y Pecuarias. Carretera Durango-Mezquital Km. 4.5, Durango, Dgo., 34170, México. E-mail: quinonez.geronimo@inifap.gob.mx

[2] PhD in Natural Resources Management, Universidad Autónoma de Nuevo León, México. Affiliation: Researcher-Professor, Laboratorio de DendroEcología, Facultad de Ciencias Forestales y Ambientales, Universidad Juárez del Estado de Durango. Río Papaloapan y Blvd. Durango s/n, Valle del Sur, Durango, Dgo., 34120, México. E-mail: mpgarcia@ujed.mx

[3] Forest engineer, Universidad Autónoma Chapingo, México. Affiliation: Master's student, Maestría en Geomática Aplicada a Recursos Forestales y Ambientales, Facultad de Ciencias Forestales y Ambientales, Universidad Juárez del Estado de Durango. Río Papaloapan y Blvd. Durango s/n, Valle del Sur, Durango, Dgo., 34120, México. E-mail: 1161194@alumnos.ujed.mx

[4] Master in Geomatics Applied to Forest and Environmental Resources, Universidad Juárez del Estado de Durango, México. Affiliation: Instituto de Investigaciones Agropecuarias y Forestales, Universidad Michoacana de San Nicolás de Hidalgo, México. Gral. Francisco Mujica s/n, Ciudad Universitaria, Morelia, Michoacán, 58030, México. E-mail: luis@qgis.mx

[5] PhD in Plant Science, Oklahoma State University, USA. Affiliation: Researcher-Professor, Instituto Tecnológico de El Salto. Mesa del Tecnológico s/n, Forestal, El Salto, Durango, 34942, México. E-mail: fcojhernan@yahoo.com.mx

[6] PhD in Agricultural and Forestry Sciences, Universidad Juárez del Estado de Durango, México. Affiliation: Researcher-Professor, Ingeniería en Tecnología Ambiental, Universidad Politécnica de Durango. Carretera Durango-México, Km. 9.5, Dolores Hidalgo, Durango, Dgo., 34120, México. E-mail: felipa.rodriguez@unipolidgo.edu.mx

[7] PhD in Natural Resources Management, Universidad Autónoma de Nuevo León, México. Affiliation: Researcher-Professor Facultad de Ciencias Forestales y Ambientales, Universidad Juárez del Estado de Durango. Río Papaloapan y Blvd. Durango s/n, Valle del Sur, Durango, Dgo., 34120, México. E-mail: rsolis@ujed.mx

[8] PhD in Forest Management and Silviculture. University of New Brunswick (Faculty of Forestry), Canada. Affiliation: Researcher-Professor, Facultad de Ciencias Forestales y Ambientales, Universidad Juárez del Estado de Durango. Río Papaloapan y Blvd. Durango s/n, Valle del Sur, Durango, Dgo., 34120, México. E-mail: jmbretado@ujed.mx

[9] PhD in Agricultural Sciences, Universidad Autónoma de Nuevo León, México. Affiliation: Researcher-Professor, Centro Regional Universitario Centro Norte, Universidad Autónoma Chapingo. Cruz del Sur No. 100, Col. Constelación, El Orito, Zacatecas, 98085, México. vacrida@hotmail.com

[10] PhD in Forest Economics, Colorado State University, USA. Affiliation: Researcher-Professor, Instituto de Silvicultura e Industria de la Madera, Universidad Juárez del Estado de Durango. Blvd. Guadiana No. 501, Ciudad Universitaria, Durango, Dgo., 34120, México. E-mail: jciroh@ujed.mx

How to cite: Quiñonez-Barraza, G., Pompa-García, M., Vivar-Vivar, E. D., Gallardo-Salazar, J. L., Hernández, F. J., Rodríguez-Flores, F. J., Solís-Moreno, R., Bretado-Velázquez, J. L., Valdez-Cepeda, R. D., and Hernández-Díaz, J. C. (2023). Modeling biometric attributes from tree height using unmanned aerial vehicles (UAV) in natural forest stands. *Ingeniería e Investigación, 43*(2), e98945. http://doi.org/10.15446/ing.investig.98945

Introduction

Forest inventory methods are subject to constant changes that allow reducing costs and destructive effects while achieving accurate estimations. Conventional methods for biometric estimations are usually derived from destructive sampling, with a subsequent negative impact on the ecosystem. In addition, they use empirical models that require manual measurements, which are costly and inaccurate (Peña *et al*., 2018).

Unmanned aerial vehicle (UAV) technology has great potential as a suitable tool for the scientific community (Brede *et al*., 2019). Its use avoids destructive sampling and excessive time consumption, including high spatial and spectral resolutions. Previous studies in Mexico and other places around the world have used this technology in plantations, where there is a regular arrangement of individual trees (Peña *et al*., 2018; Gallardo-Salazar *et al*., 2021). However, there is limited or no research whatsoever in Mexican natural forest stands because of their structural complexity. UAVs make it possible to obtain digital images with increased spectral and spatial resolutions (Tu *et al*., 2019), and UAV digital color images have been increasingly applied in vegetation analysis due to their advantages (high resolution, high frequency, and easy operation) (Skorobogatov *et al*., 2019). Thus, information from UAV digital color images can be related with some field information for individual trees and stand variables.

It is well known that forest biomass includes the largest carbon sinks in terrestrial ecosystems (Ciais *et al*., 2013; Sinha *et al*., 2015). Even so, traditional estimates of forest inventories based on allometric relationships remain a challenge in forest modeling (Chave *et al*., 2014). For instance, tree height is a typical parameter to quantify the commercial and ecological value of a stand, since it allows calculating the volume, biomass, and carbon contents, besides being an indicator of site quality (Krause *et al*., 2019). However, to the best of our knowledge, in Mexican forests, this variable is still estimated with field techniques based on trigonometric principles, which is time consuming and biased. Particularly, the estimation accuracy usually depends on the technician's experience, with the error that implies over- or underestimating reality in irregular mixed-species and high-density forests.

In northern Mexico, Ejido El Brillante, municipality of Pueblo Nuevo, state of Durango, has a great diversity of species and provides several forest ecosystems services that contribute to forest conservation and the social economy of its inhabitants. Thanks to their constant search for appropriate actions and policies, this Ejido has a sustainable management certification (Figueroa *et al*., 2013). Besides, it has been open to accept and promote modern technologies to refine the knowledge of its forest stands and improve their productivity.

The aim of this study was to assess parameters such as canopy height (CH), diameter at breast height (DBH), basal diameter (BD), above-ground biomass (AGB), volume (V), and carbon contents (C) using estimations via allometric equations, all of them based on the automated valuation of tree height (THUV) measured from UAV images. It was hypothesized that THUV is a statistically reliable predictor of such attributes.

Materials and Methods

Study area and data acquisition

The study area is located inside Ejido El Brillante, in the municipality of Pueblo Nuevo, Durango, Mexico. It is considered to be a site of great ecological, economic, and environmental importance. Its vegetation includes a mixture of pine and oak species with similar ecological preferences. The dominant elements of the vegetation are various species of pine (González *et al*., 2012), like *Pinus cooperi* C.E. Blanco, coexisting with *P. teocote* Schied. Ex Schltdl. and Cham., *P. durangensis* Martínez, *P. leiophylla* Schiede ex Schltdl. and Cham., and *P. strobiformis* Engelm. Figure 1 illustrates the geographical location of the study area.

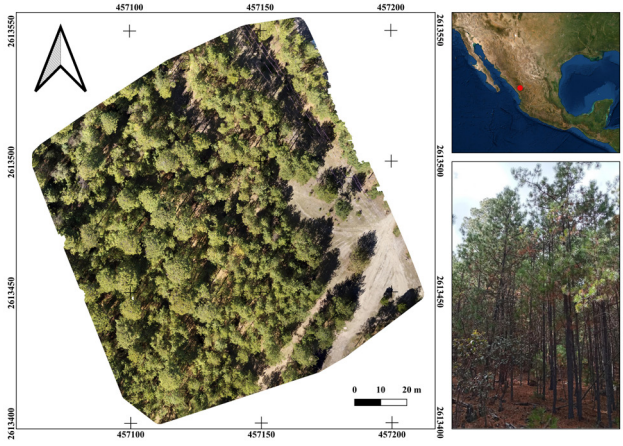

Figure 1. Location of the study area corresponding to Ejido El Brillante in northern Mexico
Source: Authors

In a previously selected forest area, data were collected at ground level over a delimited 100 x 100 m plot. The following variables were recorded for each tree (DBH > 7 cm): diameter at breast height (DBH, cm) and diameter at the base of the tree (DB, cm), measured with a diametric tape; height at the base of the live crown (HLC, m) and total height (TH, m), measured rigorously, mainly telescoped and in some cases involving tree climbing; and the lower tree crown width (CDM, m) and higher tree crown width (CDG, m), taken with measuring tape to calculate the average tree crown area (CA, m^2). The distribution of the measured variables and their relationship with UAV images is represented as a flow chart in Figure 2.

Using DBH as a predictor variable, the above-ground tree volume and biomass were estimated using allometric

equations, which had been previously done by Návar (2009) in the forests of northwestern Mexico. Biomass estimates were transformed into annual carbon accumulation (C), whose content was calculated while assuming a 50% concentration (Rodríguez *et al*., 2016).

A flight was conducted to obtain and compile aerial photographs of the study area, with overlaps between the images and lines of 80 and 75%, respectively. This flight took place on February 21, 2021, which was a sunny day, with favorable wind conditions (<25 kph) and temperatures of 14-25 °C. A DJI Phantom 4 Multispectral (P4M) quadcopter was flown over the study area. The P4M camera has a total of six imaging sensors: five multispectral sensors (*i.e.*, blue, green, red, red-edge, and near-infrared bands) and 1 RGB sensor, all with a 2 MP global shutter. The focal length of the P4M camera is 5,74 mm, the image size is 1600 × 1300 pixels, and the sensor size is 4,87 × 3,96 mm. The flight plan for automatic image collection was programmed with the DJI Ground Station Pro application (www.dji.com/mx/ground-station-pro).

A quadruple grid was established (Figure 3), covering the study area corresponding to 1 ha. The flight height was 70 m above ground level, with an angle of 90° for the first two grids and 70° for the last two grids.

Since the P4M operates under the principle of direct onboard georeferencing, it was not necessary to geo-reference the images; this quadcopter has a Global Positioning System (GPS) that geotags the coordinates of each image taken. Once the images were captured, photogrammetric and computer vision procedures were applied using the free and open-source OpenDroneMap software (ODM, www.opendronemap.org).

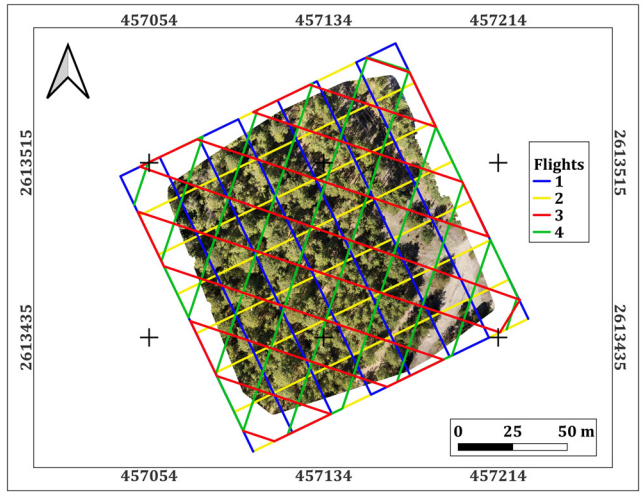

Figure 3. Flight lines in the study area to generate point clouds
Source: Authors

Data processing

For data processing, this study employed a computer with an AMD Ryzen 3900x processor, with 24 cores at 3.8 GHz, an integrated NVidia Quadro p620 quadcore 2 GHz video card, and 32 GB of RAM, running a Linux operating system based on Ubuntu, *i.e.*, Pop!_OS version 22.04 lts.

A photogrammetric procedure was applied to the captured RGB images using ODM. This software uses the modern Structure from Motion (SfM) and Multi-View Stereo (MVS) algorithms, which generates a 3D point cloud of 1 000-20 000 points m^{-2} (Puliti et al., 2020), producing a digital surface model (DSM) and a digital elevation model (DTM), which are in turn used to orthorectify each image and construct an orthomosaic. Finally, the total tree height

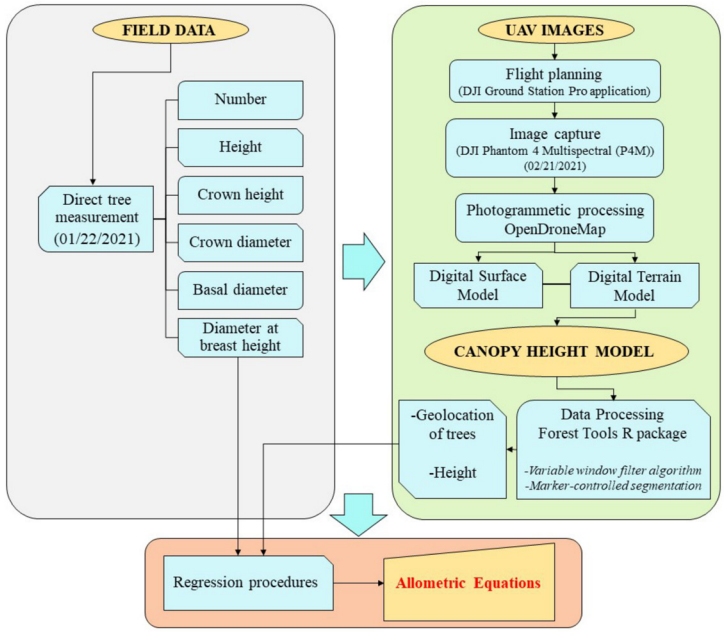

Figure 2. Flow chart of stages of field measurements and unmanned aerial vehicle (UAV) image pre-processing to generate allometric equations
Source: Authors

(canopy height model) was calculated from the elevation difference between DSM and DTM, detecting the top of the trees. This process was performed using the RStudio statistical software (R Core Team, 2020) and applied to the elevation models calculated by two methods (RGB and multispectral images). The P4M operates under the principle of direct onboard georeferencing, so the acquired images were directly georeferenced through GPS capabilities during the course of the flight. It was not necessary to use the real-time-kinematic (RTK) system, since the P4M manufacturer reported that the georeferencing system can reach vertical and horizontal location accuracies of ±0,1 and ±0,3 m, respectively (https://www.dji.com/p4-multispectral/specs).

The ForestTools package of the R statistical software (R Core Team, 2020) allowed calculating the height (H, m) and other parameters useful for modeling individual attributes. The vector and raster files created in R studio were processed in the free and open-source QGIS 3.16.2-Hannover software.

From 30 randomly selected trees, the estimates of the tree-level attributes obtained with the UAV were compared to those rigorously measured in the field. First, all the variables were correlated to identify linear relationships in order to explore statistic correspondences between attributes. Through linear regression procedures, allometric equations were generated (Equation 1); the fulfilment of regression assumptions was verified (Gujarati *et al*., 2012).

The summary description of the variables used in the regression is shown in Table 1, while the correlation matrix for the variables is illustrated in Figure 4.

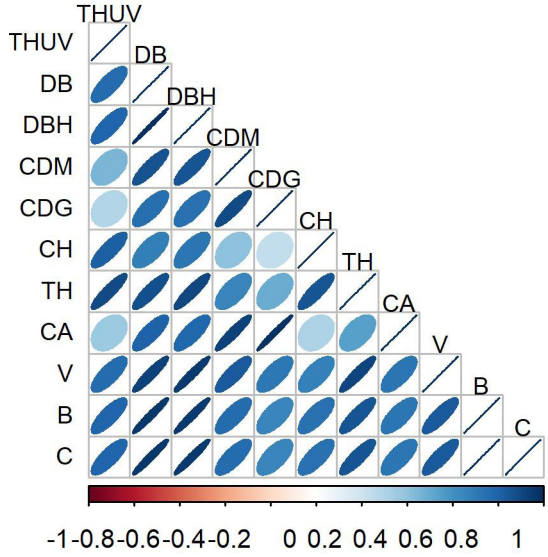

Figure 4. Correlation matrix of studied variables
Note: The highest correlation was observed for THUV—TH relationship (ρ = 0.8979) and poorest for THUV—CDG (ρ = 0.2930). THUV = tree height measured from UAV; DB = diameter at base height (cm); DBH = diameter at breast height (cm); CDM = lower tree crown width (m); CDG = higher tree crown width (m); CH = tree crown height (m); TH = total tree height (m); CA = tree crown area (m^2); V = calculated tree volume (m^3); B = calculated biomass (kg); C = calculated carbon content (kg).
Source: Authors

In order to test the goodness of fit, the determination coefficient (R^2), the root mean square error (RMSE), and Akaikes's information criterion (AIC) were considered as fitting statistics for model classification. Although there are multiple regression approaches (Gujarati *et al*., 2012), a linear regression model (Equation 1) was used to relate the total tree height measured from UAV (THUV) with other individual tree variables.

$$y_i = \beta_0 + \beta_1 x_i + \varepsilon_i \quad (1)$$

where y_i is the dependent variable (THUV) vector; x_i represents the matrix of values of independent variables for the studied relationships (DB, DBH, CDM, CDG, CH, TH, CA, V, B, C); β_i (i = 0,1) is the vector of the intercept and slope parameters; and ε_i represents the error vector [$\varepsilon_i \approx$idd N(μ,σ)].

Table 1. Descriptive statistic for used variables in the correlation and regression analysis

Variable	Statistics					
	Min	1st Qu	Median	Mean	3rd Qu	Max
THUV	5,300	8,945	10,390	11,774	11,960	21,230
DB	15,000	30,500	38,500	41,730	51,000	84,000
DBH	10,000	25,000	30,500	33,270	41,750	68,000
CDM	2,700	5,100	6,600	6,673	8,375	11,300
CDG	2,900	5,925	7,200	7,869	9,050	15,000
CH	2,070	2,925	4,350	6,472	7,275	21,000
TH	8,600	14,320	16,000	16,820	17,980	29,000
CA	6,158	24,683	37,410	46,154	59,107	124,690
V	0,339	1,019	1,163	1,166	1,379	1,780
B	42,580	347,310	547,920	846,9601	124,5103	437,040
C	21,290	173,660	273,960	423,480	562,2501	718,520

Note: THUV = tree height measured from UAV images; DB = diameter at base height (cm); DBH = diameter at breast height (cm); CDM = lower tree crown width (m); CDG = higher tree crown width (m); CH = tree crown height (m); TH = total tree height (m); CA = tree crown area (m^2); V = calculated tree volume (m^3); B = calculated biomass (kg); C = calculated carbon content (kg); Qu = quantile.
Source: Authors

The ten allometric relationships were fitted by lm in RStudio (R Core Team, 2020), and the RMSE, R^2, and AIC fitting statistics were calculated with the residuals of each model.

Results

A total of 479 RGB images were collected and processed to generate the digital elevation model (DEM) and the digital surface model (DSM), whose difference resulted in the canopy model via the ODM algorithm (Figure 5).

Since the height obtained by the UAV (THUV) explains the height measured in the field (R^2 = 95%, RMSE = 0,36 m), this was the explanatory variable that produced the results of Table 2 for the top six relationships (CH-THUV, B-THUV, C-THUV, DBH-THUV, DB-THUV, and V-THUV). The highest accuracy was achieved by the CH-THUV relationship, and the poorest one by the V-THUV relationship. The tree crown

height can also be estimated as a function of the tree height measured from UAV images. This allometric relation had R^2 = 0,6567 and values of 3,166 m and 137,6294 for the RMSE and AIC statistics, respectively. Regarding the top six allometric relations, only for the DBH-THUV and DB-THUV models, the intercept parameters are not significant (equal to zero at a 5% significance level).

According to the fitting statistics, CH is an attribute remarkably well modelled by the THUV, with a 65% of the total variability explained by the model. Furthermore, the THUV acceptably predicted B, C, and V with $R^2 > 0,61$, and DBH and DB with $R^2 > 0,57$. The statistical significance values (Pr(>| t |)) strengthen the assertion (Table 2), indicating a non-random relationship. The linear relationship between the numerical predictors was also verified, where the residuals were randomly distributed around zero, with constant variability along the x-axis. The rest of the variables had no satisfactory models (Figure 6).

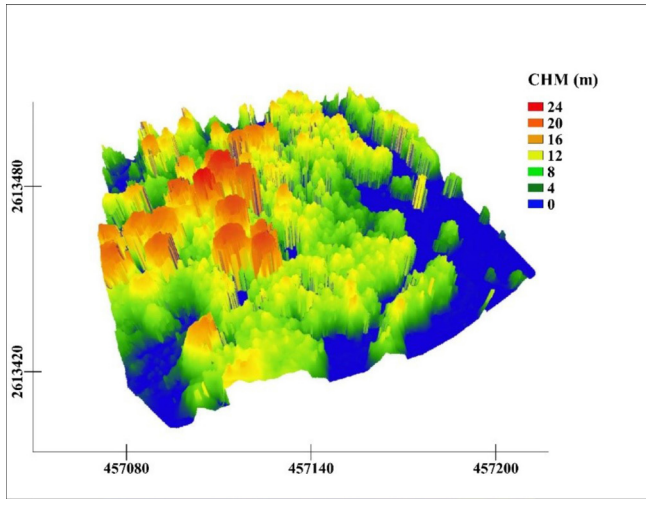

Figure 5. 3D perspective view of the study area based on the canopy height model
Source: Authors

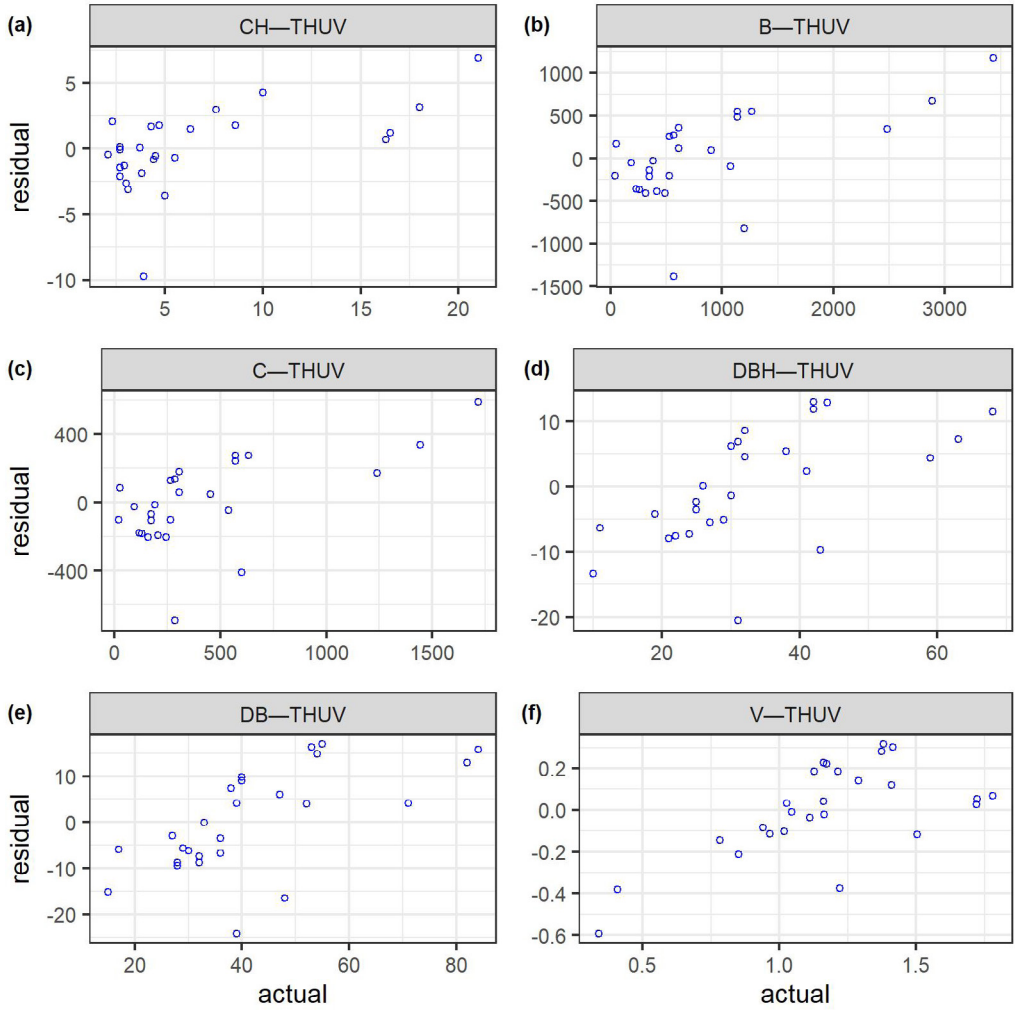

Figure 6. Residuals of the top six relationships
Note: THUV = tree height measured from UAV; CH = tree crown height (m); B = biomass (kg); C = calculated carbon content (kg); DBH = diameter at breast height (cm); DB = diameter at base height (cm); V = tree volume (m^3): (a) CH-THUV relationship; (b) B-THUV relationship; (c) C-THUV relationship; (d) DBH-THUV relationship; (e) DB-THUV relationship; (f) V-THUV relationship.
Source: Authors

Discussion

The findings of our study indicate that tree height is one of the parameters that can be best estimated with UAVs. This result agrees with Krause *et al*. (2019) and Karpina *et al*. (2016). As it is well known, the maximum error allowed for a typical forest management inventory is 10% of the standing volume, considering the entire forest property, which is valid for practical purposes (SEMARNAT, 2006).

Total height estimation becomes relevant because it is rarely subject to precision evaluations, knowing that, in dense forests stands, it is difficult to visually detect this variable from the ground. The occlusion of branches, neighboring trees, and the ruggedness of the relief complicate the inspection of the top of the trees and, consequently, its precise estimation, so it usually depends on the good judgment and experience of the forest technician. Although the aim of this study was not to evaluate the quality of the estimations made by technicians, it is evident that indirect measurements lead to a bias that should be reduced. This error is exacerbated when the data have been obtained by several different technicians, as well as when the forest stands are very dense. Thus, an important limitation is that automated tree height detection was disrupted by the presence of overlapping crowns. Consequently, in the near future, we suggest including more sophisticated sensors to prevent this. Drones can have an important role in forest management, but progress is incremental.

Quantitative analysis during data processing made it clear that the accuracy of the estimations is highly dependent on the density of points to generate the cloud, as previously documented in Krause (2019). Therefore, we recommend increasing the number of flight lines and testing different camera settings according to technical possibilities. It is known that the application of Structure from Motion (SfM) algorithms works by matching equal pairs of points located on overlapping images, and the correct generation of output results depends on the quantity of points in the cloud. For instance, Peña *et al*. (2018) argue that a good quality of the UAV images allows for the easy detection of such points, which could be improved by optimizing the values of image contrast, saturation, and brightness. The correct measurement of height has direct implications in the calculation of volume, biomass, and carbon content, among others, which has a direct impact on decision-making for forest management. From a practical point of view, this strategy allows enhancing the use of individual tree-level attribute measurements, saving time and improving certainty.

For the estimation of CH, DB, DBH, V, B, and C based on height (THUV), it was found that the models explain more than 57% of the variability in the data. It is advisable to perform a stratification of crown size classes because it is well known that dimensions and arrangement of branches play a major role in the estimation of volume (Gallardo-Salazar and Pompa-García, 2020).

These findings can contribute to global efforts to understand the magnitude of carbon contributions to ecosystem dynamics (Dubaya *et al*. 2020). For example, Brede *et al*. (2019) report that global estimates are biased, requiring validation of pilot sites for calibration. Thus, stand datasets such as this one, with high resolution and high heterogeneity, are ideal for this purpose. The ability to acquire information from multispectral remote sensing potentially broadens its application, given the large amount of low-cost data collected in a short period of time. In that sense, our data collection and processing appeared to be efficient (*e.g.*, an experienced team would require 3 to 6 days for a 1,0 ha plot) and to be consistent with similar research (Wilkes *et al*., 2017).

Table 2. Parameter estimates, standard error, and fitting statistics for the studied relationships

Relationship	Parameter	Estimate	SE	t-value	Pr(>¦t¦)	RMSE	R^2	AIC
CH-THUV	α_1	-4,8871	1,7402	-2,808	<0,0001	3,166	0,6567	137,6294
	α_2	0,9647	0,1381	6,987	<0,0001			
B-THUV	α_1	-907,14	288,85	-3,140	0,00443	525,500	0,6227	403,4491
	α_2	148,98	22,92	6,500	<0,0001			
C-THUV	α_1	-453,57	144,43	-3,140	0,00443	262,700	0,6227	367,4054
	α_2	74,49	11,46	6,500	<0,0001			
DBH-THUV	α_1	4,2807	4,8861	0,876	0,3900	8,889	0,6114	191,3136
	α_2	2,4620	0,3877	6,351	<0,0001			
DB-THUV	α_1	7,6251	6,2128	1,227	0,2320	11,300	0,5729	203,8049
	α_2	2,8966	0,4929	5,876	<0,0001			
V-THUV	α_1	0,4849	0,1247	3,889	<0,0001	0,2270	0,5703	0,5616
	α_2	0,0578	0,0098	5,840	<0,0001			

Note: THUV = tree height measured from UAV images; DB = diameter at base height (cm); DBH = diameter at breast height (cm); CH = tree crown height (m); V = tree volume (m^3); B = biomass (kg); C = calculated carbon content (kg). SE = standard error of parameters; RMSE = root mean square error; R^2 = coefficient of determination; AIC= Akaike information criterion.
Source: Authors

The efficient application of these technologies to large forest areas would depend on benefit-cost ratios in the framework of forest management programs. For those interested in replicating these technologies, it is advisable to seek partnerships, with the consequent benefit of generating multipurpose knowledge. For example, the resulting products offered at stand level by the sensors used in this work seem to promise attractive perspectives that should be addressed in future studies (phenology and stand dynamics, among others).

The challenge posed by constructing tree geometry and counting at the individual tree level in the whole forest seems to be a limitation of this study when compared to regular plantations (Tu *et al*., 2019). The cameras of our UAV have limitations, such as low efficiency in closed forest areas due to the relatively poor penetrating capacity of natural light. Consequently, the allometric equations could improve the estimations of forest attributes. However, in future research, tree metrics could be estimated by combining many types of equations and several regressions (Chave *et al*., 2014; Gujarati *et al*., 2012). As shown by the literature (Lin *et al*., 2018; Jones *et al*., 2020), accurate individual tree attributes extraction is improved by choosing tree height as predictor variable. Nevertheless, we recognize that, even though the UAV's image-based total height estimations were very capable predictors, there are still a lot of challenges for better predicting tree attributes. As a complementary strategy, it is advisable to complement the current efforts with different sensors such as terrestrial laser scanning, including a larger sample size with sophisticated remote sensing platforms and other modeling strategies (Brede *et al*., 2019; Gao *et al*., 2021). To the best of our knowledge, this is the first study in Mexico that documents the generation of allometric equations in natural forests upon the basis of UAV images.

Finally, we recognize that, although destructive methods for estimating biomass and carbon content are often reported to be reliable (Karpina *et al*., 2019), our results offer the advantage of being able to make faster and less expensive re-measurements and adjustments depending on stand structure and dynamics. Under a multitemporal perspective, the periodical re-measurement of forest attributes also represents a source of indicators on the response of site productivity to the hydroclimatic variations faced by forests (Pompa-García *et al*., 2021). Thus, our findings, in terms of the use of total height measured using UAVs (THUV), offer a promising future in forest resource management towards precision forestry.

Conclusions

This study reports that height measurements from unmanned aerial vehicles (UAVs) show proficiency in estimating tree measurements in an unevenly aged pine stand. Currently, direct tree height measurement represents a large operational effort. However, it is possible to generate efficient biometric height estimates using UAV images while avoiding destructive sampling. The long times required for individual field estimations are considerably reduced by our methodology. Its extensive implementation depends on the technical and financial possibilities of forest managers, so institutional partnerships are recommended. It was also found that increasing flight missions produce better resolutions, which translates into better possibilities for periodic and permanent monitoring, in order to generate long-term series. Our estimates of biomass, volume, carbon content, and diameters can be calibrated and validated in future studies, which could also support mission estimates on a sort of hectometric-scale.

Despite the promising results, certain limiting factors that merit further research can be highlighted. For instance, a range of models and deep statistical analysis are important, as well as highly technical requirements and trained personnel. It is therefore advisable to test more sophisticated approaches.

Acknowledgements

We would like to thank COCYTED, DendroRed; ITES, FCFyA-UJED, Ejido El Brillante. Furthermore, we are particularly grateful to Jaime de la Cruz Alemán, Roxana Meza Aragón, Manuel Delgado Ávila, Martin Delgado, Minhoru Meza Aragón, Daniel Rocha Rodríguez, Jesús Soto García, Basilio Lugo Camacho, Jesús Andrés Rosales Hernández, Heriberto Aragón Guevara, Ever Alfredo Flores Delgado, Yordy Arath Adame Villanueva, and Ramiro Martínez Acosta.

Funding

The Science and Technology Council of the State of Durango (COCYTED) and Mexican National Science and Technology Council (CONACYT) projects (A1-S-21471) have funded this research.

CRediT author statement

Conceptualization and experimental design, MP-G; software, EDV-V and JLG-S; field data gathering, EDV-V, FJH, and JBV; formal analysis, GQ-B and MP-G; investigation, FJR-F and JCH-D; resources, FJR-F and RS-M; writing (original draft), MP-G and GQ-B; writing (review and editing), RDV-C, JCH-D, MP-G, FJH, EDV-V, JLG-S, RS-M, and FJR-F; project administration, MP-G; funding acquisition, MP-G, FJR-F, and JB-V. All authors contributed to writing the manuscript and approved its definitive version for publication.

Conflicts of interest

The authors declare no conflict of interest.

References

Brede, B., Calders, K., Lau, A., Raumonen, P., Bartholomeus, H. M., Herold, and M., Kooistra, L. (2019). Non-destructive tree volume estimation through quantitative structure modelling: Comparing UAV laser scanning with terrestrial LIDAR. *Remote Sensing of Environment, 233*, 111355. https://doi.org/10.1016/j.rse.2019.111355

Chave, J., Rejou-Mechain, M., Burquez, A., Chidumayo, E., Colgan, M. S., Delitti, W. B. C., Duque, A., Eid, T., Fearnside, P. M., Goodman, R. C., Henry, M., Martinez-Yrizar, A., Mugasha, W. A., Muller-Landau, H. C., Mencuccini, M., Nelson, B. W., Ngomanda, A., Nogueira, E. M., Ortiz-Malavassi, E., ... Vieilledent, G. (2014). Improved allometric models to estimate the aboveground biomass of tropical trees. *Global Change Biology, 20*(10), 3177-3190. https://doi.org/10.1111/gcb.12629

Ciais, P., Sabine, C., Bala, G., Bopp. L., Brovkin, V., Canadell, J., Chhabra, A., DeFries, R., Galloway, J., and Heimann, M. (2013). Carbon and other biogeochemical cycles. In IPCC (Eds.), *Climate Change 2013: The Physical Science Basis*. (pp. 465-570). Cambridge University Press.

Dubayah, R., Blair, J. B., Goetz, S., Fatoyinbo, L., Hansen, M., Healey, S., Hoffton, M., Hurtt, G., Kellner, J., Luthcke, S., Armston, J., Tang, H., Duncanson, L., Hancock, S., Jantz, P., Marselis, S.,Patterson, P. L, Qi, W., and Silva, C. (2020). The global ecosystem dynamics investigation: High-resolution laser ranging of the Earth's forests and topography. *Science of Remote Sensing*, *1*, 100002.

Figueroa, E. G., Arrieta, D. D, Moreno, L. H., González, H. M., and Monsiváis, B. M. (2013). La percepción del clima organizacional en el personal de producción de un ejido forestal en México. *Revista Global de Negocios, 1*(2), 81-89. https://ssrn.com/abstract=2327258

Gallardo-Salazar, J. L., Carrillo-Aguilar, D. M., Pompa-García, M., and Aguirre, S. C. (2021). Multispectral indices and individual-tree level attributes explain forest productivity in a pine clonal or-chard of Northern Mexico. *Geocarto International, 37*(15), 441-4453. https://doi.org/10.1080/10106049.2021.1886341

Gallardo-Salazar, J. L., and Pompa-García, M. (2020). Detecting individual tree attributes and multispectral indices using unmanned aerial vehicles: Applications in a Pine clonal orchard. *Remote Sensing, 12*(24), 4144. https://doi.org/10.3390/rs12244144

Gao, Y., Quevedo, A., Szantoi, Z., and Skutsch, M. (2021). Monitoring forest disturbance using time-series MODIS NDVI in Michoacán, Mexico. *Geocarto International, 36*(15), 1768-1784. https://doi.org/10.1080/10106049.2019.1661032

González-Elizondo, M. S., González-Elizondo, M., Tena-Flores, J. A., Ruacho-González, L., and López-Enríquez, I. L. (2012). Vegetación de la Sierra Madre Occidental, México: una síntesis. *Acta Botanica Mexicana, 100*, 351-403. https://doi.org/10.21829/abm100.2012.40

Gujarati, D. N., Porter, D. C., and Gunasekar, S. (2012). *Basic econometrics*. Tata McGraw-Hill Education.

Jones, A. R., Raja Segaran, R., Clarke, K. D., Waycott, M., Goh, W. S., and Gillanders, B. M. (2020). Estimating mangrove tree biomass and carbon content: A comparison of forest inventory techniques and drone imagery. *Frontiers in Marine Science, 6*, 784. https://doi.org/10.3389/fmars.2019.00784

Karpina, M., Jarząbek-Rychard, M., Tymków, P., and Borkowski, A. (2016). UAV-Based automatic tree growth measurement for biomass estimation. *The International Archives of the Photogrammetry, Remote Sensing and Spatial Information Sciences, XLI-B8*, 685-688. https://doi.org/10.5194/isprsarchives-XLI-B8-685-2016

Krause, S., Sanders, T. G. M., Mund, J. P., and Greve, K. (2019). UAV-Based photogrammetric tree height measurement for intensive forest monitoring. *Remote Sensing 11*(7), 758. https://doi.org/10.3390/rs11070758

Lin, J., Wang, M., Ma, M., and Lin, Y. (2018). Aboveground Tree Biomass Estimation of Sparse Subalpine Coniferous Forest with UAV Oblique Photography. *Remote Sensing 10*(11), 1849. https://doi.org/10.3390/rs10111849

Návar J. (2009). Allometric equations for tree species and carbon stocks for forests of northwestern Mexico. *Forest Ecology and Management, 257*(2), 427-434. https://doi.org/10.1016/j.foreco.2008.09.028

Peña, J., M, Castro, A. D., Torres-Sánchez, J., Andújar, D., San Martín, C., Dorado, J., Fernández-Quintanilla, C., and López-Granados, F. (2018). Estimating tree height and biomass of a poplar plantation with image-based UAV technology. *AIMS Agriculture and Food, 3*(3), 313-326. https://doi.org/10.3934/agrfood.2018.3.313

Pompa-García, M., Camarero, J. J., Colangelo, M., and Gallardo-Salazar, J. L. (2021). Xylogenesis is uncoupled from forest productivity, *Trees, 35*, 1123-1134. https://doi.org/10.1007/s00468-021-02102-1

Rodríguez-Veiga, P., Saatchi, S., Tansey, K., and Balzter, H. (2016). Magnitude, spatial distribution and uncertainty of forest biomass stocks in Mexico. *Remote Sensing of Environment, 183*, 265-281. https://doi.org/10.1016/j.rse.2016.06.004

SEMARNAT (2006). *Norma Oficial Mexicana. NOM-152-SEMARNAT-2006: Que establece los lineamientos, criterios y especificaciones de los contenidos de los programas de manejo para el aprovechamiento de recursos forestales maderables en bosques, selvas y vegetación de zonas*. http://www.diariooficial.gob.mx/nota_detalle.php?codigo=5064731&fecha=17/10/2008

Skorobogatov, G., Barrado, C., and Salami, E. (2019). Multiple UAV systems: A survey. *Unmanned Systems, 8*(2), 149-169. https://doi.org/10.1142/s2301385020500090

Sinha, S., Jeganathan, C., Sharma, L. K., and Nathawat, M. S. (2015). A review of radar remote sensing for biomass estimation. *International Journal of Environmental Science and Technology, 12*, 1779-1792. https://doi.org/10.1007/s13762-015-0750-0

R Core Team (2020). *Language and environment for statistical computing*. R Foundation for Statistical Computing. https://www.R-project.org/

Tu, Y. H., Johansen, K., Phinn, S., and Robson, A. (2019). Measuring canopy structure and condition using multi-spectral UAS imagery in a horticultural environment. *Remote Sensing, 11*(3), 269. https://doi.org/10.3390/rs11030269

Wilkes, P., Lau, A., Disney, M., Calders, K., Burt, A., Gonzalez de, T. J., Bartholomeus, H., Brede, B., and Herold, M. (2017). Data acquisition considerations for Terrestrial Laser Scanning of forest plots. *Remote Sensing of Environment, 196*, 140-153. https://doi.org/10.1016/j.rse.2017.04.030

Research Article/Chemical, Food, and Environmental Engineering https://doi.org/10.15446/ing.investig.100834

Evaluation of Potential Substrates for Biogas Production in Colombia using Anaerobic Digestion Systems

Evaluación de sustratos potenciales para la producción de biogás en Colombia utilizando sistemas de digestión anaerobia

Aura A. Ramón[1], Juan E. Vásquez[2], Juan M. Delgado[3], Daniel Domínguez-Carvajal[4], Ana M. Mosquera-Mena[5], Francisco Molina[6], and Mariana Peñuela-Vásquez[7]

ABSTRACT

Increasing energy demands around the globe require alternative sources of energy. Considering the large amount of agro-industrial and agriculture-related activities in Colombia, energy generation from biomass waste is a promising option to meet the energy needs of the country. Anaerobic digestion (AD) is a good alternative to use these wastes. In this study, several potential substrates for biogas generation using AD systems were identified through a literature review. Vinasses, palm oil industry residues, swine manure, coffee industry residues, and municipal solid wastes were found as potential substrates for AD. Considering factors such as composition, the amount of waste production, availability, and their relationship with important Colombian economic activities, three substrates were selected to perform biochemical methane potential (BMP) experiments. The selected substrates were swine manure (SM), palm oil mill effluent (POME), and coffee residues (CR). The obtained BMP values were 240, 465, and 314 $NmLCH_4/g$ VS, respectively. An analysis of kinetic parameters analysis was conducted for the BMP experiments, based on the logistic and Gompertz models. It was seen that the AD of SM starts faster than in the other evaluated substrates. Nevertheless, the overall methane production rate was the highest for POME, followed by CR. SM had the lowest methane production yield. The obtained values of BMP, kinetic parameters, and those collected during the literature review can be useful for the design and implementation of AD systems in Colombia. Moreover, attention should be paid to substrates such as POME, which have a high energy production potential.

Keywords: anaerobic digestion, biogas, biochemical methane potential, wastes

RESUMEN

El aumento de la demanda de energía en el mundo hace necesaria la búsqueda de fuentes alternativas de energía. Considerando la amplia actividad agroindustrial y agropecuaria en Colombia, la generación de energía a partir de residuos de biomasa es una opción promisoria para satisfacer las necesidades energéticas del país. La digestión anaerobia (DA) es una buena alternativa para aprovechar estos residuos. En este estudio se identificaron varios sustratos potenciales para la generación de biogás utilizando sistemas de DA a través de una revisión de la literatura. Las vinazas, los residuos de la industria del aceite de palma, el estiércol porcino, los residuos de la industria del café y los desechos sólidos municipales se consideraron como sustratos potenciales para la DA. Considerando factores como la composición, la cantidad de residuos producidos, la disponibilidad y su relación con importantes actividades económicas colombianas, se seleccionaron tres sustratos para realizar experimentos de potencial bioquímico de metano (BMP). Los sustratos seleccionados fueron estiércol porcino (SM), efluente de la industria de aceite de palma (POME) y residuos de café (CR). Los valores de BMP obtenidos fueron 240, 465 y 314 y $NmLCH_4/g$ SV respectivamente. Se realizó un análisis de parámetros cinéticos para los experimentos de BMP con base en los modelos logístico y de Gompertz. Se vio que la digestión anaerobia de SM inicia más rápido que en los otros sustratos evaluados. Sin embargo, la tasa de producción de metano fue más alta para POME, seguida por CR. SM tuvo la tasa más baja de producción de metano. Los valores obtenidos de BMP, parámetros cinéticos y los recolectados durante la revisión de la literatura pueden ser de utilidad para el diseño e implementación de sistemas AD en Colombia. Aún más, debe prestarse atención a los sustratos como POME, que presentan un alto potencial de producción de energía.

Palabras clave: digestión anaerobia, biogás, potencial bioquímico de metano, residuos

Received: February 2nd, 2022
Accepted: October 19th, 2022

[1] Chemical engineer, Universidad Industrial de Santander, Colombia. PhD-c in Biotechnology, Universidad de Antioquia, Colombia. Affiliation: PhD student, Universidad de Antioquia, Colombia. Email: aura.ramonv@udea.edu.co

[2] Biological engineer, Universidad Nacional de Colombia, Colombia. Msc in Biotechnology, Universidad de Antioquia, Colombia. PhD, Tokyo Institute of Technology, Japan. Affiliation: Researcher, Universidad de Antioquia, Colombia. Email: juan.vasquezb@udea.edu.co

[3] Food engineer, Universidad de Antioquia, Colombia. PhD-c in Biotehcnology, Universidad de Antioquia, Colombia. Affiliation: Researcher, Bioprocess Research Group, Universidad de Antioquia, Colombia. Email: martin.delgado@udea.edu.co

[4] Chemical Engineering student, Universidad de Antioquia, Colombia. Affiliation: Student, Universidad de Antioquia, Colombia. Email: daniel.dominguezc@udea.edu.co

[5] Chemical engineer, Universidad de Antioquia, Colombia. Affiliation: Researcher, Bioprocess Research Group, Universidad de Antioquia, Colombia. Email: amarcela.mosquera@udea.edu.co

[6] Sanitary engineer, Universidad de Antioquia, Colombia. MSc in Sanitary Engineering, Universidad del Valle, Colombia. PhD in Chemical and Environmental Engineering, Universidad Santiago de Compostela, España. Affiliation: Full professor, Universidad de Antioquia, Colombia. Email: francisco.molina@udea.edu.co

[7] Chemical engineer, Universidad de Antioquia, Colombia. MSc in Chemical and Biochemical Process Technology, Universidade Federal do Rio de Janeiro, Brasil. PhD in Chemical and Biochemical Process Technology, Universidade Federal do Rio de Janeiro, Brasil. Affiliation: Full professor, Universidad de Antioquia, Colombia. Email: mariana.penuela@udea.edu.co

How to cite: Ramón, A., Vásquez, J., Delgado, J., Domínguez, D., Mosquera, A., Molina, F. and Peñuela, M. (2023). Evaluation of Potential Substrates for Biogas Production in Colombia using Anaerobic Digestion Systems. *Ingeniería e Investigación, 43*(2), e100834. https://doi.org/10.15446/ing.investig.100834

Introduction

In recent decades, global energy consumption has had a progressive increase (British Petroleum Company, 2020). The current world energy demand, added to the depletion of fossil fuels, has aroused the scientific community's interest in conducting research for the development and subsequent use of new, complementary energy sources. Attention has been focused on renewable energies such as biofuels, solar, wind, hydroelectric, biomass, among others, which are more environmentally friendly (REN21, 2020). One of the alternatives to meet the future energy demands lies in the use of residual biomass, given that its use as an energy source can also provide a solution to the issues regarding its final disposal. Among the different methodologies for the use of the organic substrates contained in residual biomass, anaerobic digestion (AD) has emerged as one of the most appealing options in recent years.

AD is a biochemical process in which organic matter is decomposed by the action of different microorganisms in the absence of oxygen, thus producing biogas and a liquid effluent known as *digestate*. Biogas is a gaseous mixture composed mainly of methane (55-65%), carbon dioxide (35-45%), and some small amounts of ammonia and other gasses (Uddin *et al*., 2019). The AD process involves four successive types of reaction: hydrolysis, acidogenesis, acetogenesis, and methanogenesis. These reactions are performed by different bacterial groups working together as a consortium. The process is mainly divided into two stages: in the first stage, complex organic compounds are degraded to Volatile Fatty Acids (VFA), H_2, and CO_2 through hydrolysis, acidogenesis, and acetogenesis reactions; in the second stage, VFAs are transformed into CH_4 and CO_2 through methanogenesis reactions (Wong *et al*., 2013).

At a global level, AD is a technology with broad development and high industrial application, with an estimate of more than 100 000 anaerobic digestion plants with the capacity to produce electrical energy around the world, as well as about 50 million micro-scale biodigesters located mainly in rural areas of China and India (Jain *et al*., 2019; Linville *et al*., 2015; Wu *et al*., 2019). In Colombia, the industrial application of this technology has been relatively low, and the number of anaerobic digestion plants currently operating in the country is uncertain. However, different projects have been known to take advantage of this technology in sectors such as the swine and poultry industry, the palm-growing industry, companies in the dairy sector, and some plants dedicated to the production of beer (Velásquez *et al*., 2018). Some institutions in Colombia carry out different activities aimed at encouraging the use of AD systems for utilizing waste. Among them, it is worth highlighting the association of the national pig farming fund (PORKCOLOMBIA), the mining and energy planning unit (UPME), and the Colombian network of biodigesters (REDBIOCOL).

Regarding research on AD processes, Figure 1 shows the number of articles published on different topics regarding AD in Colombia and the world as of December 2021, according to the Web of Knowledge database. While there is an evident and rapid growth in the volume of research on this topic around the world in the last decade, in Colombia, increasing research on this topic has just recently made itself evident (*i.e.*, since 2018). Considering the extensive agro-industrial and livestock activity in Colombia, the use of organic waste in these activities in the form of AD systems represents a great potential to obtain energy and other interesting by-products of the AD process. It is therefore necessary to carry out more and better research to generate knowledge and technologies adaptable to the needs of the country, as well as to expand the practical applications of AD. This should include a general assessment of the potential use of different organic wastes generated in the country as substrates for biogas production.

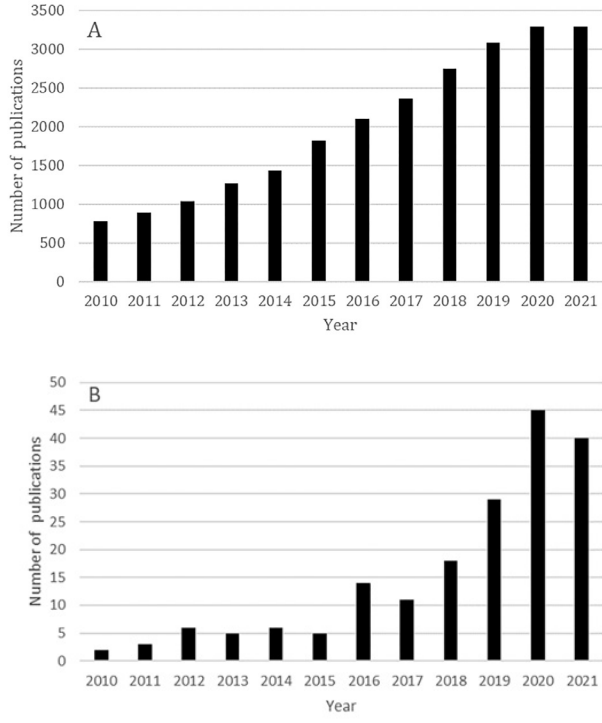

Figure 1. Number of scientific articles published annually in indexed journals on topics of anaerobic digestion by research carried out in the world (a) and in Colombia (b)
Source: Web of Knowledge

Some research carried out in the country on this topic has focused on exploring and identifying different substrates that could be used in AD systems. Rincón *et al*. (2018) carried out a study in order to identify the different types of residual biomass available for the generation of biogas in Colombia and theoretically estimate their energy and biogas production potential. To this effect, they relied on the *Biomass Atlas of Colombia*, on information from the Colombian Agricultural Institute, and on data from the sectoral associations. Residual biomass from the agricultural, livestock, and urban sectors was identified. The energy potential was determined using the amount of organic matter contained in the biomass, the lower heating value of methane, and the concentration of methane in the biogas generated by each residual biomass.

According to the results, the cattle sector has the highest potential, with more than 70 000 TJ/year. However, according to availability and feasibility criteria in terms of ease of collection, quantity of supply, other possible uses, and transportation, the exploitable potential was higher for the Panela production sector, with 22 660 TJ/year at the national level.

Velásquez *et al*. (2018) studied the potential of biomass conversion to biogas in Colombia in a joint project involving Universidad Nacional de Colombia and UPME. This study presents the identification of different types of residual biomass available in the country for the generation of biogas, and it estimates the potential of biogas production from some of these sources. The study included the economic analysis for the possible establishment of AD projects in light of the theoretically estimated potential. Among the results reported in this work, several promising biomasses were identified in different sectors. In the livestock sector, biomasses from pig, bovine, and poultry waste are mentioned. The study concludes that, in general, the use of these biomasses for the production of biogas seems favorable. It also presents few data on BMP measurements, but these are not presented in detail, and the experimental results are not largely discussed.

Amado *et al*. (2021) simulated the AD of three different residual biomasses using the ADM1 model, in order to evaluate the energy recovery potential in Colombia from those substrates. The study included validation with experimental data obtained from batch AD processes with the three substrates. According to this work, the energy recovery potential from coffee mucilage, cocoa mucilage, and Swine manure in Colombia is about 155,1 Ktoe. The local availability of these three biomasses was identified as the most influential parameter to estimate the potential recovery from the substrates. Moreover, Gutiérrez *et al*. (2020) carried out an extensive literature review to create an inventory of available biomass residues with potential application as energy sources, including their use in AD. Several wastes were summarized, including different agricultural and agro-industrial wastes, waste from crops, and livestock waste. The combined bioenergy potential of these residues was calculated to be 216 000 to 432 000 TJ per year.

On a different approach, Mosquera *et al*. (2020) developed a statistical model to evaluate the anaerobic co-digestion potential of several biomass sources commonly found in Colombia. BMP assays for different combinations of the substrates were performed. They found that the best co-digestion occurs when mixing residues from the bottled fruit drinks industry and the organic fraction of municipal solid waste, reaching a BMP value of 382,17 mL CH_4/g VS.

The aforementioned studies have mainly focused on identifying potential substrates for AD in Colombia and evaluating their theoretical potential for energy production. Only in a few cases, limited experimental data have been shared regarding the AD process of the considered substrates. This kind of empirical information is important for the design and implementation of AD systems, and more detailed data on the methane production from potential substrates in the country is needed to stimulate biogas production technologies in Colombia.

The objective of this study was to compare the different potential substrates for biogas production in Colombia using different criteria based on an extensive literature review, as well as to select the most promising substrates to experimentally evaluate their methanogenic potential and kinetic parameters within the AD process.

Materials and methods

Substrate evaluation

The selection of potential substrates for biogas production was performed through a literature review, considering different criteria such as the annual national production of each waste and its availability, the adequacy of the biomass or the pretreatment requirement for its use in the anaerobic digestion process, and the values reported for physicochemical factors associated with the process, *i.e.*, the methanogenic potential, the organic matter content represented by the amount of volatile solids, and the presence of nutrients such as carbon and nitrogen, with an optimal carbon-nitrogen ratio (C /N) from 20 to 30, which is essential for the growth of microbial communities (Rivas *et al*., 2016; Lohani *et al*., 2018). Then, the ones considered to be substrates with the most interesting features for AD and biogas production in Colombia were characterized, and their methanogenic potential was experimentally evaluated.

Substrate selection and physicochemical characterization

Following the literature review, different substrates were selected for the BMP tests. In order to characterize the selected substrates evaluated in this work, experimental measurements of different physicochemical parameters were carried out. These parameters were pH, percentage of humidity, chemical oxygen demand (COD), total solids (TS), and volatile solids (VS). All measurements were carried out following the standard methods of the American Public Health Association (APHA, 2019).

Methanogenic potential (BMP) of selected substrates

For the evaluation of the methanogenic potential, an automated volumetric method was implemented using the AMPTS II – Light equipment developed by Bioprocess Control (BPC). Testing was carried out in triplicate in batch assays at different times, within reactors with a working volume of 2 L and a headspace of 300 mL. The assays were run under mesophilic conditions at 35°C for 30 days. The inoculum used for the experiments was obtained from the biodigester of the San Fernando wastewater treatment plant,

located in Medellín, Colombia. An inoculum to substrate ratio in terms of volatile solids content of 2 was employed. The vessels were gassed with pure N_2 for 1 minute in order to ensure anaerobic conditions. All reactors were mechanically stirred at 60 RPM in cycles (each cycle consisted of 10 minutes with mixing and 10 minutes without mixing). The biogas produced in each vial passed through a vessel containing an alkaline solution of 1 M NaOH, allowing only CH_4 to pass through the gas flow in-line measuring device. Finally, data on methane volume production were collected from the equipment. The volume data was normalized at a temperature of 0°C and a pressure of 1 atm.

Determination of kinetic parameters

To evaluate and compare the degradation kinetics of the different substrates in the BMP tests, two different equations were used, corresponding to models widely used in anaerobic digestion processes. Equation (1) represents the calculation of accumulated methane produced (B) by the logistic model.

$$B = \frac{K}{1 + e^{\left(\frac{4r(\delta - t)}{K} + 2\right)}} \quad (1)$$

$$B = K * e^{-e^{\left(\frac{(r*e)}{K}(\delta - t) + 1\right)}} \quad (2)$$

In the above Equations, K represents the maximum methane production, **δ** represents the lag phase, r represents the maximum methane production rate, and t represents time. To find the values of the kinetic parameters, an optimization was carried out using Excel's Solver tool in order to minimize the square error between the experimentally measured methane production and the methane production calculated with the models.

Results and discussion

Considered substrates

For the literature review, national published documents were taken into account, such as the Biomass Atlas of Colombia, information on the elaboration of the productive censuses of the Colombian Agricultural Institute (ICA). In addition, a search was carried out (in academic databases such as Dialnet, Scielo, and Redalyc, among others) of recent publications, using the name of the substrate, anaerobic digestion, or biogas as a keywords in their title.

The information found allowed collecting relevant data to compare the potential use in AD systems of substrates such as vinasse, coffee residues (CR), palm oil wastewater (POME, rachis and almond), pig slurry (SM), and urban solid waste (RSU). Other wastes that have been mentioned as possible substrates by other studies for the AD process in Colombia were excluded here because there was not enough information to make a comparison according to the criteria mentioned in the *Materials and methods* section. 1

Appendices 1 and 2, summarize the information on the selection criteria and the main characteristics of the substrates reviewed. Some details of the considered substrates are described in this section.

Vinasse

Vinasse stems from the industrial process of obtaining ethanol as fuel. Specifically, vinasse is a residual effluent from the distillation stage that allows obtaining a purer alcohol (Durán *et al*., 2015; Fedebiocombustibles 2020).

Currently, the National Federation of Biofuels of Colombia (Fedebiocombustibles) reports seven production plants of ethanol fuel produced from sugar cane, which in turn are the largest producers of stillage in the country. These plants are located in Valle del Cauca, Meta, and Risaralda. The joint ethanol production of these facilities reached 2 150 000 L/d in 2019 (Fedebiocombustibles, 2020; Asocaña, 2019). It is estimated that the amount of vinasse produced per liter of ethanol is between 0,8 and 3 L. However, the information provided by ethanol producing companies shows that the amount of stillage obtained in the process is between 7 and 14 L of stillage/L of ethanol, depending on whether the distillation is carried out with or without recycling (Asocaña, 2019, Rincón, 2018).

Generally, the alternative use of vinasse is low. One of the most studied ones is the use of vinasse as a fertilizer due to its high content of phosphorus, nitrogen, and potassium. Other uses that are given to vinasse include dehydration and subsequent composting or incineration (Asocaña, 2019). In general, these alternative uses are attempts to give a better disposition to the vinasse. In this sense, almost all of the vinasse produced is available for use in other processes such as AD. The availability of vinasse for its use in other processes such as AD is almost full. It should be taken into account, however, that the use of vinasse in this process usually requires its pretreatment by means of an ozone process to reduce the phenols that it contains and can be inhibitory for microorganisms producing biogas (Durán *et al*., 2015).

Coffee residues (mucilage and pulp)

Coffee pulp is obtained through the pulping process, which consists of removing the pulp around the coffee fruit. As the coffee cherry passes through a rotating drum, the coffee is brought to a point where the pressure exerted separates the pulp from the fruit, given the slime or mucilage contained in ripe coffee. Coffee pulp accounts for about 42% of the mass of the coffee cherry on a wet basis.

Mucilage is a gelatinous film that that is exposed when the coffee fruit is pulped. It is characterized by a strong water retention capacity. In Colombia, coffee mucilage is

removed from the pulp by natural fermentation (12 to 18 hours), mechanical means, and the addition of enzymes (Moreno and Jiménez, 2016). Coffee mucilage represents approximately 15% of cherry coffee on a wet basis.

The coffee industry, one of the most important in the country, reported a production of 13,8 million bags of coffee in the 2017-2018 period, according to the National Federation of Coffee Growers (Moreno and Jiménez, 2016). This high activity of the coffee industry generates large amounts of pulp and mucilage, close to 2,25 and 0,76 tons/year * ha, respectively (Rodríguez and Zambrano, 2010). The high production of these wastes and their high sugar content make them potential substrates for the production of biogas via AD.

Mucilage and coffee pulp have several alternative uses. Among them are the production of ethanol and its use in vermicomposting processes. It has also been tested as a raw material for the production of coffee mucilage concentrates, thanks to the fact that it contains high concentrations of fructose, glucose, pectin, chlorogenic acid, and polyphenols that contribute to health and well-being (Moreno and Jiménez, 2016; Rodríguez and Zambrano, 2010). Some pretreatments that may be required by coffee mucilage before its use in anaerobic digestion processes include leaching processes and pH adjustments. The pulp may also require pH adjustments or the mechanical reduction of particle sizes.

Palm oil industry residues

In Colombia, palm cultivation has spread throughout the territory, reaching 480 000 ha in 2020, making the country the first palm oil producer in America and the fourth in the world (Fedepalma, 2021). During the palm oil extraction process, a large amount of waste is generated, such as fibers (12%), palm kernels or shells (5%), empty fruit clusters or rachis (23%), and wastewater from each cluster of processed fresh fruit (Saelor *et al*., 2017).

Palm oil mill effuent (*POME*): is a combination of effluents from cluster sterilization condensate (36%), clarification wastewater (60%), and hydrocyclone wastewater (4%) (Ahmed *et al*., 2015). POME is a concentrated brownish acidic liquid with a pH in the range of 3,5 to 5,0. It is discharged at a temperature of 80-90 °C and is characterized by a high chemical oxygen demand. It is estimated that, for each ton of processed fresh fruit bunch, 0,5 to 0,7 m^3 of POME are produced (Suksong *et al*., 2017).

The use of POME as a feedstock for biogas production has been applied on an industrial scale in the countries with the highest palm oil production, *i.e.*, Malaysia and Indonesia. The conversion of POME to biogas provides different benefits such as reducing waste contamination parameters such as organic solids, microbial pathogens, and toxicity. Under mesophilic conditions, it is estimated that 28 m^3 of biogas can be produced from 1 m^3 of POME (Shakib *et al*., 2019).

In Colombia, Nabarlatz *et al*. (2012) conducted a study with the purpose of evaluating the production of methane using POME and sludge and pig manure as inoculum. The maximum accumulated methane production was 2 740 mL (343 mL CH_4/g VS). Currently, at the national level, there are nine palm oil beneficiation plants that have a system of lined anaerobic lagoons in order to capture methane and reduce the generation of greenhouse gasses. Three of those companies have developed cogeneration projects implementing biodigesters for the use of methane gas from POME, generating approximately 8 MW of clean energy per year and selling surplus energy to the external network (Fedepalma, 2020).

Palm rachis: The cluster of empty fruit or palm rachis is a lignocellulosic material composed mainly of polysaccharides (66%) such as cellulose, xylan, and glucan; and polymers (12%) such as lignin. Palm rachis has a moisture content in the range of 60-65% and 1 to 2,5% of impregnated vegetable oil. In addition, it is rich in nutrients such as potassium and, to a lesser extent, in magnesium, nitrogen, and phosphorus (Ramírez *et al*., 2011). The main use of rachis is to incorporate it into the soil as organic fertilizer due to its potassium content.

There has been little interest in using palm rachis for biogas production due to its lignocellulosic composition. However, it shows great potential to produce methane, given its biodegradability and high moisture content. Some studies, such as those by Paepatung *et al*. (2009), Nieves *et al*. (2011), and O-Thong *et al*. (2012), have estimated the potential yield of specific methane for rachis at different operating conditions. The results express maximum methane productions of 370, 181, and 202 mL/g VS, respectively. Likewise, Suksong *et al*. (2019) have investigated the fungal pre-treatment with TRICHODERMA reesei TISTR 3080 in order to produce enzymes capable of degrading cellulose, hemicellulose, and lignin, thus improving methane recovery. The results express a maximum methane yield of 315 mL/g VS for the retention of 15 days.

Palm kernel is the shell that covers the almond and corresponds to approximately 7% of the weight of the fresh fruit cluster. It is characterized by a low moisture content and a high content of volatile matter. Among the residues from palm oil extraction, the shell has the lowest sulfur content and the highest calorific value, which is why palm shells are used as fuel for preheating boilers and are important in the search for different processes of energy use of this biomass. Jekayinfa *et al*. (2013) developed a study of biogas production using palm shell as a substrate on a laboratory scale under mesophilic conditions at 35 °C for 30 days. A maximum methane production of 50 mL/g VS and a biogas yield of 80 mL/g VS were achieved.

Swine manure

Swine manure are the feces produced in operations involving swine, which can be used as fertilizer. They contain nutrients

such as nitrogen, phosphorus, and potassium among others (Grisales *et al*., 2016).

In Colombia, the swine population is estimated to be about 6,4 million. With an average of 2,35 kg of manure produced per pig every day, the manure produced in the country reaches values close to 5,5 million ton/year (Mosquera *et al*., 2020). As manure is sometimes used as a fertilizer, not all of it is available to be used in energy production. Gutiérrez *et al*. (2020) estimated that only about 61% of the total manure produced is available. The potential for methane production of manure varies greatly. The literature reports values between 210 and 437 mL CH_4/gVS (Rodríguez *et al*., 2017; Gutiérrez *et al*., 2020). In Colombia, the swine industry has shown great interest in the development and implementation of AD processes to use their residues.

Organic Fraction of Municipal Solid Waste (OFMSW)

Municipal solid waste refers to all waste consisting of organic and inorganic material generated in private homes from institutional and commercial sources, such as offices, hotels, and restaurants, among others. The organic fraction of municipal solid waste (OFMSW) represents, on average, between 50 to 70% of the composition of urban solid waste, consisting mainly of garden waste, food scraps, and paper (Malik *et al*., 2013).

OFMSW has great potential as a substrate in AD due to the large volumes of generation related to population growth and its organic content, availability, and geographic location. In Colombia, an average of 0,74 kg is estimated per day of waste generated per inhabitant (CEPAL, 2021). According to the 2018 Solid Waste Final Disposal report, the final disposal of solid waste in Colombia amounts to 11 390 329 tons per year, which corresponds to more than 14 500 daily tons of organic waste for use (Superintendencia de Servicios Públicos Domiciliarios, 2019). Among the current treatment methods for OFMSW, composting and AD stand out (López *et al*., 2020). Composting is considered to be the best option due to its low cost and ease of implementation, transforming waste into a homogeneous material with nutritional contents that contributes to the recovery of degraded soils (Tortosa, 2020). The use of OFMSW in AD systems for biogas production is very recent. According to CONPES 3874 of 2016, energy recovery is included as a strategy for the alternative treatment of this type of waste before its final disposal in landfills (Departamento Nacional de Planeación, 2016).

Residues selection and characterization

Swine manure (SM), POME, and coffee residues (CR) were selected as substrates to conduct the BMP test. The selection was based on their high content of VS, high volume of production in Colombia, high availability, and few pretreatment requirements, as well as for their key role in the Colombian industry with regard to the commercial sectors that produce these wastes. To conduct the BMP test, the residues were collected from different sources.

Swine manure was collected from a pig farm located in the outskirts of Medellín, Colombia. The solid manure was diluted with water in a manure:water ratio of 1:5, and then it was filtered with an 18 mesh to remove large solids in the mixture. The liquid obtained after filtration was used for the BMP. POME was obtained from the COOPAR palm oil extraction plant located in El Zulia, Colombia. Coffee residues consisted of the wastewater resulting from the washing and centrifugation of coffee fruits. They were collected from a coffee processing plant located in Andes, Colombia. No pretreatment was made to POME or CR before the BMP tests. Table 1 shows the values for different parameters of the collected samples.

Table 1. Measured parameters of the substrates used in the BMP test

Substrate	pH	COD [mg/L]	Humidity [%]	TS [mg/L]	VS [mg/L]
POME	4,2 ± 0,5	59 600 ± 3 818	94,94 ± 0,76	50 590 ± 7 660	42 838 ± 7 863
SM	7,38 ± 0,08	35 270 ± 9 310	97,44 ± 0,31	25 633 ± 3 135	18 991 ± 2 527
CR	3,35 ± 0,09	87 561 ± 40 765	91,41 ± 0,3	85 876 ± 3 032	75 546 ± 1 620

Source: Authors

BMP assays

Figure 2 presents the BMP results obtained for the three selected substrates. It can be seen that POME has the highest BMP, with a value close to 465 NmL CH_4/gVS after 30 days of experimentation. The BMP values for SM and CR were 240 and 314 NmL CH_4/gVS, respectively. It is interesting that AD processes in Colombia have focused mostly on one substrate (SM), which has a lower BMP value than other potential substrates. New projects of AD using alternative substrates such as CR and POME are a potential way to generate larger amounts of energy in the country.

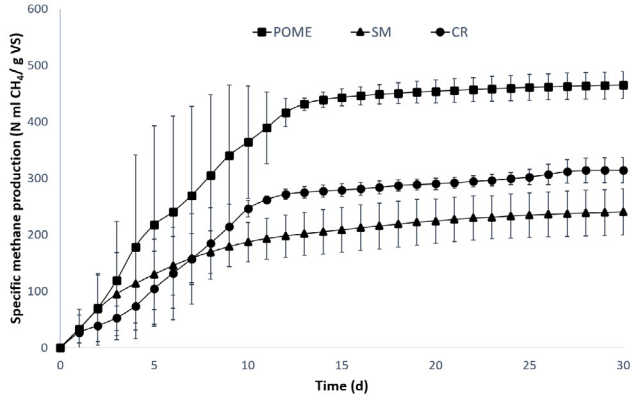

Figure 2. Evolution of methane production during the BMP test for the selected substrates. Error bars represent the standard deviation for the triplicates.
Source: Authors

The BMP values obtained in this study can be compared to the information found in the literature. In the case of CR, no reliable BMP values are found in Colombian studies. In a study conducted in Ethiopia, Chala *et al*. (2018) reported BMP values for different fractions of coffee wastes, ranging from 159 to 294 mL CH_4/gVS. The BMP value found for CR in this study was slightly higher. In the case of POME, other studies have reported BMP values below 400 mL CH_4/gVS. The value found in this study is considerably higher. In the case of SM, reported values rank from 210 to 437 mL CH_4/gVS. In this study, the value found was close to the lower reports. Nevertheless, it should be stated that, in this study, the SM was diluted in water and then filtered for large particles that could cause complications during its use in reactors requiring feeding by pumps. Unfiltered SM preparations may show a higher BMP, as they could contain larger amounts of organic matter. However, preliminary assays have shown that the methane production rate for the unfiltered SM (with the same dilution ratio) is much lower than that of the filtered SM (data not shown).

It is also noticeable that methane production from CR had almost finished on day 11, while POME showed methane production until day 13. The behavior of CR at the beginning of the fermentation was slower. However, after day 8, it surpassed SM. After days 11 and 13, POME showed no significant changes in methane production. However, CR showed a slightly higher daily methane production on day 28 in one of the reactors. This is less clear for SM, as the methane production seems to become fully established only after day 24, with an increase in daily methane production of less than 1,0% compared to previous days. This is important when it comes to defining the hydraulic retention time (HRT) of an AD process with any substrate. In the case of SM, as the complete degradation of organic matter can take longer, a higher HRT should be ensured, whereas, for CR and POME, the HRT can be lower. Additionally, in the first 13 days, POME showed a large standard deviation reflected in the speed of adaptation of the sludge to said substrate, due to the use of a more active sludge for performing the tests at different times.

Kinetic parameters

The logistic and Gompertz models were applied, and their parameters optimized, for the BMP assays carried out with POME, SM, and CR as substrates. Both models showed a good fitting to the experimental data in all cases (Figure 3).

The estimated kinetic parameters for the selected substrates are shown in Table 2. According to the experimental results, POME had the highest K value, and SM had the lowest, indicating a higher BMP of POME, followed by CR, and a lower BMP for SM. Interestingly, the shortest lag phase (represented by **δ**) was observed for SM. A **δ** value of 0 d for SM indicates that there is practically no lag phase during the AD of this substrate. This value was higher for POME, while CR showed the highest value of **δ**. A larger lag phase in an AD process implies that the microorganisms in charge of degrading the substrates take longer to adapt to it, and the biogas production will thus take longer to start during the early stages of the process.

As for the maximum methane production rate (represented by r), the highest value was obtained for POME, followed by CR and, finally, by SM with the lowest value. This indicates that, once the microbial community has adapted to the substrate, POME can be more easily transformed into biogas than CR and SM. This parameter is important for the design of AD systems using a given substrate, and having it calculated for different substrates can support the design and implementation of AD plants in Colombia.

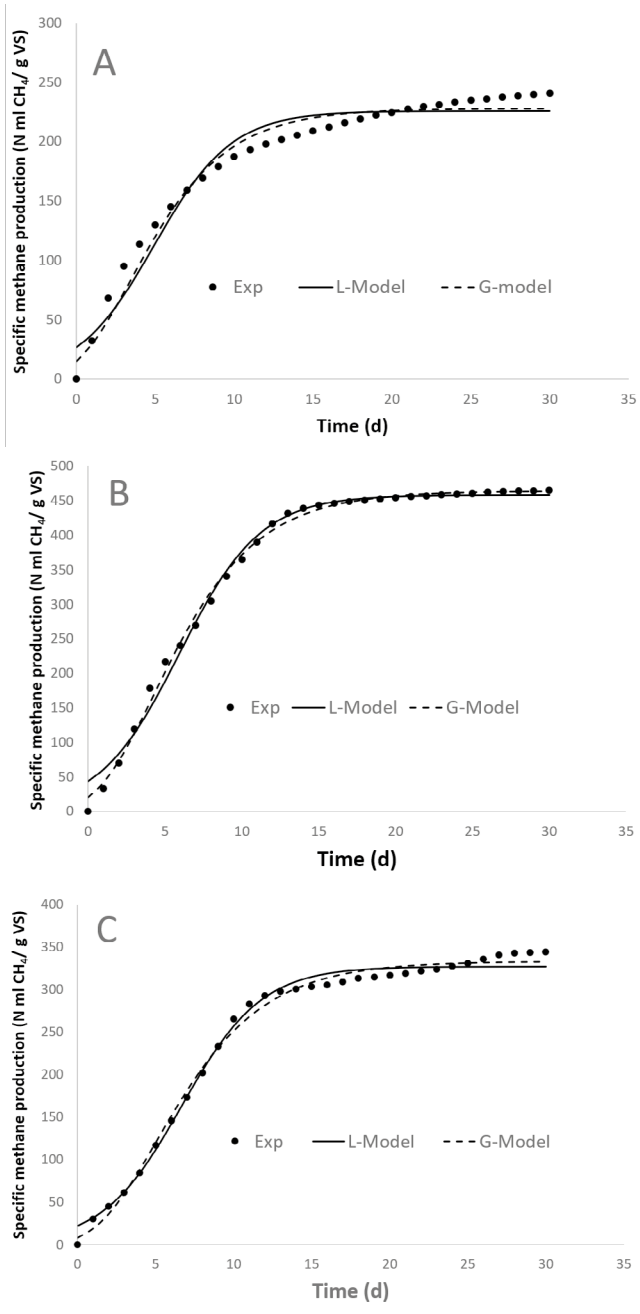

Figure 3. Model fitting for the BMP of the selected substrates: a) SM, b) POME, c) CR
Source: Authors

It can be seen that the previous discussion is similar considering the results of both models, thus implying that the calculations are consistent with different calculation approaches and in accordance with the experimental results.

Table 2. Estimated kinetic parameters for the logistic and Gompertz models applied to the anaerobic digestion of swine manure, POME, and coffee residues

		Parameters		
Substrate	**Model**	**K (N mL CH_4)**	**δ (d)**	**r (N mLCH_4 / d)**
SM	Logistic	225,65	0	22,91
	Gompertz	227,72	0	24,28
POME	Logistic	458,59	0,67	43,44
	Gompertz	464,10	0,53	45,21
CR	Logistic	327,03	1,57	32,04
	Gompertz	333,09	1,19	31,56

Source: Authors

Conclusions

The wide agriculture and agro-industrial activity of Colombia provides large amounts of different organic wastes that are potential substrates for biogas generation using anaerobic digestion (AD) processes. Among said wastes, swine manure (SM), POME, and coffee residues (CR) are especially interesting considering their chemical composition, their amount of production and availability to be used in energy generation processes, and their importance in Colombian economic activities, which allows solving problems related to the inappropriate use of solutions and constitutes an alternative to the final disposal of said residues. The biochemical methane potentials of SM, POME, and CR were found to be 240, 465, and 314 and NmLCH_4/gVS respectively. Kinetic parameters for the AD process of these substrates show that, while methane production starts earlier for SM, in later stages of the process, the production rates of CR and POME are higher. Although the few AD systems currently operating in Colombia are focused on using SM as substrate, new systems should be considered for substrates with high BMP, such as CR and POME. The design and implementation of AD systems for this kind of substrates should be supported by more experimental data such as those reported in this study.

Acknowledgements

The authors gratefully acknowledge the financial support provided by the Colombia Scientific Program, within the framework of the call Ecosistema Científico (Contract No. FP44842-218-2018).

CRediT author statement

All authors: Conceptualization–Methodology–Software–Validation–Formal analysis–Investigation– Writing-Original Draft preparation, Writing, Reviewing, and Editing–Data Curation–Supervision–Project administration–Resources–Funding acquisition.

References

Ahmed, Y., Yaakob, Z., Akhtar, P., and Sopian, K. (2015). Production of biogas and performance evaluation of existing treatment processes in palm oil mill effluent (POME). *Renewable and Sustainable Energy Reviews*, *42*, 1260-1278. https://doi.org/10.1016/j.rser.2014.10.073

Amado, M., Barca, C., Hernández, M. A., and Ferrasse, J. H. (2021). Evaluation of energy recovery potential by anaerobic digestion and dark fermentation of residual biomass in Colombia. *Frontiers in Energy Research*, *9*, 690161. https://doi.org/10.3389/fenrg.2021.690161

Asocaña (2019). *Aspectos generales del sector agroindustrial de la caña 2018-2019 informe anual*. https://www.asocana.org/modules/documentos/15331.aspx

Blandón-Castaño, G., Dávila-Arias, M. T., and Rodríguez-Valencia, N. (1999). Caracterización microbiológica y físico-química de la pulpa de café sola y con mucílago, en proceso de lombricompostaje. *Cenicafé*, *50*(1), 5-23. https://www.cenicafe.org/es/publications/arc050(01)005-023.pdf

Bristish Petroleum Company (2020). *Statistical review of world energy, 69th edition*. https://www.bp.com/content/dam/bp/business-sites/en/global/corporate/pdfs/energy-economics/statistical-review/bp-stats-review-2020-full-report.pdf

Campuzano, R., and González, S. (2016). Characteristics of the organic fraction of municipal solid waste and methane production: A review. *Waste Management, 54,* 3-12. https://doi.org/10.1016/j.wasman.2016.05.016

Chala, B., Oechsner, H., Latif, S., and Müller, J. (2018). Biogas potential of coffee processing waste in Ethiopia. *Sustainability*, *10*(8), 2678. https://doi.org/10.3390/su10082678

Comisión Económica para América Latina y el Caribe (CEPAL). (2021). *Encuesta a municipios sobre gestión de residuos sólidos domiciliarios 2019 – Colombia. Documentos de Proyectos* (*LC/TS.2021/67*). https://www.cepal.org/es/publicaciones/46988-encuesta-municipios-gestion-residuos-solidos-domiciliarios-2019-colombia

Departamento Nacional de Planeación. (2016). CONPES 3874 – Política Nacional para la Gestión Integral de Residuos Sólidos. https://www.minambiente.gov.co/wp-content/uploads/2021/08/conpes-3874-de-2016.pdf

Durán, M., Sanabria, I., and Gutiérrez, N. (2015). Evaluación de la producción de metano en la digestión anaerobia de vinazas pretratadas con ozono. *Revista EIA, 12*(*24*), 167-177. https://doi.org/10.24050/reia.v12i24.881

Fedebiocombustibles (2021). *Etanol*. http://www.fedebiocombustibles.com/main-pagina-id-4-titulo-proceso_de_los_biocombustibles.htm

Fedepalma (2019). *Anuario estadístico: principales cifras de la agroindustria de la palma de aceite en Colombia*. https://publicaciones.fedepalma.org/index.php/anuario

Fedepalma (2021). *La palma de aceite en Colombia*. https://web.fedepalma.org/la-palma-de-aceite-en-colombia-departamentos

Grisales, J., Osorio, N., and Gómez, J. (2016). *Manual de uso de la porcinaza en la agricultura "De la granja al cultivo"*. https://www.porkcolombia.co/manual-de-uso-de-la-porcinaza-en-la-agricultura/

Gutierrez, A., Cabello, J., Hens, L., and Vandecasteele, C. (2020). The energy potential of agriculture, agroindustrial, livestock, and slaughterhouse biomass wastes through direct combustion and anaerobic digestion. The case of Colombia. *Journal of cleaner production, 269*, 122317. https://doi.org/10.1016/j.jclepro.2020.122317

Jain, S. (2019). *Global potential of biogas*. World Biogas Association. https://www.worldbiogasassociation.org/wp-content/uploads/2019/09/WBA-globalreport-56ppa4_digital-Sept-2019.pdf

Jekayinfa, S., and Scholz, V. (2013). Laboratory scale preparation of biogas from cassava tubers, cassava peels, and palm kernel oil residues. *Energy Sources, Part A: Recovery, Utilization, and Environmental Effects. 35*(*21*), 2022-2032. https://doi.org/10.1080/15567036.2010.532190

Linville, J., Shem, Y., Wu, M., and Urgun, M. (2015). Current state of anaerobic digestion of organic wastes in North America. *Current Sustainable/Renewable Energy Reports, 2*, 136-144. DOI: https://doi.org/10.1007/s40518-015-0039-4

Lohani, S. P., Havukainen, J. (2018). Anaerobic digestion: Factors Affecting anaerobic digestion process. In S. Varjani, E, Gnansounou, B. Gurunathan, D. Pant, and Z. Zakaria (Eds.) *Waste Bioremediation. Energy, Environment, and Sustainability* (pp. 343-359). Springer. https://doi.org/10.1007/978-981-10-7413-4_18

López, Y., and Franco, B. (2020). Gestión de residuos sólidos urbanos: Un enfoque en Colombia y el departamento de Antioquia. *Cuaderno Activa, 11,* 120-134. https://ojs.tdea.edu.co/index.php/cuadernoactiva/article/view/808/916

Lorenzo, Y., Chanfón, J., and Pereda, I. (2013). Estudio de la digestión anaerobia mediante el ensayo de actividad metanogénica empleando vinazas con diferentes contenidos de sulfatos. *ICIDCA sobre los derivados de la caña de azúcar, 47*(*1*), 45-50. https://www.redalyc.org/pdf/2231/223126409006.pdf

Malik, A., Masood, F., and Grohmann, E. (2013). Management of microbial resources in the environment: A broad perspective. In A. Malik, E. Grohmann, and M. Alves (Eds.), *Management of Microbial Resources in the Environment* (pp. 1-15). Springer. https://doi.org/10.1007/978-94-007-5931-2_1

Mejía, M. (2015). *Efecto del cuesco de la palma africana en la reducción de emisiones NOX en la combustión de gas natural*. [Undergraduate tesis, Universidad de los Andes]. https://repositorio.uniandes.edu.co/bitstream/handle/1992/18583/u722464.pdf?sequence=1&isAllowed=y

Moreno, N., and Jiménez, R. (2016). *Evaluación de diferentes métodos para la transformación de la pulpa de café en abono orgánico en fincas cafeteras* [Master's thesis, Universidad de Manizales]. https://ridum.umanizales.edu.co/xmlui/handle/20.500.12746/2620

Mosquera, J., Varela, L., Santis, A., Villamizar, S., Acevedo, P., and Cabeza, I. (2020). Improving anaerobic co-digestion of different residual biomass sources readily available in Colombia by process parameters optimization. *Biomass and Bioenergy, 142*, 105790. https://doi.org/10.1016/j.biombioe.2020.105790

Nabarlatz, D., Arenas, L., Herrera, D., and Niño, D. (2013). Biogas production by anaerobic digestion of wastewater from palm oil mill industry. *CT&F - Ciencia, Tecnología y Futuro, 5*(*2*), 73-83. https://doi.org/10.29047/01225383.58

Nieves, D. C., Karimi, K., and Horváth, I. S. (2011). Improvement of biogas production from oil palm empty fruit bunches (OPEFB). *Industrial Crops and Products*, *34*(1), 1097-1101. https://doi.org/10.1016/j.indcrop.2011.03.022

O-Thong, S., Boe, K., and Angelidaki, I. (2012). Thermophilic anaerobic co-digestion of oil palm empty fruit bunches with palm oil mill effluent for efficient biogas production. *Applied Energy, 93*, 648-654. https://doi.org/10.1016/j.apenergy.2011.12.092

Paepatung, N., Nopharatana, A., and Songkasiri, W. (2009). Bio-methane potential of biological solid materials and agricultural wastes. *Asian Journal on Energy and Environment, 10*(*01*), 19-27. https://www.thaiscience.info/Journals/Article/AJEE/10262486.pdf

Puerta, G., and Ríos, S. (2011). Composición química del mucílago de café, según el tiempo de fermentación y refrigeración. *Cenicafé, 62*(*2*), 23-40. https://www.cenicafe.org/es/documents/2.pdf

Ramírez, C., Nidia, E., Garzón, E. M., Silva, R., Ángela, S., Yáñez, A., and Edgar, E. (2011). *Caracterización y manejo de subproductos del beneficio del fruto de palma de aceite*. https://publicaciones.fedepalma.org/index.php/boletines/article/view/10502

REN21 (2020). *Renewables 2020 global status report*. (*Paris: REN21 Secretariat*). https://www.ren21.net/gsr-2020/

Rincón, J., Durán, D., Quintero, O., Duarte, C., Guevara, P., and Velásquez, M. (2018). Disponibilidad de biomasa residual y su potencial para la producción de biogás en Colombia. *CIDET*, *2018*, 16-21. https://www.cidet.org.co/sites/default/files/documentos/2-compressed.pdf

Rivas-Solano, O., Faith-Vargas, M., and Guillén-Watson, R. (2016). Biodigesters: Chemical, physical and biological factors related to their productivity. *Revista Tecnología En Marcha, 29*(*5*), 47-53. https://doi.org/10.18845/tm.v29i5.2516

Rodríguez, A., Ángel, J., Rivero, E., Acevedo, P., Santis, A., Cabeza, I., Acosta, M., and Hernández, M. (2017). Evaluation of the methane potential of pig manure, organic fraction of municipal solid waste and Cocoa industry residues In Colombia. *Chemical Engineering Transactions, 57,* 55-60. https://doi.org/10.3303/CET1757010

Rodríguez, N., and Zambrano, D. (2010). Los subproductos del café: fuente de energía renovable. *Avances técnicos Cenicafé*, *393*, 1-8. https://biblioteca.cenicafe.org/bitstream/10778/351/1/avt0393.pdf

Saelor, S., Kongjan, P., and O-Thong, S. (2017). Biogas production from anaerobic co-digestion of palm oil mill effluent and empty fruit bunches. *Energy Procedia, 138,* 717-722. https://doi.org/10.1016/j.egypro.2017.10.206

Shakib, N., and Rashid, M. (2019). Biogas production optimization from POME by using anaerobic digestion process. *Journal of Applied Science & Process Engineering, 6*(2), 369-377. https://doi.org/10.33736/jaspe.1711.2019

Siciliano, A., Limonti, C., and Curcio, G. (2021). Improvement of biomethane production from organic fraction of municipal solid waste (OFMSW) through alkaline hydrogen peroxide (AHP) pretreatment. *Fermentation 2021, 7*(3), 197. https://doi.org/10.3390/fermentation7030197

Suksong, W., Promnuan, K., Seengenyoung, J., and O-Thong, S. (2017). Anaerobic co-digestion of palm oil mill waste residues with sewage sludge for biogas production. *Energy Procedia, 138,* 789-794. https://doi.org/10.1016/j.egypro.2017.10.068

Suksong, W., Tukanghan, W., Promnuan, K., Kongjan, P., Reungsang, A., Insam, H., and O-Thong, S. (2019). Biogas production from palm oil mill effluent and empty fruit bunches by coupled liquid and solid-state anaerobic digestion. *Bioresource Technology, 296*, 122304. https://doi.org/10.1016/j.biortech.2019.122304

Super Intendencia de Servicios Públicos Domiciliarios. (2019). Informe de Disposisición Final de Residuos Sólidos – 2018. https://www.superservicios.gov.co/sites/default/files/inline-files/informe_nacional_disposicion_final_2019.pdf

Torres, C., and Quintero, L. (2019). Análisis de residuos sólidos de palma africana, como alternativa de aprovechamiento de energías renovables en el departamento del Cesar. *Investigación Científica y Tecnológica, 10*(1), 3662. https://doi.org/10.21500/20275846.3662

Tortosa, G. (2020). *La agricultura regenerativa como motor económico de la España rural*. Compostando Ciencia Lab. http://www.compostandociencia.com/2020/07/la-agricultura-regenerativa-como-motor-economico-de-la-espana-rural/#:~:text=La%20agricultura%20regenerativa%20es%20un,y%20la%20generaci%C3%B3n%20de%20comunidad.

Tosun, I., Gönüllü, M., Arslankaya, E., and Günay, A. (2008). Co-composting kinetics of rose processing waste with OFMSW. *Bioresource Technology, 99,* 6143-6149. https://doi.org/10.1016/j.biortech.2007.12.039

Uddin, M., Rahman, M., Taweekun, J., Techato, K., Mofijur, M., and Rasul, M. (2019). Enhancement of biogas generation in up-flow sludge blanket (UASB) bioreactor from palm oil mill effluent (POME). *Energy Procedia, 160,* 670-676. https://doi.org/10.1016/j.egypro.2019.02.220

Velásquez, M., Rincón, J., Guevara, P., Duarte, S., Quintero, O., Durán, D., Morales, Y., Zarama, L., and Quintero, J. (2018). *Estimación del potencial de conversión a biogás de la biomasa en Colombia y su aprovechamiento. Bogotá*. https://bdigital.upme.gov.co/bitstream/handle/001/1317/Informe%20final.pdf?sequence=1&isAllowed=y

Water Environment Federation and American Public Health Association (2005). *Standard methods for the examination of water and wastewater*. American Public Health Association.

Wong, Y., Teng, T., Ong, S., Norhashimah, M., Rafatulah, M., and Lee, H. (2013). Anaerobic acidogenesis biodegradation of palm oil mill effluent using suspended closed anaerobic bioreactor (SCABR) at mesophilic temperature. *Procedia Environmental Sciences, 18,* 433-441. https://doi.org/10.1016/j.proenv.2013.04.058

Wu, N., Moreira, C., Zhang, Y., Doan, N., Yang, S., Phlips, E., Svoronos, S., and Pullammanappallil, P. (2019). *Techno-economic analysis of biogas production from microalgae through anaerobic digestion*. IntechOpen. http://dx.doi.org/10.5772/intechopen.86090

Appendix 1. Selection criteria for the evaluated substrates

Selection criteria	Vinasse	Coffee Mucilage	Coffee pulp	POME	Palm rachis	Palm kernel	Swine Manure	Organic Fraction of Municipal Solid Waste
National production	7-14 L vinasse /L ethanol	129 270 ton/year	366 960 ton/ year	3 770 004 ton/year	1 649 735 ton/year	502 093 ton/year	5 434 524 ton/year]	11 390 329 ton/ year
Availability [%]	100	-	-	95	45	35	61	100
BMP* [NmL CH_4/g VS]	210	311	15	397	225	41	325	175
Required pretreatments	pH adjustment and ozonation	pH adjustment and leachate production	pH adjustment and size reduction	pH adjustment	Size reduction	Size reduction	None	pH adjustment
VS (mg/L)	28 785	3 515	5 335	26 530-984 45	81,3%	75,66%	4,2 %	10 200 ± 400
C/N ratio	17,9	29,8	27,44	27	45-65	50-65	10,7	20

Appendix 2. Reported characteristics and parameters of the considered substrates

Parameters	Vinasse	Coffee Mucilage	Coffee pulp	POME	Palm rachis	Palm kernel	Swine Manure	Organic Fraction of Municipal Solid Waste
VS (mg/L)	28 785	3 515	5 335	10 500- 98 445	81,3%	75,66%	4,2%	10 200 ± 400
TS (mg/L)	7 450	4 650	7 400	13 400-111029	97,04%	-	6,4%	21 600 ± 700
BOD (mg O_2/L)	-	6 200	6 435	25 500	-	-	-	-
COD (mg O_2/L)	56 712	10 650	14 305	62 973	-	-	71 592	12 500 ± 600
TOC (mg/L)	44 762	-	-	-	54,02 % TS	-	-	37,8 %
pH	4,5	4,4	4,4	4,58	7,4	-	7,7	5,3
Humidity content (%)	-	90,05	74,83	-	4,89	7,6	95,6	80,3
NTK (g/L)	1,227	-	-	0,75	1,14 % TS	-	3,75	1,61
Fixed carbon	-	-	-	-	14,88	15,67	-	-
Calorific value	-	2 (MJ/kg fresh mucilage)	0,54 (MJ/kg fresh mucilage)	22 480 kJ/m^3	11 920 kJ/kg	20 110 kJ/kg	-	-
Elemental composition (%)	-	-	-	-	C: 43,94 H: 5,66 O:37,87 N: 0,73 S: 0,09	C: 47,53 H: 6,21 O: 35,86 N: 1,58 S: 0,08	C: 37,24 H: 5,06 O: 34,89 N: 4,08 S: 0,28	C: 46,6 H: 6,6 N: 2,9 S: 0,3
Metals content (%)	-	K= 1,60 Mg= 0,08 Fe= 0,04 Zn= 0,007 Mn= 0,004 Cu= 0,002	P= 0,13 K= 2,82 Ca= 0,32 Mg= 0,08	P: 180 mg/L K: 2 270 mg/L Ca: 439 mg/L B: 7,6 mg/L Mn: 2,0 mg/L Cu: 0,89 mg/L Mg: 615 mg/L Zn: 2,3 mg/L	B: 10 mg/kg Cu: 23 mg/kg Zn: 51 mg/kg Mn: 48 mg/kg Fe: 473 mg/kg	-	P= 1 406 K= 4 929 Cu= 41,3 Zn= 63,4	-
Ashes (%)	-	0,43	6,66	-	6,84	3,82	-	-
References	Durán *et al.* (2015) Lorenzo *et al.* (2013)	Puerta *et al.* (2011) Rodríguez *et al.* (2011)	Blandón *et al.* (1999) Rodríguez *et al.* (2010)	Saelor *et al.* (2017) Suksong *et al.* (2017)	Ramírez *et al.* (2011) Saelor *et al.* (2017) Suksong *et al.* (2019)	Mejía, (2015) Torres *et al.* (2019)	Gutiérrez *et al.* (2020) Rodríguez *et al.* (2017) Amado *et al.* (2021)	Siciliano *et al.* (2021) Tosun *et al.* (2008) Campuzano *et al.* (2016)

Research Article/Chemical, Food and Environmental Engineering https://doi.org/10.15446/ing.investig.97848

Bench-Scale Biopile Hydrocarbons Removal Optimization Using the Response Surface Methodology and Simultaneous Optimization

Optimización de la remoción de hidrocarburos en biopilas a escala de banco utilizando metodología de superficie de respuesta y optimización simultánea

Omar Gutiérrez-Benítez[1], David J. Castro Rodríguez[2*], Víctor M. Serrano-Suárez[3], Enmanuel Casals-Pérez[4], Dayana Rabassa-Rabassa[5], Roberto Núñez-Moreira[6], Eudalys Ortiz-Guilarte[7], and María V. Iglesias-Rodríguez[8]

ABSTRACT

Nowadays, the generation of vast volumes of oily sludges is associated with industrial operations such as production, pretreatment, processing, water separation, and storage tank maintenance. Biopiles can be more efficient than other techniques for removing hydrocarbons in sludges, but their removal efficiency depends on operating variables. The goal of this study was to determine the best operating variable ranges at the bench scale to simultaneously optimize hydrocarbons removal in a biopile prototype. This research was conducted within the framework of a Cuban project and used an experimental protocol that integrates several standardized methods and engineering procedures into a series of steps. A Box-Behnken design was implemented for three factors and two response variables: the mass of Total Petroleum Hydrocarbons (TPH) removed and the final concentration of TPH. A simultaneous optimum was obtained for an initial TPH concentration of 39 278 mg.kg^{-1} and contents of texturizer and moisture of 6,45 and 25,95%, respectively. The obtained variable ranges ensure a compromise solution that maximizes the mass of TPH removed and keeps the contaminant concentration under the Cuban disposal regulations. The results have been used to set up the biopiles at a pilot scale as a subsequent stage of the project.

Keywords: biopile, Box-Behnken, hydrocarbon removal, response surface methodology, simultaneous optimization

RESUMEN

La generación de volúmenes de lodos oleosos está asociada a operaciones industriales como producción, pretratamiento, procesamiento, tratamiento de aguas y mantenimiento de tanques de almacenamiento. Las biopilas pueden ser más eficientes que otras técnicas para degradar los hidrocarburos en lodos, pero su eficiencia en la remoción depende de variables operativas. El objetivo de este estudio fue determinar los mejores rangos de variables operativas a escala de banco para optimizar simultáneamente la eliminación de hidrocarburos en un prototipo de biopila. Esta investigación se desarrolló en el marco de un proyecto cubano y utilizó un protocolo experimental que integra varios métodos estandarizados y procedimientos de ingeniería en una serie de pasos. Se implementó un diseño Box-Behnken para tres factores y dos variables de respuesta: la masa de Hidrocarburos Totales de Petróleo (HTP) removida y la concentración final de HTP. Se obtuvo un óptimo simultáneo para una concentración inicial de HTP de 39 278 mg.kg^{-1} y porcentajes de texturizante y humedad de 6,45 y 25,95 % respectivamente. Los valores obtenidos garantizan una solución de compromiso que maximiza la masa de HTP removida y mantiene los hidrocarburos bajo lo establecido en la normativa cubana de eliminación de residuos. Los resultados fueron utilizados para establecer biopilas a escala piloto en una siguiente etapa del proyecto.

Palabras clave: biopila, Box-Behnken, metodología de superficie de respuesta, optimización simultánea, remoción de hidrocarburos

Received: August 19th, 2021
Accepted: September 17th, 2022

* Corresponding author.

[1] Chemical Engineering, Central University of Las Villas, Cuba. Master in Processes Analysis of the Chemical Industry, Central University of Las Villas, Cuba. Affiliation: Associate professor at the Chemistry Department of Carlos Rafael Rodríguez University of Cienfuegos, Cuba. E-mail: ogutierrez@ucf.edu.cu

[2] Industrial Engineering, Carlos Rafael Rodríguez University of Cienfuegos, Cuba. Master's in industrial engineering, Carlos Rafael Rodríguez University of Cienfuegos, Cuba. Affiliation: PhD student in the Chemical Engineering program, Applied Science and Technology Department (DISAT), Politecnico di Torino (POLITO), Italy. E-mail: david.castro@polito.it

[3] Chemical Engineering, Carlos Rafael Rodríguez University of Cienfuegos, Cuba. Affiliation: Lecturer at the Chemistry Department of Carlos Rafael Rodríguez University of Cienfuegos, Cuba. E-mail: victormanuelserranosuarez@gmail.com

[4] Chemical Engineering, Carlos Rafael Rodríguez University of Cienfuegos, Cuba. Master in Environmental Engineering, Central University of Las Villas, Cuba. Affiliation: Research assistant at the Cienfuegos Center of Environmental Studies (CEAC), Cuba. E-mail: ecasalsperez@gmail.com

[5] Chemical Engineering, Carlos Rafael Rodríguez University of Cienfuegos, Cuba. Master from the Cleaner Production program, Carlos Rafael Rodríguez University of Cienfuegos, Cuba. Affiliation: Master's student, Chemical Engineering program of the University of Sonora, México. E-mail: a221230080@unison.mx

[6] Chemical Engineering, José Antonio Echeverría Technical University of Havana, Cuba. PhD in Biological Sciences, University of Havana, Cuba. Affiliation: Senior researcher at the Institute of Marine Sciences (ICIMAR), Cuba. E-mail: robertico@icimar.cu

[7] Microbiology bachelor, University of Havana, Cuba. PhD in Biological Sciences, University of Havana, Cuba. Affiliation: Senior researcher at the Institute of Marine Sciences (ICIMAR), Cuba. E-mail: laly@icimar.cu

[8] Microbiology bachelor, University of Havana, Cuba. Master's in Microbiology, University of Havana, Cuba. Affiliation: Junior researcher at the Institute of Marine Sciences (ICIMAR), Cuba. Email: victoria@icimar.cu

How to cite: Gutiérrez-Benítez O., Castro-Rodríguez D. J., Serrano V., Casals-Pérez E., Rabassa D., Núñez R., Ortiz E., and Iglesias, M.V. (2023). Bench-scale biopile hydrocarbons removal optimization using the response surface methodology and simultaneous optimization. *Ingeniería e Investigación, 43*(2), e97848. https://doi.org/10.15446/ing.investig.97848

Introduction

It is generally accepted that chemical, physical, and biological processes intervene in the remediation of waste and soils contaminated with hydrocarbons (Volke and Velasco 2002; Riser-Robert, 2019). The use of bioremediation methods has aroused a considerable research interest and currently provides advantages over other treatment processes (Kumar *et al*., 2011; Tyagi *et al*., 2011; Thapa *et al*., 2012; Varjani, 2017; Yuniati, 2017; de Oliveira *et al*., 2018). Among the bioremediation methods, biopiles are an *ex situ* technology where the stimulation of microbial activity is achieved through the direct addition of nutrients and texturizers (agro-industrial organic wastes), as well as aeration and humidity control (Velasco and Volke, 2003; Prakash *et al*., 2015; EPA, 2017; Martínez *et al*., 2017; Ossai *et al*., 2020).

The removal efficiency of biopiles is influenced by a considerable number of variables, which can be grouped into three categories: the characteristics of the soil and texturizers, the characteristics of the pollutant, and climatic conditions. Among the essential factors are the hydrocarbon concentration, the texturizer content, the moisture content, and the C:N:P:K ratio (Velasco and Volke, 2003; Prakash *et al*., 2015; EPA, 2017; Yuniati, 2017; Al-Hawash *et al*., 2018).

Moreover, the response surface methodology is widely known as an experimental strategy that allows finding the best-operating conditions for a process. Particularly, the Box-Behnken experimental design is an excellent economic alternative because it requires a minimum of experimental runs to study three or more factors at three levels (Gutiérrez and de la Vara, 2012; Montgomery, 2017). During the past decade, the Box-Behnken design has been extensively applied to hydrocarbon bioremediation research (Agarry and Ogunleye, 2012; Martínez *et al*., 2015; Khaled *et al*., 2016; Shuo *et al*., 2019; Zhang *et al*., 2020).

Although these procedures guarantee an individual optimum, when more than one response variable is of interest in the arrangement, the global optimum is generally not the combination of the optimizations performed by the independent variables. Therefore, it is necessary to find a compromise solution where all the variables have a satisfactory level. This solution is recognized as a *simultaneous optimum* (Montgomery, 2017).

Statistical data report that, in the province of Cienfuegos, Cuba, there is still confined oiled sludge resulting from the territorial companies' collection, which amounts to 2 993 740 kg (CITMA, n.d.; Castro *et al*., 2022a). In this vein, the Environmental Studies Center of Cienfuegos (CEAC), the Institute of Marine Science (ICIMAR), and the Soil Research Institute (IIS) are three Cuban Institutions that have developed the project *Evaluation of the ecotechnology of biopiles for the bioremediation of oily waste using local texturizers* (BIOPILA).

The BIOPILA project aims to address an innovative and resilient technique to cope with the environmental problem of soil polluted with hydrocarbons in Cuba, specifically with the residues generated by the local industry which remain confined without a solution (Castro *et al*., 2022a). Previous research carried out within the framework of the aforementioned project has shown, at the bench scale, the relevance of biopile ecotechnology for the degradation of soils polluted with hydrocarbons (Gutiérrez *et al*., 2021; Castro *et al*., 2022b, Gutiérrez, *et al*., 2022; Castro *et al*., 2022c). Significant removal rates were reported for oils and grease concentrations (between 50,05 and 66,08%). For TPH, values between 40,00 and 59,12% were reported for all experimental treatments tested. However, neither the way in which the biopile design variables reported by Gutiérrez *et al*. (2020) should be operated nor the abiotic factors described by Casals *et al*. (2020) were sufficiently clear in terms of their influence on the bioremediation efficiency of waste and soil polluted with hydrocarbons. Hence, as part of the research-development BIOPILA project, this paper focuses on determining the best operating variable ranges of biopile ecotechnology at the bench scale. Moreover, the simultaneous optimization of biopile hydrocarbons removal was implemented as a prototype to obtain a compromise solution that maximized the mass of TPH removed while keeping the pollutant concentration under the Cuban disposal regulations.

Materials and methods

Some bench-scale experiments were carried out with biopile ecotechnology to bioremediate hydrocarbons. This technique has proven to be more efficient than others in removing hydrocarbons from sludges (Shahryar, 2017). Moreover, it has the advantage that the microorganisms are already adapted to the site conditions (Casale *et al*., 2018).

Figure 1 presents the heuristic diagram of the experimental protocol used in the bench-scale experimentation phase. The operating variables of interest for this research only comprised those related to the *Evaluation of hydrocarbon degradation* stage (highlighted in bold in Figure 1).

Under methodological convergence, several engineering tools were used, such as the design of experiments, mass balance, analytical chemistry, engineering design, and statistical analysis. The experimental polygon consisted of an industrial warehouse, roofed, with a concrete floor and provided with open windows, where 15 experimental units were settled within identical polyethylene basins that were 1,10 m long and 0,95 m wide. Each basin acted as a container to avoid mixing materials and leakage, separating each experimental unit from the surroundings.

Selection, collection, and characterization of materials

The critical materials used for the experimentation are detailed below:

- A mix of solid waste and soils contaminated with hydrocarbons, collected from the bottom of a settler.
- Representative soil from the central region of Cuba with low agricultural potential, selected as a pattern soil.
- A predetermined combination of two different agro-industrial wastes, which were mixed as a texturizer.

Firstly, the oily sludge was retrieved during the cleaning procedures in the waste treatment plant of an oil refinery.

Secondly, a typical greyish-brown soil from the central region of Cuba was used (density = 1 190 kg.m^{-3}). The soil was classified as silty clay sand, with low plasticity and moderate permeability. It was sieved using an industrial mesh for particles smaller than 4,75 mm, according to Cuban standards based on ASTM norms (ASTM International, 2002, 2017).

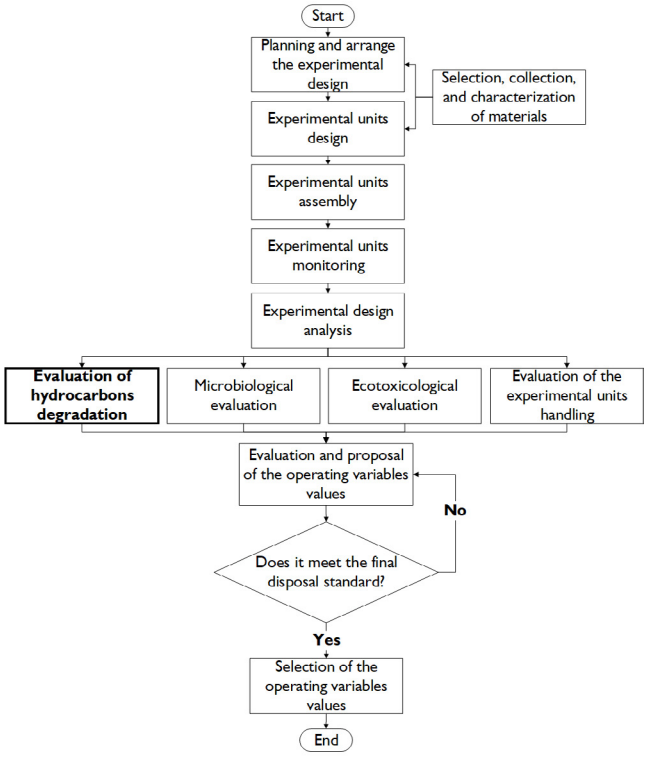

Figure 1. Heuristic diagram of the experimental protocol used in the bench-scale experimentation phase of the BIOPILA project
Source: Authors

For the mixture of texturizers, the best candidates for different treatments were selected, which had been tested in previous stages of the BIOPILA project (Casals *et al*., 2020; Gutiérrez *et al*., 2020; Castro *et al*., 2022c; Castro *et al*., 2022d). On the one hand, the candidate which reported the lowest TPH concentrations at 240 days, the highest degradation kinetic rate, and the shortest half-life ($t_{1/2}$) among all the considered treatments was used. On the other hand, the treatment that maintained the necessary water content requirements in the biopiles was also included in the mixture, with values of up to 35% moisture, increasing the soil porosity and contributing to soil moisture retention according to the criteria of Zang *et al*. (2020).

Finally, it is remarkable that the flora stimulated during the technological process was composed of the individual contributions of the microorganisms in each component of the biopile mixture (oily sludge, soil, and texturizers). The kinds and initial concentrations of the main groups of microorganisms identified in the mixture were total heterotrophic bacteria, filamentous fungi and yeasts, and hydrocarbon degraders, in the orders of 10^6 CFU.g^{-1}, 10^4 CFU.g^{-1}, and 10^5 CFU.g^{-1}, respectively. The concentrations above ensured a total heterotrophic bacteria concentration greater than 10^3 CFU.g^{-1}, in line with the initial requirements established for biopile efficacy (EPA, 2017).

Planning and organizing the experimental design

The procedure used to conduct this study was developed by following the criteria given by Gutiérrez and de la Vara (2012) and Montgomery (2017). Its seven steps are contextualized below:

1. Defining the problem: The problem matches the focus and goal of the paper, as declared in the introduction section.

2. Choosing the response variables: The mass of TPH removed and the final concentration of TPH (240 days). The TPH was determined by adapting the EPA Method 1664 to the biopile system, which was determined analogously to the previous stages of the BIOPILA Project described in Castro *et al*. (2022). The analysis is based on TPH extraction from a solid by an organic solvent and the gravimetric evaluation of the TPH mass. This method is reliable when the solid sample is over 5 g and the TPH concentration is over 0,3% by weight.

   The applied method consists of extracting a dry soil sample with n-hexane in a microwave at 120 °C for 20 min. Then, the extract (n-hexane + TPHs) is filtered through a funnel containing anhydrous Na_2SO_4. Afterwards, the solution is distilled at 85 °C in a water bath. Then, the residual mass is weighted in order to estimate the TPH quantity by gravimetry. The TPH concentration is achieved by the ratio of TPH mass to the dry sample soil mass.

   The TPH mass removed was determined from the initial and final concentrations of TPH and the mass of the experimental unit according to the following Equation:

$$MR = \frac{(TPH_{t=0} - TPH_{t=240}) \cdot Mb_i}{1000000} \quad (1)$$

where:

MR: Mass of TPH removed in the experimental unit (kg)
$TPH_{t=0}$: TPH concentration in the experimental unit at 0 days (mg.kg^{-1})
$TPH_{t=240}$: TPH concentration in the experimental unit at 240 days (mg.kg^{-1})
Mb_i: Mass of the experimental unit (kg)

3. Determining which factors should be studied according to the supposed influence on the response: Since biopile is an *ex situ* technique, the factors of interest were established and organized. The step *Selection, collection, and characterization of materials* constituted the cornerstone to implementing the material balance according to the procedure described in previous research (Gutiérrez *et al*., 2020).

   The factors of interest in the experiment were: texturizer content (% mass), moisture content (% mass), and the initial concentration of TPH ($mg.kg^{-1}$) in each experimental unit. The latter should be less than 50 000 $mg.kg^{-1}$ according to the effectiveness criterion established by EPA (2017).

4. Selecting the levels of each factor: The levels of the factors studied are shown in Table 1.

Table 1. Levels of the factors studied

Factors/Levels	Low (-1)	Medium (0)	High (+1)
Initial TPH concentration-X_1 ($mg.kg^{-1}$)	22 000	30 500	39 000
Texturizer content-X_2 (%)	4	8	12
Moisture content-X_3 (%)	20	25	30

Source: Authors

5. Selecting the appropriate design for the experiment goal and the factors of interest: the Response Surface Methodology was adopted, and a three-factor Box-Behnken was selected based on the criteria stated below.

   Box-Behnken designs are built by combining 2^n designs and incomplete block designs. This design is still considered to be more proficient and potent than other designs –such as the three-level complete factorial design, the central composite design (CCD), and the Doehlert design–, despite its poor coverage of the corner of the nonlinear design space (Karmoker *et al*., 2019). Specifically, for three factors, the Box-Behnken design has 15 treatments, where the coded factor levels exhibit a complete set of the treatment combinations for a 2^n factorial for each pair of factors at their high and low levels (-1; 1), accompanied by the middle level (0) of the remaining factor (12 treatments). In addition, three replicates of the center of the design (0, 0, 0) are included in accordance the criteria of Kuehl (2001) and Gutiérrez and de la Vara (2012).

   The design was executed in a single block. In addition, the order of the experiments was entirely randomized with the aim to protect the effect of hidden variables.

6. Planning and organizing the experimental work: A worksheet was designed with the specifications of each treatment, the order of the runs, and how the data would be collected. Furthermore, the personnel involved in each activity were defined, as well as the general and specific instructions to be followed at any moment, including the logistical needs and the work schedule.

7. Implementing the experiment: Implementation was carried out according to the design plan described in the previous items.

Experimental unit design

According to previous research, the established design principles, and criteria for biopile ecotechnology were adapted to the bench scale (BATTELLE-NFESC,1996; Wu and Coulon, 2015; Abdul and Webb, 2017; EPA, 2017; Martínez *et al*., 2017). In addition, the constraints imposed not only by the experimental array, but also by the dimensions of the experimental polygon, were considered.

As previously reported by Gutiérrez *et al*. (2020), a validated technical design protocol was implemented. This design included mass balance at the level of each experimental unit to determine the mass of each component in the biopile. According to the planning levels in the experimental design, the balance calculations assumed TPH concentrations of the only material in the biopile mixture, as well as the predefined percentage of texturizing agent in each experimental unit. Similarly, not only were the dimensions of the biopiles determined, but also the mass of nutrient amendments required to maintain the C:N:P:K ratio in the order of 100:10:1:0,1 respectively. Moreover, a simple random procedure was employed to intercalate each experimental unit in the polygon layout.

Experimental unit assembly

The preparation and stabilization of the system composed of waste and soils contaminated with hydrocarbons, as well as the conformation of the experimental units, were carried out according to previously established protocols (Gutiérrez *et al*., 2020). Furthermore, the mass balance calculations determined the mass of water to be added in order to achieve the required moisture percentage. Each biopile was shaped like a truncated pyramid, with a height of 0,2 m and an angle of 45° between the lateral pyramid faces and the bases. The initial total mass of each bench-scale biopile was set at 38 kg, varying the mass of the mixture's components depending on the experimental conditions in Table 1, and according to the adopted experimental array (Box-Behnken). Accordingly, the experimental units (treatments) had different dimensions (except for the three central points), varying in the range of 0,82-0,92 m regarding the length of the more extensive base of the truncated pyramid, and 0,55-0,61 m regarding its width. The shorter base dimensions varied in proportion to the larger ones, and their relationships with the established height and the angle of repose.

Experimental unit monitoring

The biopiles were monitored and controlled according to the following activities and times:

1. Homogenization and aeration (every 15 days): The solid substratum of each experimental unit was manually homogenized and aerated in its tray, destroying the initial geometry design (truncated pyramid) and intensively mixing all the mass, emphasizing the destruction of lumps.

2. Handling and shaping (every 15 days): Each time the experimental unit was homogenized and aerated, it was subsequently modeled according to the standardized relationship between the dimensions of the base, the height, and the angle of repose of each treatment, as well as the moisture content. To reduce variability, shape templates were established for this operation.

3. Humidification (every four days): The weight of water to be added to each experimental unit was determined via mass balance calculations, starting from the percentage of absolute water content, to achieve the final moisture percentage required, which agreed with the level array of this variable assigned to each treatment.

4. Temperature and water content monitoring (every seven days): The temperature (T) and water content (WC) were monitored and recorded on a worksheet designed for that purpose.

5. Physical-chemical monitoring (time: 0, 50, 100, and 240 days): The content of each experimental unit was sampled to determine the concentration of TPH by following the method described above. The biopiles were appropriately homogenized before the collection according to that described in item 1. Five samples with a mass of around 100 g were taken from the four corners of the basin and the center, alternating between bottom and surface samples. Finally, quartering was performed, and 100 g were taken to determine the TPH concentration. The samples were uniformly dried and grounded as part of the pretreatment to increase homogeneity. Then, they were spread on aluminum foil inside a room at a controlled temperature of 30 °C for 48 h.

Experimental design analysis

Afterwards, all of the data were statistically processed, and analyses were performed using a confidence level of 95% via the professional software STATGRAPHICS Centurion v. 16.1.18. In addition, Excel calculation books were used. During this stage, both tabular and graphical tests were performed. The main tests conducted were an Analysis of Variance (ANOVA), a Correlation Matrix and a Regression Coefficients Analysis, a Standardized Pareto Diagram, a Main Effects Graph, Interaction Graphs, and Response Graphs. Furthermore, the orthogonality and rotational properties were analyzed and associated with the model quality estimation.

The contribution of each term in the simple ANOVA to the explanation of the response variable was evaluated using the individual model coefficients, where p-Value<Statistic significance (α=0,05) indicates that the model terms are significant. The model was refined using variable selection by backward steps. Furthermore, it was verified that the model-adjusted coefficient of determination (R^2_{aj}) would be more significant than 70%, as recommended by Montgomery (2017).

Subsequently, the surface described by the validated individual models was explored in order to find the factor levels combination, which turned to be at an optimal point for the response variable. Moreover, simultaneous optimization was performed to obtain a compromise solution, not only to maximize the mass of TPH removed, but also to ensure compliance with the final concentration of TPH in the Cuban regulation for hydrocarbons final disposal, which establishes a maximum limit of 10 000 mg.kg^{-1} (ONN, 2017). In this line, the analytical method based on the desirability function was implemented as described in Montgomery (2017).

Finally, the assumptions of normality (normal probability plot), constant variance (residuals *vs.* predicted), and independence of the residuals (residuals *vs.* run number) were verified.

Results and discussion

Interpretation of the experimental design analysis results

Using the methods described above, the refined models' ANOVA for both response variables can be observed in Tables 2 and 3.

Table 2. ANOVA for the removed mass of TPH

Source	Sum of squares	Degree of freedom	Mean Squared	F-Ratio	P-Value
A: Initial TPH concentration	0,515 113	1	0,515 113	116,25	0,000 0
B: texturizer content	0,000 05	1	0,000 05	0,01	0,918 4
C: moisture content	0,009 112 5	1	0,009 112 5	2,06	0,194 7
AA	0,028 810 3	1	0,028 810 3	6,50	0,0381
BB	0,012 925 6	1	0,012 925 6	2,92	0,131 4
BC	0,065 025	1	0,065 025	14,68	0,006 5
CC	0,027 733 3	1	0,027 733 3	6,26	0,040 9
Total error	0,031 016 7	7	0,004 430 95		
Total (corr.)	0,694 693	14			

Source: Authors

In the individual model of removed mass, the initial TPH concentration (A) was significant. It was also corroborated that it was the factor with the most influence on the response variability. Furthermore, the initial TPH concentration (A) is also significant in the individual model of final TPH concentrations. It is also noteworthy that the effects of factors A and C are greater than that of factor B, given that, when the former are increased, they further modify the variability of the response.

Table 3. ANOVA for the TPH final concentration

Source	Sum of squares	Degree of freedom	Mean Squared	F-Ratio	P-Value
A: Initial TPH concentration	3,311 15E7	1	3,311 15E7	10,78	0,013 4
B: texturizer content	7,200E3	1	7,200E3	0,00	0,962 7
C: moisture content	6,183 77E6	1	6,183 77E6	2,01	0,198 8
AA	1,990 99E7	1	1,990 99E7	6,48	0,038 3
BB	9,270 06E6	1	9,270 06E6	3,02	0,125 9
BC	4,421 92E7	1	4,421 92E7	14,40	0,006 8
CC	2,046 68E7	1	2,046 68E7	6,67	0,036 4
Total error	2,149 3E7	7	3,070 43E6		
Total (corr.)	1,581 02E8	14			

Source: Authors

Although the first-order effects of the texturizer (B) and moisture (C) contents did not turn out to be significant, they were maintained in the models given the need to obtain a hierarchical model. Indeed, it is recognized that, in the Response Surface Methodology, this kind of model is preferred (Gutiérrez and de la Vara, 2012; Montgomery, 2017). Therefore, both terms were maintained in both models, as the BC interaction resulted to be significant. On the other hand, the quadratic interaction BB was also kept in both models because its elimination implied a decrease in the R^2_{aj}.

The fitted mathematical models that describe the behavior of the mass of TPH removed and the final TPH concentration are presented in Equations (2) and (3), respectively.

$$MR = -2,80477 - 0,0000417203 \cdot A + 0,217917 \cdot B + 0,231083 \cdot C + 1,15665 \cdot 10^{-9} \cdot A^2 - 0,00369792 \cdot B^2 - 0,006375 \cdot BC - 0,00346667 \cdot C \quad (2)$$

$$TPH_{t=240} = 75587 + 2,09287 \cdot A - 5733,09 \cdot B - 6214,54 \cdot C - 3,04062 \cdot 10^{-5} \cdot A^2 + 99,0312 \cdot B^2 + 166,244 \cdot BC + 94,175 \cdot C^2 \quad (3)$$

where:

MR: mass of TPH removed in the experimental unit (kg)
$TPH_{t = 240}$: TPH concentration in the experimental unit at 240 days (mg.kg^{-1}) (final concentration)
A: Initial TPH concentration (mg.kg^{-1})
B: Texturizer content (% mass)
C: Moisture content (% mass)

Reasonable coefficients of determination were obtained from Equations (2) and (3), R^2_{MR} = 95,54% and $R^2_{TPHt=240}$ = 86,41%. Although these results are barely lower than the R^2 reported in similar research (Agarry and Ogunleye, 2012; Zhang *et al.*, 2020), it could be inferred that the models, adjusted in this way, explain a considerable percentage of the total variability. On the other hand, according to the criteria given by Gutiérrez and de la Vara (2012), the adjusted coefficient of determination (R^2_{aj}) is more suitable for comparing the models of Equations (2) and (3). Regarding this issue, it yields values of R^2_{ajMR} = 91,07% and $R^2_{ajTPHt=240}$ = 72,81%; in both cases, the required 70%, in agreement with the criterium of Montgomery (2017), is appreciably exceeded. Consequently, Table 4 shows the final TPH concentration values obtained through laboratory tests of the samples obtained from monitoring and the values adjusted by the model of both response variables for each treatment and levels assigned to the three factors under study.

Table 4. Results of the observed and adjusted response variables

Treatments	Factors studied			Final concentration of TPH (mg·kg^{-1})		TPH mass removed (kg)	
	TPH (mg.kg^{-1})	Texturizer (%)	Moisture (%)	Observed value	Adjusted value	Observed value	Adjusted value
T1	39 000	8	20	11 639,00	11 318,40	1,05	1,07
T2	30 500	8	25	10 372,50	8 372,50	0,77	0,84
T3	30 500	12	30	15 040,00	14 787,10	0,59	0,60
T4	30 500	8	25	5 273,50	8 372,50	0,96	0,84
T5	22 000	8	20	7 432,00	7 249,50	0,55	0,56
T6	30 500	4	20	1 6232,50	16 485,40	0,55	0,54
T7	39 000	12	25	9 727,50	9 699,31	1,12	1,12
T8	30 500	12	20	9 645,50	9 895,69	0,80	0,79
T9	22 000	8	30	4 048,50	5 491,13	0,68	0,63
T10	39 000	4	25	8 351,00	9 639,31	1,18	1,13
T11	30 500	4	30	8 327,50	8 077,31	0,85	0,86
T12	22 000	12	25	5 599,50	5 630,44	0,62	0,62
T13	30 500	8	25	9 471,50	8 372,5	0,80	0,84
T14	22 000	4	25	6 861,50	5 570,44	0,57	0,62
T15	39 000	8	30	10 499,50	9 560,00	1,10	1,13

Source: Authors

By comparing the observed and adjusted values in Table 4, a similar behavior could be appreciated in the 15 treatments, with no sudden changes and variations, which is consistent with Agarry and Ogunleye (2012) and Shuo *et al*. (2019).

Figures 2 and 3 illustrate the estimated response surface mesh for both response variables under analysis.

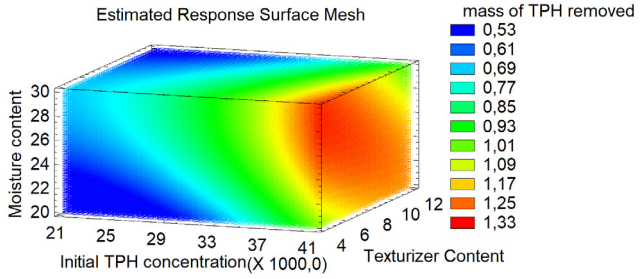

Figure 2. Estimated response surface mesh for the model regarding the mass of the TPH removed (kg)
Source: Authors

As shown in Figure 2, the highest mass of TPH removed (between 1,17 and 1,33 kg) is found in the region comprised simultaneously by the low and high levels of moisture and texturizer content, along with the high level of the initial TPH concentration.

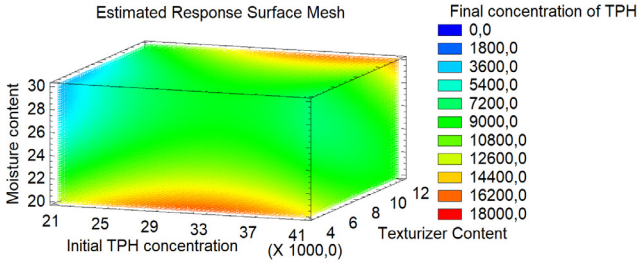

Figure 3. Response surface mesh for the final TPH concentration model (mg/kg)
Source: Authors

On the other hand, in Figure 3, it can be observed that the region with lower final concentrations of TPH (up to 5 400 mg.kg^{-1}) was found where there was a lower initial concentration of TPH and lower texturizer content but higher moisture content.

Table 5 shows the values of the studied factors for which the desirability was maximum (1), according to the results of the simultaneous optimization.

Table 5. Optimization of the desirability function

Factors /Levels	Low	High	Simultaneous optimum
Initial TPH concentration (mg.kg^{-1})	21 848	39 326	39 278
Texturizer content (%)	4	12	6,446 11
Moisture content (%)	20	30	25,946 4

Source: Authors

For the levels associated with desirability, a significant TPH mass of 1,19 kg was removed, representing 79,58% of the initial TPH concentration. Likewise, a final TPH concentration of 8 000 mg/kg was obtained, which reasonably complies with the final disposal standards of Cuba.

Figure 4 shows the estimated response surface plot for the desirability function, and Figure 5 shows the contour of the estimated response surface for the same function. In both cases, the moisture content factor was kept at its optimum value (25,95 %).

The optimum moisture content where the desirability was maximum (approximately 26%) is under the levels of moisture percentage by weight (12-30%) recommended by EPA (2017) for the design of biopiles.

In addition, the optimum also fits the qualitative criteria of manipulation, as evidenced during the experimental phase, because the experimental units with a high moisture content had severe difficulties in their handling. Specifically, these biopiles (30% of moisture content) exhibited marked differences from the ones in the medium and low levels regarding moisture content, thus producing puddling of the mass and a more significant generation of leachates, with a proven transfer of the pollutant to the aqueous medium.

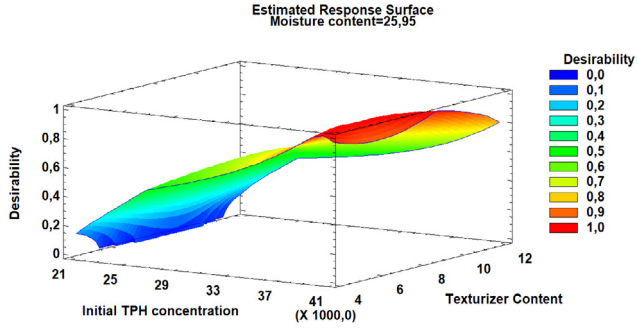

Figure 4. Estimated response surface for the desirability function keeping the % of moisture at its optimum level
Source: Authors

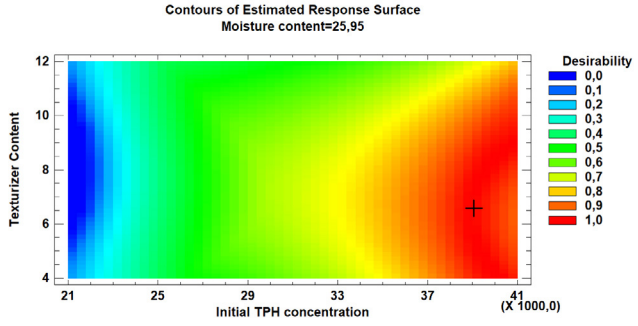

Figure 5. The contour of the estimated response surface for the desirability function keeps the moisture content at its optimum level
Source: Authors

By interpreting Figures 4 and 5, it can be confirmed how the values of the factors shown in Table 5 could achieve optimum desirability. In addition, it was observed that the desirability function is maintained around the maximum for texturizer content values between 6 and 10%, keeping the other two studied factors at their optimal values.

Additionally, the models' assumptions can be graphically verified for both response variables, as shown in the Appendices (Figures 6 and 7).

Conclusions

It was remarkable that the statistical analyses and the closeness of the experimental results and model predictions show the reliability of the regression model. The highest mass of TPH removed was obtained in the region defined by the high initial concentration of TPH and the levels from low to high regarding the texturizer and moisture contents. On the other hand, the lowest values for the final TPH concentrations were found in the region defined by the high moisture content factor and the low levels of both the initial TPH concentration and the texturizer content.

It was crucial to obtain a simultaneous optimum with initial concentration values of TPH of 39 278 $mg.kg^{-1}$, a texturizer content of 6,45%, and a moisture content of 25,95%. For these values, it was possible to maximize the mass of TPH removed and maintain the final TPH concentration of 8 000 $mg.kg^{-1}$, lower than that stipulated by the Cuban disposal standard. The mass of TPH removed remained in the range of the compromise solution for texturizer content values between 6 and 10%. At the same time, the other two factors studied were kept at their optimal values.

Finally, this research responded to a scientific demand for the continuity of the subsequent stage of the research-development BIOPILA project. The results are encouraging and should be validated during the ecotechnology scale-up processes, *i.e.*, into a pilot scale.

Acknowledgments

The authors are grateful for the funding provided by the Science of National Interest Program *Sustainable use of the components of biological diversity in Cuba*, managed by the Cuban Environment Agency of the Ministry of Science, Technology, and the Environment.

CRediT author statement

All authors: Conceptualization, methodology, validation, formal analysis, investigation, writing (original draft preparation, review, and editing), data curation, supervision, project administration, resources, and funding acquisition.

References

Abdul, M., and Webb, C. (2017). Design aspects of solid-state fermentation as applied to microbial bioprocessing. *Journal of Applied Biotechnology & Bioengineering, 4*(1), 1-25. https://doi.org/10.15406/jabb.2017.04.00094

Agarry, S., and Ogunleye, O. (2012). Box-Behnken design application to study enhanced bioremediation of soil artificially contaminated with spent engine oil using biostimulation strategy. *International Journal of Energy and Environmental Engineering, 3*(31), 1-14. https://doi.org/10.1186/2251-6832-3-31

Al-Hawash, A. B., Dragh, M. A., Li, S., Alhujaily, A., Abbood, A., Zhang, X., and Fuying, M. (2018). Principles of microbial degradation of petroleum hydrocarbons in the environment. *The Egyptian Journal of Aquatic Research, 44*(2), 71-76. https://doi.org/10.1016/j.ejar.2018.06.001

ASTM International (2002). *D 422 -63. Standard test method for particle-size analysis of soils*. ASTM International. https://civillabs.kashanu.ac.ir/file/download/page/1593845138-d-422-63-r02-rdqymg-.pdf

ASTM International (2017). *D2487. Standard practice for engineering purpose soil classification*. ASTM International. https://civilnode.com/download-standard/10667907375737/astm-d2487-standard-practice-for-classification-of-soils-for-engineering-purposes-unified-soil-classification-system

BATTELLE-NFESC (1996). *Biopile design and construction manual. Technical Memorandum TM-2189-ENV*. BATTELLE Environmental Restoration Department and Naval Facilities Engineering Service Center (NFESC). https://clu-in.org/download/techfocus/bio/Biopile-design-and-construction-1996-tm-2189.pdf

Casals, E., Rabassa, D., Viera, O., Gutiérrez, O., and Castro, D. (2020). Comportamiento de factores abióticos en la biorremediación de residuos petrolizados mediante biopilas a escala semi-piloto. *Centro Azúcar, 47*(3), 36-46. http://hdl.handle.net/11583/2870192

Castro Rodríguez, D. J., Jiménez González, Y., Gutiérrez Benítez, O., Viera Ribot, O. M., Rabassa Rabassa, D., Casals Pérez, E., and Demichela, M. (2022a). Quality function deployment to determine the design requirements in experimental biopiles at bench-scale, evaluated as a resilient strategy for the degradation of oily waste. *Ingeniare. Revista Chilena de ingeniería,* 30(3), 439-454. https://dx.doi.org/10.4067/S0718-33052022000300439

Castro, D., González, Y., Gutiérrez, O., Viera, O., Casals, E., Rabassa, D., and Demichela M. (2022b). QFD to determine experimental biopiles requirements, evaluated at bench-scale as a resilient strategy against soil contamination with oil residues. *Chemical Engineering Transactions, 91*, 1-6. https://dx.doi.org/10.3303/CET2291084

Castro, D., Gutiérrez, O., Casals, E., Demichela, M., Godio, A., and Chiampo, F. (2022c). Bioremediation of hydrocarbon-polluted soil: Evaluation of different operative parameters. *Applied Sciences, 12*(4) 2012. https://doi.org/10.3390/app12042012

Castro Rodríguez, D. J., Gutiérrez Benítez, O., Casals Pérez, E., Demichela, M., Godio, A., and Chiampo, F. (2022d). Categorical multifactor design to evaluate different operative

parameters during the bioremediation of hydrocarbon-polluted soil in early experimental stages. In AIDIC (Eds.), *Proceedings of the GRICU 2022: Centralità dell'Ingegneria Chimica in un-Mondo che cambia. Book of abstracts*. AIDIC-Associazione Italiana di Ingegneria Chimica. (pp. 294-297) https://dx.doi.org/10.3303/BOA2201

Casale, A., Bosco, F., Chiampo, F., Franco, D., Ruffino, B., Godio, A., and Pujari, P. R. (2018). Soil microcosm set up for a bioremediation study. In The IRED (Eds.), *Proceedings of the Sixth International Conference on Advances in Bio-Informatics, Bio-Technology and Environmental Engineering* (pp. 12-15). The IRED. https://doi.org/10.15224/978-1-63248-148-1-03

CITMA (n.d.). *Proyecto Estrategia Ambiental Territorial. Provincia de Cienfuegos 2021/2030. Etapa 2021-2025". 2021*. Ministerio de Ciencia, Tecnología y Medio Ambiente de Cuba (CITMA). https://www.scribd.com/document/556922951/Estrategia-Ambiental-Territorrial-Cienfuegos-2021-2030

de Oliveira, J. V., Alves, Y. L., De Souza, L. L., De Lacerda, I. M., Brandão, S., and Ferro, I. M. (2018). Use of bioremediation for the removal of petroleum hydrocarbons from the soil: An overview. *International Journal of Environment, Agriculture and Biotechnology, 3*(5), 1831-1838. http://dx.doi.org/10.22161/ijeab/3.5.35

Environmental Protection Agency (EPA) (2017). *How to evaluate alternative cleanup technologies for underground storage tank sites. A guide for corrective action plan reviewers. Chapter: IV Biopiles* (*EPA 510-B-17-003*). EPA. https://www.epa.gov/sites/production/files/2014-03/documents/tum_ch4.pdf

Gutiérrez, H., and de la Vara, R. (2012). *Análisis y diseño de experimentos* (3rd ed.). McGraw-Hill/Interamericana Editores, S. A. de C. V..

Gutiérrez, O. Castro, D., Viera, O., Casals, E., and Rabassa, D. (2021). Cinética de la degradación de hidrocarburos mediante biopilas a escala de banco. *Tecnología Química, 41*(2), 349-369. https://tecnologiaquimica.uo.edu.cu/index.php/tq/article/view/5197

Gutiérrez, O., Castro, D., Viera, O., Casals, E., and Rabassa, D. (2020). Diseño ingeniero y montaje de unidades experimentales para la biorremediación de residuos petrolizados a escala de banco. *Tecnología Química, 40*(3), 564-562. https://tecnologiaquimica.uo.edu.cu/index.php/tq/article/view/5168

Khaled, M., Saleh, M., and Majid A. (2016). Bioremediation of diesel fuel by fungal consortium using statistical experimental designs. *Polish Journal of Environmental Studies, 25*(1), 1-10. https://doi.org/10.15244/pjoes/42493

Kumar, A., Bisht, B., Joshi, V., and Dhewa, T. (2011). Review on bioremediation of polluted environment: a management tool. *International Journal of Environmental Sciences, 1*(6), 1079-1093. https://www.researchgate.net/publication/284061537_Review_on_bioremediation_of_polluted_environment_A_management_tool

Karmoker, J. R., Hasan, I., Ahmed, N., Saifuddin, M., and Reza, M. S. (2019). Development and optimization of acyclovir loaded mucoadhesive microspheres by Box -Behnken design. *Dhaka University Journal of Pharmaceutical Sciences, 18*(11), 1-12. https://doi.org/10.3329/dujps.v18i1.41421

Kuehl, R. O. (2001). *Principios estadísticos para el diseño y análisis de investigaciones* (2nd ed.). Thompson/Learning.

Martinez L., Ruberto, L., Lo Balbo A., and Mac Cormack, W. (2017). Bioremediation of hydrocarbon-contaminated soils in cold regions: Development of a pre-optimized biostimulation biopile-scale field assay in Antarctica. *Science of the Total Environment, 590-591*, 194-203. https://doi.org/10.1016/j.scitotenv.2017.02.204

Martinez, L. M., Lo Balbo A., Mac, W. P., and Ruberto, A. M. (2015). Bioremediation of a petroleum hydrocarbon-contaminated Antarctic soil: Optimization of a biostimulation strategy using response-surface methodologyn (RSM). *Cold Regions Science and Technology, 119*, 61-67. https://doi.org/10.1016/j.coldregions.2015.07.005

Montgomery, D. C. (2017). *Design and analysis of experiments* (9th ed.). John Wiley & Sons Inc.

Oficina Nacional de Normalización (ONN) (2017) *Manejo de fondaje de tanques de almacenamiento de petróleo y sus derivados*. (*NC 819: 2017*). *Norma Cubana*. Oficina Nacional de Normalización (ONN).

Ossai, I. C., Ahmed, A., Hassan, A., Shahul, F., and Ball, A. S. (2020). Remediation of soil and water contaminated with petroleum hydrocarbon: A review. *Environmental Technology and Innovation, 17*, 100526. https://doi.org/10.1016/j.eti.2019.100526

Prakash, V., Saxena, S., Sharma, A., Singh, S., Silva, A., and Kumar, S. (2015). Treatment of oil sludge contamination by composting. *Journal of Bioremediation & Biodegradation, 6*(3), 1-6. https://doi.org/10.4172/2155-6199.1000284

Riser-Robert, E. (2019) *Remediation of petroleum contaminated soils: Biological, physical, and chemical processes*. CRC Press. Taylor & Francis Group. https://doi.org/10.1007/BF03037726

Shuo, S., Qiyou, L., Shuiquan, C., Wenhe, Y., Chaocheng Z., and Hongkun, C. (2019) Optimization for microbial degradation of petroleum hydrocarbon (TPH) by Enterobacter sp. S-1 using response surface methodology. *Petroleum Science and Technology, 37*(7), 821-828. https://doi.org/10.1080/10916466.2019.1566256

Shahryar, J. (2017). Environmental impacts of the petroleum industry. In J. Sharyar (Ed.), *Petroleum Waste Treatment and Pollution Control* (vol. 3, pp. 86-115). Butterworth-Heinemann. https://doi.org/10.1016/B978-0-12-809243-9.00007-9

Thapa, B., Kumar, A., and Ghimire, A. (2012) A review on bioremediation of petroleum hydrocarbon contaminants in soil. *Kathmandu University Journal of Science, Engineering and Technology, 8*(1), 164-170. https://doi.org/10.3126/kuset.v8i1.6056

Tyagi, M., da Fonseca M. M. R., and de Carvalho, C. C. R. (2011). Bioaugmentation and biostimulation strategies to improve the effectiveness of bioremediation processes. *Biodegradation, 22*, 231-241. https://doi.org/10.1007/s10532-010-9394-4

Varjani, S. (2017). Microbial degradation of petroleum hydrocarbons. *Bioresource Technology, 223*(2017), 276-286. https://doi.org/10.1016/j.biortech.2016.10.037

Velasco, J. A., and Volke, T. L. (2003). El composteo: una alternativa tecnológica para la biorremediación de suelos en México. *Gaceta Ecológica, 66*, 41-53. https://www.redalyc.org/pdf/539/53906604.pdf

Volke, T. L., and Velasco, J. A. (2002). *Tecnologías de remedia-*

ción para suelos contaminados. Instituto Nacional de Ecología (INE-SEMARNAT). http://www.ecopuerto.com/Bicentenario/informes/TecnologiasRemediacion.pdf

Wu, G., and Coulon, F. (2015). Protocol for biopile construction treating contaminated soils with petroleum hydrocarbons. In T, McGenity, K. Timmis, and B. Nogales (Eds.), *Hydrocarbon and Lipid Microbiology Protocols* (pp. 181-194). Springer. https://doi.org/10.1007/8623_2015_149

Yuniati, M. D. (2017). Bioremediation of petroleum-contaminated soil: A Review. I*OP Conference Series: Earth and Environmental Science, 118*, 18-19. http://doi.org/10.1088/1755-1315/118/1/012063

Zhang, C., Wu, D., and Ren, H. (2020). Bioremediation of oil contaminated soil using agricultural wastes via microbial consortium. *Scientific Reports, 10*, 9188. https://doi.org/10.1038/s41598-020-66169-5

Appendices

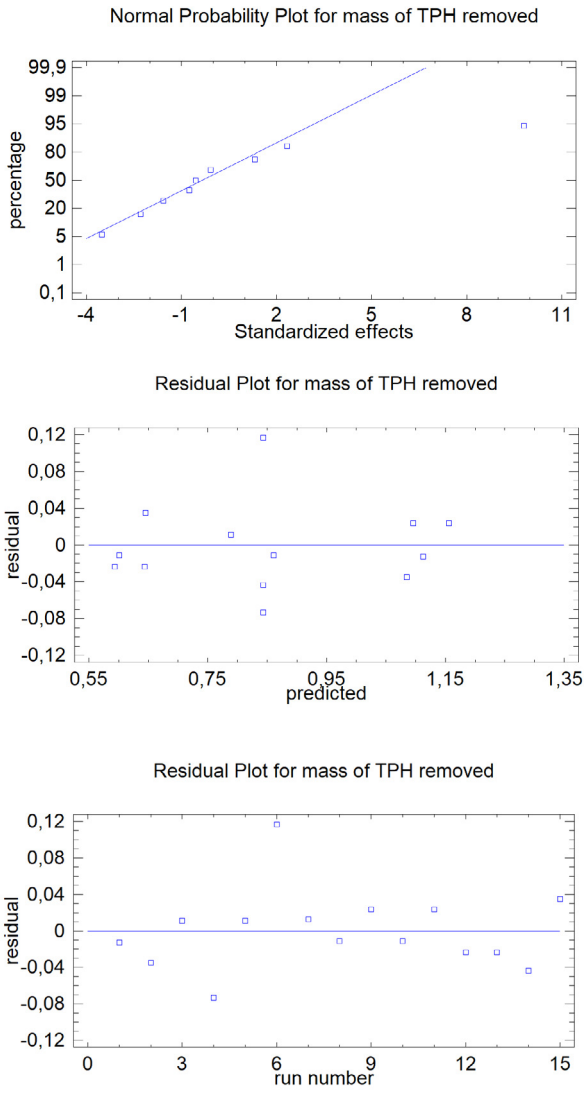

Figure 6. Assumption analysis of the mass model of TPH removed: a) normal probability plot, b) residuals *vs.* predicted (equality of variance), and c) residuals *vs.* row number (independence)
Source: Authors

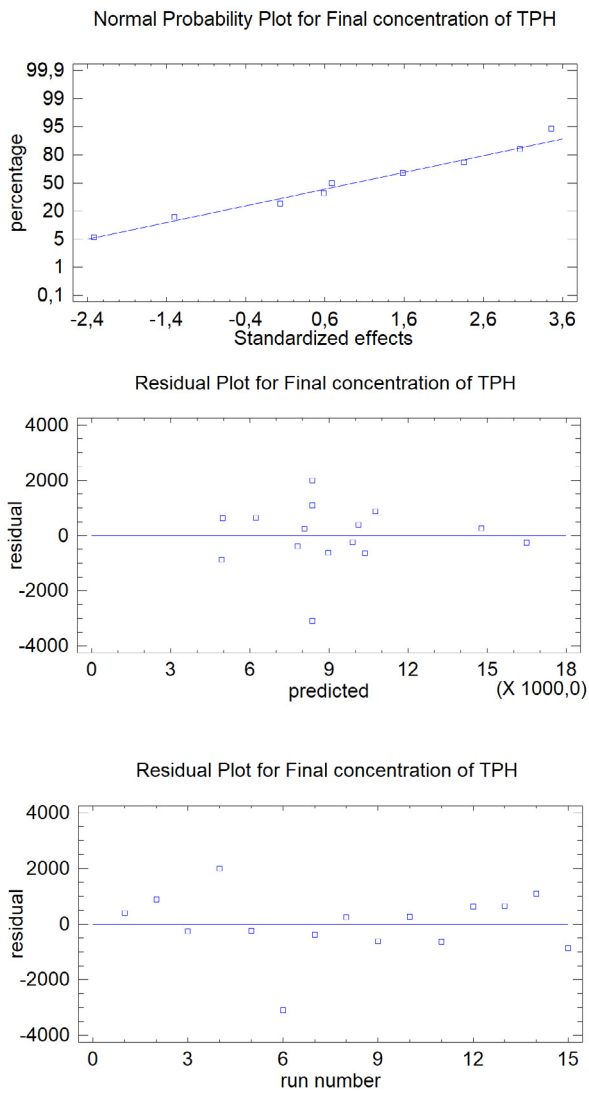

Figure 7. Assumption analysis of the final TPH concentration model: a) normal probability plot, b) residuals *vs.* predicted (equality of variance), c) residuals *vs.* row number (independence)
Source: Authors

Regarding the graphical analyses corresponding to Figure 6a and Figure 7a, a good fitness to the normal distribution was corroborated for both models. Similarly, in Figures 6b and 6c, as well as in Figures 7b and 7c, there were no significant patterns indicating a lack of randomness or independence.

Ingeniería e Investigación vol. 43 No. 2, August - 2023 (e96125)
Research Article/ Chemical, Food, and Environmental Engineering
https://doi.org/10.15446/ing.investig.96125

School Children's exposure to $PM_{2,5}$ in a high pollution area of Bogotá, Colombia

Exposición de niños en edad escolar a $PM_{2,5}$ en una zona de alta contaminación de Bogotá, Colombia

Yisel A. Vargas-Legarda [1], Adriana K. Toro-Martínez [2], Néstor Y. Rojas-Roa [3], and Oscar A. Fajardo-Montaña [4]

ABSTRACT

Approximately 93% of the world's children under 15 are exposed to ambient $PM_{2,5}$ levels exceeding the World Health Organization's guidelines. $PM_{2,5}$ and other air pollutants affect children's mental and motor development, as well as their lung function, even at low concentrations. In low- and middle-income countries, the effects are potentially stronger because of the weaker land-use policies in place, which increases households' proximity to industrial sources. Such is the case of areas with mixed land use in western Bogotá, Colombia. In this work, the exposure of children to $PM_{2,5}$ at a school in the Puente Aranda district was estimated. $PM_{2,5}$ concentrations were measured using low-volume area samplers during school hours in February 2020. Information on the children's daily activity was recorded in order to estimate the physical effort applied during their normal school activities, and the minors' respiratory symptomatologies were consulted with their parents. The inhaled dose was estimated using inhalation rates. The results showed that children aged three to five inhale the highest doses and report higher rates of respiratory symptoms. Indoor $PM_{2,5}$ concentrations were consistently higher, agreeing with previous reports, probably because of dust resuspension and poor classroom ventilation. Air pollution mitigation measures must be put into effect in order to protect this highly vulnerable population. These measures will also positively affect the safe return of students to school activities after the pandemic lockdown.

Keywords: air pollution, children's exposure, fine particulate matter, inhalation of pollutants

RESUMEN

Aproximadamente el 93 % de los niños menores de 15 años del mundo están expuestos a niveles ambientales de $PM_{2,5}$ que superan las directrices de la Organización Mundial de la Salud. El $PM_{2,5}$ y otros contaminantes del aire afectan el desarrollo mental y motor de los niños, así como su función pulmonar, incluso en concentraciones bajas. En los países de ingresos bajos y medios, los efectos son potencialmente más fuertes debido a la existencia de políticas de uso de la tierra más débiles, lo cual aumenta la proximidad de los hogares a las fuentes industriales. Tal es el caso de las áreas con uso mixto de suelo en el occidente de Bogotá, Colombia. En este trabajo se estimó la exposición de niños a $PM_{2,5}$ en una escuela del distrito de Puente Aranda. Las concentraciones de $PM_{2,5}$ se midieron utilizando muestreadores de área de bajo volumen durante el horario escolar en febrero de 2020. Se registró información sobre la actividad diaria de los niños para estimar su tasa metabólica en base al esfuerzo físico aplicado a cada actividad escolar. Además, la dosis inhalada se estimó utilizando las tasas de inhalación, y se consultaron sintomatologías respiratorias de los menores con sus padres. Los resultados mostraron que los niños de 3 a 5 años inhalan las dosis más altas y reportan las tasas más altas de síntomas respiratorios. Las concentraciones de $PM_{2,5}$ en interiores fueron consistentemente más altas, probablemente debido a la resuspensión del polvo y la mala ventilación del aula. Se deben implementar medidas de mitigación de la contaminación del aire para proteger a esta población altamente vulnerable. Estas medidas también afectarán positivamente el retorno seguro de los estudiantes a las actividades escolares después del confinamiento de la pandemia.

Palabras clave: contaminación atmosférica, exposición infantil, material particulado fino, inhalación de contaminantes

Received: May 25th, 2021
Accepted: February 10th, 2023

Introduction

Air pollution is the world's most considerable environmental risk to human health, according to the World Health Organization (WHO, 2019). It has become a global problem of great importance, which is associated with environmental deterioration and morbidity from respiratory diseases in specific populations such as children, pregnant women, and elderly adults (UNICEF, 2016). In the case of children, vulnerability is due to their higher breathing rate, lower body mass, and developing immune system (American Academy of Paediatrics, 2004). Fine particles can penetrate deep into the airways and even reach the bloodstream, causing a variety of harmful effects (Oyarzún, 2010). Increases in $PM_{2,5}$ concentrations are associated with increases in daily and long-term mortality and morbidity (WHO, 2018), and they can entail school absenteeism for children under the age of five in areas of high air pollution. On the other hand, and considering the current situation with

[1]Environmental engineer, Universidad Central, Colombia. E-mail: yvargasl@ucentral.edu.co
[2]Environmental engineer, Universidad Central, Colombia. E-mail: atorom@ucentral.edu.co
[3]PhD University of Leeds, UK. Affiliation: Associate professor, Universidad Nacional de Colombia, Colombia. E-mail: nyrojasr@unal.edu.co
[4]PhD in Environmental Science and Engineering, Tsinghua University, China. Affiliation: Associate professor, Research Cluster of Converging Sciences and Technologies, Universidad Central, Colombia. E-mail: ofajardom@ucentral.edu.co

How to cite: Vargas-Legarda, Y. A., Toro-Martínez, A. K., Rojas-Roa, N. Y., and Fajardo-Montaña, O. A. (2023). School Children's exposure to $PM_{2,5}$ in a high pollution area of Bogotá, Colombiae. *Ingeniería e Investigación*, *43*(2), e96125. https://doi.org/10.15446/ing.investig.96125

regard to COVID-19, scientific studies have shown that air pollution increases the risk of medical complications. In countries such as Italy, France, Germany, and Spain, it is inferred that high concentrations of pollutants in the air could be the most critical aggravating factor of the mortality caused by the virus (Ogen, 2020). Multiple scientific studies worldwide have analyzed schoolchildren's exposure to $PM_{2,5}$ in order to assess impacts. In China, Chen *et al.* (2019) determined the exposure of minors to $PM_{2,5}$ concentrations by gravimetric analysis using a battery-powered mini-sampler, taking samples for 24 hours for two years and evidencing long-term problems in the neuronal, respiratory, and cardiac systems. Likewise, in a study carried out in New Zealand, Bennett *et al.* (2019) performed measurements of $PM_{2,5}$ indoors in order to analyze the concentrations and sources of air pollution in a primary school for children between the ages of five and 11 over a period of three weeks, indicating that the main driver of $PM_{2,5}$ indoors was the infiltration of pollutants, whose main contributor were the by-products of emissions from motor vehicles. On the other hand, in the national context, Franco *et al.* (2009) characterized the concentration levels of PM10, for district schools located in high traffic corridors of the city of Bogotá, obtaining high concentrations of the pollutant inside the institutions, which exceeded the values considered harmful for sensitive populations according to the WHO.

This study aimed to evaluate particulate matter concentrations to which schoolchildren are exposed, as well as the potential inhaled doses that they may receive during their schooling time in an industrial sector of Bogotá.

Materials and methods

Sampling site selection

The interest of this study was to evaluate the air quality of a school located within industrial area of the city, in order to assess the levels of PM that students are exposed to. The district of Puente Aranda was designated as an industrial zone since 1974 and became a pole of industrial development in the capital, with an extensive production of plastic, chemicals, textiles, metalworking, beverages, and food, with a large number of industries in the sector. However, its use has been changing, and it has lately become a more commercial and residential area. A number of industrial plants have left the area for other municipalities, especially Mosquera, Funza, Madrid, and Fusagasugá in the outskirts of the city (Bogotá City Hall, 2012).

For this study, the sampling sites were located in Gimnasio San Valery, which offers grades from preschool to fifth grade and a total of 103 students with an age range between four and ten. The school is located in a single, three-level building with immediate access to a public park for recreational and sport activities. This school maintains the typical structure of many small private institutions, nowadays common in the city, with a single building containing all academic spaces and using the public parks nearby for sport and leisure activities.

The Puente Aranda and Carvajal-Sevillana stations of the air quality monitoring network (RMCAB) are located 1,9 km north and 3,6 km southwest of the school (Figure 1), respectively. This study used $PM_{2,5}$ concentrations and wind direction reports from these stations for reference. Data are accessible in the network's website http://rmcab.ambientebogota.gov.co/.

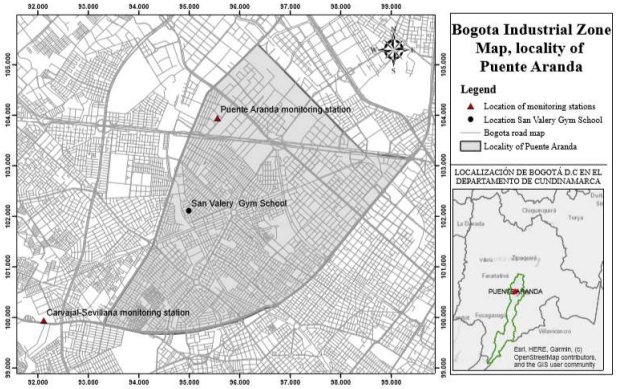

Figure 1. Location of the sampling site and the Puente Aranda and Carvajal-Sevillana air quality monitoring stations
Source: Authors

Data obtained from the RMCAB allowed for a comparison of concentration behaviors with the *in situ* samplings carried out during this research, in ranges of 48 hours corresponding to the same sampling times.

In the surroundings of the sampling site (Gimnasio San Valery School, Figure 2), there is a road axis with circulation of collective public transport, as well as abundant adjacent industries outside a radius of 1 km. In the district, the landscape is predominantly industrial, with warehouses, factories, and large houses established for commerce and services.

Figure 2. Images of Gimnasio San Valery and its surroundings
Source: Authors

A green zone in the area corresponds to the Camelia neighbourhood park, located in front of the school, an area used daily as a rest area, as well as for recreation and school activities, as seen in Figure 2.

Estimation of potential doses inhaled and inhalation rates

To calculate the potential dose inhaled by age range and gender, the following relationship was used:

$$Potential\ dose = PM_{2,5} \cdot ventilation\ rate \cdot t \qquad (1)$$

where the potential dose is in μg, $PM_{2,5}$ denotes the particulate matter concentration ($\mu g/m^3$), the ventilation

rate is in m^3/min, and t is the exposure time by exertion level (min).

As a method to calculate the inhalation rate and obtain statistical data regarding human exposure to environmental agents, the *EPA Exposure Factors Handbook* was used as a reference document (EPA, 2011), which provides inhalation rates with descriptive statistics for the average ventilation rate (m^3/min), based on variables of gender and age range for activities of diverse exertion levels.

Sedentary and passive activities are defined as sitting and standing; light intensity activities as walking at a speed between 0,7 and 1,3 m/s; moderate intensity activities as fast walking (between 1,4 and 1,8 m/s) and slow running (between 1,6 and 1,8 m/s); and high intensity activities are defined as fast running (between 2,0 and 2,7 m/s).

Through a rubric, the activities performed by the students and their times were collected, in order to establish a relationship with the inhalation rates and the duration of such events. The activities considered in this study were class time, recess time in common areas (indoors), and outdoor sports activities.

$PM_{2,5}$ mass concentrations

Particulate matter concentrations were determined during school days for sampling periods of 48 hours over a two-week sampling campaign. Indoor and outdoor $PM_{2,5}$ sampling was performed using two low-volume area samplers (Chemcomb 3500) (Figure 3) and 37 mm, 2 microns pore Teflon filters (Whatman, GE Healthcare). The filters were weighed before and after sampling using a Sartorius analytical balance (M5P-000V001), after conditioning in a desiccator at 23 °C and 45% relative humidity for 24 hours.

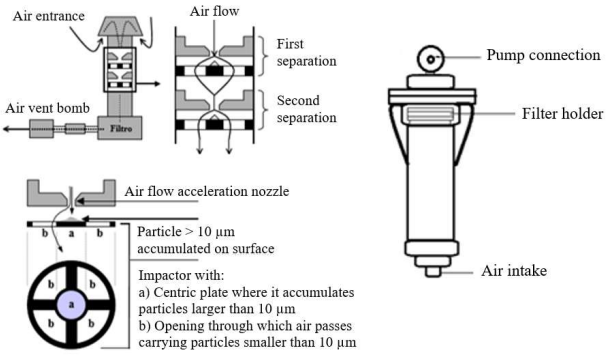

Figure 3. Schematic diagram of the area samplers
Source: Oliva *et al.* (2001)

Respiratory symptoms in children

A survey was conducted to characterize children's respiratory symptoms, which was based on the ISAAC questionnaire (International Study on Asthma and Allergies in Childhood) and its adaptation in Colombia, *i.e.*, *Validation of the Spanish version of the ISAAC phase III questionnaire on asthma* (Mata-Fernández *et al.*, 2005), which collected information on intramural and extramural factors, referring to the existing conditions both in Gimnasio San Valery and at the students' homes.

Results and discussion

$PM_{2,5}$ concentrations in the study area

Figure 4 shows the $PM_{2,5}$ concentrations obtained *in situ* during the monitoring campaign. Similarly, Figure 5a shows the concentrations at the Puente Aranda and Carvajal-Sevillana stations, reported by RMCAB in the same time frame, *vs.* the *in situ* concentrations. During the sampling period, a high air pollution alert was declared in the city, whose duration can be observed in the Figure (shadow colors).

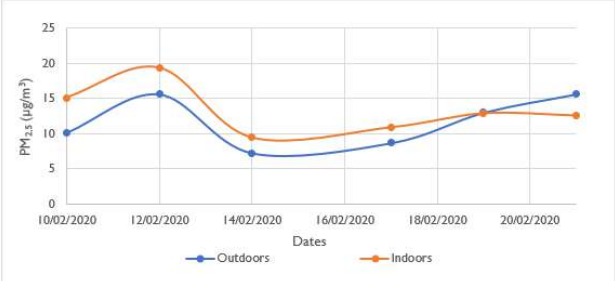

Figure 4. Concentrations of extramural *vs.* intramural $PM_{2,5}$ from the sampling site
Source: Authors

Within the school, indoor concentrations were off up to 19,3 $\pm$ 0,6 $\mu g/m^3$, always higher than those outdoors, where concentrations reached 15,6 $\pm$ 0,2 $\mu g/m^3$. This difference is considered to be possible due to the resuspension of dust and the low air exchange capacity, which causes the particles to accumulate inside. These findings are in apparent agreement with Bennett *et al.* (2019), Carrion *et al.* (2019), Hernández *et al.* (2013), and Franco *et al.* (2009), where indoors concentrations were reported over the outdoor levels.

An inversion of indoors and outdoors concentrations occurred from 02/19/2020 onwards (Figure 5a). Outdoor concentrations followed a similar trend to that of Puente Aranda station, evidencing a more significant influence of industrial emissions from the air currents of this specific area, which was caused by the local winds.

The concentrations determined *in situ* were found to be lower than those reported by the monitoring stations, albeit with similar trends. During 12/02/2020, a $PM_{2,5}$ concentration peak was observed (the maximum for the period analyzed). This behavior may be associated with the low wind speeds that occurred on that date, reducing the dispersion capacity of the atmosphere and causing higher concentrations of $PM_{2,5}$. Under those meteorological conditions, which were occurring for some days at the time, the environmental authority of the city (SDA) responded to the contingency by declaring a yellow alert for some districts, including the one studied herein (*i.e.*, Puente Aranda). This is represented in Figure 5a with a yellow shadow for the duration of the yellow alert, with green showing the sampling concentrations after the yellow alert was lifted. The Puente Aranda monitoring station recorded concentrations of up to 32,42 $\mu g/m^3$, and Carvajal-Sevillana significantly showed higher concentrations, *i.e.*, up to 43,73 $\mu g/m^3$, possibly evidencing regional transport (Carrion *et al.*, 2019). For the sake of comparison regarding the pollution levels in this industrial area, it is possible to visualize the difference

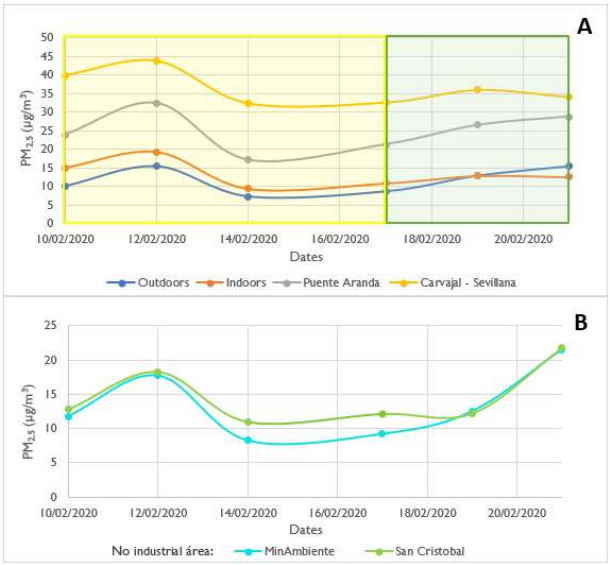

Figure 5. a) $PM_{2,5}$ concentrations from the sampling site and the air quality monitoring stations (Puente Aranda and Carvajal-Sevillana), b) monitoring stations in non-industrial areas of the city for the same period
Source: Authors

in concentration with non-industrial areas of the city for the same sampling period, as shown in Figure 5b. The selected non-industrial areas are located in the district of Santa Fe, in the Northeast (NE) of Bogotá, as reported by the MinAmbiente air quality monitoring station; and in the district of San Cristóbal, in the Southeast (SE) of the city, via the San Cristóbal station. In Figure 5b, it can be seen that the concentrations in this industrial zone can double the exposure concentrations of the other two non-industrial stations. Note that the MinAmbiente monitoring station reaches concentration peaks of up to 21,49 $\mu g/m^3$, followed by San Cristóbal with concentrations of up to 21,76 $\mu g/m^3$, unlike the industrial zone corresponding to the Carvajal-Sevillana monitoring station, with significantly higher $PM_{2,5}$ concentrations (up to 43,73 $\mu g/m^3$) and the Puente Aranda station, with concentration peaks of up to 32,42 $\mu g/m^3$.

Estimated inhalation rates

The inhalation rates of children shown in Tables 1 and 2, which are presented by gender, age-range, and type of activity as indicated in the EPA Exposure Factors Handbook, along with the daily activity times, allowed assessing the air volumes that each evaluated group might be inhaling during their school time. The volume of inhaled air was determined by multiplying the activity time by the inhalation rate according to the level of activity or physical effort of each time slot, by course and by gender.

Table 1. Descriptive statistics for average ventilation rate, unadjusted for body weight, while performing activities within the specified category (males by age category)

Age	Activity level	Inhalation rate (m^3/min)
3 to <6	Sedentary	0,00458
	Light	0,0114
	Moderate	0,0210
	Heavy	0,0390
6 a <11	Sedentary	0,00487
	Light	0,0116
	Moderate	0,0223
	Heavy	0,0436

Source: EPA (2011)

Table 2. Descriptive statistics for average ventilation rate, unadjusted for body weight, while performing activities within the specified category (females by age category)

Age	Activity level	Inhalation rate (m^3/min)
3 to <6	Sedentary	0,0044
	Light	0,0109
	Moderate	0,0200
	Heavy	0,0345
6 a <11	Sedentary	0,00464
	Light	0,0111
	Moderate	0,0210
	Heavy	0,0394

Source: EPA (2011)

The children activities considered herein are categorized as sedentary activity (sitting and standing), light activity (walking), moderate activity (fast walking and slow running), and heavy activity (fast running during sports classes). All these activities were recorded by gender and age range (three to five and six to ten years old) (Tables 3 and 4):

Table 3. Daily activity times for preschool and first grade (three to five years of age)

	Duration (min)	Description of activities	Activity density
Time in class-rooms	355	The school day begins at 6:30 a.m. and continues until 9:30 a.m. It is resumed at 10:15 a.m. and goes until 1:00 p.m. Students generally remain in the classroom during each class, sitting at their desks or sometimes doing short play activities in the classroom.	Sedentary
Recreation time, common areas within the insti-tution	20	At this time, the students eat their snacks on the first floor in a small *patio* and then go out to the park. In this space, they remain mostly seated, except when they go to throw the garbage in the trash can.	Light
Exposure time outside	25	The students are accompanied by their course director to move around the park as they wish while sharing with their classmates. Some children sit and others participate in play and recreation activities, being active and dynamic, such as running or moving to the small playground.	Moderate
Sports class	45	Sports classes last 45 minutes and are given once a week, where the students, accompanied by the teacher, in charge go out and perform an exercise routine, such as running, fast walking, and active games. This, in order to develop coordination and object manipulation skills.	Heavy

Source: Authors

Table 4. Daily activity times for second to fifth grades (six to ten years of age)

	Duration (min)	Description of activities	Activity density
Time in class-rooms	355	Classes start at 6:30 a.m. and continue until 9:30 a.m.. They are resumed at 10:15 a.m. and go until 1:00 p.m. Students generally remain in the classroom during each class hour, sitting at their desks. Here, they sometimes carry out short play activities.	Sedentary
Recreation time, common areas within the insti-tution	20	Students in second and third grade share in the first-floor hallway, whereas the fourth and fifth grades are usually in the classrooms. Fifth graders are also selected to help maintain order in the classrooms. Once the snack time is over, the children leave for the park.	Light
Exposure time outside	25	Students in second and third grade move around the park as they please, walking or sitting beside their peers. Fourth and fifth graders mostly play soccer or run around the park. They are active and dynamic.	Moderate
Sports class	90	Physical education classes for grades 2-5 last 90 minutes and are given once a week, where the students, accompanied by the teacher in charge, go out and perform an exercise routine based on speed, coordination, and motor skills development.	Heavy

Source: Authors

Estimated potential doses

The $PM_{2,5}$ dose was determined via Equation 1, with the inhalation volumes and the concentrations determined *in situ*. The following Figures display the daily doses by age and gender evaluated.

Figure 6 presents the behavior of the potential doses received in each analyzed group during the sampling period. The greatest dose values correspond to boys, in comparison with girls' doses during different activities, which is due to their slightly larger inhaled volumes. The trend observed in the Figures is similar to that of Figure 5a, implying that the $PM_{2,5}$ concentrations in the children's environment are directly proportional to the potential dose that can be received, particularly during sports class day. Hence, heavy activity is the most significant parameter, even with less exposure time, due to the greater exertion required during the activity.

Preschool grade children reported high dose peaks on 12/02/2020 and 19/02/2020 for activities of heavy intensity, where the daily doses reached maximum levels (Figure 6a). On those dates, these children were exposed to an outdoors average hourly concentration of $14{,}3 \pm 0{,}2\ \mu g/m^3$ during their sports class, ordinarily lasting 45 minutes. During this time, the inhalation rate increased significantly, so the children received a higher potential dose. For the whole

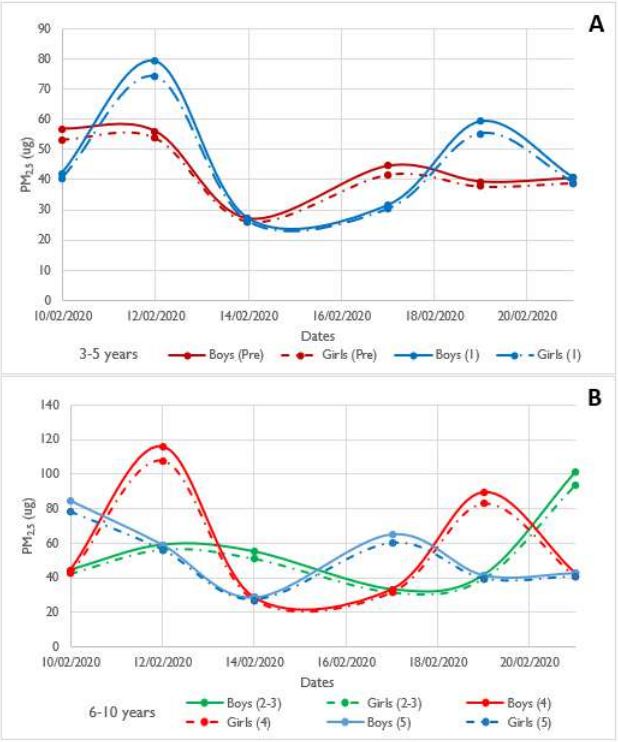

Figure 6. Potential dose by gender and grade: a) three to five years old (preschool, first year), b) six to ten years old (second, third, fourth, and fifth years). Dashed lines for girls, continuous lines for boys.
Source: Authors

sampling period, the potential inhaled doses of $PM_{2,5}$ ranged from a maximum of 70,1 μg to a minimum of 21,6 μg.

A similar case occurred with older children (Figure 6b) on 12/02/2020 and 21/02/2020. They reported the highest peaks within an exposure time of 90 minutes, facing average hourly concentrations of up to 15 $\mu g/m^3$ during sports class, reaching higher doses than first-year children (up to 102 μg), only because of higher environmental concentrations.

Figure 7 shows that boys and girls in the fourth grade received the highest calculated total dose for the entire sampling period (355 and 332,5 μg, respectively). This is followed by the second and third grades (both with equal doses, *i.e.*, 334,9 and 314,4 μg, given that both sport classes take place on the same weekday).

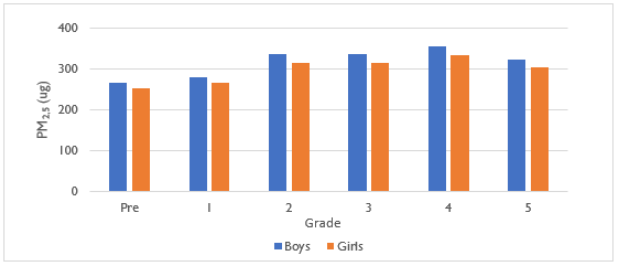

Figure 7. Total potential inhaled dose by grades for boys (blue) and girls (orange)
Source: Authors

Findings of respiratory symptoms in children

The survey was applied to 62 students (parental authorization was provided for their participation) in order

to find out about any respiratory symptoms associated with $PM_{2,5}$ pollution exposure. When implementing the ISAAC questionnaire, the following results were obtained for the symptomatology variables: cough, expectoration or phlegm, nasal congestion, nasal discharge, wheezing, dyspnea, and school absenteeism due to some respiratory disease (Figures 8 and 9).

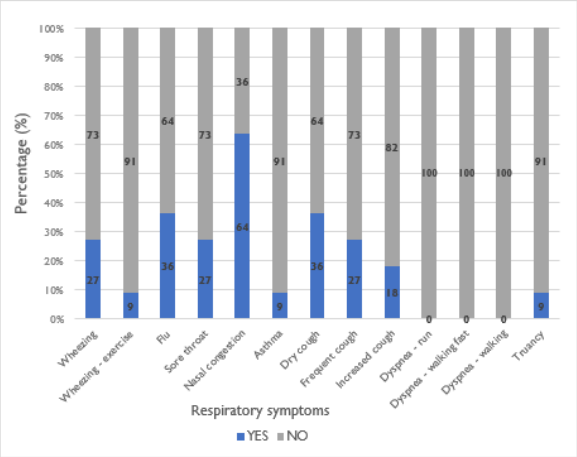

Figure 8. Respiratory symptoms for children three to five years of age
Source: Authors

The group with the highest incidence of respiratory symptoms corresponds to children three to five years of age (transition and first grade). This might be due to their higher respiration rate, lower body mass, and the incomplete development of their respiratory system, as their calculated doses were shown to be lower. Those with wheezing in the chest correspond to 27%, but few reported this symptom during or after physical activity. As for wheezing with flu symptoms (36%), children are more prone to contracting this type of symptoms due to their weak immune systems. Some minors (27%) reported a sore throat when swallowing. The most common symptomatology (64%) is nasal congestion and discharge, which could be associated with exposure to $PM_{2,5}$. Minors who have a dry cough at night which cannot be linked to a cold or chest infection amount to 36%, out of which 27% cough frequently, and that cough occurs when getting up or when they first go out to the street. Likewise, 18% of the minors reported an increase in coughing. According to the survey, no children reported dyspnea when performing physical activity, but a case of asthma (four years old) reported absenteeism in the group.

On the other hand, children between six and ten years of age (grades 2 to 5) reported dyspnea when performing physical activities such as running (10%), fast walking (6%), and walking (2%), which was directly proportional to the level of physical exertion. For this age range, a case of asthma (six years old) was found, with frequent school absenteeism. In light of these findings, within education institutions in this industrial area, but also in others with similar conditions, administrators and educators must perform a daily review of the air quality before allowing outdoor sports activities. Although this study found differences between the $PM_{2,5}$ concentrations reported by the RMCAB and the *in situ* measurements, there is a similar trend between them than can be informative of the local situation. Sports activities should only be carried out

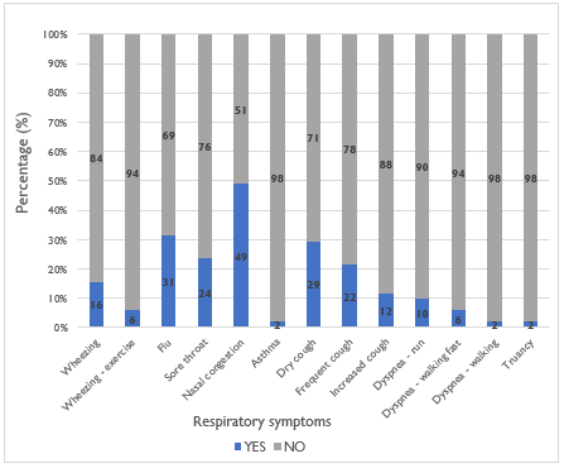

Figure 9. Respiratory symptoms of children six to ten years of age
Source: Authors

during the appropriate days and times, so the students are not forced to receive exaggerated doses of pollutants. Institutions should also consider implementing local air quality monitors both indoors and outdoors in order to obtain more accurate information. Low-cost monitors are gaining momentum around the world, providing good high spatial and temporal resolutions regarding air pollution (Bulot *et al.*, 2019; Wallace *et al.*, 2021), and there are already applications in school environments (de Souza *et al.*, 2017; Kazemi, 2018; Rogulski, 2018).

Finally, the ventilation of the premises must be ensured at all times. This is particularly relevant nowadays, when these institutions are resuming in-person activities after the national lockdown caused by COVID-19. A final recommendation would be the continuous cleaning of surfaces and floors in order to minimize dust accumulation and resuspension, and as well as to prevent fomite contagion.

Conclusions

This study dealt with the collection of $PM_{2,5}$ samples in 48-hour periods for 15 days using Harvard impactors in Gimnasio San Valery (located in Puente Aranda), finding indoor concentrations ranging between 9,45±0,1 and 19,32±0,6 $\mu g/m^3$. Outdoors concentrations varied, with minimum and maximum values of 7,28±0,1 and 15,60±0,3 $\mu g/m^3$, respectively. Indoor concentrations were consistently higher than those outdoors. However, although the sources were not evaluated in this study, it is concluded that the intramural values are due to the resuspension of particles, the penetration of emissions from motor vehicles, insufficient ventilation in the area, and transport from local sources.

By using rubrics, it was possible to analyze children's daily activities according to gender and age range during the established school day. Theoretical inhalation rates were established from the *EPA Exposure Factors Manual* for sedentary, light, moderate, and heavy activities depending on physical effort.

Maximum and minimum potential doses were calculated for the evaluated period, finding a maximum dose of 102 μg for boys and 94,1 μg for girls. It is important to underline

the need for limiting the air quality conditions under which sports activities must be performed. Institutions must complete daily validations of pollutant concentrations from the RMCAB to ensure that children are not exposed to elevated values.

Symptomatology variables such as cough, expectoration or phlegm, nasal and nasal discharge, wheezing, dyspnea, and school absenteeism due to respiratory diseases were consulted using a validated survey. The results suggested a larger prevalence of symptoms in students three to five years of age. However, dyspnea under different physical exertion levels is only reported for the higher grades.

Finally, the education sector must ensure appropriate ventilation and surface cleaning to guarantee air exchange rates that allow minimizing pollutant concentrations indoors. The implementation of new low-cost technologies may help to locally monitor air quality and ventilation conditions. This is of particular importance nowadays, when in-person activities have been fully resumed after the COVID-19 pandemic. This simple measure would reduce transmission rates, but also fine particle matter exposure from concentrations building up indoors.

Acknowledgements

We would like to thank Gimnasio San Valery for their willingness to participate in this project, as well as the Air Quality Research group and the Small Mass Metrology Laboratory of Universidad Nacional de Colombia, who supported the development of this study.

Author contributions

YAV-L and *OAF-M* conceived the idea. *YAV-L* did the background research and developed the project proposal. *YAV-L* and *AKT* collected the data and developed the workflow. *YAV-L* and *OAF-M* performed the data analysis. *NYR-R* and *OAF-M* supervised the research and provided critical feedback. *NYR-R* provided resources through the air quality research group of Universidad Nacional de Colombia as part of the development of the methodology. *YAV-L* reviewed and edited final manuscript. All authors approved the final manuscript for publication.

References

American Academy of Paediatrics (2004). Ambient air pollution: Health hazards to children, *Pediatrics*, *114*(6), 1699-1707. https://doi.org/10.1542/peds.2004-2166

Bennett, J., Davy, P., Trompetter, B., Wang, Y., Pierse, N., Boulic, M., Phipps, R., and Howden, P. (2019). Sources of indoor air pollution at a New Zealand urban primary school; a case study. *Atmospheric Pollution Research*, *10*, 435-444. https://doi.org/2156/10.1016/j.apr.2018.09.006

Bogotá City Hall (2012). *Puente Aranda, a business locality*. https://bogota.gov.co/

Bulot, F. M. J., Johnston, S. J., Basford, P. J., Easton, N. H. C., Apetroaie-Cristea, M., Foster, G. L., Morris, A. K. R., Cox, S. J., and Loxham, M. (2019). Long-term field comparison of multiple low-cost particulate matter sensors in an outdoor urban environment. *Scientific Reports, 9*(1), Article 1. https://doi.org/10.1038/s41598-019-43716-3

Carrion-Matta, A., Kang, C.-M., Gaffin, J. M., Hauptman, M., Phipatanakul, W., Koutrakis, P., and Gold, D. R. (2019). Classroom indoor $PM_{2,5}$ sources and exposures in inner-city schools. *Environment International, 131*, 104968. https://doi.org/2156/10.1016/j.envint.2019.104968

CCB (2007). *Economic and business profile: Locality of Puente Aranda*. http://hdl.handle.net/11520/2884

Chen, Z., Cui, L., Cui, X., Li, X., Yu, K., Yue, K., Dai, Z., Zhou, J., Jia, G., and Zhang, J. (2019). The association between high ambient air pollution exposure and respiratory health of young children: A cross sectional study in Jinan, China. *Science of the Total Environment*, *656*, 740-749. https://doi.org/10.1016/j.scitotenv.2018.11.368

DANE (2019). *Statistic analysis. Geoportal*. https://doi.org/10.16924/riua.v0i26.299

de Souza, P., Nthusi, V., Klopp, J. K., Shaw, B. E., Ho, W. O., Saffell, J., Jones, R., and Ratti, C. (2017). A Nairobi experiment in using low cost air quality monitors. *Clean Air Journal, 27*(2), Article 2. https://doi.org/10.17159/2410-972X/2017/v27n2a6

EPA (2011). *Exposure factors handbook: 2011 edition*. EPA.

Franco, F., Rojas, N., Sarmiento, O., and Hernández, L. (2009). Particulate matter concentrations at public schools located near major urban roads in Bogotá, Colombia: A pilot study. *Revista Facultad de Ingeniería Universidad de Antioquia*, *49*, 101-111. https://www.redalyc.org/articulo.oa?id=43019324010

Hernández, J., Aristizábal-Duque, G., Quiroz, L., Medina, K., and Sarmiento, R. (2013). Air pollution and respiratory illness in children aged less than 5 years-old in Bogotá, 2007. *Revista Salud Pública, 15*(4), 503-516. https://pubmed.ncbi.nlm.nih.gov/25124123/

Hernández, L. (2016). *Characterization of pollution by particulate material in Bogotá using solar photometry* [Master's dissertation, Universidad Nacional de Colombia]. https://repositorio.unal.edu.co/handle/unal/58964 National University of Colombia

Kazemi, F. (2018). Low-cost air monitors effectively show school-level particle matter risks are comparable across demographic groups within an impacted California air region [Master's thesis, San José State University]. https://doi.org/10.31979/etd.9w25-94nr

Mata-Fernández, C., Fernández-Benítez, M., Pérez-Miranda, M., and Guillén-Grima, F. (2005). Validation of the Spanish version of the Phase III ISAAC questionnaire on asthma. *Journal of Investigational Allergology & Clinical Immunology*, *15*(3), 201-210.

Metropol (2007). *Procedure for determining the concentration of suspended particles smaller than 10 microns in ambient air by the PM_{10} method*. https://www.metropol.gov.co

Ogen, Y. (2020). Assessing nitrogen dioxide (NO_2) levels as a contributing factor to coronavirus (COVID-19) fatality. *Science of the Total Environment*, *726*, 138605. https://doi.org/10.1016/j.scitotenv.2020.138605

Oliva, P., García, K., Cortez, R., Dávila, R., Alfaro, M., and Duke, V. (2001). *Air monitoring laboratory anual*. http://www.ingenieroambiental.com/Manual-laboratorio-analisis-aire.pdf

Othman, M., Talib, M., and Matsumi, Y. (2019). The exposure of children to $PM_{2,5}$ and dust in indoor and outdoor school classrooms in Kuala Lumpur City Centre. *Ecotoxicology and Environmental Safety*, *170*, 739-749. https://doi.org/2156/10.1016/j.ecoenv.2018.12.042

Oyarzún, M. (2010). Air pollution and its effects on health. *Chilean Journal of Respiratory Diseases*, *26*(1), 16-25. https://dx.doi.org/10.4067/S0717-73482010000100004

RMCAB (2018). Annual air quality report. Year 2018. RCMAB.

Rogulski, M. (2018). Indoor PM_{10} concentration measurements using low-cost monitors in selected locations in Warsaw. *Energy Procedia, 147*, 137{144. https://doi.org/10.1016/j.egypro.2018.07.043

Sarmiento, R., Hernández, L., Medina, E., Rodríguez, N., and Reyes, J. (2015). Respiratory symptoms associated with exposure to air pollution in five localities in Bogotá, 2008-2011. Study in a dynamic cohort. *Biomedical*, *35*(0), 167-176. https://doi.org/10.7705/biomedica.v35i0.2445

SDA (2009). *Technical elements of the 10-year decontamination plan for Bogotá*. SDA.

UNICEF (2016). *Clean the air for children*. https://www.unicef.org/reports/clean-air-children

Wallace, L., Bi, J., Ott, W. R., Sarnat, J., and Liu, Y. (2021). Calibration of low-cost PurpleAir outdoor monitors using an improved method of calculating PM2.5. *Atmospheric Environment, 256*, 118432. https://doi.org/10.1016/j.atmosenv.2021.118432

World Health Organization (WHO) (2018). *Air pollution and children's health*. https://www.who.int/es

World Health Organization (WHO) (2019). *Ten threats to global health in 2019*. https://www.who.int/es

Mechanical Engineering, Mechatronics, and Materials Science

https://doi.org/10.15446/ing.investig.99467

Monitoring via Infrared Spectrometry and Rheometry of a Vulcanization-Like Process of Chewing Gum Waste

Monitoreo por espectrometría infrarroja y reometría de un proceso similar a la vulcanización de los desechos de goma de mascar

Isabel Cristina Castellanos[1], Carolina Luque[2], Eliseo Avella[3], Stiven Huertas[4], Mischel Toro[5], and Daniel Rojas[6]

ABSTRACT

Once chewed, chewing gum becomes a disposable and non-degradable cumulative residue that causes environmental, economic, and social problems. Collecting and treating chewing gum waste until its properties are adapted for some profitable use will generate environmental and economic savings. In this work, chewing gum waste was collected, sanitized, and subjected to a laboratory-scale rubber vulcanization-like process with sulfur. The evolution of the process was monitored via sequential measurements of torque and the acquisition of a series of ATR-FTIR spectra on the raw and resulting material of aliquots isolated from the reaction medium every 10 minutes for 4 hours. The absorbance values of the signals in the series of ATR-FTIR spectra were normalized and subjected to a descriptive statistical analysis, which allowed detecting intensity variations in bands attributed to carboxylate, as well as a slight decrease in the intensity of the bands attributed to hydroxyl, carbonyl, methylene in alpha to carbonyl, and other CHn groups in aliphatic fragments. These intensity changes and the trend of rheometric measurements during the process (vulcanization curve) evidenced that chewing gum waste did indeed react. Its vulcanization process had an absolute cross-linking maximum 5,15 minutes into the process and caused a remarkable increase in the torque of the resulting material; the Shore A hardness changed from 20 to 95 units, and the density varied from 1 280 to 1 510 kg/m^3. These findings hint at an alternative treatment to reduce environmental pollution and revalue chewing gum waste.

Keywords: chewing gum waste, vulcanization, rheometry, mid-infrared, ATR-FTIR spectroscopy

RESUMEN

Una vez masticada, la goma de mascar se convierte en un residuo acumulativo desechable y no degradable que causa problemas ambientales, económicos y sociales. Recoger y tratar los desechos de goma de mascar hasta que sus propiedades se adapten a un uso rentable generará ahorros ambientales y económicos. En este trabajo se recogieron y desinfectaron desechos de goma de mascar, y se los sometió a un proceso similar a la vulcanización de caucho con azufre a escala de laboratorio. La evolución del proceso se monitoreó mediante mediciones secuenciales de torque y la adquisición de una serie de espectros ATR-FTIR de la materia prima y el material resultante de alícuotas aisladas del medio de reacción cada 10 minutos durante 4 horas. Los valores de absorbancia de las señales en la serie de espectros ATR-FTIR se normalizaron y se sometieron a un análisis estadístico descriptivo que permitió detectar variaciones de intensidad en bandas atribuidas al carboxilato, así como una ligera disminución en la intensidad de las bandas atribuidas a hidroxilo, carbonilo, metileno en alfa a carbonilo y otros grupos CHn en fragmentos alifáticos. Estos cambios de intensidad y la tendencia de las medidas reométricas durante el proceso (curva de vulcanización) evidenciaron que los residuos de goma de mascar en efecto reaccionaron. Su vulcanización tuvo un máximo absoluto de entrecruzamiento a los 5,15 minutos de proceso y causó un aumento notable en el torque del material resultante; la dureza Shore A cambió de 20 a 95 unidades, y la densidad varió de 1 280 a 1 510 kg/m^3. Estos hallazgos sugieren un tratamiento alternativo para reducir la contaminación ambiental y revalorizar los desechos de goma de mascar.

Palabras clave: desechos de goma de mascar, vulcanización, reometría, infrarrojo medio, espectroscopía ATR-FTIR.

Received: November 12th 2021
Accepted: September 09th 2022

Introduction

Chewing gum is a popular product around the world, and its consumption has been steadily increasing. Several studies claim that chewing gum has beneficial effects on oral health, weight control, and stress relief, among others, and it has even been proposed as an efficient mechanism for medication delivery (Takahashi *et al.*, 2003; Jacobsen *et al.*, 2004; Potineni, 2007; Thivya *et al.*, 2021; Tijani *et al.*, 2022). However, its insoluble fraction can not be digested by the consumer, and it is discarded to the environment as a waste. Around the world, about 250 000 tons of environmentally

[1] Chemist, Universidad Nacional de Colombia, Bogotá. MSc Biochemistry, Universidad Nacional de Colombia, Bogotá. Affiliation: Associate Professor, Universidad EAN, Faculty of Engineering, Department of Basic Sciences, Colombia. E-mail: iccastellan@universidadean.edu.co

[2] Bachelor in Mathematics, Universidad Pedagógica Nacional de Colombia, Bogotá. Specialist in Statistics, Universidad Nacional de Colombia, Bogotá. MSc Applied Statistics, Universidad Santo Tomás, Bogotá. Affiliation: Associate Professor, Universidad EAN, Faculty of Engineering, Department of Basic Sciences, Colombia. E-mail: cluque2.d@universidadean.edu.co

[3] Chemist, Universidad Nacional de Colombia, Bogotá. ScD Chemistry, Universidad Nacional de Colombia, Bogotá. Affiliation: Associate Professor, Universidad Nacional de Colombia, Faculty of Sciences, Department of Chemistry, APRENA research group, Bogotá, Colombia. E-mail:eavellamo@unal.edu.co

[4] Chemical engineer, Universidad EAN, Bogotá. Affiliation: Universidad EAN, Faculty of Engineering, Bogotá, Colombia. E-mail:

hazardous chewing gum waste are generated per year, according to Euromonitor International (Roy, 2021).

Chewing gum waste is an environmental problem, as currently available chewing gums are products made of substantially non-degradable elastomer (Roy, 2021). An important amount of chewed gum ends up on the ground, carrying harmful toxins and microorganisms (Saberi *et al.*, 2018) that can severely affect the health of any living being upon contact or by accidental or systematic ingestion. All of this implies environmental and economic costs that the inhabitants and the planet must pay.

This waste also poses an economic problem. City authorities and the people responsible for waste management must work hard to remove all of the chewed gum thrown to the environment. Such efforts are costly and not completely succesful. The removal of each bit of chewing gum thrown onto the pavement costs more than three times the average price of a piece of gum (Logan and Rudolfs, 1947; Oosthuizen *et al.*, 2022). For example, in 2012, London spent more than £3 per piece of gum removed from the pavement, and three months steam-cleaning the 300000 pieces of gum that were thrown in an area of less than two miles of a street during the Olympic Games, while the consumer of such quantity of gum bought each piece for just a nickel, and threw that waste in a short period of time (BBC, 2010).

According to reports in The Telegraph (Rudgard, 2018) and The Guardian (Carter, 2005), governmental environmental protection entities of different countries charge taxes to the whole supply chain for single-use plastics (such as plastic bags) in order to diminish harms for the environment. It has already been considered that taxes to chewing gum consumption should be implemented as a way to recover some of the resources spent cleaning the gum waste.

Chewing gum waste also represents a social problem because it substantially decreases the utility and aesthetic value of public places (Simonek, 2011), generating untidiness and discomfort, as well as promoting adverse social behavior in the population. Among the tentative strategies to reduce the amount of chewing gum waste thrown onto the streets, some chewing gum waste collection campaigns have been proposed, as well as the use of improved cleaning methods (Liu and Jiang, 2003), the incorporation of anti-sticking agents into chewing gum formulations (Sozzi and Del Visco, 2011; Bullus, 2017), the production of bio-chewing Gum (Ribadeau-Dumas and Mentink, 2004; Palabiyik *et al.*, 2018; Saberi *et al.*, 2018), the making of wraps for their hygienic disposal (Simonek, 2011), and their use as a filling in the formulation of plastic blends useful for manufacturing chewing gum waste collection containers (Bullus, 2017). The latter implies having to throw the chewed gum into special containers, rather than into ordinary trash bins without any appeal for the consumer. However, none of these strategies has contributed significantly to solving the pollution problem.

After the chewing, the base gum remains as a non-degradable residue. This is the main ingredient that manufacturers keep as reserved information (which is commonly not shared or declared). The base gum is a supremely soft food-grade chewable plastic made of polymers, plasticizers, and resins, which is not biodegradable. In the United States, Butadiene-styrene rubber, Isobutylene-isoprene copolymer (butyl rubber), paraffins (obtained by Fischer-Tropsch process), natural or synthetic petroleum waxes, polyethylene, polyisobutylene, and polyvinyl acetate are some of ingredients approved for the making, formulation, and production of chewing and bubble gum (Fritz and Elias, 1980).

In this context, our work aims to study the feasibility of modifying the properties of chewing gum waste by means of a chemical reaction carried out under conditions similar to those of cross-linking rubber by vulcanization, in order to take advantage of some similarities between chewing gum and rubber regarding their structure and properties. It is expected that the cross-linking modifies the polymeric properties of chewing gum residues, as in the vulcanization of natural material (*i.e.*, through the use of sulfur, one of the most efficient and widely employed industrial methods), generating desirable characteristics in the products at a low cost. Therefore, the polymeric structure of the chewing gum base could be modified by cross-linking in a rubber vulcanization-like process to produce a less polluting material, which might have suitable properties for some applications.

Since the discovery of vulcanization, several researchers have highlighted the effect of the filler, the plasticizer, and the anti-oxidant on the process. A free-radical mechanism for rubber cross-linking was originally suggested by Flory (1953), Shelton and McDonel (1960) and Kruželák *et al.* (2017). Other evidence suggests an ionic mechanism that leads to the formation of macromolecules by sulfur bridges (C-Sx-C), which is initialized by sulfur (the cross-linking agent) with zinc salt (the accelerator) to produce a type of perthio-salt [activator-Sx-Zn-activator]. This induces the formation of a rubber-sulfur bond, removing hydrogen from the methylene groups located in alpha to an unsaturation in the structure of the natural rubber (Niyogi and Varma, 2007). However, as it probably involves a complex sequence of reactions, the mechanisms and the chemistry involved in the rubber cross-linking process using sulfur have not been fully understood and are still a subject of prime interest.

In rubber vulcanization, different types of accelerators are used to obtain better use properties and shorter process times. The cross-linking process catalyzed solely by the action of zinc salts (activators) can take up to 4 hours (Bevilacqua, 1959; Nieuwenhuizen, 2001; Sae-oui *et al.*, 2007; Bornstein and Pazur, 2020). In the cross-linking with sulfur, the selected accelerator determines the type of network structure produced, as well as the specific properties of the material obtained (Marković, 2009). The basic characteristics of the accelerators used in rubber vulcanization are usually similar and are composed of one or two sulfur atoms located between a pair of organic groups.

shuerta52029@universidadean.edu.co
[5] Chemical engineer, Universidad EAN, Bogotá. Affiliation: Universidad EAN, Faculty of Engineering, Bogotá, Colombia. E-mail: mtorosa91317@universidadean.edu.co
[6] Chemical engineer, Universidad EAN, Bogotá. Affiliation: Universidad EAN, Faculty of Engineering, Bogotá, Colombia. E-mail: drojasm30899@universidadean.edu.co

How to cite: Castellanos, IC., Luque, C., Avella, E., Huertas, S., Toro, M. and Rojas, D. (2023). Monitoring via infrared spectrometry and rheometry of a vulcanization-like process of chewing gum waste. *Ingeniería e Investigación, 43*(2), e99467. https://doi.org/10.15446/ing.investig.99467

There are primary and secondary accelerators responsible for increasing the reaction speed in the vulcanization of rubbers, *e.g.*, cyclohexyl benzothiazole sulfenamide (CBS) and tetramethylthiuram disulfide (TMTD). The former is a primary accelerator that, at normal vulcanization temperatures (408 – 413 K), increases the speed of the process; and the latter is a secondary accelerator that acts as a sulfur donor which favors the stabilization of the torque, generates a high cross-linking density, and provides vulcanized rubbers with a resistance to thermal degradation (Sae-oui *et al.*, 2007). Binary accelerator combinations have also been widely used, as they provide higher curing rates in rubber vulcanization (Kim *et al.*, 2011; Wang *et al.*, 2019).

This paper presents information on the laboratory-scale obtainment of a material from chewing gum waste subjected to a process similar to that of the sulfur vulcanization of natural rubber, and it provides some data on its preliminary characterization by ATR-FTIR, rheometry, Shore A hardness, and density measurements taken in order to determine the curing time, as well as to analyze, through the results of these experiments, the changes generated by the process in the chewing gum waste properties. It is considered that a treatment like this could help revalue this waste by finding an appropriate use for the produced material.

The evolution of the whole process was monitored via a series of mid-infrared ATR-FTIR (attenuated total reflectance with Fourier Transform) spectra of aliquots isolated from the reaction medium every 10 minutes for 4 hours, as well as through sequential measurements of torque during the process (from the raw material until the final product was obtained). The absorbance of the bands in all ATR-FTIR spectra were normalized with regard to the absorbance of the band at 2 953 cm^{-1}, as it was practically constant in all spectra. The fundamental bands of the ATR-FTIR spectra were analyzed in terms of their maximum absorbance wave number and intensity changes, as manifested by the normalized absorbance during the process, using a descriptive statistical analysis in order to get information about changes caused by this reaction in the functional groups present in the structure of the material.

Methodology

All of the rubber vulcanization-like processes were carried out from raw material obtained via a collection campaign of chewing gum waste discarded from Colombian commercial brands, which was carried out at Universidad EAN (Bogotá, Colombia) at the beginning of 2019. The chewing gum wastes were sanitized with 1% sodium hypochlorite and by autoclaving (at an internal pressure of 98 to 103 kPa and a temperature of 373 K to 393 K), and they were dried properly before subjecting them to the vulcanization-like process.

The drying of the gum was carried out by making thin sheets in a roller mill with a thickness not greater than 0,3 mm and subjecting them to air drying for 6 hours. The kneading and formation of a new sheet was repeated to regenerate the area exposed to drying in order to foster the loss of water trapped between the polymer chains. The drying cycles were repeated until no changes were observed in the O-H stretching band (υ_{O-H}) of the ATR-FTIR spectrum. The base formulation for the rubber vulcanization-like process used in this study is summarized in Table 1.

Table 1. Base formulation of chewing gum waste compound (weight per 100 parts of chewing gum). Natural rubber was used for control.

Compound	Mix A (phr)	Control (phr)	Mix B** (*phr*)
Wasted chewing gum	100,0	0,0	100,0
Natural rubber	0,0	100	0,0
Stearic acid	1,0	1,0	1,0
ZnO	5,0	5,0	5,0
Carbon black N550 type - STERLING® SO-1*	60,0	60,0	6,0
Sulfur	3,0	3,0	3,0
CBS (N-Cyclohexyl-2-benzothiazole Sulfonamide) Premix®	1,0	1,0	0,0
TMTD (Tetramethyl thiuram disulfide) Premix®	1,0	1,0	0,0
Total	171,0	171,0	115,0

Source: Authors

* Rubber® furnace industrial-grade carbon black, from Cabot Corporation

** Mix B was the only one monitored via ATR-FTIR

Sample preparation for rheometry

Mix A and B were prepared using a 300 mm laboratory mixer roll mill at a roll speed ratio of approximately 1 100 rpm and a roll temperature of 293-303 K. The processing time after the addition of each component of Mix A was approximately 2 minutes. Rheometric characteristics were evaluated using a Prescott MDR MINI Oscillating Disk Rheometer, in accordance with the ASTM-D5289 (2019) standard test method. The hardness of the samples was measured using the PTC 306 L equipment according to ASTM-D792 (2020), while density was measured according to ASTM-D2240 (2021).

Mix B was made without the addition of accelerators (CBS and TMTD) and with a lower amount of sulfur in order to slow down the process and monitor the changes of the functional groups present in the mix via ATR-FTIR, improving the quality of the baseline of the spectra. It was subjected to heating for 4 hours at a temperature of 413 K, and samples of the reaction medium were taken every 10 minutes for the subsequent acquisition of ATR-FTIR spectra.

ATR-FTIR analysis

Each sample (aliquot isolated from the reaction medium) was cooled in liquid nitrogen to stop the reaction before acquiring its ATR-FTIR spectrum at room temperature with a Shimadzu IRTracer–10 spectrophotometer equipped with a DLATGS detector (deuterated L-alanine doped triglycine sulfate), a mid-infrared (IR) source, and a single-reflection attenuated total reflectance (ATR) zinc selenide (ZnSe) crystal. Each spectrum was collected by placing a portion of the material on the round crystal window. The ATR-FTIR spectrum of each sample was recorded in 32 scans in the range of 340 cm^{-1} - 4 000 cm^{-1}, with a spectral resolution of 2 cm^{-1}. This, with regard to a previous background spectrum acquired with a constant distance from the sample to the optic unit (guaranteed by the holding arm of the sample spacer device) in order to minimize any errors caused by non-uniform contacts when acquiring the spectra. The ATR-FTIR spectrum of each sample was recorded via the LabSolutions IR Data Collection software and analyzed in triplicate.

The entire vulcanization-like process of chewing gum waste was carried out in duplicate, starting from a variety of different chewing gum wastes. Thus, for this study, a total of 150 ATR-FTIR spectra were acquired, *i.e.*, three spectra for every aliquot isolated from the reaction medium throughout the process.

Data processing

The baseline of each spectrum was adjusted with variable slope and offset, and an advanced smoothing with three algorithms (moving average, Savitsky-Golay, and percentile filter) was carried out. The spectrum was filtered by removing the cosmic spikes that can be present in all photoelectric readout systems as random unidirectional sharp spikes that distort spectra and may affect the results of later statistical analyses (Barton and Hennelly, 2019). An average ATR-FTIR spectrum of the n-replicates acquired of each aliquot isolated from the reaction medium throughout the process was calculated. All processing (including the conversion of spectrum data to *.csv* files) was made using the Spectragryph software (https://www.effemm2.de/spectragryph/index.html21/04/2023). Statistical analyses were conducted in R version 4.0.3 with RStudio version 1.3.1093, Windows 10+ (64-bit).

Descriptive statistical analysis of the ATR-FTIR spectrum

All of the ATR-FTIR spectra were normalized for the analysis, with the aim to make them comparable. 25 average spectra, each with 3 734 point data (wave number, absorbance), were studied. 13 bands present in all of the ATR-FTIR spectra were selected for the analysis. These bands were characterized by the wave number corresponding to its maximum absorbance and assigned according to previously published tables (Anderson *et al.*, 2004; Silverstein *et al.*, 1991; Stuart, 2004). It was assumed that each point data of a band (well-defined wave number, absorbance) in any spectrum correlates with that of the band located at the same wave number in any other spectrum belonging to the series of ATR-FTIR spectra under analysis (Smith, 2011).

The absorbance of the band at 2 953 cm^{-1} served as a reference to normalize the data of each spectrum, as it showed the least variation in all of the spectra acquired during the study. This normalization allowed comparing the spectra of the series, attenuating the effects caused by the penetration of the IR beam in the sample while acquiring each spectrum, thus avoiding interpretation bias in the results. For each of the 13 selected bands, the mean of the maximum absorbance wave number and its corresponding absorbance were calculated, as well as the dispersion range and the standard deviation of the mean. The normalization process was based on Equation (1), where $a_{i,j}$ represents the absorbance of the band appearing at the j-th wave number in the i-th spectrum for $i = 1, \cdots, 25$ and $j = 1, \cdots, 3\,734$; $\bar{a}_{2\ 953\,cm^{-1}}$ denotes the average absorbance of the band at $\bar{\nu}$: 2 953 cm^{-1} in the total series of the spectra; $a_{i_{2\ 953\,cm^{-1}}}$ corresponds to the absorbance of the band at $\bar{\nu}$: 2 953 cm^{-1} for each i-th spectrum; and $a^*_{i,j}$ represents the normalized absorbance for the corresponding band at the j-th wave number. The input for the statistical analysis was a 25×3 734 matrix of normalized absorbance values.

$$a^*_{i,j} = a_{i,j}\frac{\bar{a}_{2\ 953\,cm^{-1}}}{a_{i_{2\ 953\,cm^{-1}}}} \tag{1}$$

The Pearson correlation coefficient was calculated according to Equation (2) in order to show the probable relationships between bands attributed to certain functional groups and particular bonds in the literature (Anderson *et al.*, 2004; Silverstein, *et al.*, 1991; Stuart, 2004).

$$r_{xy} = \frac{\sum_{i=1}^{n} x_i y_i - n\bar{x}\bar{y}}{(n-1)s_x s_y} \tag{2}$$

where x_i and y_i are the values of absorbance for the bands x and y at the i-th spectrum; n is the number of spectra; $\bar{x}$ and $\bar{y}$ are the mean of absorbance value for each band; and s_x and s_y are the corresponding standard deviations. This coefficient takes values between +1 and −1. Values close to +1 indicate a positive linear correlation (direct or increasing), and values close to 0 evidence no linear correlation. Those close to −1 are indicators of a negative linear correlation (inverse or decreasing). To evaluate whether the coefficient obtained was statistically significant, the hypothesis $H_0 : \rho = 0$ was evaluated with a significance of 5%. The *cor.test* function from the stats library of R was used for contrasting the hypothesis.

Results and analysis

Table 2. Test on unvulcanized and vulcanized products

Property	Units	Unvulcanized Product		Vulcanized Product	
		Natural Rubber	Chewing gum waste	Natural rubber	Chewing gum waste
Hardness*	Shore A	43	20	70	97
Density**	(kg/m^3)	930	1 280	1 150	1 510

Source: Authors

* Measurement uncertainty ±0, 03. ** Measurement uncertainty ±0, 5kg/m^3

At the industrial level, vulcanization has been extensively used for cross-linking natural rubber, and a vulcanization-like process has not been applied to chewing gum waste, which is typically disposed of as useless polluting trash. This report shows the results of applying said process on chewing gum waste, which was carried out under conditions similar to those of industrial rubber vulcanization and monitored via rheometry measurements and ATR-FTIR spectrometry from the raw material until the final product was obtained, including the aliquots isolated from the reaction medium every 10 minutes during the whole process. This was done in our laboratory under the expectation of obtaining a cross-linked product with different physical-chemical properties, perhaps suitable for a more profitable use than that of the chewing gum waste.

The measured elastic torsional (S′) data in the rubber vulcanization processes provide indication of the cross-linking level achieved (*i.e.*, the sum of the chemical bonds involved in the cross-links). Figure 1 shows the rheometric monitoring of the rubber vulcanization-like process of the chewing gum waste at 413 K in Mix A. The curve in Figure 1 has a similar behavior to that of reversion in rubber vulcanization (Bornstein and Pazur, 2020), where a steep linear drop of torque precedes the reaction stage during precursor formation, in a way analogue to the first stage occurring with uncured rubber, which will be discussed later in the ATR-FTIR analysis section. After said drop, the S′ value shows a fast rise, which can be associated with a cross-linking density increase, just up to a maximum value of 17, 46 dNcm. Then, S′ values show a slight drop, probably due to a reversion process, a term generally applied to the loss of network structures due to non-oxidative thermal

aging, as a result of an overly long vulcanization (Coran, 1964; Bornstein and Pazur, 2020).

The Mix A formulation was characterized by the addition of 3,0 phr of sulfur, a higher content of carbon black (60 phr), and the use of CBS and TMTD as accelerators. Based on the monitoring of torque during the process (Figure 1), a scorch time T_{S2} (at which cross-links begin to occur) equal to 1,96 min was determined, as well as the time at which the progress of the cross-linking in the vulcanization reached 90% of the maximum (T_{90}), equal to 5,15 min (T_{90} = 3,74 minutes for natural rubber).

The final material obtained via the vulcanization-like process of chewing gum waste using CBS and TMTD in Mix A (Table 1) was characterized in terms of density and Shore A hardness (Table 2). The density (1 510 ± 5 kg/m^3) turned out to be approximately 1,18 times higher and the shore A hardness (97 ± 0,3) 77 units larger than those of the raw material (chewing gum waste). The Shore A hardness of the raw material (20 ± 0,3 units) classifies chewing gum waste as a soft material, while that of the material obtained with this treatment is characteristic of extra-hard materials.

All of these data evidence the feasibility of the rubber vulcanization-like process of chewing gum waste. Under conditions similar to those experienced by rubberin industrial vulcanization, this process is able to change the properties of chewing gum waste and transform it into a material with characteristics that could be adapted for convenient and cost-effective uses.

The Mix B formulation was characterized by lower contents of carbon black and sulfur. The vulcanization-like process of Mix B produced a material whose Shore A hardness (70 ± 0,3 units) classifies it as a medium-hardness material. The fact that this product has a lower hardness than the product obtained from Mix A can be attributed to the lower content of carbon black, which was used as a reinforcing material in Mix B (Sánchez *et al.*, 2020), and, by analogy with rubber vulcanization, to the use of the CBS and TMTD accelerators, which have shown some influence on the final properties of vulcanized rubber (Sae-oui *et al.*, 2007; Marković *et al.*, 2009; Formela *et al.*, 2015). The increased concentration of carbon black in Mix A formulation had a positive effect on the hardness and density of the final product, possibly because, as in the case of rubber, it acts as a support material to form the bonds with the material that is being vulcanized (Bueche, 1961; Janacek, 1962).

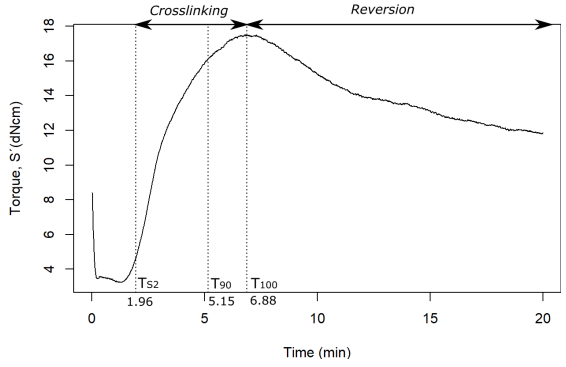

Figure 1. Rheometer curve for the vulcanization of chewing gum waste in Mix A at 413 K
Source: Authors

Monitoring the process via ATR-FTIR

Figure 2 presents the ATR-FTIR spectra series of the raw material, the reactives, the prevulcanized material, and the 25 aliquots isolated from the reaction medium every 10 minutes during the vulcanization-like process of Mix B (Table 1), which were acquired at 413 K.

Seeking to minimize any distortions due to overlapping signals in the components of the ATR-FTIR spectra of these mixtures, this study considered the intensity of the bands, which proved to be more accurate than its integral when analyzing the behavior of the set of signals in the spectra. Table 3 shows the location (wave numbers) and the average with the dispersion of the absorbance for each spectral band of interest in this analysis. The band at $\bar{\nu}$: 2 953 cm^{-1} showed the least variation in the whole the set of spectra during the whole process; it had a dispersion of 0,04 units and a coefficient of variation of 13,39% around its average value. Therefore, the band at $\bar{\nu}$: 2 953 cm^{-1} was chosen as the reference to normalize the absorbance of all other bands of interest in each spectrum of the ATR-FTIR series of the samples (raw material, pre-vulcanized material, and aliquots). It is worth adding that the term *to normalize* means to represent each data from a sample of data (each ATR-FTIR spectrum of the series) by a ratio of proportion obtained as the quotient resulting from dividing it by another data belonging to the same sample, which is chosen as a common reference for all the data in the sample, in order to unify their scale and make them comparable to other equally normalized samples, *i.e.*, with respect to the same reference (the average absorbance of the band at 2 953 cm^{-1}).

In order to obtain information on changes in the chemical composition during the vulcanization-like process of the chewing gum waste, the corresponding 13 bands of each spectrum (Table 3) were selected along with their already normalized average absorbances, considering the magnitude of the coefficients of variation found for their average values of normalized absorbance in the whole set of spectra for the aliquots isolated from the reaction medium during the process. These bands were assigned as indicated in the literature (Anderson *et al.*, 2004; Silverstein, 1991; Stuart, 2004), and their average absorbances were subjected to a statistical treatment, such as the one shown in Figure 3, looking for changes in the initial composition which could be interpreted as the occurrence of a vulcanization-like process of the chewing gum waste. Thus, changes in the carbonyl, methylene, and carboxylate groups were found and taken into consideration for the analysis.

It is very common to use the Pearson correlation coefficient to quantify a possible linear correlation between two sets of data (Zou *et al.*, 2003). This coefficient was used to analyze linearity of the absorbances of all the spectral bands chosen for this study (Jampafuang *et al.*, 2015; slouf *et al.*, 2018).

For this analysis, the data from the ATR-FTIR spectra set were represented in a 2D matrix (1 line = absorbance of the first band; 1 column = absorbance of second band), and the correlation matrix was computed for the eight spectral bands with the highest coefficient of variation during the process: the bands at $\bar{\nu}$: 1 700 cm^{-1} and $\bar{\nu}$: 1 732 cm^{-1} for the stretching of carbonyls ($\upsilon_{C=O}$); the band at $\bar{\nu}$: 1 412 cm^{-1} for the bending of methylene and/or the methyl groups (δ_{H-C-H}, δ_{H-C-C}, and δ_{H-C-O}); the bands at $\bar{\nu}$: 1 559 cm^{-1} and $\bar{\nu}$: 1 538 cm^{-1} for the bending of ester carboxylate groups

Table 3. Assignment of the bands and descriptive statistics of the average absorbance local maximum data prior to normalization for the bands of interest in the whole set of ATR-FTIR spectra of the aliquots isolated from the reaction medium during the vulcanization-like process of chewing gum waste

Wave number (cm^{-1})	Assignment	Between acquisitions of same sample				
		Absorbance		Range	Mean	Standard deviation
		Min	Max			
3 433	υ_{O-H} associated	0,01	0,04	0,04	0,02	0,01
2 953	υ_{C-H} stretching $-CH_2-$ and $-CH_3$	0,05	0,09	0,04	0,08	0,01
2 916		0,10	0,18	0,09	0,16	0,02
2 848		0,12	0,22	0,11	0,19	0,03
1 732	$\upsilon_{C=O}$	0,06	0,16	0,10	0,10	0,02
1 700		0,01	0,10	0,08	0,03	0,02
1 566	$R-COO^-$	0,01	0,06	0,05	0,04	0,01
1 542		0,01	0,10	0,09	0,06	0,02
1 412	$-CH_3$ and $-CH_2$, $-O-CO-CH_3$ and $-CH_2-C=C<$	0,08	0,23	0,15	0,15	0,03
1 234	$-C-O-$, CH_2-SH	0,03	0,12	0,09	0,06	0,02
728	long aliphatic chains $-(CH_2)n-$; n > 4	0,01	0,05	0,04	0,3	0,01
720		0,03	0,07	0,04	0,05	0,01
712		0,03	0,08	0,05	0,06	0,01

Source: Authors

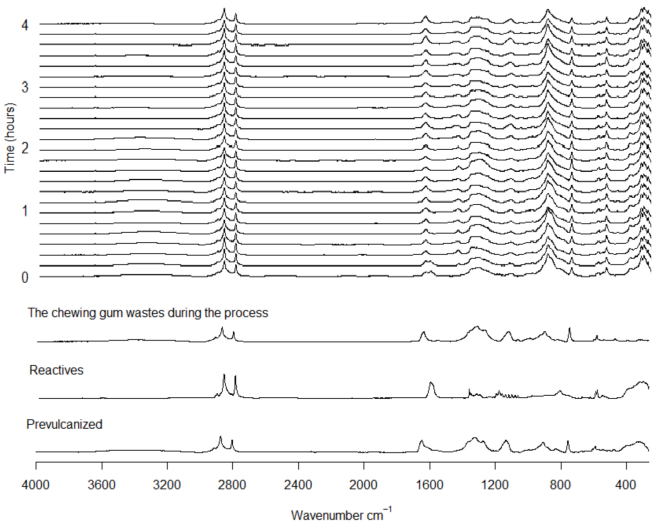

Figure 2. ATR-FTIR spectra acquired during the vulcanization-like process of the discarded chewing gum normalized at peak intensity (2 953 cm^{-1}) - Mix B at 413 K
Source: Authors

($\delta_{O=C-O}$); the band at $\bar{\nu}$: 1 232 cm^{-1} for the stretching of C–O bonds in sp^2 hybridized carbon ($\upsilon_{=C-O}$) or the stretching of υ_{C-S} bonds (υ_{C-S}) in mercaptan-methylene fragments, $–CH_2–SH$, which is most likely overlapped in this spectral region; and the bands at $\bar{\nu}$: 728 cm^{-1} and $\bar{\nu}$: 712 cm^{-1} for the rocking of CH_2 in aliphatic chains, $-(CH_2)_n-$ with n > 4.

Figure 3 depicts the 2D matrix considered for the statistical treatment when correlating the average maximum of absorbances for nine bands located at a given wave number in each ATR-FTIR spectrum of the series, which were finally chosen due to their proven relevance for interpreting the results. The form and the intensity of such spectral bands are shown by the curves appearing in the cells of the diagonal of the matrix in Figure 3. The bands at $\bar{\nu}$: 1 732 cm^{-1}, $\bar{\nu}$: 1 700 cm^{-1} ($\upsilon_{C=O}$), and the band at $\bar{\nu}$: 1 234 cm^{-1} ($\upsilon_{=C-O}$) frequently exhibited low absorbance values due to their asymmetric and variable forms (mostly with positive asymmetry). The other bands had a less pronounced yet similar tendency. For example, in Figure 3, an increasing linear relation is noticeable between the band at $\bar{\nu}$: 1 732 cm^{-1} ($\upsilon_{C=O}$) and the band at $\bar{\nu}$: 1 234 cm^{-1} ($\upsilon_{=C-O}$), supported by a linear correlation coefficient of 0,974, with a p-value of less than 5%. This means that the higher the absorbance values of the band at $\bar{\nu}$: 1 732 cm^{-1} ($\upsilon_{C=O}$), the greater the absorbance values for the band at $\bar{\nu}$: 1 234 cm^{-1} ($\upsilon_{=C-O}$).

Another possible increasing linear relation is that of the bands at $\bar{\nu}$: 1 412 cm^{-1} (δ_{H-C-H}, δ_{H-C-C}, δ_{H-C-O}) and $\bar{\nu}$: 712 cm^{-1} (δ_{H-C-H}), with a correlation coefficient of 0,684 and a lower p-value of 5%.

The absorbance values of the bands at $\bar{\nu}$: 1 542 cm^{-1} and $\bar{\nu}$: 1 700 cm^{-1} ($\upsilon_{C=O}$) or those at $\bar{\nu}$: 1 566 cm^{-1} ($\upsilon_{O=C-O}$) and $\bar{\nu}$: 1 700 cm^{-1} ($\upsilon_{C=O}$) showed a linear decreasing relation supported by negative linear correlation coefficients of −0,665 and −0,631, respectively. Both had a lower p-value of 5%, indicating that these bands are attributable to independent phenomena occurring in functional groups without common atoms or bonds, as well as in different structural fragments of the sample.

As mentioned above, these first results are only presented as a first approach, in order to collect evidence of the feasibility of the reaction of chewing gum waste under rubber vulcanization-like conditions, with the purpose of transforming these residues into materials with distinct properties, which could be suitable for profitable use. Therefore, these results do not pretend to clarify the mechanism involved in the chemical reactions occurring during the process; they aim to serve as a descriptive analysis of the changes observed, based on some similarities and differences with the processes recorded by the authors of previous studies on rubber vulcanization.

The most noticeable spectral features that were modified in the ATR-FTIR spectra of the materials isolated from the reaction medium during the treatment (Figure 2) can be thus described: the medium intensity of the band at $\bar{\nu}$: 3 433 cm^{-1}, attributable to the stretching vibration of associated O–H(υ_{O-H}), was present in the spectrum of the chewing gum waste and in those of the aliquots initially isolated from the reaction mixture, but this intensity decreased slightly in the spectra of aliquots, with some grade of cross-linking (vulcanized samples). Its appearance in the spectrum can be explained by residues of sweetener and acids as original components of the chewing gums, by the product of partial deacetylation of its major constituent (the polyvinyl acetate, PVAc) (Rimez *et al.*, 2008), or by occluded water that was not removed by drying, as revealed by the band at $\bar{\nu}$: 1 640 cm^{-1}, attributed to H–O–H bending (δ_{H-O-H}), in the spectrum of the chewing gum waste.

The bands at $\bar{\nu}$: 2 953 cm^{-1}, $\bar{\nu}$: 2 916 cm^{-1}, and $\bar{\nu}$: 2 848 cm^{-1}, due to C-H stretching vibrations on sp^3 hybridized carbon atoms in aliphatic fragments (υ_{C-H}), correlate with the bands of bending in planes H–C–H of methylene groups (δ_{H-C-H}), or in planes H–C–C or H–C–O of methyl groups (δ_{H-C-C}, δ_{H-C-O}) that appear at $\bar{\nu}$: 1 450 cm^{-1} and $\bar{\nu}$: 1 433 cm^{-1}, and their changes in the ATR-FTIR spectra have been previously associated with the progressive cross-linking occurring in rubber vulcanization

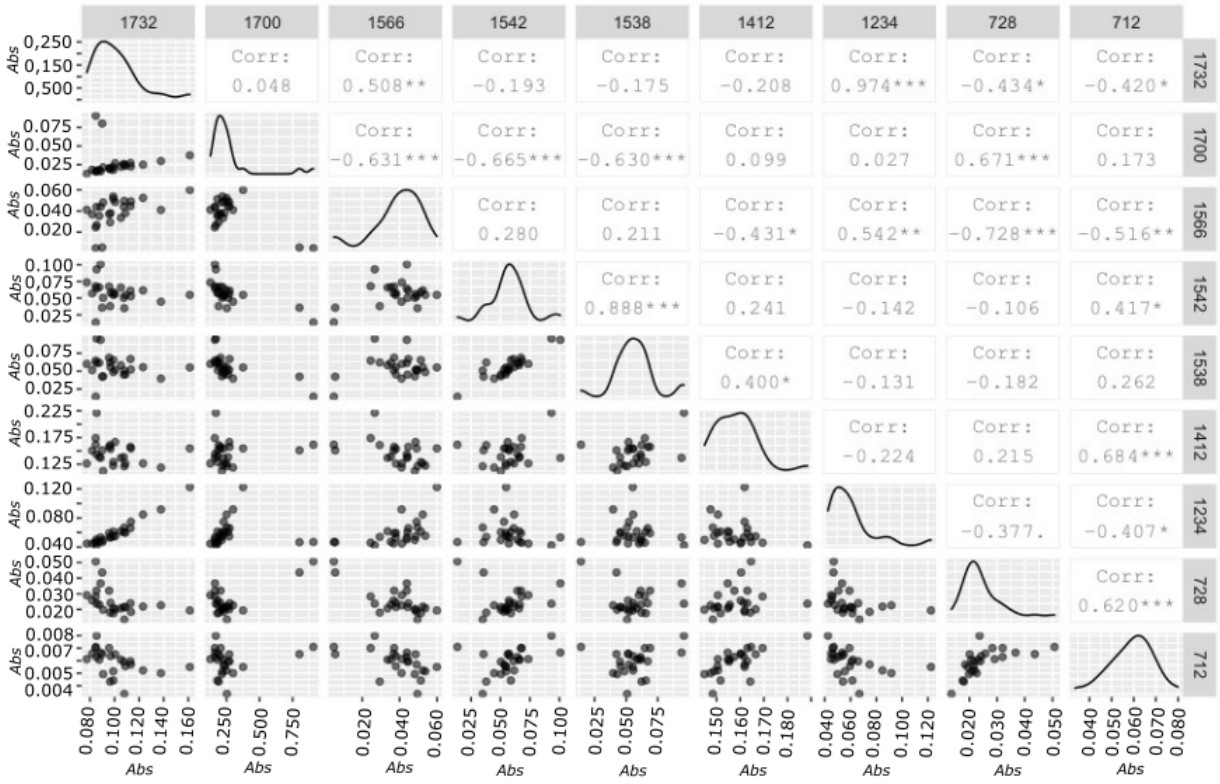

Figure 3. Linear correlation 2D matrix for the absorbance variation of the chosen bands of interest to analyze the set of ATR–FTIR standard reference spectra (normalized) of aliquots isolated from the reaction medium during the vulcanization-like process of chewing gum waste. Statistical significance level: * 0,05, ** 0,01 and *** 0,001. The first line and the last column are wave numbers (cm^{-1}).
Source: Authors

with sulfur (Koenig, 1975), as a result of the decrease in α-methylene hydrogen contents caused by the vulcanization reaction, in which hydrogen, located in alpha, is abstracted to unsaturation as something concomitant to the formation of sulfur bridges (C–Sx–C). For the set of spectra acquired throughout this research, the variation coefficient of the average absorption in the band at $\bar{\nu}$: 1 412 cm^{-1} was 19, 07%. At $\bar{\nu}$: 1 475 – 1 365 cm^{-1}, besides the bands of bending in planes of the $–CH_3$ and $-CH_2-$ groups, those of bending in planes H–C–O of the $–O–CO–CH_3$ fragment appear overlapped and interfere with the analysis of their behavior throughout the process.

There are also three bands in the interval comprising $\bar{\nu}$: 735 – 700 cm^{-1} which are attributable to the rocking or asymmetrical bending in planes H–C–H in aliphatic chains with four or more consecutive methylene groups. This set of bands, with maxima at $\bar{\nu}$: 728 cm^{-1}, at $\bar{\nu}$: 720 cm^{-1}, and at $\bar{\nu}$: 712 cm^{-1}, are complementary to the two sets of signals described before. Its appearance in the spectra can be associated with the gum base and the presence of stearic acid. This analysis shows the band at $\bar{\nu}$: 712 cm^{-1} correlated to that at $\bar{\nu}$: 1 412 cm^{-1} (0, 684 Pearson correlation coefficient, 5% significance) while the band at $\bar{\nu}$: 728 cm^{-1} is correlated to that at $\bar{\nu}$: 1 700 cm^{-1}, which is attributable to stretching of carbonyl (with Pearson correlation coefficient of 0, 671 and a significance of 5%).

When it comes to studying rubber vulcanization and taking into account the IR spectra acquired before and after the process, different approaches have been proposed. Shipman and Golub (1962) reported that the most prominent change in the infrared spectrum of rubber after vulcanization with sulfur is the appearance of a new absorption at $\bar{\nu}$: 961 cm^{-1}. This signal was associated with a carbon-carbon double bond formation (–CH=CH–) by elimination (Shipman and Golub, 1975), *i.e.*, one from the various possible reactions considered in rubber cross-linking. Nevertheless, this signal did not appear in any spectrum of the ATR-FTIR monitoring of the vulcanization-like process of chewnig gum waste under similar conditions, albeit without the use of accelerators.

Additionally, this set of ATR-FTIR spectra allowed detecting some modifications undergone by the zinc oxide and stearic acid present in the reaction medium since the beginning of the process as precursors of zinc-derived accelerators in the vulcanization (Ikeda *et al.*, 2009).

A critical step to attaining efficient curing is the formation of zinc stearate via the reaction of stearic acid and zinc oxide (Figure 4). In the vulcanization-like process of chewing gum waste, this was monitored based on the band at $\bar{\nu}$: 1 542 cm^{-1}, attributable to the asymmetric stretching vibration of the carboxylate anion, which stands for the

complete resonance in the C-O bonds of the carbonyl group due to coordination with the metal (Figure 4). During the first minutes of the process, this band showed an increase in absorbance (a sign of zinc stearate production), while the absorbance of the band at $\bar{\nu}$: 1 700 cm^{-1}, attributable to the stretching of carbonyl ($\upsilon_{C=O}$) in the carboxyl group of the acid, had a proportional decrease, a sign of stearic acid consumption (Figure 3).

In other words, the carbonyl absorption decrease (at $\bar{\nu}$: 1 700 cm^{-1}) was replaced by the increase of that of the band at $\bar{\nu}$: 1 542 cm^{-1} appearing in the spectrum (this was supported by a Pearson correlation coefficient of -0,665). The band at $\bar{\nu}$: 1 542 cm^{-1} appeared as a unique band in the spectra of aliquots isolated until 90 minutes after heating began. From that time onward, a second band appeared at $\bar{\nu}$: 1 566 cm^{-1}, attributable to the anti-symmetric stretching of bands for the bidentate association with zinc ions, which has a Pearson correlation coefficient of -0,631 with the band at $\bar{\nu}$: 1 700 cm^{-1}. A similar behavior was reported for rubber vulcanization (Musto *et al.*, 2013; Ikeda *et al.*, 2015).

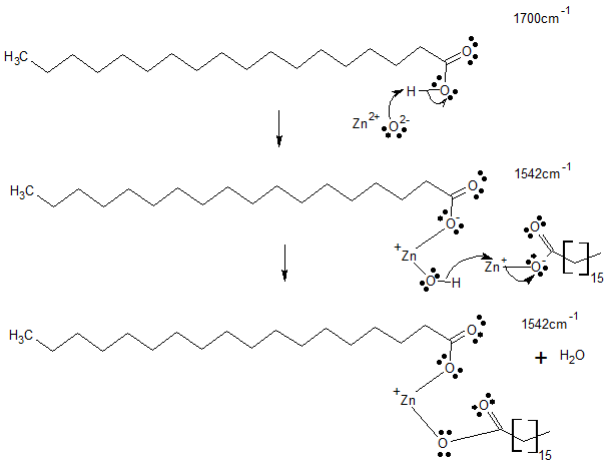

Figure 4. Reaction scheme for the zinc stearate formation related to ATR-FTIR signals recorded during the vulcanization-like process of chewing gum waste
Source: Authors

In the whole set of ATR-FTIR spectra for aliquots isolated from the reaction medium during the studied process, major variations were observed in the absorbance of the bands at $\bar{\nu}$: 1 700 cm^{-1}, at $\bar{\nu}$: 1 566 cm^{-1}, and at $\bar{\nu}$: 1 542 cm^{-1} for the first monitoring intervals times (0-10 min); whereas the bands at $\bar{\nu}$: 1 732 cm^{-1} and $\bar{\nu}$: 1 234 cm^{-1} varied noticeably in the spectra of aliquots isolated at the end of the reaction (220-240 min). Both sets of bands are related to phenomena occurring in carboxylate or carboxyl functional groups, but the variations in the band at $\bar{\nu}$: 1 732 cm^{-1} do not behave similarly to those of $\bar{\nu}$: 1 700 cm^{-1}. This suggests that the band at $\bar{\nu}$: 1 732 cm^{-1} might be a result of the overlapping between bands from the −COOH group of stearic acid associated with hydrogen bridges (Musto *et al.*, 2013) and those from carbonyl of the carboxylate groups of PVAc in the chewing gum waste, as evidenced by the appearance of said bands in the spectrum of the residues, as well as by their absence in the spectrum of the other reagents (Figure 2).

The absorbance of the band at $\bar{\nu}$: 1 732 cm^{-1} ($\upsilon_{=C-O}$) varied just as that at $\bar{\nu}$: 1 234 cm^{-1} ($\upsilon_{=C-O}$); it showed a significant drop in the spectra of aliquots isolated from the reaction medium during the monitoring time, as well as a Pearson correlation coefficient of 0,974 with a 5% significance, suggesting a progressive PVAc degradation under the oxidative conditions inherent to the process applied to chewing gum waste, which was statistically supported by a Pearson correlation coefficient of 0,974 and a 5% significance. This indicates the feasibility of the reaction of such residues under rubber vulcanization-like conditions.

Conclusions

These findings are the first to show that, under conditions such as those of rubber vulcanization, chewing gum residues react to produce materials with different properties, thus evidencing the cross-linking of the lineal chains initially existing in their components, as it probably happens in the aforementioned process.

Monitoring via rheometric measurements and ATR-FTIR spectrometry of a vucanization-like process involving chewing gum waste on a laboratory scale allowed determining the occurrence of cross-linking in a reaction time of 5, 15 minutes. A harder (Shore A hardness: 95 units) and denser (1510 kg/m^3) material than chewing gum wastes was obtained (Shore A hardness: 20 units and density: 1280 kg/m^3).

Monitoring via the ATR-FTIR spectra of the vulcanization-like process of chewing gum waste evidenced the occurrence of structural changes throughout the process, which was also proven by the distinct values of their corresponding rheometric properties, always indicating a progressive evolution in the reaction, similar to that of cross-linking in rubber vulcanization.

These initial findings suggest the possibility of reincorporating chewing gum waste into market value chains and promoting the search for profitable alternatives to treat this type of environmental contaminant. This work encourages readers to consider further research, the scaling of the process, and the characterization of the final product with more rheometric measurements such as the storage and loss modulus, together with viscosity parameters that could enrich the prospects of this research.

Acknowledgements

This study was supported by Universidad EAN (Bogotá, Colombia) namely the Basic Sciences area of the Department of Engineering; and by Universidad Nacional de Colombia (Bogotá campus), represented by the APRENA research group of the Chemistry area, Department of Science. The authors declare their affiliation to one institution or the other, and they appreciate the support received from them.

CRedit author statement

All authors: Conceptualization, methodology, validation, formal analysis, investigation, writing (original draft preparation, review, and editing), data curation, supervision, project administration, resources, and funding acquisition.

References

Anderson, R. J., Bendell, D. J., and Groundwater, P. W. (2004). *Organic spectroscopic analysis* (vol. 22). Royal Society of Chemistry.

ASTM International (2019). *ASTM-D5289-19a: Standard test method for rubber property -Vulcanization using rotorless cure meters. ASTM International*. ASTM International. https://doi.org/10.1520/D5289-19A

ASTM International (2020). *ASTM-D792-20: Standard test methods for density and specific gravity (relative density) of plastics by displacement*. ASTM International. https://doi.org/10.1520/D0792-20

ASTM International (2021). ASTM-D2240-15(2021): *Standard test method for rubber property -Durometer hardness*. ASTM International. https://doi.org/10.1520/D2240-15R21

Barton, S. J., and Hennelly, B. M. (2019). An algorithm for the removal of cosmic ray artifacts in spectral data sets. *Applied Spectroscopy, 73*(8), 893-901. https://doi.org/10.1177/0003702819839098

BBC (2010). *Mayor to tackle London's gum litter problem*. http://news.bbc.co.uk/local/london/hi/people_and_places/newsid_8804000/8804328.stm21/04/2023

Bevilacqua, E. M. (1959). Vulcanization with TMTD. *Rubber Chemistry and Technology, 32*(3), 721-738. https://doi.org/10.5254/1.3542441

Bornstein, D., and Pazur, R. J. (2020). The sulfur reversion process in natural rubber in terms of crosslink density and crosslink density distribution. *Polymer Testing, 88*, 106524. https://doi.org/10.1016/j.polymertesting.2020.106524

Bueche, F. (1961). Mullins effect and rubber–filler interaction. *Journal of Applied Polymer Science, 5*(15), 271-281. https://doi.org/10.1002/app.1961.070051504

Bullus, A. L. (2017). *Composition comprising chewing gum, method for producing the same and use thereof* (France, Patent WO2010046667A1).

Carter, H. (2005). *Liverpool leads campaign for chewing gum tax*. https://www.theguardian.com/uk/2005/apr/28/localgovernment.politics21/04/2023

Coran, A. Y. (1964). Vulcanization. Part VI. A model and treatment for scorch delay kinetics. *Rubber Chemistry and Technology, 37*(3), 689-697. https://doi.org/10.3390/polym11122010

Flory, P. J. (1953). *Principles of polymer chemistry*. Cornell University Press.

Formela, K., Wąsowicz, D., Formela, M., Hejna, A., and Haponiuk, J. (2015). Curing characteristics, mechanical and thermal properties of reclaimed ground tire rubber cured with various vulcanizing systems. *Iranian Polymer Journal, 24*(4), 289-297. https://doi.org/10.1007/s13726-015-0320-9

Fritz, D. P., and Elias, R. J. (1980). *Low density chewing gum product and method of making the same* (US, Patent US4233319A).

Hofko, B., Alavi, M. Z., Grothe, H., Jones, D., and Harvey, J. (2017). Repeatability and sensitivity of FTIR ATR spectral analysis methods for bituminous binders. *Materials and Structures, 50*, 187. https://doi.org/10.1617/s11527-017-1059-x

Ikeda, Y., Higashitani, N., Hijikata, K., Kokubo, Y., Morita, Y., Shibayama, M., Osaka, N., Suzuki, T., Endo, H., and Kohjiya, S. (2009). Vulcanization: New focus on a traditional technology by small-angle neutron scattering. *Macromolecules, 42*(7), 2741-2748. https://doi.org/10.1021/ma802730z

Ikeda, Y., Yasuda, Y., Ohashi, T., Yokohama, H., Minoda, S., Kobayashi, H., and Honma, T. (2015). Dinuclear bridging bidentate zinc/stearate complex in sulfur cross-linking of rubber. *Macromolecules, 48*(3), 462-475. https://doi.org/10.1021/ma502063m

Jacobsen, J., Christrup, L. L., and Jensen, N. H. (2004). Medicated chewing gum. *American Journal of Drug Delivery, 2*(2), 75-88. https://doi.org/10.2165/00137696-200402020-00001

Jampafuang, Y., Tongta, A., and Waiprib, Y. (2015). Impact of crystalline structural differences between α-and β-chitosan on their nanoparticle formation via ionic gelation and superoxide radical scavenging activities. *Polymers, 11*(12), 1-16. https://doi.org/10.3390/polym11122010

Janacek, J. (1962). Reactions of polymers in bulk. I. Influence of fillers on the degree of crosslinking of natural rubber. *Rubber Chemistry and Technology, 35*(3), 563-571. https://doi.org/10.5254/1.3539930

Kim, S. M., Nam, C. S., and Kim, K.J. (2011). TMTD, MBTS, and CBS accelerator effects on a silica filled natural rubber compound upon vulcanization properties. *Applied Chemistry for Engineering, 22*(2), 144-148.

Koenig, J. L. (1975). Application of Fourier Transform infrared spectroscopy to chemical systems. *Applied Spectroscopy, 29*(4), 293-308.

Kruželák, J., Sỳkora, R., and Hudec, I. (2017). Vulcanization of rubber compounds with peroxide curing systems. *Rubber Chemistry and Technology, 90*(1), 60-88. https://doi.org/10.5254/rct.16.83758

Liu, H., and Jiang, Y. (2003). *Chewing gum waste eliminating method* (China, Patent CN1421282A).

Logan, R. P., and Rudolfs, W. (1947). Treatment of wastes from natural gums in chewing gum manufacture. *Industrial and Engineering Chemistry, 39*(12), 1673-1675. https://doi.org/10.1021/ie50456a032

Marković, G., Radovanović, B., Marinović-Cincović, M., and Budinski-Simendić, J. (2009). The effect of accelerators on curing characteristics and properties of natural rubber/chlorosulphonated polyethylene rubber blend. *Materials and Manufacturing Processes, 24*(10), 1224–1228. https://doi.org/10.1080/10426910902967087

Musto, P., Larobina, D., Cotugno, S., Straffi, P., Di Florio, G., and Mensitieri, G. (2013). Confocal Raman imaging, FTIR spectroscopy and kinetic modelling of the zinc oxide/stearic acid reaction in a vulcanizing rubber. *Polymer, 54*(2), 685-693. https://doi.org/10.1016/j.polymer.2012.12.021

Nieuwenhuizen, P.J. (2001). Zinc accelerator complexes: Versatile homogeneous catalysts in sulfur vulcanization. *Applied Catalysis A: General, 207*(1-2), 55-68. https://doi.org/10.1016/S0926-860X(00)00613-X

Niyogi, D. U. K., and Varma, I. K. (2007). *Polymer additives and compounding: Additives for rubbers*. Shri Ram Institute for Industrial Research.

Oosthuizen, T., Howes, L. M., and White, R. (2022). Forensic science and environmental offences: Litter, DNA analysis and surveillance. *Forensic Science International: Animals and Environments, 2*, 100042. https://doi.org/10.1016/j.fsiae.2022.100042

Palabiyik, I., Toker, O. S., Konar, N., Oner, B., and Demirci, A. S. (2018). Development of a natural chewing gum from plant based polymer. *Journal of Polymers and the Environment, 26*(5), 1969-1978. https://doi.org/10.1007/s10924-017-1094-2

Potineni, R. V. (2007). *Mechanisms of flavor release and perception in sugar-free chewing gum* [Doctoral thesis, Pennsylvania State University]. https://www.proquest.com/openview/b3e4c9d491c3fb0b9b7acc9f5096ac95/1?pq-origsite=gscholar&cbl=1875021/04/2023

Rimez, B., Rahier, H., Van Assche, G., Artoos, T., Biesemans, M., and Van Mele, B. (2008). The thermal degradation of poly (vinyl acetate) and poly (ethylene-co-vinyl acetate), Part I: Experimental study of the degradation mechanism. *Polymer Degradation and Stability, 93*(4), 800-810. https://doi.org/10.1016/j.polymdegradstab.2008.01.010

Ribadeau-Dumas, G., and Mentink, L. (2004). *Environment-friendly chewing gum and method of its manufacture* (Mexico, Patent MXPA04000669).

Roy, A. S. (2021). Improper disposal of non-biodegradable chewing gum is one of the biggest threats to our ecology: A review. *Current World Environment, 16*(3), 916-927. http://dx.doi.org/10.12944/CWE.16.3.22

Rudgard, O. (2018). *Introduce a chewing gum tax to pay for cleaning up British streets, LGA says*. https://www.telegraph.co.uk/news/2018/03/02/introduce-chewinggum-tax-pay-cleaning-british-stree/ /ts-lga-says/21/04/2023

Saberi, F., Naderi, M., and Naeli, M. H. (2018). Production of Bio-chewing Gum Based on Saqqez as the Biopolymer: Its Biodegradability and Textural Properties. *Journal of Polymers and the Environment, 26*(9), 3889-3901. https://doi.org/10.1007/s10924-018-1244-1

Sae-oui, P., Sirisinha, C., Thepsuwan, U., and Thapthong, P. (2007). Influence of accelerator type on properties of NR/EPDM blends. *Polymer Testing, 26*(8), 1062-1067. https://doi.org/10.1016/j.polymertesting.2007.07.004

Sánchez, M. A. G., Giraldo-Vásquez, D. H., and Sánchez, R. M. (2020). Rheometric, transient, and cyclic tests to assess the viscoelastic behavior of natural rubber-based compounds used for rubber bearings. *Materials Today Communications, 22*, 100815. https://doi.org/10.1016/j.mtcomm.2019.100815

Savitzky, A., and Golay, M. J. E. (1964). Smoothing and differentiation of data by simplified least squares procedures. *Analytical Chemistry, 36*(8), 1627-1639. https://doi.org/10.1021/ac60214a047

Shelton, J. R., and McDonel, E. T. (1960). Investigation of radical and polar mechanisms in vulcanization reactions. *Rubber Chemistry and Technology, 33*(2), 342-356. https://doi.org/10.5254/1.3542150

Shipman, J. J., and Golub, M. A. (1962). Infrared study of the reaction of polyisoprene and polybutadiene with sulfur by use of deuterated polymers. *Journal of Polymer Science, 98*(166), 1063-1082.

Simonek, M. (2011). *Wrapping for used chewing gum* (US Patent 7.959.001).

Silverstein, R. M., Bassler, G. V., and Morril, T. C. (1991). *Spectrometric identification of organic compound*. John Wiley and Sons.

Smith, B. C. (2011). *Fundamentals of Fourier Transform infrared spectroscopy*. CRC Press.

Šlouf, M., Pilař, Jan., Dybal, J., Šloufová, I., Michálková, D., Lukešová, M., Zgadzai, O., Blank, A., and Filippov, S. K. (2018). UV degradation of styrene-butadiene rubber versus high density poly (ethylene) in marine conditions studied by infrared spectroscopy, micro indentation, and electron spin resonance imaging. *Polymer Degradation and Stability, 156*, 132-143. https://doi.org/10.1016/j.polymdegradstab.2018.08.005

Sozzi, G., and Del Viscio, G. (2011). *Non sticky gum base for chewing gum* (US Patent 7.871.650).

Stuart, B. H. (2004). *Infrared spectroscopy: Fundamentals and applications*. John Wiley and Sons.

Sullivan, A.B., Hann, C.J. and Kuhls, G.H. (1991). *Vulcanization Chemistry Fate of Elemental Sulfur and Accelerator During Scorch Delay as Studied by Modern HPLC*. Papers of the American Chemical Society, Division of Rubber Chemistry.

Takahashi, K., Fukazawa, M., Motohira, H., Ochiai, K., Nishikawa, H., and Miyata, T. (2003). A pilot study on antiplaque effects of mastic chewing gum in the oral cavity. *Journal of Periodontology, 74*(4), 501-505. https://doi.org/10.1902/jop.2003.74.4.501

Thivya, P., Durgadevi, M., and Sinija, V.R.N. (2021). Biodegradable medicated chewing gum: A modernized system for delivering bioactive compounds. *Future Foods, 4*, 100054. https://doi.org/10.1016/j.fufo.2021.100054

Tijani, A. O., Garg, J., Frempong, D., Verana, G., Kaur, J., Joga, R., Sabanis, C. D., Kumar, S., Kumar, N., and Puri, A. (2022). Sustained drug delivery strategies for treatment of common substance use disorders: Promises and challenges. *Journal of Controlled Release, 348*, 970-1003. https://doi.org/10.1016/j.jconrel.2022.06.034

Wang, M., Zhu, J., Zhang, S., You, G. and Wu, S. (2019). Influencing factors for vulcanization induction period of accelerator/natural rubber composites: Molecular simulation and experimental study. *Polymer Testing, 80*, 106145. https://doi.org/10.1016/j.polymertesting.2019.106145

Zou, K. H., Tuncali, K., and Silverman, S. G. (2003). Correlation and simple linear regression. *Radiology, 227*(3), 617-628. https://doi.org/10.1148/radiol.2273011499

Research Article/Civil and Sanitary Engineering http://doi.org/10.15446/ing.investig.96880

Evaluation of Tunnel Elastic and Elasto-Plastic Deformations with Approximations Obtained from 3D-FEM Simulations

Evaluación de las deformaciones elásticas y elastoplásticas en túneles usando aproximaciones obtenidas de simulaciones 3D-FEM

Luisa Equihua-Anguiano[1], Emmanuel Álvarez-Cornejo[2], and Yajaira Concha-Sánchez[3]

ABSTRACT

Nowadays, there are computer tools designed to simulate engineering problems. Numerical simulations in three dimensions (3D) are the closest to reality, but they require a significant amount of time and experience. In this paper, the aim is to present formulae and graphs obtained from numerical simulations using the finite element method (FEM). Their application decreases the time required to obtain deformations in the periphery of different tunnel sections and further serves to evaluate them for different excavation lengths in the face of unexpected geotechnical changes during drilling. Using the RS2 and RS3 software, 3D analyses were carried out according to the Mohr-Coulomb (MC) model, considering elastic and elasto-plastic perfect be-haviors as well as isotropic and anisotropic conditions. The graphs presented herein allow obtaining displacements from an axisymmetric model to infer the 3D displacements horseshoe tunnels, and the polynomial expressions aid in determining the displacements of an established excavation length. Finally, comparisons between the displacements reported by other authors and those obtained with the polynomial expressions are presented as a means of validation for this research.

Keywords: tunnels, finite element method, Mohr-Coulomb, elastic-elastoplastic

RESUMEN

En la actualidad existen herramientas computacionales diseñadas para simular problemas de ingeniería. Las simulaciones numéricas tridimensionales (3D) son las más cercanas a la realidad, pero requieren una cantidad importante de tiempo y experiencia. En este artículo, el objetivo es presentar fórmulas y gráficos obtenidos de simulaciones realizadas utilizando el método de elementos finitos (FEM). La aplicación de estos disminuye el tiempo requerido para obtener deformaciones en la periferia de distintas secciones de túnel, e incluso funciona para evaluarlas con respecto a distintas longitudes de excavación cuando se encuentren cambios geotécnicos inesperados durante la perforación. Mediante el software RS2 y RS3, se realizaron análisis 3D de acuerdo con el modelo Mohr-Coulomb, teniendo en cuenta comportamientos elásticos y elastoplásticos perfec-tos, así como condiciones isotrópicas y anisotrópicas. Los gráficos aquí presentados permiten obtener los desplazamientos a partir de un modelo axisimétrico para a su vez inferir los desplazamientos 3D de túneles con forma de herradura, y las expresio-nes polinómicas ayudan a determinar los desplazamientos de una longitud de excavación establecida. Por último, se presen-tan comparaciones entre los desplazamientos reportados por otros autores y aquellos obtenidos con las expresiones polinómicas como medio para la validación de esta investigación.

Palabras clave: túneles, método de elementos finitos, Mohr-Coulomb, elástico-elastoplástico

Received: June 22th, 2021
Accepted: September 12th, 2022

Introduction

Tunnel infrastructure is a fundamental part of modern life, as it reduces the impact on the surface and improves travel times. Research on tunnel design and construction continues, given the large amount of data, knowledge, and expertise that are required for these civil works. In practice, many methods are used in the design phase, such as empirical, analytical, and numerical analysis. Empirical methods have used equations based on experience (Khan *et al*., 2019; Rehman *et al*., 2018; Terzaghi, 1942), analytic methods use rupture schemas to emulate soil or rock failure (Lu *et al*., 2020; Kong *et al*., 2019; Langford and Diederichs, 2013), and numerical analysis methods are integrated into specialized software and are applied in practice and research (Sadique *et al*., 2022; Zaid, 2021; Zaid and Shah, 2021; Equihua-Anguiano *et al*., 2017; Vlachopoulos and Diederichs, 2014). The goal in all types of methods is to determine the stress and deformations of the medium, which is decisive in tunnel behavior (Zhang *et al*., 2020; Qiu *et al*., 2017; Ngueyep *et al*., 2015). Nevertheless, each method is implemented under

[1] PhD, INPGrenoble, France. Engineer, Affiliation: CFE Subgerencia de Geotecnia y Materiales, Mexico, E-mail: luisa.equihua@cfe.mx
[2] MSc, FIC-UMSNH, Mexico. Engineer, Affiliation: CFE Subgerencia de Geotecnia y Materiales, Institution, E-mail: emalvarez1115@gmail.com
[3] PhD, UMSNH, Mexico, Professor, Affiliation: FIC-UMSNH, Mexico, E-mail: yajacs26@gmail.com

How to cite: Equihua-Anguiano, L., Álvarez-Cornejo, E., and Concha-Sánchez, Y. (2023). Evaluation of Tunnel Elastic and Elasto-Plastic Deformations with Approximations Obtained from 3D-FEM Simulations. *Ingeniería e Investigación, 43*(2), e96880. http://doi.org/10.15446/ing.investig.96880

specific conditions due to the high variability of the design process. All methodologies and theories are complemented in practice using *in situ* testing and field monitoring (Ma *et al*., 2022; Du *et al*., 2020).

In general, geotechnical determination constitutes one of the greatest sources of unknown data prior to the construction of an engineering underground project (Soldo *et al*., 2019), which becomes a challenge for each specific tunnel (Kaya and Bulut, 2019). Nowadays, the development of new methods to predict tunnel behavior continues (Vitali *et al*., 2020), and, on the other hand, laboratory tests are necessary to have a better comprehension of the tunnels (Zhao *et al*., 2020). Due to the complexity of tunnel construction, a problem that has been widely studied around the world is the squeezing phenomenon, which can be analyzed using empirical and numerical solutions (Hanumanthappa and Maji 2017; Zhiming *et al*., 2019). Other particular challenges are the effect of the superstructure on the stability of underground tunnels (Naqvi *et al*., 2021), the failure behavior of horseshoe-shaped tunnels in hard rock under high stress while aiming to determine the fracture around a tunnel based on numerical simulations (Hao and Zhao, 2022), the deformations taking place during ground settlement in clay soil (Sadique *et al*., 2021), and the effect of blast loading (Zaid and Rehan Sadique, 2021; Zaid *et al*., 2022) among others.

Thus, numerical simulations constitute a useful tool, as they allow for different considerations adapted to particular designs. Nevertheless, it is necessary to calibrate and validate numerical models. Tunnels are not the exception, in light of the multiple possibilities to be considered. Commercial codes allow solving complex problems, *e.g.*, using the finite element method (FEM), which involves differential equations adapted to the studied problem and is recurrently used in practice to solve all kind of engineering problems. Some examples of its application are simulations of the effect of weathering (Mishra *et al*., 2022; Zaid *et al*., 2022); the challenges involved in the selection of excavation techniques, support types, and dynamic effects (Khan *et al*., 2022); and static loading (Zaid and Mishra, 2021). Come things to consider in order to obtain a useful numerical model are the mesh characteristics (Azimi *et al*., 2016), the parameters selected according to actual data or the methodology used for construction (Forsat *et al*., 2022), and the impact of the constitutive model employed (Huang *et al*., 2020, Hejazi *et al*., 2008); if these are carefully considered, they will allow for an accurate reproduction of geotechnical conditions.

Other methods to consider for managing uncertainties during construction are the reliability and hybrid approaches, which integrate machine learning methods or deterministic and probabilistic analysis (Li *et al*., 2021; Zhang and Lin, 2021; Chen *et al*., 2019; Johansson *et al*., 2016; Spross, 2016; Celestino *et al*., 2006; Lombardi and Amberg, 1974), as well as observational methods (Bjureland *et al*., 2017; Spross, 2017; Holmberg and Stille, 2007). The latter have been pointed out by some design codes (CEN 2004). However, decisive progress in the field is obtained by the availability of powerful computers for making calculations (Lunardi 2008), due to the complexity and time required for designing this type of structures. Regarding the above, it is evident that each work requires studies that require long calculation times, as well as field and laboratory validations.

Methodology and application

In this study, a numerical analysis using the FEM was conducted while applying RS2 and RS3 and modeling tunnels with circular and horseshoe cross-sections. Deformations in three dimensions (3D) were analyzed in the periphery of the tunnels at different lengths of the excavation, with the objective of elaborating graphs that allowed determining elastic and elasto-plastic deformations without using FEM software and aiding in the preliminary design of a tunnel. Based on the numerical evaluation, it was possible to establish polynomial expressions for both cases. In this methodology, a circular section was first selected, and then the results were compared against axisymmetric (AX) conditions and 3D dimensions. From equivalent meshes (Equihua-Anguiano *et al*., 2018) obtained from the comparisons made between the models in 2D and 3D, it was possible to obtain results for different tunnel sections, using equivalent area criteria proposed from the circular original section (RT). The construction process of the displacement graphs was iterative.

From the elastic results, deformation factors (Fi) were obtained in order to infer the maximum displacements for different excavation lengths in horseshoe tunnel sections. For the sake of validation, a comparison of the displacement obtained by the proposed polynomial expression and that of other authors is presented in this document.

The polynomial expressions and graphs proposed in this work allow reducing the time required via a quick evaluation of the deformations taking place in the tunnel periphery. They would be applicable in drilling, when unexpected geotechnical changes may arise, or for the initial study phase, with the advantage that it is possible to infer displacements for different tunnel sections and excavation lengths.

Numerical modeling

Characteristics of the analyzed models: stress state and geometrical conditions

The following stress states were simulated as constant in the models: the vertical stress σ1 and two horizontal stresses σ2 = σ3, as obtained from the geostatic conditions of the material. Vertical stress σ1 was obtained as a product of multiplying the depth from the ground surface to the center of the tunnel (Ho) and the soil unit weight (γ). The isotropic state (Is) considers the same magnitude for vertical and horizontal stresses (σ1 = σ2 = σ3) and the anisotropic state

(An), a coefficient of lateral earth pressure (K) (AASHTO, 2012; NCMA, 2010) equal to 0,6 was selected (Tamez-González *et al*., 1997). Soil radial stresses in the tunnel periphery (*Pa*) of 609 and 300 kPa were analyzed. These values were selected based on Equihua-Anguiano *et al*. (2018). Figure 1 shows the employed nomenclature. Three pressure conditions were considered from *Pa* = 0 kPa in order to evaluate the elastic theory, despite the fact that the deformations obtained are higher the actual ones. *Pa* = 609 and 300 kPa were the numerical artifices that allowed considering the presence of the lining system.

Table 1 lists the studied tunnels. Two modeling phases can be observed: in the first modeling phase, the influence of the geometry of the cross-tunnel sections was evaluated for soils with the same characteristics; in the second phase, the consequences of varying some parametric soil conditions were studied, as well as the stress state in the soil, and complemented for a third phase; and the last phase allowed elaborating the graphs proposed in this work.

In this Table, *General Information* indicates the descriptive nomenclature used to identify the results.

Table 1. Several studied cases and nomenclature used for the parametric study

Phase	General Information				Geometry			Parameter Variation			Discretization		
	#	Nomenclature	Cross Section	Type of Analysis	Evaluation point	Tunnel Depth *Ho* (m)	Tunnel radius *r* (m)	Pressure uniformity	*Pa* (kPa)	Elasticity Module *E* (kPa)	Number of nodes #ND	Number of elements #EL	Type of Finite Elements
1st	RMR	*2D-Original Section*	*Ci*	*2D*	*C*	50	5	*Is*	0	15 000	6 394	2 083	TRIA-6N
	1	*Ci-AX-15-Is*	*Ci*	*AX*	*C*	50	5	*Is*	0	15 000	3 268	3 114	TRIA-6N
	2	*Ci-3D-15-Is*	*Ci*	*3D*	*C*	50	5	*Is*	0	15 000	84, 90	63 078	TETH-4N
	RMR		*H1*	*2D*	*C*	50	-	*Is*	0	15 000	4 525	1 486	CUAD-8N
					S	50	-	*Is*	0	15 000	4 525	1 486	CUAD-8N
	3	*H1-3D-15-Is-C*	*H1*	*3D*	*C*	50	-	*Is*	0	15 000	33 327	204 486	TETH-4N
		H1-3D-15-Is-S			*S*	50	-	*Is*	0	15 000	33 327	204 486	TETH-4N
	RMR		*H2*	*2D*	*C*	50	-	*Is*	0	15 000	4 503	1 476	CUAD-8N
					S	50	-	*Is*	0	15 000	4 503	1 476	CUAD-8N
	4	*H2-3D-15-Is-C*	*H2*	*3D*	*C*	50	-	*Is*	0	15 000	27 665	170 054	TETH-4N
		H2-3D-15-Is-S			*S*	50	-	*Is*	0	15 000	27 665	170 054	TETH-4N
2nd	RMR		*Ci*	*2D*	*C*	50	5	*Is*	0	5 000	6 394	2 083	CUAD-8N
	RMR		*Ci*	*2D*	*C*	50	5	*Is*	0	24 000	6 394	2 083	CUAD-8N
	5	*Ci-AX-5-Is*	*Ci*	*AX*	*C*	50	5	*Is*	0	5 000	3 260	3 109	CUAD-4N
	6	*Ci-AX-24-Is*	*Ci*	*AX*	*C*	50	5	*Is*	0	24 000	3 253	3 100	CUAD-4N
	7	*Ci-3D-15-Is*	*Ci*	*3D*	*C*	50	5	*Is*	0	15 000	843 900	630 780	TETH-4N
	RMR		*H1*	*2D*	*C*	50	-	*Is*	0	15 000	4 525	1 486	TRIA-6N
					S	50	-	*Is*	0	15 000	4 525	1 486	TRIA-3N
	RMR		*H2*	*2D*	*C*	50	-	*Is*	0	15 000	4 503	1 476	TRIA-6N
					S	50	-	*Is*	0	15 000	4 503	1 476	TRIA-6N
	8	*H1-3D-5-Is-C*	*H1*	*3D*	*C*	50	-	*Is*	0	5 000	33 327	204 486	TETH-4N
	9	*H2-3D-15-Is-C*	*H2*	*3D*	*C*	50	-	*Is*	0	15 000	276 650	170 054	TETH-4N
		H2-3D-5-Is-S			*S*	50	-	*Is*	0	15 000	276 650	170 054	TETH-4N
	10	*Ci-AX-5-Is-3.0*	*Ci*	*AX*	*C*	75	3	*Is*	0	5 000	13 269	6 674	CUAD-4N
	11	*Ci-AX-15-Is-7.0*	*Ci*	*AX*	*C*	100	7	*Is*	0	15 000	4 183	4 022	CUAD-4N
	12	*Ci-3D-15-Is-609*	*Ci*	*3D*	*C*	50	5	*Is*	609	15 000	84 390	630 780	TETH-4N
	13	*Ci-3D-24-An*	*Ci*	*3D*	*C*	50	5	*An*	0	24 000	103 220	630 780	TETH-4N
3rd	14	*r = 3 m (Ci)*	*Ci*	*3D*	*C*	30	3	*Is*	0	15 000	33 063	203 790	TETH-10N
	15	*r = 5 m (Ci)*	*Ci*	*3D*	*C*	30	5	*Is*	0	15 000	40 496	236 541	TETH-10N
	16	*r = 7 m (Ci)*	*Ci*	*3D*	*C*	50	7	*Is*	0	15 000	231 849	170 988	TETH-10N
	17	*r = 3 m (H2-C)*	*H2*	*3D*	*C*	30	3	*Is*	0	15 000	211 098	154 701	TETH-10N
		r = 3 m (H2-S)			*S*	30	3	*Is*	0	15 000	211 098	154 701	TETH-10N
	18	*r = 5 m (H2-C)*	*H2*	*3D*	*C*	40	5	*Is*	0	24 000	324 214	239 611	TETH-10N
		r = 5 m (H2-S)			*S*	40	5	*Is*	0	24 000	324 214	239 611	TETH-10N

Note: 2D = Two-dimensional; AX = Axisymmetric; 3D = Three-dimensional; Is = Isotropic; An = Anisotropic; Ci = Circular; C = Tunnel key; S = Tunnel floor; (-) = Not applicable; RMR = Reference models for results; CUAD-4N = Quadrilaterals-4 nodes; TRIA-6N = Triangular-6 nodes; TETH-4N = Tetrahedrons-4 nodes; TETH-10N = Tetrahedrons-10 nodes.

Source: Authors

The *Geometry* column mentions the two points where deformations were analyzed: the tunnel key (C) and the floor (S) (Figure 2), as well as the radii (r) of the circular sections that were modeled and the depth (Ho). In addition, the *Parameter Variation* column presents the stress state conditions (Is and An). The *Pa* shows the normal pressure applied in the tunnel periphery, as well as the elastic modulus (E) used in each simulation. Finally, the discretization details of the characteristics of the continuous medium are presented, namely the number of nodes and the number and type of finite elements.

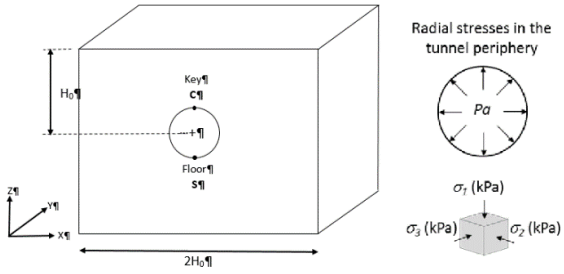

Figure 1. Stress state, geometry, convention axes (-x, -y, and -z), and nomenclature used in the 3D-RS3 numerical models
Source: Authors

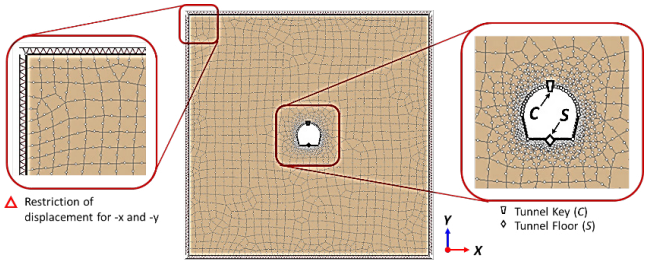

Figure 2. Geometry, boundary conditions, convention axes (-x and -y), and nomenclature used in the 2D-RS2 numerical models
Source: Authors

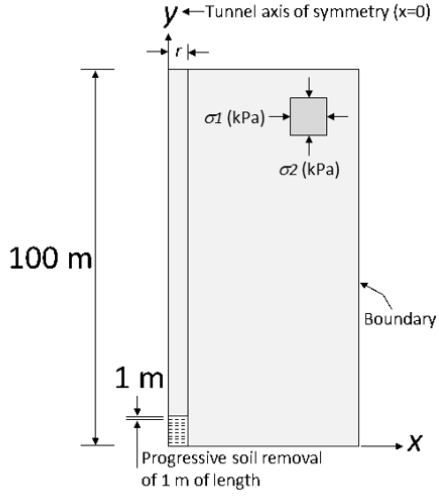

Figure 3. Geometry, convention axes (-x and -y), and nomenclature used in the AX-RS2 numerical models
Source: Authors

The 2D models were simulated in two stages: the *in situ* conditions without material removal in the tunnel section, and material removal to simulate the excavation. The excavation of the AX and 3D tunnels was simulated in stages based on *in situ* conditions. Afterwards, a progressive soil removal of 1 m of material length was considered, for a total of 101 excavation stages (Figure 3). The boundaries of the models were restricted as follows: the rims of the model were restricted in all directions (-x, -y, and -z), and the border of the excavation was restricted in the direction of the longitudinal axis (-y, *i.e.*, the direction in which the excavation advanced) (Figure 4).

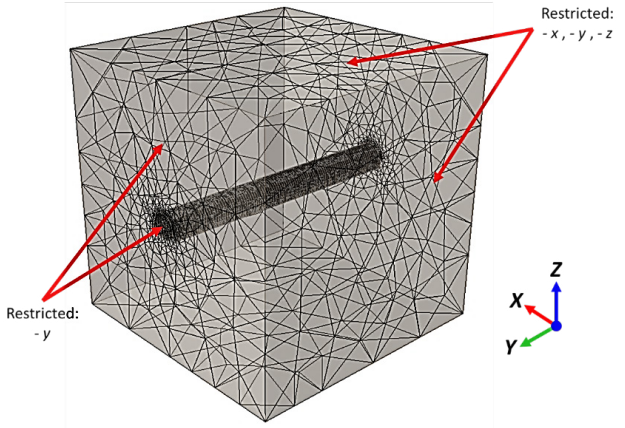

Figure 4. Mesh 3D model, axes convention, and boundary conditions, with FEM tetrahedron elements
Source: Authors

Tunnel sections

For the elastic study, three tunnel sections were analyzed, as indicated in Table 1, whose geometries are presented in Figure 5. The proposal was to form the models by matching the position of the tunnel key (C) of the different sections (Figure 6). To regard them as equivalent sections, the same transversal area was considered. The transversal area of the circular sections was obtained, and, from it, two equivalent horseshoe sections named *H1* and *H2* were calculated. The parametric conditions of the soil and the stress states were similar to those assigned to the original circular tunnels.

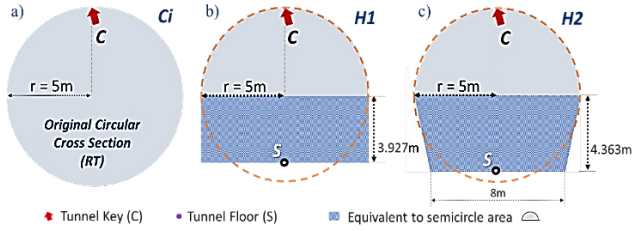

Figure 5. Original circular cross-section (Ci) for r = 5 m and two horseshoe cross-sections (H1 and H2) used in the elastic numerical modeling
Source: Authors

Geotechnical parameters

The soil parameters considered are shown in Table 2. The constitutive model was the Mohr-Coulomb one regarding

the elastic and elastic perfectly plastic behavior. The elastic modulus (E) was varied to study the influence of different soil rigidities with three different values. The soil parameters were taken from typical material found in Morelia, Mexico, as a reference for this study.

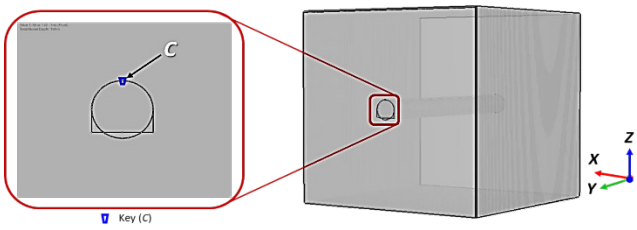

Figure 6. Coincidence of the key (C) of the tunnels with different cross-sections (Ci) for r = 5 m and the horseshoe equivalent section (H1)
Source: Authors

Table 2. Geotechnical soil parameters

Constitutive model	γ (kN/m³)	c (kPa)	φ (°)	ν (-)	E (kPa)
Mohr-Coulomb	17,4	12	22	0,35	5 000 15 000 24 000

Source: Authors

Elastic mesh validation

Via Equation (1) (Deere *et al*., 1969), the radial displacements of a circular tunnel were obtained and compared with the results obtained from the 2D and 3D models.

$$u = \left(H_o - P_a \right) \frac{(1+)D}{2E} \quad (1)$$

Where:

u = elastic displacement in the tunnel periphery
γ = soil unit weight
Ho = depth from the ground surface to the center of the tunnel
Pa = soil radial stress in the tunnel periphery
ν= Poisson ratio
D = tunnel diameter
E = soil elastic modulus

The results of the 2D models served as a reference for an approximation of the expected results in 3D. Figure 7 presents the mesh sizes for the 2D and 3D analyses. The mesh dimensions were 100 x 100m and for the 3D model, and a thickness of 1 m in the y-axis was modeled. Figure 8 shows the results obtained from the analytical Equation (1) and the numerical results of 2D-RS2 and 3D-RS3. The radial stress (*Pa*) in the tunnel periphery was varied, starting from the *in situ* stress condition (*Pa* = 870 kPa) until it reached zero. The analytical displacements, which are represented in Figure 8 with rhombuses, and the 2D displacements in points A and B (stars and squares, respectively) of the tunnel periphery, are very similar to each other. In the same way, the results obtained from the 3D numerical model (dashed line) are similar to the 2D results. Based on the above, the thickness of the 3D mesh was extended in length (L) in order to analyze the effect of the excavation.

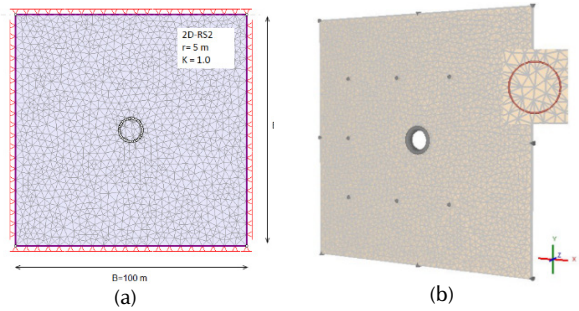

Figure 7. Equivalent meshes in a) 2D-RS2, 100 x 100 m, r = 5 m, 2 750 triangular elements and 1 418 nodes; and b) 3D-RS3, 100 x 100 x1 m, r = 5 m, 500 triangular elements and 10-node tetrahedron
Source: Authors

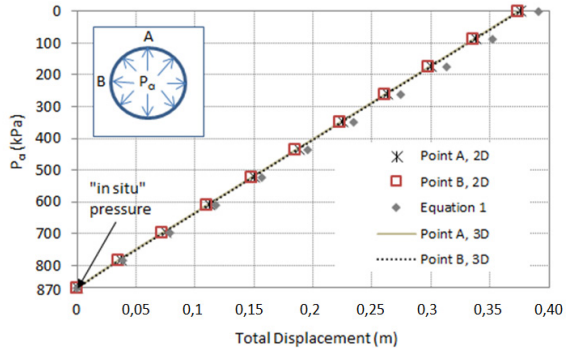

Figure 8. Numerical and analytical radial displacements obtained for a circular tunnel, r = 5 m, K = 1,0, using Equation (1), 2D-RS2 and 3D-RS3
Source: Authors

Results

First modeling phase – elastic behavior

In this phase, the deformations were evaluated while considering an isotropic medium with the soil characteristics shown in Table 2, as well as with an elastic modulus of E = 15 000 kPa. The influence exerted by the use of different cross-sections (circular and horseshoe) was studied for 2D, AX, and 3D conditions.

First, the analyzed tunnel section had a circular (Ci) shape with r = 5 m. To obtain the relationship between the deformations for the different geometries, the deformations (δ) were evaluated in the key (C) and in the floor (S) for the horseshoe sections H1 and H2. In Figure 9, it can be seen that, for all models, the trend of the deformations describes the same behavior, and the maximum deformation is always the 2D response, as shown by 2D H1-S, 2D H1-C, and 2D H2-C show. The continuous line describes deformations for the reference tunnel (Ci 3D-15-Is). From this line, it is possible to observe the influence of the change in tunnel geometries. The measured points C and S are shown, and it can be noted that the S point exhibits the most unfavorable deformations (cross and square void symbols). Furthermore, the H1 section

exhibits greater displacements. On the other hand, the C point reports virtually the same deformations as the reference tunnel. The analyzed behavior shows that the S point is the critical deformation in design, and it moves in a similar proportion depending of the geometry H1 or H2. It is concluded that the trend is similar in the key (C) of the three numerical results.

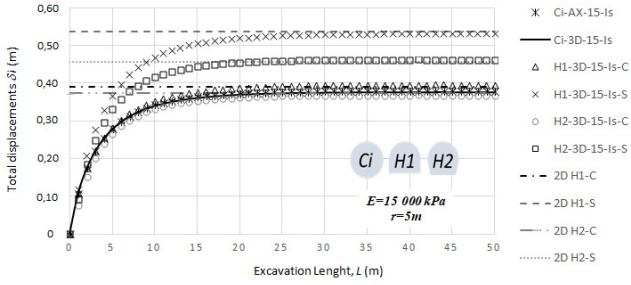

Figure 9. Comparisons between the total displacements (i) and length of excavation (L) of the original tunnel (Ci, r = 5 m), E = 15 000 kPa, *Pa* = 0 kPa in the H1 and H2 sections
Source: Authors

In Figure 9, the results correspond to a *Pa* = 0 kPa. This simulation is only valid as a theoretical reference and as a starting point for this study. In practice, its condition will never occur, given the lining system that is placed in tunnels. In this sense, the displacements observed in the floor of the H1 and H2 sections have a difference of approximately 10 cm and are greater in section H1 because the difference in the length floor is 2 m.

Second modeling phase – elastic behavior

For the second phase, the soil geometry and parametric conditions were varied in accordance with Table 1. The total displacements (δ) *vs.* excavation length (L) graphs were obtained for the models in AX and 3D dimensions, and they were normalized as shown in Figure 10. The normalization was carried out based on the deformations (δi) taking place along of the length (L) with respect to the maximum deformation (δi max) in ten cases. The graphs describe a similar trend to those of the first modeling phase, and the separation observed between the lines only shows the influence of r on the deformations; a greater r causes greater displacements in shallower excavation lengths, as seen with the filled square symbols. It can also be noted that there is an interval for the r = 5m (Ci), as well as in its corresponding equivalent horseshoe sections (H1 and H2), where the trend shows a very good match. In Figure 10, it can be seen that the normal pressure of *Pa* = 609 kPa, described with triangles (Ci-3D-15-Is-609), agrees with the results of the models with *Pa* = 0 kPa (*e.g.*, Ci-3D-15-Is void circles and H1-3D-5-Is-C dashed symbols).

In the same way, the anisotropic and isotropic conditions were compared, as well as the variation of the E and the simulated conditions (3D and AX). This means that, by modifying *Pa*, the cross-section, E, K, analysis type, and the two evaluated points (C and S), the trend of deformations is not affected when normalizing the lines while considering the same radius (r = 5m). The lines with a similar behavior are Ci-3D-15-Is, Ci-AX-24-Is, H2-3D-15-Is-C, H2-3D-15-Is-S, Ci-3D-24-An, H1-3D-5-Is-C, and Ci-3D-15-Is-609. Figure 11 shows the 3D kinematics of the deformation, obtained for the conditions of Ci-Is in a circular tunnel and an H1 tunnel section. In the same Figure, the displacements tend to zero, as observed via the blue area. This happens when the simulated excavation length is next to the end of the progressive soil removal of 1 m in length of the material (L = 18 m in Figure 11). Nevertheless, when the excavated length is the total simulated one, the displacements in the tunnel periphery correspond to the same deformations in the entire tunnel periphery.

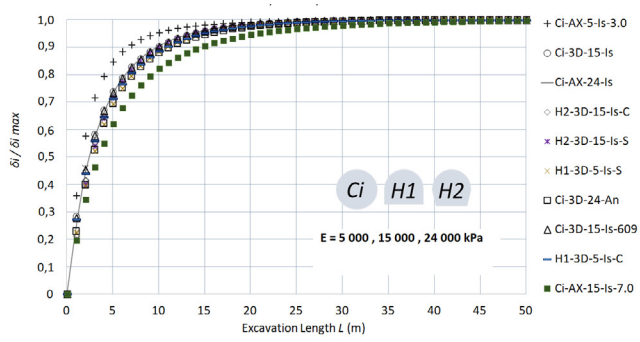

Figure 10. Normalized graph of deformations (δi) along of the length of excavation (L) with respect to the maximum deformation (δi max) for different tunnels and parametric conditions
Source: Authors

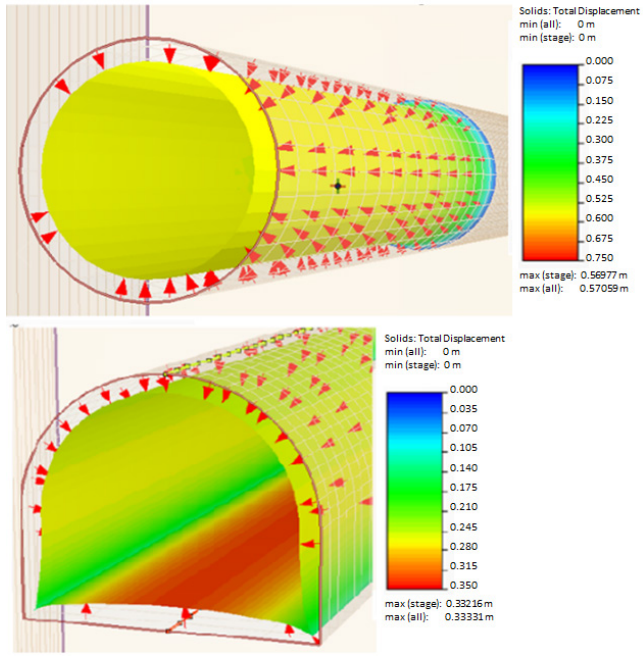

Figure 11. Deformation kinematics for Ci-r = 5 m and H1-r = 7 m
Source: Authors

Displacement graphs and polynomial expressions – elastic behavior

The displacement graphs were elaborated based on Figure 12. The trend lines Ci-AX-24-Is, Ci-3D-15-Is, Ci-3D-15-Is-609, Ci-3D-24-An, H1-3D-5-Is-C, and H2-3D-15-Is-C represent the FEM results obtained for r = 5m in the key (C) of the

tunnel, in which the displacements δ were normalized with respect to γ, Ho, *Pa*, E, and the maximum elasticity modulus considered for rigid soil (Emax = 24 000 kPa). The lines are very close to each other; thus, it is possible to consider the same behavior. On the other hand, the separation observed in the H1-3D-Is-5-C and H2-3D-Is-5-S lines is attributed to the automatic building of the mesh refinement. As a result, it is determined that parameters such as E, *Pa*, Is, An, and the shape H1 and H2 do not have a great influence on the normalized displacements of the C point for all tunnel sections. Greater displacements take place at the S point in the H1 and H2 sections with respect to the C point, and they can be obtained from this graph. From these results, it is concluded that this normalization works for every numerical simulation performed in FEM (3D and AX).

Another normalization was performed for the three radii studied, adding rmax/r multiplication (rmax = 7 m) to the normalization shown in Figure 13. Note that the three radii have the same maximum normalized value, and only the first meters of the excavation length have different displacements, with greater displacements for longer radii (r=7m). In this way, the results show the possibility to obtain the displacements by using any radius between 3 and 7 m (Figure 14).

Based on the above-presented analyses, the polynomial expressions (2), (3), and (4) were calculated by polynomial interpolation (Teodorescu *et al.*, 2013; Stoer and Bulirsch, 1993; Hamming, 1987; Conte and de Boor, 1972) using the Mathematica software (Wolfram Research, 2020), which provides a simple and good way to estimate the analytical expression –which is essentially a function– over the range of the measured points. These polynomial expressions are presented to obtain the displacements δ in the tunnel periphery for r = 3, 5, and 7 m, respectively. Figures 14apresents the adjustment.

$$\frac{\delta\ \gamma}{\gamma\ H_o - P_a} \cdot \frac{E}{E_{max}} \cdot \frac{r_{max}}{r} 1000 = \quad (2)$$

$$0.0002L^5 - 0.0072L^4 - 0.107L^3 - 0.7918L^2 + 3.1832L$$

Until L = 20 m - r=5m

$$\frac{\delta\ \gamma}{\gamma\ H_o - P_a} \cdot \frac{E}{E_{max}} \cdot \frac{r_{max}}{r} 1000 = \quad (3)$$

$$-0.0002L^4 + 0.0103L^3 - 0.1967L^2 + 1.7237L$$

Until L = 20 m - r = 7m

$$\frac{\delta\ \gamma}{\gamma\ H_o - P_a} \cdot \frac{E}{E_{max}} \cdot \frac{r_{max}}{r} 1000 = \quad (4)$$

$$-0.0001L^4 + 0.0068L^3 - 0.1395L^2 + 1.3784L$$

Where:

δ = total displacement in the tunnel periphery
γ = soil unit weight
Ho = depth from the ground surface to the center of the tunnel
Pa = radial stresses in the tunnel periphery
E = Elastic modulus of the soil
Emax = maximum elasticity modulus (24,000 kPa)
r = radius of the tunnel
rmax = maximum radius used (7m)
L = length of the excavation

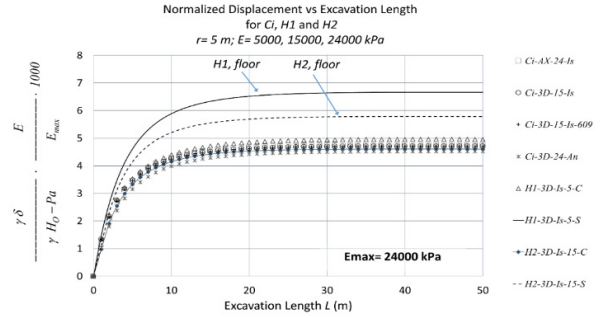

Figure 12. Excavation length (L) *vs.* normalized elastic displacements for r = 5 m, Ci, H1, H2, E = 5 000, 15 000, and 24 000 kPa under isotropic Is and anisotropic An conditions, considering models in AX and 3D and for different Pa
Source: Authors

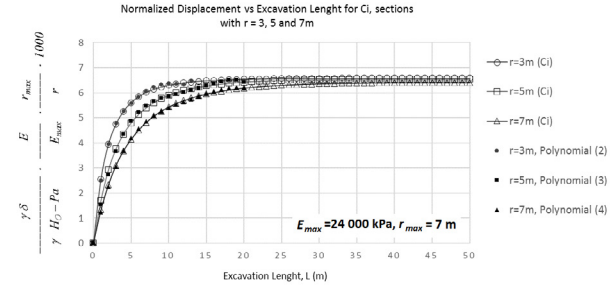

Figure 13. Excavation length (L) *vs.* normalized elastic displacements for r = 3, 5, and 7 m for the circular section Ci
Source: Authors

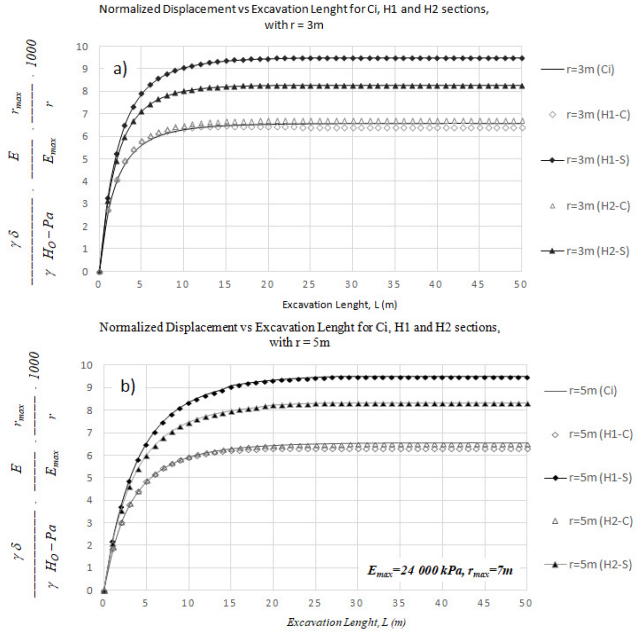

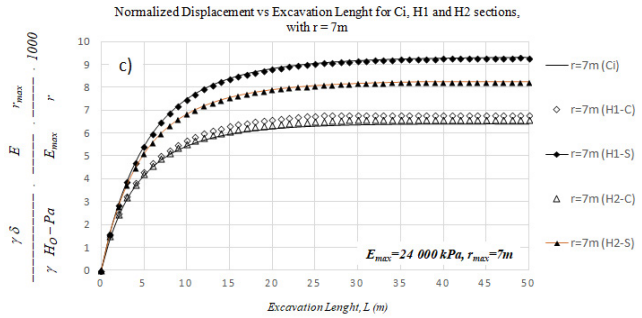

Figure 14. Elastic displacement for (a) r = 3 m, (b) r = 5 m, and (c) r = 7 m for Ci, H1 and H2 sections
Source: Authors

Deformation factors (Fi)

Figures 14a, 14b, and 14c present the average of the lines of the deformations δ for all reported simulations. Note that the trends are the same for all simulations, with similar values for all lines. From the maximum displacement obtained from the AX-FEM simulations, a relationship was proposed by comparing these results against the displacements (δimax) obtained from the two horseshoe sections.

$$F_i = \frac{\delta_{maxAX}}{\delta_{imax}} \tag{5}$$

Where:

Fi = deformation factor
δmaxAX = maximum deformation in AX FEM model
δimax = maximum deformation in FEM models for H1 and H2

This relationship allows obtaining the maximum displacements in the key (C) and in the floor (S) of a horseshoe section (H1 or H2) from axisymmetric (AX) simulations while using the equivalent criterion is proposed in this article. The deformation factors (Fi) obtained are presented in Table 3.

Elasto-plastic behavior

In this section, the steps followed for the elastic study were emulated, and the normalization curves were obtained in the same way. The numerical models were replicated according to Table 1, and, in order to obtain a perfectly elasto-plastic behavior, the shear parameters c and ϕ were duplicated according to RS3. In this case, a *Pa* = 300 kPa was modeled. Even though this pressure is low, this value allows soil to go from its elastic interval to its plastic interval. Figure 15 presents the normalized curves for the three radii studied, considering only circular sections, as well as the adjustment obtained from the proposed polynomial expressions (6), (7), and (8). For the case of the r = 3m (Ci), a leap is observed in the first meters of the excavation length, which is due to the fact that, for this radius, the *Pa* is high, so it decreases the displacements in the first meters, although there is an L where de maximal displacement is reached.

Table 3. Deformation factors Fi, r = 5 m (FEM models)

Model	E (kPa)	Deformation Factor (Fi)	Coincidence
H1-3D-5-Is-S	5 000	0,71	H1-Floor
H1-3D-24-Is-S	24 000		
H1-3D-15-Is-S	15 000		
H2-3D-5-Is-S	5 000	0,82	H2-Floor
H2-3D-24-Is-S	24 000		
H2-3D-15-Is-S	15 000		
H1-3D-5-Is-C	5 000	0,96	H1-Key
H1-3D-24-Is-C	24 000		
H1-3D-15-Is-C	15 000		
Ci-AX-5-Is	5 000	1,00	Ci-AX
Ci-AX-15-Is	24 000		
Ci-AX-24-Is	15 000		
Ci-3D-5-Is	5 000	1,00	Ci-3D
Ci-3D-24-Is	24 000		
Ci-3D-15-Is	15 000		
H2-3D-5-Is-C	5 000	1,03	H2-Key
H2-3D-24-Is-C	24 000		
H2-3D-15-Is-C	15 000		
Ci-3D-5-An	5 000	1,05	K = 0,6
Ci-3D-24-An	24 000		
Ci-3D-15-An	15 000		

Source: Authors

The polynomial expressions proposed to obtain elasto-plastic displacements δ in the tunnel periphery for r = 3, 5, and 7 m respectively are as follows:

Until L = 30 m - r = 3 m

$$\frac{\delta\ \gamma}{\gamma\ H_o - P_a} \cdot \frac{E}{E_{max}} \cdot \frac{r_{max}}{r} 1000 = \tag{6}$$

$$4.5024L - 0.5708L^2 + 0.0339L^3 - 0.00095L^4 + 1.003\text{x}10^{-5}L^5$$

Until L = 30 m - r = 5 m

$$\text{r = 5 m}\ \frac{\delta\ \gamma}{\gamma\ H_o - P_a} \cdot \frac{E}{E_{max}} \cdot \frac{r_{max}}{r} 1000 = \tag{7}$$

$$2.3157L - 0.2441L^2 + 0.0133L^3 - 0.00036L^4 + 3.71309\text{x}10^{-6}L^5$$

Until L = 30 m - r = 7 m

$$\frac{\delta\ \gamma}{\gamma\ H_o - P_a} \cdot \frac{E}{E_{max}} \cdot \frac{r_{max}}{r} 1000 \tag{8}$$

$$1.7549L - 0.1641L^2 + 0.0085L^3 - 0.00022L^4 + 2.26\text{x}10^{-6}L^5$$

Comparisons with other works

Comparisons with the results reported by other authors were conducted by applying the expressions proposed in

this work and the displacements and data informed in the following papers: Arnau and Molins (2012) studied the 3D structural response of segmental tunnel linings, and their results constitute the obtained displacements in isolated rings and joints; Katebi *et al*. (2015) studied the influence of ground stratification and tunnel and surface building specifications on shield tunnel lining loads using FEM; Miro *et al*. (2014) presented the study of a global sensitivity analysis for subsoil parameter estimation in mechanized tunneling; Xing-Tao *et al*. (2019) presented a three-dimensional stress transfer mechanism and soil arching evolution as induced by shield tunneling in sandy ground.

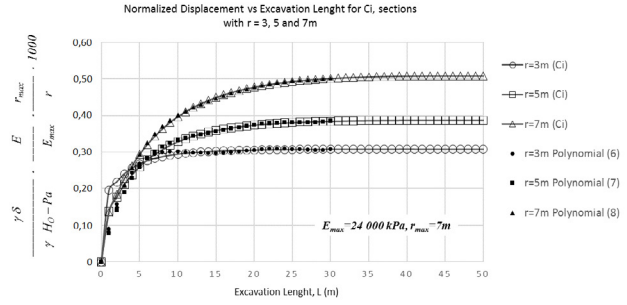

Figure 15. Excavation length (L) *vs.* normalized elasto-plastic displacements for r = 3, 5, and 7 m, circular section Ci
Source: Authors

Table 4 shows a summary of the parameters collected from the papers, with the purpose of comparing them with the results obtained using the expressions (2), (3), (4), (6), (7), and (8). The displacements selected from the papers are labeled with δmax_art, and those obtained with the polynomial expressions are labeled with δ Elastic and δ Elasto-Plastic for the elastic and elasto-plastic displacements, respectively. The parameters substituted in equations correspond to those found in the papers. The L considered is the excavation length corresponding to one day or to the ring thickness placed in the tunnels.

Figure 16 shows the displacements calculated with the polynomial expressions *vs.* the displacements reported by other authors. For the five first cases, the *Pa* was not reported. For said cases, two values (*Pa* = 0 and 50 kPa) were considered, and the displacements obtained are presented in Table 4 and Figure 16. The results for the three cases mentioned by Arnau and Molins (2012) –which consider a *Pa* = 0 kPa– are lower than those reported in this paper. As expected, if *Pa* = 50 kPa, the displacements decrease and are closer to the displacements found by Arnau and Molins (2012). In general, it can be noted that all of the calculated displacements follow the same trend and are very close to those found by other authors. In the case where the *Pa* applied is greater than the geostatic conditions, the polynomial expressions are not applicable, as in case 6 (Miro *et al*., 2014)

For cases 6, 7, and 9, the displacements obtained with the proposed equations and those of other papers are very similar. In all cases, the elasto-plastic response is greater that the elastic displacements obtained, so this is a conservative way to evaluate displacements before the design phase.

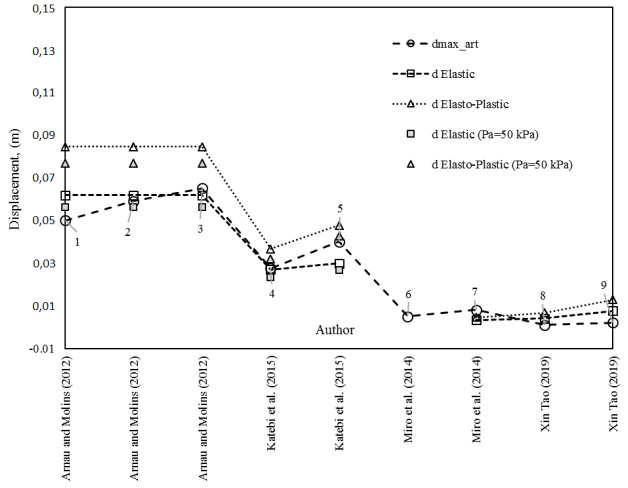

Figure 16. Comparisons between the displacements obtained from the polynomial expressions proposed in this work and those reported by other authors
Source: Authors

Table 4. Summary of data used by other authors and results obtained from the polynomial expressions

Author	Conditions	γ (kN/m3)	E (kN/m2)	Ho (m)	r (m)	Pa (kPa)	L (m)	δmax_art (m)	δ Elastic (m)	δ Elasto-Plastic (m)
Arnau and Molins (2012)	Linear	18	25 000	30,8	5,8	*	1,8	0,050	0,06	0,08
									0,056	0,077
Arnau and Molins (2012)	Non-Linear	18	25 000	30,8	5,8	*	1,8	0,059	0,062	0,085
									0,056	0,077
Arnau and Molins (2012)	Isolated ring	18	25 000	30,8	5,8	*	1,8	0,065	0,062	0,085
									0,056	0,077
Katebi *et al*. (2015)	ML	20,35	25 000	18,98	4,745	*	1,5	0,0275	0,027	0,037
									0,023	0,032
Katebi *et al*. (2015)	SM	20	23 000	23,44	3,44	*	1,0	0,040	0,03	0,05
									0,027	0,043
Miro *et al*. (2014)	Geostatic	16	25 000	8,5	4,25	136	1,5	0,0050	-	-
Miro *et al*. (2014)	Long term	16	25 000	17	4,25	230	1,5	0,0080	0,003	0,005
Xin Tao (2019)	Sandy Ground	19,5	37 800	12	3	147,3	1,5	0,0010	0,004	0,007
Xin Tao (2019)	Sandy Ground	19,5	37 800	15	3	128,7	1,5	0,0020	0,008	0,013

* Not reported; *Pa* values of 0 kPa and 50kPa were substituted in the equations
Source: Authors

Conclusions

This study presents polynomial expressions and graphs to obtain 3D deformations in the periphery of different tunnel sections. These were obtained from the numerical simulations of a parametric study carried out in RS2 and RS3. This approach reduces the time required to obtain said deformations and evaluate them for different excavation lengths in the face of unexpected geotechnical changes encountered during drilling, as well as when a rapid evaluation of deformations is required.

The polynomial expressions were obtained from numerical 3D results and through an interpolation with the Mathematica software. As a complement of the polynomial equations, deformation factors (Fi) were obtained, which can be applied to predict deformations in the key or floor of two horseshoe tunnel sections. Fi relationships depend on the maximum displacements obtained from an axisymmetric simulation (AX).

In the numerical simulations, different displacements were observed in the first meters of the 3D excavation, and there was a distance at which the maximum displacement takes place depending on the tunnel characteristics. Thus, the application of the graphs supersedes the use of a 3D-FEM analysis, and it is possible to evaluate 3D displacements for different excavation lengths until the displacement reaches its maximum value.

Despite the fact that elastic theory is a classical and a relatively simple design method, it provides reliable designs for the case of tunnels that are based primarily on displacements in the tunnel periphery. 2D analysis provides the maximum displacement in a tunnel. If this value is used in design, it can cause an overdesign of the infrastructure, *i.e.*, if it is considered for an excavation length greater than L = 13 m for r = 3 m and L = 20m for r = 5 and 7 m.

In the same way, a first elasto-plastic approximation is presented, along with polynomial equations considering a low internal pressure, aiming to ensure that the soil is in its elasto-plastic interval.

The influence of the variation in parametric conditions and the stress state of the tunnels were studied. It was observed that soil rigidities do not have an influence on the normalized results, unlike radii, as larger displacements are caused in smaller excavation lengths for larger tunnel diameters of the tunnels. Shorter diameters result in lower displacements. In this regard, the displacement is not proportional to the radius.

At higher normal pressures, there are lower deformations. Nevertheless, when this is normalized, there is no influence on the displacements. The polynomial expressions or graphs presented herein can be used to obtain displacements for different *Pa* values, determined as a function of the value taken for the tunnel lining while considering the length of the tunnel excavation.

For the case of the anisotropic conditions, it can be stated that the average is very similar. Graphs including the results obtained from the representative models of the parametric variations normalized with the maximum deformation were presented in order to understand the impact of modifying them. It was observed that the same deformation tendency was maintained.

The displacements obtained by other authors are very close to those of this study (elastic and elastoplastic). However, the elasto-plastic response is higher that the elastic one, which makes this a conservative way to evaluate displacements before the design phase.

Finally, this is the beginning of other considerations that need to be made, such as the determination of the displacements along the construction length and the possibility of a three-dimensional understanding of the effect on the internal pressure, with the aim to determine the time to place the lining or to improve tunnel design. It is necessary to carry out more studies that allow understanding displacements under plastic conditions in order to provide better estimations according to the real soil behavior.

CRediT author statement

Conceptualization, methodology, validation, formal analysis, investigation, writing (original draft preparation, review, and editing), data curation, supervision, project administration, resources, and funding acquisition.

References

American Association of State Highway and Transportation Officials (AASHTO). (2012). *AASHTO LRFD bridge design specifications* (6th ed). AASHTO.

Arnau, O., and Molins, C. (2012). Three dimensional structural response of segmental tunnel linings. *Engineering Structures, 44*, 210-221. https://doi.org/10.1016/j.engstruct.2012.06.001

Azimi, M., Mirjavadi, S. S., and Asli, S. A. (2016). Investigation of mesh sensitivity influence to determine crack characteristic by finite element methods. *Journal of Failure Analysis and Prevention, 16*(3), 506-512. https://doi.org/10.1007/s11668-016-0117-y

Bjureland, W., Spross, J., Johansson, F., Prästings, A., and Larson, S. (2017). Reliability aspects of rock tunnel design with the observational method. *International Journal of Rock Mechanics and Mining Sciences, 98*, 102-110. https://doi.org/10.1016/j.ijrmms.2017.07.004

Celestino, T. B., Aoki, N., Silva, R. M., Gornes, R. A. M. P., Bortolucci, A. A., and Ferreira, D. A. (2006). Evaluation of tunnel support structure reliability. Tunneling and Underground Space Technology, 21(3-4), 311. https://doi.org/10.1016/j.tust.2005.12.028

CEN (2004) Eurocode 7: Geotechnical design – Part 1: General rules. European Committee for Standardization, EN 1997-1:2004.

Chen, F., Wang, L., and Zhang, W. (2019). Reliability assessment on stability of tunnelling perpendicularly beneath an existing tunnel considering spatial variabilities of rock mass properties. *Tunnelling and Underground Space Technology, 88*, 276-289. https://doi.org/10.1016/j.tust.2019.03.013

Conte, S. D., and De Boor C. (1972). *Elementary numerical analysis* (2nd ed.). McGraw-Hill Inc.

Deere, D. U., Peck, R. B., Monsees, J. E., and Schmidt, B. (1969). *Design of tunnel liners and support systems*. US Department of Transportation.

Du, M., Wang, X., Zhang, Y., Li, L., and Zhang, P. (2020). *In-situ* monitoring and analysis of tunnel floor heave process. *Engineering Failure Analysis, 109,* 104323. https://doi.org/10.1016/j.engfailanal.2019.104323

Equihua-Anguiano, L. N., Rubio-Saldaña, I., Orozco-Calderón, M., Arreygue-Rocha, J. E., and Chávez-Negrete, C. (2018). Equivalent FEM meshes from Axisymmetric (AXID) to three (3D) dimensions applied to tunnels in clay. In S. Shu, L. He, and Y. Kai (Eds.), *New Developments in Materials for Infrastructure Sustainability and the Contemporary Issues in Geo-environmental Engineering* (pp. 11-22). Springer. https://doi.org/10.1007/978-3-319-95774-6_2

Equihua-Anguiano, L. N., Viveros-Viveros, F., Pérez-Cruz, J. R., Chávez-Negrete, C., Arreygue-Rocha, J. E., Orozco-Calderón, M. (2017). *Displacement nomograph from two (2D) to three (3D) dimensions applied to circular tunnels in clay using finite element* [Conference paper]. International Conference on Soil Mechanics and Geotechnical Engineering, Seoul, Korea.

Forsat, M., Taghipoor, M., and Palassi, M. (2022). 3D FEM model on the parameters' influence of EPB-TBM on settlements of single and twin metro tunnels during construction. *International Journal of Pavement Research and Technology, 15*(3), 525-538. https://doi.org/10.1007/s42947-021-00034-0

Hamming R. W. (1987). *Numerical methods for scientists and engineers* (2nd ed.). Dover Publications.

Hanumanthappa, M., and Maji, V. B. (2017). Empirical and numerical analyses of tunnel closure in squeezing rock. *International Journal of Geosynthetics and Ground Engineering, 3*, 38. https://doi.org/10.1007/s40891-017-0118-2

Hao, W. U., and Zhao, G. Y. (2022). Failure behavior of horseshoe-shaped tunnel in hard rock under high stress: Phenomenon and mechanisms. *Transactions of Nonferrous Metals Society of China, 32*(2), 639-656. https://doi.org/10.1016/S1003-6326(22)65822-9

Hejazi, Y., Dias, D., and Kastner, R. (2008). Impact of constitutive models on the numerical analysis of underground constructions. *Acta Geotechnica, 3*(4), 251-258. https://doi.org/10.1007/s11440-008-0056-1

Holmberg, M., and Stille, H. (2007). *The application of the observational method for design of underground excavations*. SveBeFo.

Huang, M., Zhan, J. W., Xu, C. S., and Jiang, S. (2020). New creep constitutive model for soft rocks and its application in the prediction of time-dependent deformation in tunnels. *International Journal of Geomechanics, 20*(7), 04020096. https://doi.org/10.1061/(ASCE)GM.1943-5622.0001663

Johansson, F., Bjureland, W., and Spross, J. (2016). *Application of reliability-based design methods to underground excavation in rock*. BeFo.

Katebi, H., Rezaei, A. H., Hajialilue-Bonab, M., and Tarifard, A. (2015). Assessment the influence of ground stratification, tunnel and surface buildings specifications on shield tunnel lining loads (by FEM). *Tunnelling and Underground Space Technology, 49*, 67-78. https://doi.org/10.1016/j.tust.2015.04.004

Kaya, A., and Bulut, F. (2019). Geotechnical studies and primary support design for a highway tunnel: A case study in Turkey. *Bulletin of Engineering Geology and the Environment, 78*(8), 6311-6334. https://doi.org/10.1007/s10064-019-01529-8

Khan, B., Jamil, S. M., Jafri, T. H., and Akhtar, K. (2019). Effects of different empirical tunnel design approaches on rock mass behaviour during tunnel widening. *Heliyon, 5*(12), e02944. https://doi.org/10.1016/j.heliyon.2019.e02944

Khan, M. A., Sadique, M., Harahap, I. H., Zaid, M., and Alam, M. M. (2022). Static and dynamic analysis of the shielded tunnel in alluvium soil with 2D FEM model. *Transportation Infrastructure Geotechnology, 9*(1), 73-100. https://doi.org/10.1007/s40515-021-00160-z

Kong, F., Lu, D., Du, X., and Shen, C. (2019). Elastic analytical solution of shallow tunnel owing to twin tunnelling based on a unified displacement function. *Applied Mathematical Modelling, 68*, 422-442. https://doi.org/10.1016/j.apm.2018.11.038

Langford, J. C., and Diederichs, M. S. (2013). *Evaluating uncertainty in intact and rock mass parameters for the purpose of reliability assessment* [Conference paper]. 7th US Rock Mechanics/Geomechanics Symposium, ARMA, San Francisco, California, United States.

Li, B., Fu, Y., Hong, Y., and Cao, Z. (2021). Deterministic and probabilistic analysis of tunnel face stability using support vector machine. *Geomechanics and Engineering, 25*(1), 17-30. https://doi.org/10.3208/jgssp.v08.c13

Lombardi, G., and Amberg, W. (1974). *Une méthode de calcul élasto-plastique de l'état de tension et de déformazion autour d'une cavité souterraine* [Conference paper]. Congresso Internazionale, ISRM, Denver, Colorado, United States.

Lu, D., Shen, C., Kong, F., and Du, X. (2020). Viscoelastic analytical solution for shallow tunnel considering time-dependent displacement boundary. *Japanese Geotechnical Society Special Publication, 8*(11), 430-435.

Lunardi, P. (2008). *Design and construction of tunnels. Analysis of controlled deformation in rocks and soils (ADECO-RS)*. Springer. https://doi.org/10.1007/978-3-540-73875-6

Ma, K., Zhang, J., Zhang, J., Dai, Y., and Zhou, P. (2022). Floor heave failure mechanism of large-section tunnels in sandstone with shale stratum after construction: A case study. *Engineering Failure Analysis, 140*, 106497. https://doi.org/10.1016/j.engfailanal.2022.106497

Miro, S., Hartmann, D., and Schanz, T. (2014). Global sensitivity analysis for subsoil parameter estimation in mechanized tunneling. *Computers and Geotechnics, 56*, 80-88. https://doi.org/10.1016/j.compgeo.2013.11.003

Mishra, S., Zaid, M., Rao, K. S., and Gupta, N. K. (2022). FEA of urban rock tunnels under impact loading at targeted velo-

city. *Geotechnical and Geological Engineering, 40*(4), 1693-1711. https://doi.org/10.1007/s10706-021-01987-6

National Concrete Masonry Association (NCMA). (2010). *Design manual for segmental retaining walls* (3rd ed.). NCMA.

Naqvi, M. W., Akhtar, M. F., Zaid, M., and Sadique, M. R. (2021). Effect of superstructure on the stability of underground tunnels. *Transportation Infrastructure Geotechnology, 8*(1), 142-161. https://doi.org/10.1007/s40515-020-00119-6

Ngueyep Mambou, L. L., Ndop, J., and Ndjaka, J. (2015). Numerical investigations of stresses and strains redistribution around the tunnel: Influence of transverse isotropic behavior of granitic rock, in situ stress and shape of tunnel. *Journal of Mining Science, 51*(3), 497-505. https://doi.org/10.1134/S1062739115030102

Qiu, L., Wang, E., Song, D., Liu, Z., Shen, R., Lv, G., and Xu, Z. (2017). Measurement of the stress field of a tunnel through its rock EMR. *Journal of Geophysics and Engineering, 14*(4), 949-959. https://doi.org/10.1088/1742-2140/aa6dde

Rehman, H., Ali, W., Naji, A. M., Kim, J. J., Abdullah, R. A., and Yoo, H. K. (2018). Review of rock-mass rating and tunneling quality index systems for tunnel design: Development, refinement, application and limitation. *Applied sciences, 8*(8), 1250. https://doi.org/10.3390/app8081250

Rocscience Inc. (n.d.). *RS2, 2D Geotechnical Finite Element Analysis, version 9.0 64 bits* [Computer software]. Rocscience Inc.

Rocscience Inc. (n.d.). *RS3, 3D Geotechnical Finite Element Analysis, version 2.0 64 bits* [Computer software]. Rocscience Inc.

Sadique, M., Ali, A., Zaid, M., and Masroor Alam, M. (2021). Experimental and numerical modeling of tunneling-induced ground settlement in clayey soil. In S. Kumar Shukla, S. N. Raman, B. Bhattacharjee, and J. Bhattacharjee (Eds.), *Advances in Geotechnics and Structural Engineering* (pp. 23-33). Springer. https://doi.org/10.1007/978-981-33-6969-6_3

Sadique, M., Zaid, M., and Alam, M. (2022). Rock tunnel performance under blast loading through finite element analysis. *Geotechnical and Geological Engineering, 40*(1), 35-56. https://doi.org/10.1007/s10706-021-01879-9

Soldo, L., Vendramini, M., and Eusebio, A. (2019). Tunnels design and geological studies. *Tunnelling and Underground Space Technology, 84*, 82-98. https://doi.org/10.1016/j.tust.2018.10.013

Spross, J. (2016). *Toward a reliability framework for the observational method* [Doctoral thesis, KTH Royal Institute of Technology].

Spross J., and Johansson, F. (2017). When is the observational method in geotechnical engineering favourable. *Structural Safety, 66*, 17-26. https://doi.org/10.1016/j.strusafe.2017.01.006

Stoer, J., and Bulirsch, R. (1993). *Introduction to numerical analysis* (2nd ed.). Springer-Verlag. https://doi.org/10.1007/978-1-4757-2272-7

Tamez-González, E., Rangel-Núñez, J. L., and Holguín, E. (1997). *Diseño geotécnico de túneles*. TGC Geotecnia S.A. de C.V.

Teodorescu, P., Stanescu N-D., and Pandrea N. (2013). *Numerical analysis with applications in mechanics and engineering* (1st ed.). Wiley, IEEE Press. https://doi.org/10.1002/9781118614563

Terzaghi, K. (1942). Liner-plate tunnels on the Chicago (IL) subway. *Proceedings of the American Society of Civil Engineers, 68*(6), 862-899.

Vitali, O. P., Celestino, T. B., and Bobet, A. (2020). Analytical solution for a deep circular tunnel in anisotropic ground and anisotropic geostatic stresses. *Rock Mechanics and Rock Engineering, 53*(9), 3859-3884. https://doi.org/10.1007/s00603-020-02157-5

Vlachopoulos, N., and Diederichs, M. S. (2014). Appropriate uses and practical limitations of 2D numerical analysis of tunnels and tunnel support response. *Geotechnical and Geological Engineering, 32*(2), 469-488. https://doi.org/10.1007/s10706-014-9727-x

Wolfram Research Inc. (2020). *Mathematica* [Computer software]. https://www.wolfram.com/mathematica

Xing-Tao, L., Ren-Peng, C., Huai-Na, W., and Hong-Zhan C. (2019). Three-dimensional stress-transfer mechanism and soil arching evolution induced by shield tunneling in sandy ground. *Tunnelling and Underground Space Technology, 93*, 103104. https://doi.org/10.1016/j.tust.2019.103104

Zaid, M. (2021). Preliminary study to understand the effect of impact loading and rock weathering in tunnel constructed in quartzite. *Geotechnical and Geological Engineering, 2021*, s10706-021-01948-z. https://doi.org/10.1007/s10706-021-01948-z

Zaid, M., and Mishra, S. (2021). Numerical analysis of shallow tunnels under static loading: a finite element approach. *Geotechnical and Geological Engineering, 39*(3), 2581-2607. https://doi.org/10.1007/s10706-020-01647-1

Zaid, M., and Rehan Sadique, M. (2021). A simple approximate simulation using coupled Eulerian–Lagrangian (CEL) simulation in investigating effects of internal blast in rock tunnel. *Indian Geotechnical Journal, 51*(5), 1038-1055. https://doi.org/10.1007/s10706-021-01927-4

Zaid, M., Sadique, M., and Alam, M. (2022). Blast resistant analysis of rock tunnel using abaqus: Effect of weathering. *Geotechnical and Geological Engineering, 40*(2), 809-832. https://doi.org/10.1007/s10706-021-01927-4

Zaid, M., and Sadique, M. R. (2021). Blast resistant behaviour of tunnels in sedimentary rocks. *International Journal of Protective Structures, 12*(2), 153-173. https://doi.org/10.1177/2041419620951211

Zaid, M., and Shah, I. A. (2021). Numerical analysis of imalayan rock tunnels under static and blast loading. *Geotechnical and Geological Engineering, 39*(7), 5063-5083. https://doi.org/10.1007/s10706-021-01813-z

Zhang, L., and Lin, P. (2021). Multi-objective optimization for limiting tunnel-induced damages considering uncertainties. *Reliability Engineering & System Safety, 216*, 107945. https://doi.org/10.1016/j.ress.2021.107945

Zhang, M., Li, S., and Li, P. (2020). Numerical analysis of ground displacement and segmental stress and influence of yaw excavation loadings for a curved shield tunnel. *Computers and Geotechnics, 118*, 103325. https://doi.org/10.1016/j.compgeo.2019.103325

Zhao, H., Liu, C., Huang, G., Yu, B., Liu, Y., and Song, Z. (2020). Experimental investigation on rockburst process and failure characteristics in trapezoidal tunnel under different lateral stresses. *Construction and Building Materials, 259*, 119530. https://doi.org/10.1016/j.conbuildmat.2020.119530

Zhiming, L., Jian, C., Mitsutaka, S., and Hongyan, G. (2019). Numerical simulation model of artificial ground freezing for tunneling under seepage flow conditions. *Tunneling and Underground Space Technology, 92*, 103035. https://doi.org/10.1016/j.tust.2019.103035

Research Article/Chemical, Food and Environmental Engineering https://doi.org/10.15446/ing.investig.94617

Influence of Conventional and Hybrid Septic Tank-Anaerobic Filter Configurations on the Hydrodynamics and Performance of Wastewater Treatment

Evaluación de la influencia de las configuraciones convencional e híbrida de tanque séptico-filtro anaerobio sobre la hidrodinámica y desempeño del tratamiento de aguas residuales

Maricel Arias-Henao[1], Diego Paredes-Cuervo[2], and Patricia Torres-Lozada[3]

ABSTRACT

Decentralized treatment is an adequate strategy to more sustainably treat municipal wastewater in rural and peri-urban areas. In light of the above, this study evaluated, on a pilot scale, the performance of an anaerobic configuration consisting of a septic tank (ST) and an anaerobic filter (AF) in two modalities: (i) a conventional system (CS) in separate reactors and (ii) a hybrid system (HS) with a ST and an AF in a single reactor –both with theoretical hydraulic retention times (HRTs) of 36, 30, 24, and 18 hours. The results indicated that the HS had a better performance (less variability) under the different conditions evaluated, achieving, at an HRT of 18 hours, higher reduction efficiencies (52,0±16,8% COD and 73,06±18,5% TSS) compared to the CS (39,8±13,1% COD and 65,8±20,52% TSS). Although hydrodynamic analysis showed dual flow (full mix and plug flow) in both configurations, the HS exhibited a greater predominance of plug flow (62%) than the CS (52%), which allowed the former to reach a real HRT closer to the theoretical value than the latter (23/24 *vs*. 19/24 hours). This behavior guarantees the lowest occurrence of dead zones and short circuits, as well as a higher Persson hydraulic efficiency (0,62) and lower area requirements for the HS in comparison with the CS (0,5).

Keywords: anaerobic digestion, anaerobic filter, decentralized wastewater treatment, hydrodynamic performance, septic tank

RESUMEN

El tratamiento descentralizado es una estrategia adecuada para tratar las aguas residuales municipales en áreas rurales y periurbanas de manera más sostenible. Con base en esto, este estudio evaluó, a escala piloto, el desempeño de una configuración anaerobia conformada por un tanque séptico (TS) y un filtro anaerobio (FA) en dos modalidades: (i) un sistema convencional (SC) en reactores separados y (ii) un sistema híbrido (SH) con TS y FA en un solo reactor –ambos con tiempos teóricos de retención hidráulica (TRH) de 36, 30, 24 y 18 horas. Los resultados indicaron que el SH presentó un mejor desempeño (menor variabilidad) bajo las diferentes condiciones evaluadas, logrando, a un TRH de 18 horas, mayores eficiencias de reducción (52,0±16,8 % DQO y 73,06±18,5 % SST) en comparación con el SC (39,8±13,1 % DQO y 65,8±20,52 % SST). Aunque el análisis hidrodinámico mostró flujo dual (mezcla completa y flujo pistón) en ambas configuraciones, el SH presentó mayor predominio del flujo pistón (62 %) que el SC (52 %), lo que permitió que el primero alcanzara un TRH real más cercano al valor teórico que el segundo (23/24 vs. 19/24 horas). Este comportamiento garantiza la menor ocurrencia de zonas muertas y cortocircuitos, así como una mayor eficiencia hidráulica de Persson (0,62) y menores requerimientos de área para el SH en comparación con el SC (0,5).

Palabras clave: digestión anaerobia, filtro anaerobio, tratamiento descentralizado de aguas residuales, comportamiento hidrodinámico, tanque séptico

Received: March 19th, 2021
Accepted: January 6th, 2023

[1] MSc Engineering-Sanitary and Environmental Engineering, Universidad del Valle, Colombia. Universidad Tecnológica de Pereira, Faculty of Engineering, Water and Sanitation Research Group, Carrera 27 #10-02, Pereira, Colombia. E-mail: maricel.arias@utp.edu.co

[2] PhD Engineering, Martin Luther Universität Halle-Wittemberg, Germany. Associate professor, Universidad Tecnológica de Pereira, Faculty of Environmental Sciences, Water, and Sanitation Research Group, Carrera 27 #10-02, Pereira, Colombia. E-mail: diparede@utp.edu.co

[3] PhD Civil Engineering-Hydraulics and Sanitation, São Paulo University, Brazil. Full professor, Universidad del Valle, Faculty of Engineering, Study and Control of Environmental Pollution (ECCA) Research Group, Calle 13 # 100-00, Cali, Colombia. E-mail: patricia.torres@correounivalle.edu.co – Corresponding author

How to cite: Arias-Henao, M., Paredes-Cuervo, D., and Torres-Lozada, P. (2023). Influence of conventional and hybrid septic tank-anaerobic filter configurations on the hydrodynamics and performance of wastewater treatment.. *Ingeniería e Investigación, 43*(2), e94617. https://doi.org/10.15446/ing.investig.94617

Introduction

The sixth sustainable development goal (SDG) involves ensuring access to water and sanitation. Thus, clean and accessible water for all is an essential part of the world we want to live in, and there is enough fresh water on the planet to achieve this. However, due to bad economic management and poor infrastructure, millions of people –including children– die every year from diseases associated with inadequate water supply, sanitation, and hygiene (United Nations Sustainable Development, 2019).

Most of the population living in rural and peri-urban areas of developing countries depend on decentralized systems for the treatment of domestic wastewater, with conventional septic tanks (ST) being the oldest and most popular method for on-site wastewater treatment, given their favorable economic and functional features, such as simple design, low cost, easy installation, and minimal maintenance (Stazi and Tomei, 2018; Sharma *et al*., 2014). However, these devices have several inherent drawbacks, with the most significant being their limited treatment efficiency in terms of COD and TSS reductions for compliance with discharge or reuse requirements (30-40% COD and 55-65% TSS) (Nasr and Mikhaeil, 2013).

In light of the above, ST are usually sequentially combined with anaerobic filters (AF), in which the organic matter not removed in the ST is stabilized by microorganisms retained in the interstices or adhered to the support medium or biofilm in order to achieve a better effluent quality. This configuration (ST-AF, commonly called conventional system or CS), in addition to its simplicity, low cost, and easy operation, is highly accepted by environmental control bodies, mainly for small and dispersed populations, where there are few resources to build conventional sewer treatment systems (van Haandel *et al*., 2006).

Despite these advantages, these types of alternatives require larger reactors associated with high operating and construction costs. In addition, they sometimes demand a completely new structure, thus increasing the costs and resulting in greater space and maintenance requirements (Sharma *et al*., 2014).

Therefore, hybrid system (HS) strategies have been implemented, considering a wide range of technologies, *i.e.*, from ST and AF to other combinations with up-flow anaerobic sludge blanket (UASB) reactors, activated sludge, reverse osmosis, and ultrafiltration, among others (Dorji *et al*., 2022; Fernández del Castillo *et al*., 2022; Vicuña *et al*., 2009).

Some examples of HS include:

i) The full-scale compact system developed by Sousa and Chernicharo (2005), called *SISCOTE* and composed of a modified ST (MST) and two hybrid anaerobic reactors operating in series, with removal efficiencies of 85-90% COD and 95% TSS;

ii) the full scale up-flow septic tank/baffled reactor (USBR) MST, built and tested in a small town in Egypt (Sabry, 2010), with removal efficiencies of 84% COD and 89% TSS;

iii) an MST followed by an up-flow AF, housed within a single cylindrical unit, designed for the *in situ* treatment of domestic wastewater (DWW), evaluated at laboratory scale by Sharma *et al*. (2014), which showed removal efficiencies of 86,3±4,9% COD and 91,2±9,7% TSS;

iv) an MST followed by an AF for the *in situ* treatment of the wastewater generated in a boarding school, with efficiencies on the order of 72,6% COD and 83,2% TSS (Sharma and Kazmi, 2015);

v) an isolated AF (IAF) system incorporating a waste heat input for wastewater treatment in buildings, tested at full scale in the Phitsanulok province of northern Thailand, with removal efficiencies of 61,3% COD and 67,7% TSS (Bouted and Ratanatamskul, 2018);

vi) the demonstration by Santiago-Díaz *et al*. (2019, 2021) of the potential of decentralized wastewater management in Mexico, through the use of a UASB-septic tank strategy for the treatment of municipal wastewater, finding that this system can be built with low-cost local materials and does not require sophisticated equipment (it is also an economical alternative due to the simplicity of the technology and its easy operation); and

vii) the HS comprising ST-AF, where the suspended biomass (present in the ST) is combined with adhered biomass (present in the AF) in the same reactor.

HS are compact, do not require large areas, and improve biological system performance. Additionally, these HS are also convenient in places where it is desired to increase the biological system's capacity without making substantial modifications involving civil works (Garrido Aranda *et al*., 2003; von Sperling and Chernicharo, 2005).

One of the aspects that defines treatment process efficiency is the hydrodynamic behavior of the reactors, which considers aspects such as the presence of dead zones and short circuits and the determination of the distribution of residence times (DRT) of the particles within the system (Levenspiel, 2004). However, in general, reactor design has focused mainly on aspects of biochemical process efficiency.

Hydrodynamic aspects can be evaluated by tracer tests, in which an easily detectable tracer substance (which does not participate in any physical, chemical, or biological transformations that can alter the actual hydrodynamics of the fluid) with a known concentration is injected. Among the models used to evaluate hydrodynamics, the most applicable are the Wolf Resnick method, the axial dispersion model, and the model of complete mixing tanks (CMT) in series (Pérez and Torres, 2008; Hassanvand-Jamadi and Alighardashi, 2017). Authors such as Santiago-Díaz *et al*.

(2021) have also applied a comprehensive analysis of a zeolite-packed up-flow baffled septic tank using tracer tests and mathematical modeling.

Although HS are presented as a promising wastewater treatment technology, there are few reported full-scale studies (Soroa *et al*., 2005). Thus, it is to continue with the research and application of these systems in order to respond to the need for more compact and more sustainable systems, as well as to reduce maintenance operations. Thereupon, this study presents the results of a pilot-scale evaluation of the performance of two wastewater treatment system configurations: (i) a conventional system (CS) involving a ST and an up-flow AF in separate units and (ii) a hybrid system (HS) involving ST-AF in a single reactor. This, from a perspective of both performance (COD and TSS removal efficiency) and hydrodynamic behavior.

Materials and methods

Area of study

The study was conducted in a university campus located at coordinates N 4°47'19,65" W 75°41'27,01", in the Central Mountain Range of the Colombian Andes, in the coffee-growing region, with an altitude of 1 465 meters above the sea level, in an urban area with intermediate climate (17 to 26 °C), and an average annual precipitation of 2 750 mm.

Characterization of the substrate

The raw wastewater (DWW) used as a substrate came from a building located in the Faculty of Arts (35 restrooms, one cafeteria, and three workplaces for painting, ceramics, and sculptures); and the inoculum came from the septic tank of the institutional wastewater treatment plant (WWTP), applying 40% of the useful volume of the reactors (Pérez *et al*., 2009). Table 1 shows the variables measured regarding the substrate.

Treatment system configurations and experimental conditions

Two system configurations consisting of septic tanks (ST) and an anaerobic up-flow filter (AF) were evaluated: (i) a conventional system (CS: ST followed by AF in separate units) and (ii) a hybrid system (HS: ST in the lower part and AF in the upper part of the same reactor).

The height of the AF, both in the CS and the HS, was 70 cm, and, as filling material, polypropylene rosettes of 186 mm diameter with a porosity of 95% were used (Balasundaram *et al*., 2014), placing 100 units on each filter. Figure 1 shows the evaluated CS and HS configurations.

The reactor volumes were: CS: 0,75 m^3 (0,50 ST and 0,25 AF); and HS: 0,96 m^3. Given that the porosity percentage of the rosettes was 95%, their incorporation in the reactors had little effect on their volume, leaving a useful volume of 0,74 and m^3, respectively. These values were considered in the hydrodynamic analysis of the two systems.

Table 1. Substrate variables measured

Substrate variables	Units	Measuring technique
Temperature	°C	Mercury thermometer
pH	units	Potentiometric
Chemical oxygen demand (COD)	mg/L	Closed reflux, titrimetric
Total (TA) and bicarbonate (BA) Alkalinity	mg $CaCO_3$/L	Titrimetric
Total (TSS) and Volatile Suspended Solids (VSS)	mg/L	Gravimetric
Volatile Fatty Acids (VFA)	meq/L	Titrimetric
Inlet and outlet flow	L/s	Volumetric

Source: APHA *et al*. (2012)

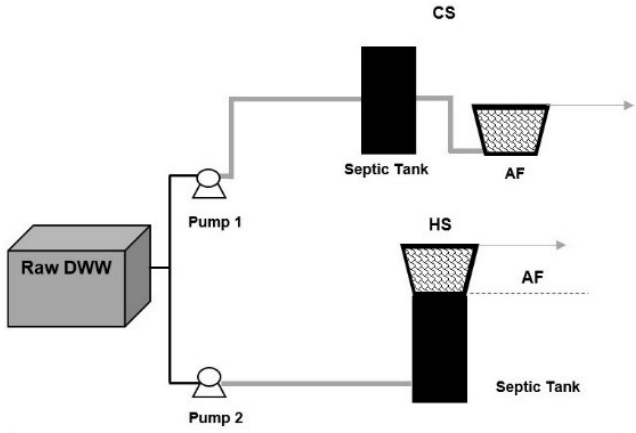

Figure 1. Conventional (CS) and hybrid (HS) configurations evaluated
Source: Authors

Raw wastewater was fed by a distribution system with hoses, and, in order to improve the distribution of the AFs, a 1-inch PVC pipe with 0,5 mm perforations was installed at the bottom of the reactors. The hydraulic load was regulated using peristaltic pumps, ensuring the same initial HRT in both configurations (36 hours), which is based on studies conducted for the start-up of anaerobic systems with municipal wastewater in Colombia and Mexico (Méndez-Novelo *et al*., 2012; Orozco-Gaviria *et al*., 2014).

Considering that STs require HRTs between 12 and 24 hours, as well as the fact that, when AFs are used to treat ST effluents, HRTs are between 4 and 10 hours (Chernicharo, 2007), the operating strategy consisted of a progressive reduction of the HRT until the lowest value in each reactor with stable conditions was reached. This was done as the reactors responded favorably in terms of the COD removal efficiency and the behavior of the control variables (pH, TA, BA, VFA, buffer (BI) and alpha indices, and AI/AP ratio), in order to guarantee the conditions for metabolic equilibrium between the different process stages and, therefore, the

adaptability of biomass to controlled substrate overloads (Pérez *et al*., 2009).

The BI corresponds to the relationship between alkalinity due to VFA and the total alkalinity; the alpha index is the relationship between BA and TA; and the AI/AP is the relationship between alkalinity due to VFAs and BA (Pérez and Torres, 2008). According to this criterion, the duration of each operating stage was variable (Table 2). Additionally, the COD and TSS reduction efficiencies were determined, and the temperature and pH were measured *in situ*.

Table 2. Operational conditions

Stage	HRT (CS)		HRT (HS)	Operation period (days)	
	ST (hours)	AF (hours)	Hybrid (hours)	*Total	**Real
1	24	12	36	85	63
2	20	10	30	84	49
3	16	8	24	42	42
4	12	6	18	35	35
Total				246	189

* Includes stops due to the students' holiday period (absence of wastewater to feed the systems). **Does not include stops.
Source: Authors

A multivariate factorial design was proposed in which eight treatments resulting from the combination of two factors were evaluated: the type of configuration (CS and HS) and the HRT (36, 30, 24, and 18 hours), as shown in Table 3.

Table 3. Factors and levels

Factors	Levels	No. of levels	No. of treatments	Response variables
System	CS: conventional	2	4 x 2 = 8	COD and TSS removal efficiency
	HS: hybrid			
Hydraulic retention time (HRT)	HRT 36	4		
	HRT 30			
	HRT 24			
	HRT 18			

Source: Authors

Descriptive statistics tools were used to analyze the results obtained, including the average and the standard deviation. In the first instance, it was verified whether the assumptions of the analysis of variance were met for the response variables (COD and TSS removal efficiency), for which the Shapiro-Wilk and Levene tests were used with regard to the normality and homogeneity of variance, respectively. Additionally, to establish the significance of the factors evaluated for each of the response variables, as well as to examine factor interactions, an analysis of variance was performed based on the multivariate factorial model at a confidence level of 95% (σ = 0,05). Statistical processing was performed with the Statistical Package for Social Science (SPSS) software.

Reactor hydrodynamic performance

To evaluate the hydrodynamic behavior of the two configurations and validate the real HRT with respect to the theoretical HRT, a hydrodynamic test was performed using sodium chloride (NaCl) as a tracer, which is not absorbed by sludge particles, has no inhibitory effects on anaerobic bacteria, and is not absorbed as a nutrient by microorganisms (Li *et al*., 2016). Equations (1) and (2) were used to calculate the tracer dose (Pérez and Torres, 2008), and the tracer injection was instantaneous.

$$\mathbf{P} = \frac{\forall \times \boldsymbol{K} \times \boldsymbol{Co}}{\boldsymbol{I} \times 10^3} \quad (1)$$

$$K = \frac{Weight\ NaCl}{Weight\ Cl} = \frac{23 + 35,5}{35,5} = 1,65 \quad (2)$$

where P represents the weight of the tracer to be added (kg); ∀ represents the useful reactor volume (m^3); K represents the correction constant; Co represents the concentration (mg/L or g/m^3); and I represents the degree of purity of the tracer (fraction of the unit).

The theoretical HRT was 24 hours, and, taking into account that the tracer test must last three times longer than the theoretical HRT, during which the concentration of the tracer is expected to approach zero, a period of 72 hours was considered, measuring conductivity every 20 minutes during the first 48 hours and then every hour until completing 72 hours. Table 4 shows the final value of P for each configuration according to these Equations.

Table 4. P_{final} for each configuration (conventional and hybrid systems)

CONVENTIONAL SYSTEM (CS)			
P	4,64	kg	Amount of salt added
P_{final}	0,89	kg	NaCl concentration after 72 hours (1203 mg/l NaCl)
C-Co	0,01	kg	Initial-final concentration after 72 hours (19,4 mg/l NaCl)
HYBRID SYSTEM (HS)			
P	3,64	kg	Amount of salt added
P_{final}	1,19	kg	NaCl concentration after 72 hours (1271 mg/l NaCl)
C-Co	0.13	kg	Initial-final concentration after 72 hours (137,62mg/l NaCl)

Source: Authors

Data analysis was performed by constructing tracer concentration and time distribution (E(t)) trend curves to determine the real or experimental HRT, and the Wolf-Resnick mathematical model, the axial dispersion model, and the complete mix reactors in series model were applied (Levenspiel, 2004; Pérez and Torres, 2008), with the objective of identifying the type of flow in each system and the presence of hydraulic phenomena such as short circuits and dead zones.

To evaluate the real HRT when compared to the theoretical one, the mean, variance, and standard deviation of the HRT were calculated according to the CS and HS reactor concentration results measured in known time intervals. Likewise, the mean residence time from the E curves was used to determine the hydraulic efficiency associated with a reactor's ability to distribute the flow uniformly within its useful volume, maximizing the pollutant contact time and optimizing its removal (Persson *et al.*, 1999; Latrach *et al.*, 2018). Equation (3) allows evaluating the effective volume and the number of complete mix tanks in series (Persson *et al.*, 1999).

$$\ddot{e} = V_e\left(1-\frac{1}{N}\right) \quad (3)$$

where V_e represents the effective volume, and N represents the number of tanks in series.

Results and discussion

Substrate evaluation and experimental unit performance

Table 5 shows the physicochemical characteristics of the wastewater (influent), which is characterized by the temperature, pH, and VFA of the DWW. However, a high alkalinity and COD were observed, which allows classifying the substrate as having a medium to strong DWW concentration (Bureau of Sale Drinking Water, 2016), which may be associated with the fact that the wastewater comes from 35 sanitary batteries (without showers) that have water-saving devices. Additionally, wastewater is received from the washing of materials in the ceramic, painting, and sculpture workplaces. Lew *et al.* (2011) found similar values (COD: 1 576±376 mg/L) in Israel and elsewhere in the Middle East, which were caused by low *per capita* water consumption in these areas.

Throughout the experimental period, the reactors operated under environmental conditions in the mesophilic temperature range, as well as with pH values close to the ranges recommended for anaerobic digestion (6,5-8,0 units). As for alkalinity, an adequate buffer capacity was observed, given the predominance of bicarbonate alkalinity (Chernicharo, 2007).

Reactor performance

Table 6 shows the effluent characteristics of the two configurations (CS and HS) in terms of temperature, pH, VFA, TA, and BA. In general, both effluents reached higher alkalinity values than those of the affluent, which, according to Orozco-Gaviria et al. (2014), occurs because the system seeks to generate bicarbonate ions to reach equilibrium with buffer capacity.

Figure 2 shows the COD and TSS reduction efficiencies in each of the evaluated operating stages, allowing to observe that efficiencies higher than 60% were achieved during HRTs longer than 36 and 30 hours for both the CS and HS and in the samples. For HRTs of 24 and 18 hours, although efficiency decreased overall, it was higher in the HS. It was observed that, in terms of the removal efficiency of both COD and TSS, the HS configuration exhibited a better performance under all of the evaluated operating conditions.

From a statistical point of view, significant differences ($p<0,05$) were found between the HRTs of 36 and 18 hours in the removal of COD: (i) CS: 69,4±5,2 and 39,8±13,1%, respectively, which represents an efficiency reduction of 29,6%; (ii) HS: 64,0±5,4 and 52,0±16,8%, respectively, which constitutes an efficiency reduction of just 12% regarding the two HRTs. This indicates that CS was more susceptible than HS to a decrease in HRT.

Chernicharo (2007) reports COD removal efficiencies for the CS between 40 and 70% (for temperatures below 15 °C and above 25 °C), a range in which the results of this study fall, also coinciding with other studies, such as that by Méndez-Novelo et al. (2012) in Mexico with HS, in which removal efficiencies of 56% COD and 61% TSS were obtained while operating at HRs of 36 and 24 hours. In contrast, Pacheco and Magaña (2003) obtained low efficiencies in Mexico, in the order of 38%, when starting an HS in a continuous phase,

Table 5. Summary of evaluated influent physicochemical parameters

	Parameters	Stage 1 (HRT 36)				Stage 2 (HRT 30)				Stage 3 (HRT 24)				Stage 4 (HRT 18)			
		max	min	mean	σ	max	min	mean	σ	max	Min	mean	σ	max	min	mean	σ
Influent	Temperature (°C)	30,0	23,1	25,5	1,9	28,7	23,7	25,6	1,6	26,6	22,3	24,4	1,7	24,5	23,1	23,5	0,6
	pH (units)	8,08	7,19	7,64	0,26	8,18	7,78	7,99	0,16	8,23	7,77	7,98	0,19	8,34	8,02	8,21	0,12
	VFA (mgHAc/L)	360	84	245	88	156	84	110	33	156	108	132	19	204	120	180	35
	TA ($mgCaCO_3$/L)	765	405	605	129	780	500	662	115	690	495	587	75	790	660	738	56
	BA ($mgCaCO_3$/L)	640	285	499	133	670	400	537	92	630	375	465	91	640	530	574	43
	COD (mg/L)	1 333,3	383,5	878,5	250,5	1 743,6	383,6	700,8	480,5	1 487,2	860,8	1 103,7	268,0	1 063,3	842,1	893,8	100,7
	TSS (mg/L)	866,7	56,0	283,9	258,9	223,3	53,3	105,7	61,7	90,0	27,0	65,2	23,4	131,0	29,0	137,2	105,3

HRT 36 hours (n = 10); HRT 30 hours (n = 7); HRT 24 hours (n = 6); HRT 18 hours (n = 5).
Source: Authors

Table 6. Summary of the control variables in the effluent of the conventional (CS) and hybrid systems (HS)

Configuration/ system	Parameters	Stage 1 (HRT 36)				Stage 2 (HRT 30)				Stage 3 (HRT 24)				Stage 4 (HRT 18)			
		max	min	Mean	σ	Max	min	mean	σ	max	min	mean	σ	max	min	mean	σ
CS	Temperature (˚C)	30,5	20,7	25,99	2,98	28,2	23,1	25,56	1,80	26,5	22,6	24,6	1,7	26,3	23,2	24,6	1,5
	pH (units)	8,25	7,83	8,10	0,12	8,51	8,13	8,25	0,14	8,32	8,01	8,14	0,13	8,33	8,07	8,22	0,10
	VFA (mgHAC/L)	300	120	199	59	126	72	93	18	156	60	94	34	144	96	118	20
	TA ($mgCaCO_3$/L)	710	460	614	87	810	590	717	82	660	465	578	63	770	650	726	57
	BA ($mgCaCO_3$/L)	630	310	521	117	700	520	621	67	530	365	466	56	640	550	583	35
HS	Temperature (˚C)	30,5	20,6	26,2	3,0	26,7	23,2	25,2	1,5	26,6	22,2	24,5	1,8	25,5	23,2	24,0	0,9
	pH (units)	8,20	7,77	8,04	0,11	8,42	8,00	8,21	0,15	8,24	7,95	8,07	0,10	8,39	7,99	8,21	0,15
	VFA (mgHAC/L)	560	108	223	127	120	72	89	18	120	36	89	29	180	144	163	18
	TA ($mgCaCO_3$/L)	680	305	515	140	840	620	710	77	600	435	540	61	750	720	736	13
	BA ($mgCaCO_3$/L)	590	215	436	139	690	530	610	61	470	355	422	44	600	550	572	18

HRT 36 hours (n = 10); HRT 30 hours (n = 7); HRT 24 hours (n = 6); HRT 18 hours (n = 5).
Source: Authors

due to the slow growth of the reactor biomass and the high affluent concentration variations (1 375-565 mg/L of COD). They also found that the higher the affluent concentration, the greater the removal percentage.

Other studies with anaerobic HS operated under different conditions exhibit higher efficiencies than those obtained in this study (Soroa *et al.*, 2005; Sousa and Chernicharo, 2005; Sharma and Kazmi, 2015), possibly because the wastewater composition evaluated in this study includes waste from activities such as painting, ceramics, and sculpture, which can provide some potentially inhibiting substances to the microbial population responsible for the anaerobic digestion of the substrate.

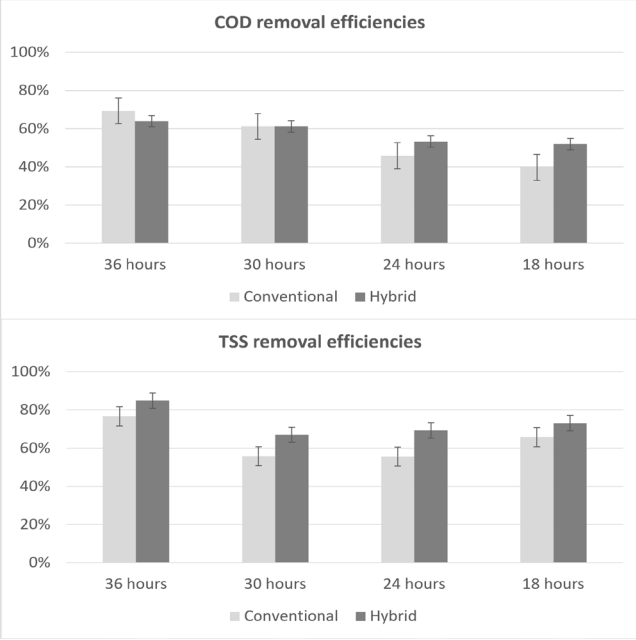

Figure 2. Comparison of the COD and TSS removal efficiencies in the conventional and hybrid systems
Source: Authors

Hydrodynamic evaluation of reactors

Figure 3 presents the CS and HS tracer concentration curves over time, and Table 7 shows the trend curve analysis through the relationships between the parameters.

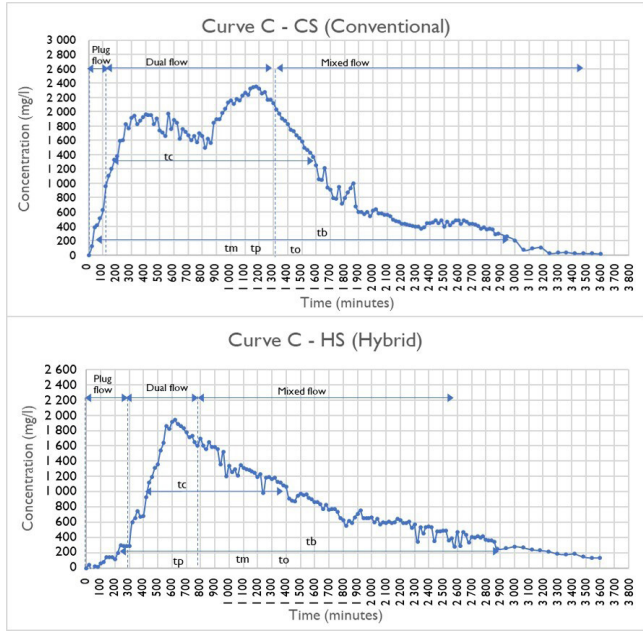

Figure 3. CS and HS tracer concentration curve *vs.* time
Source: Authors

An analysis of the CS and HS trend curves shows a dual or arbitrary behavior. According to Pérez and Torres (2008), plug flow occurs during the time elapsed from the tracer addition until it can be measured in the effluent and the curve changes from concave to convex. From this point and until a second inflection is observed in the descending curve, dual flow occurs. Henceforth, the flow is of mixed character. In this sense, the HS curve shows a greater predominance of plug flow than that of the CS.

Table 7. Systems' tracer trend curve analysis

Parameters	CS	HS	Meaning
t_i/t_o	0,03	0,07	Measures big **short circuits** (SC) t_i/t_o = 1: plug flow **t_i/t_o = 0: mixed flow** t_i/t_o < 0,3: SC (direct passage between inlet and outlet)
t_m/t_o	0,7	0,8	**t_m/t_o < 1 short circuits** t_m/t_o > 1 experimental errors or unwanted tracer accumulation (dead zones)
t_p/t_o	0,82	0,43	**t_p/t_o = 1: plug flow** t_p/t_o = 0: mixed flow t_p/t_o = 1 and t_i/t_o >0,5: predominance of plug flow, **if =0: mixed flow predominance**
t_c/t_o	1,1	0,97	**t_c/t_o = 0,7 complete mix flow**
t_b/t_o	2,1	2	**t_b/t_o = 2,3 complete mix flow**
E	0,51	1,71	e ≥ 2,3: complete mix flow e = 0: plug flow

Source: Authors

According to the relationships between t_i/t_o and t_p/t_o, there is a predominance of mixed flow in the systems, and large short circuits, with a value below 0,3, which indicates the probable direct passage of water between the inflow and outflow of the tanks.

Similarly, the relationship between the mean time and the theoretical time (t_m/t_o), with a value <1, proves the existence of short circuits. In terms to the Wolf-Resnick, axial dispersion, and tanks in series models, Table shows the analysis of the two systems; the first section allows identifying the percentages of the reactor that behave as plug flow or as complete mixture, in addition to dead zones and short circuits, showing a very equitable dual behavior involving plug flow (52%) and complete mix (48%) at the CS outlet, as well as more dead zones compared to the HS, which exhibits a dual hydraulic regime, albeit with a predominance of plug flow (62%), thus confirming the trend curve findings.

Table 8. Application of the Wolf-Resnick, axial dispersion, and tanks in series models

Wolf-Resnick model analysis results								
System	**Reactor**	**θ**	**t_1/t_o**	**t_2/t_o**	**tag ∝**	**Plug flow**	**Mix flow**	**Dead zones**
CS	ST+AF	0,50	0,50	1,50	1,00	52%	43%	5%
HS	HS	0,71	0,71	1,67	1,05	62%	38%	0%

Axial dispersion and tanks in series model results					
System	**Real HRT (hours)**	**σ^2**	**θ**	**No. dispersion (D/uL)**	**No. tanks (1/N)**
CS	8,96	124,88	0,347	0,118	3
HS	21,85	142,85	0,299	0,105	3

Source: Authors

According to Levenspiel (2004), all reactors showed a dispersion number between intermediate (0,025) and large (0,200), which confirms the presence of PF and CM. According to the tanks in series model, the greater the number of tanks, the greater the tendency towards PF; and, with fewer tanks, there is a tendency towards CM. In short, the CS behaves like a completely mixed reactor (CMR) in a series of three, with a high dispersion coefficient and a dual regime and a predominance of plug flow (52%) and 5% dead zones. The CMR model showed a correlation of 88%.

The HS behaves as a CMR in series of three, with a high degree of dispersion and a dual flow regime with a greater predominance of plug flow (62%) than the CS (52%), without the presence of dead zones. There was also a higher correlation (91%) with the axial dispersion model. Similar results were found in the hydrodynamic evaluation at the end of the optimization of a full-scale AUFF (Pérez and Torres, 2008), as well as in studies conducted in Brazil (Baettker, 2015), evaluating different AF support media on a laboratory scale.

Table 9 shows the results of the estimation of real HRT for the systems, which indicate that the mean experimental or real HRT, calculated through the median variance and E curve methods, are similar. For the CS (ST+AF), the real HRT is 19,29 hours (in comparison with 16,50 for the ST and very close to the theoretical value of 16 hours), which means that, in this system, short circuits are mainly found in the AF, which have a real HRT of only 2,79 hours compared to the theoretical HRT of 8 hours.

Table 9. Estimated real HRT for the CS and HS

Configuration	Reactors	Theoretical HRT	Real HRT	
			HRT method: median and variance	HRT method: E and F curves
		Median (hours)	Median (hours)	Median (hours)
CS	ST	16,00	15,98	16,50
	AF	*8,00	*2,98	*2,79
	ST+AF	24,00	18,96	19,29
HS	Hybrid	24,00	21,85	23,07

*These values were calculated as the difference between the HRT of the complete system (ST+AF) minus that of the septic tank (ST)
Source: Authors

This may be the cause of the low COD removal efficiency (45,9±19,7%) in the 24-hour HRT (insufficient wastewater contact time with the retained AF biomass). Thus, a large portion of the removal takes place in the septic tank (von Sperling and Chernicharo, 2005; Oliveira and von Sperling, 2008).

In the HS, the real HRT approaches the theoretical HRT with a difference of just 56,35 minutes, which guarantees a better performance of the HS with respect to the CS because the water mass has a longer contact time with

the microorganisms responsible for removing organic matter. Table 10 shows that the HS also exhibits a greater hydraulic efficiency (0,63%) compared to the CS (0,50%) because, according to Persson *et al*. (1999), λ values ≥ 0,75 indicate good hydraulic efficiency, 0,75 ≤ λ <0,5 indicates satisfactory efficiency, and λ ≤ 0,5 denotes poor efficiency.

Table 10. Persson method hydraulic efficiencies

System	Reactor	Ve (m^3)	N	Persson H.E. (λ) %
CS	**ST+AF**	0,74	3	0,50
HS	**H**	0,94	3	0,63

Source: Authors

Conclusions and recommendations

The evaluated wastewater shows adequate levels of pH and total and bicarbonate alkalinity, which guarantees a good buffer capacity in the systems. The alkalinity indices, as well as the operating variables, showed that the systems operated in a stable manner, without acidification due to the accumulation of VFA. However, the presence of paints and clay residues, among other additives used in painting, ceramics, and sculpture in the fine arts workplaces, can generate inhibitory effects on the process, which must be further evaluated.

In the conventional and hybrid systems evaluated, conformed by septic tank and anaerobic filters, the hybrid configuration had a better performance, with greater stability by better supporting the different hydraulic loads evaluated and achieving an 18-hour HRT removal efficiency of 52,0±16,8% for COD and 73,06±18,5% for TSS, in comparison with 39,8±13,1% for COD and 65,8±20,52% for TSS with the conventional configuration. Additionally, the hybrid system had lower performance variations as the HRT was reduced.

This hydrodynamic evaluation confirms the improved performance of the hybrid system, which is associated with a predominance of plug flow (62%) compared to the conventional system (52%), leading to a real HRT closer to the theoretical one, as well as to a greater hydraulic efficiency than the conventional system.

CRediT author statement

All authors contributed equally to the research.

References

APHA, AWWA, and WEF (2012). *Standard methods for examination of water and wastewater* (22nd ed.). American Water Works Association and Water Environment Federation, Water Environment Federation.

Baettker, E. C. (2015). *Avaliação do desempenho de filtros anaeróbios preenchidos com diferentes meios suportes no tratamento de água residuária sintética* [Master's tesis, Universidade Tecnológica Federal do Paraná]. https://repositorio.utfpr.edu.br/jspui/handle/1/2744

Balasundaram, N., Meenambal, T., Balasubramanium, N., and Loganath, R. (2014). Comparative study of different media in the treatment of sago wastewater using HUASB reactor. *Nature Environment and Pollution Technology*, *13*(3), 511-516. https://neptjournal.com/upload-images/NL-49-12-(10)B-3010Com.pdf

Bouted, C., and Ratanatamskul C. (2018). Effects of temperature and HRT on performance of a novel insulated anaerobic filter (IAF) system incorporated with the waste heat input for building wastewater treatment. *Journal of Environmental Management*, *206*, 698-706. https://doi.org/10.1016/j.jenvman.2017.10.071

Bureau of Safe Drinking Water (2016). Wastewater operator certification training. Module 1: Introduction to wastewater treatment, unit 2 – Characteristics of wastewater. Department of Environmental Protection. https://cutt.ly/Az0dfix

Chernicharo, C. A. L. (2007). *Biological wastewater treatment series. Volume 4. Anaerobic reactors* (1st ed.). IWA Publishing.

Dorji U., Dorji P., Shon H., Badeti U., Dorji C., Wangmo C., Tijing L., Kandasamy J., Vigneswaran S., Chanan A., and Phuntsho S. (2022). On-site domestic wastewater treatment system using shredded waste plastic bottles as biofilter media: Pilot-scale study on effluent standards in Bhutan. *Chemosphere, 286*(2), 131729. https://doi.org/10.1016/j.chemosphere.2021.131729

Fernandez del Castillo A, Verduzco-Garibay M, Sénes-Guerrero, C, Orozco-Nunnelly D.A., de Anda J., and Gradilla-Hernandez M.S. (2022). A review of the sustainability of anaerobic reactors combined with constructed wetlands for decentralized wastewater treatment. *Journal of Cleaner Production, 371*, 133428. https://doi.org/10.1016/j.jclepro.2022.133428

Garrido-Aranda, J. M., Oyanedel, V. and Méndez, R. (2003). Nuevos biorreactores híbridos para el tratamiento de aguas residuales. *Ingeniería Química, 401*, 171-178. https://dialnet.unirioja.es/servlet/articulo?codigo=623582

Hassanvand-Jamadi, M., and Alighardashi, A. (2017). Application of Froude dynamic similitude in anaerobic baffled reactors to prediction of hydrodynamic characteristics of a prototype reactor using a model reactor. *Water Science and Engineering, 10*(1), 53-58. https://doi.org/10.1016/j.wse.2017.03.002

Latrach, L., Ouazzani, N., Hejjaj, A., Zouhir, F., Mahi, M., Masunaga, T., and Mandi, L. (2018). Optimization of hydraulic efficiency and wastewater treatment performances using a new design of vertical flow Multi-Soil-Layering (MSL) technology. *Ecological Engineering, 117*, 140-152. https://doi.org/10.1016/j.ecoleng.2018.04.003

Levenspiel, O. (2004). *Ingeniería de las reacciones químicas* (2nd ed.). Reverté, S.A..

Lew, B., Lustig, I., Beliavski, M., Tarre, S., and Green, M. (2011). An integrated UASB-sludge digester system for raw domestic wastewater treatment in temperate climates. *Bioresource Technology, 102*(7), 4921-4924. https://doi.org/10.1016/j.biortech.2011.01.030

Li, S., Nan, J., and Gao, F. (2016). Hydraulic characteristics and performance modeling of a modified anaerobic baffled reactor (MABR). *Chemical Engineering Journal, 284*, 85-92. https://doi.org/10.1016/j.cej.2015.08.129

Méndez-Novelo R. I., Chan-Gutiérrez, E. A., Castillo-Borges, E. R., Vázquez-Borges, E. R., and Espadas-Solís, A. E. (2012). Digestión anaerobia de efluentes de fosas sépticas. *Ingeniería, Investigación y Tecnología, 13*(3), 339-349. https://www.scielo.org.mx/scielo.php?script=sci_arttext&pid=S1405-77432012000300008

Munavalli, G. R., Sonavane, P. G., Koli, M. M., and Dhamangaokar, B. S. (2022). Field-scale decentralized domestic wastewater treatment system: Effect of dynamic loading conditions on the removal of organic carbon and nitrogen. *Journal of Environmental Management, 302*(Part A), 114014. https://doi.org/10.1016/j.jenvman.2021.114014

Nasr, F. A., and Mikhaeil, B. (2013). Treatment of domestic wastewater using conventional and baffled septic tanks. *Environmental Technology*, *34*(16), 2337-2343. http://dx.doi.org/10.1080/09593330.2013.767285

Oliveira, S. C., and von Sperling, M. (2008). Reliability analysis of wastewater treatment plants. *Water Research, 42*(4-5), 1182-1194. https://doi.org/10.1016/j.watres.2007.09.001

Orozco-Gaviria, C. A., Triviño-Cabrera, C. C., and Manrique-Losada, L. (2014). Arranque de un reactor UASB para el tratamiento de aguas residuales domésticas en condiciones andino amazónicas. *Revista Facultad de Ciencias Básicas*, *10*(2), 170-185. https://doi.org/10.18359/rfcb.328

Pacheco, J., and Magaña, A. (2003). Arranque de un reactor anaerobio. *Ingeniería*, *7*(*1*), 21-25. https://www.redalyc.org/pdf/467/46770102.pdf

Pérez-Vidal, A., and Torres-Lozada, P. (2008). Evaluación del comportamiento hidrodinámico como herramienta para optimización de reactores anaerobios de crecimiento en medio fijo. *Revista Facultad de Ingeniería Universidad de Antioquia, 45*, 27-40. http://www.scielo.org.co/scielo.php?script=sci_arttext&pid=S0120-62302008000300003

Pérez-Vidal, A., Torres-Lozada, P. and Silva-Leal, J. (2009). Tratamiento anaerobio de las aguas residuales del proceso de extracción de almidón de yuca. Optimización de variables ambientales y operacionales. *DYNA*, *76*(160), 139-148. http://www.scielo.org.co/pdf/dyna/v76n160/a13v76n160.pdf

Persson, J., Somes, N. L., and Wong, T. H. F. (1999). Hydraulics efficiency of constructed wetlands and ponds. *Water science and technology, 40*(3), 291-300. https://doi.org/10.1016/S0273-1223(99)00448-5

Sabry, T. (2010). Evaluation of decentralized treatment of sewage employing Upflow Septic Tank/Baffled Reactor (USBR) in developing countries. *Journal of Hazardous Materials, 174*(*1-3*), 500-505. https://doi.org/10.1016/j.jhazmat.2009.09.080

Santiago-Díaz, Á. L., García-Albortante, J., and Salazar-Peláez, M. L. (2019) UASB-septic tank as an alternative for decentralized wastewater treatment in Mexico. *Environmental Technology, 40*(14), 1780-1792. https://doi.org/10.1080/09593330.2018.1430170

Santiago-Díaz, Á. L., Benítez-Olivares, G., Salazar-Peláez, M. L., de los Cobos Vasconcelos, D., and Mugica-Álvarez, V. (2021). Comprehensive analysis of a zeolite-packed upflow baffled septic tank using tracer tests and mathematical modelling. *Water and Environment Journal, 36*(2), 332-342. https://doi.org/10.1111/wej.12740

Sharma, M. K., Khursheed, A., and Kazmi, A. A. (2014). Modified septic tank-anaerobic filter unit as a two-stage onsite domestic wastewater treatment system. *Environmental Technology, 35*(17-20), 2183-2193. http://dx.doi.org/10.1080/09593330.2014.896950

Sharma, M. K., and Kazmi, A. A. (2015). Anaerobic onsite treatment of black water using filter-based packaged system as an alternative of conventional septic tank. *Ecological Engineering*, *75*, 457-461. https://doi.org/10.1016/j.ecoleng.2014.12.014

Singh. S. P., Sharma, M. K., and Gaur, R. C. (2022). Effects of aqwise carrier media and brick media as filter materials on performance of biofilm reactor. *Materials Today: Proceedings, 60*(Part 1), 782-787. https://doi.org/10.1016/j.matpr.2022.04.486

Soroa del Campo, S., Lopetegui-Garnika, J., Almandoz-Peraita, A., and García de las Heras, J. L. (2005). Diseño de reactores híbridos anaerobios para el tratamiento de aguas residuales industriales. *Revista Tecnología del Agua*, *267*, 60-67. http://www.bibliotecagbs.com/archivos/ta_267_1_05.pdf

Sousa V. P., and Chernicharo, C. A. L. (2005). *Sistema compacto de tratamento de esgostos domiciliares composto de tanque séptico modificado e reatores anaeróbios Híbridos operando em série* [Conference presentation]. 23° Congresso Brasileiro de Engenharia Sanitária e Ambiental, Campo Grande, Brasil. https://acortar.link/xT2KfT

Stazi, V., and Tommei, M. C. (2018). Enhancing anaerobic treatment of domestic wastewater: State of the art, innovative technologies and future perspectives. *Science of the Total Environment, 635*, 78-91. https://doi.org/10.1016/j.scitotenv.2018.04.071

United Nations Sustainable Development (2019). *Water and sanitation*. Retrieved from: https://www.un.org/sustainabledevelopment/water-and-sanitation/

van Haandel, A., Kato, M., Cavalcanti, P., and Florencio, L. (2006). Anaerobic reactor design concepts for the treatment of domestic wastewater. *Reviews in Environmental Science and Bio/Technology*, *5*, 21-38. https://doi.org/10.1007/s11157-005-4888-y

Vicuña, E., Ara, L., and Loayza, J. (2009). Sistemas híbridos de tratamiento de aguas residuales. *Revista Peruana de Química e Ingeniería Química*, *12*(1), 10-17. https://revistasinvestigacion.unmsm.edu.pe/index.php/quim/article/view/4953

von Sperling, M., and Chernicharo, C. A. (2005). *Biological wastewater treatment in warm climate regions – Volume 1* (1st ed.). IWA Publishing.

Research Article/Civil and Sanitary Engineering https://doi.org/10.15446/ing.investig.97253

Strapping Spiral Ties for Short Tie-Columns in Confined Masonry Walls Using a Micro-Numerical Model

Estribos flejados en espiral para castillos cortos de paredes de mampostería confinada mediante el empleo de micro modelación numérica

José Álvarez-Pérez[1], Milena Mesa-Lavista[2], Jorge Humberto Chávez-Gómez[3], Bernardo T. Terán-Torres[4], Román Hermosillo-Mendoza[5] and Diego Cavazos-de-Lira[6]

ABSTRACT

Many dwellings in the world are built using confined masonry walls. Confinement is achieved by tie-columns and bond beams of reinforced concrete. These tie-columns are traditionally reinforced by using closed loop ties. In this paper, a new type of ties for tie-columns is presented: *strapping spiral ties*. These strapping ties are compared against traditional ties by a three-dimensional micro-numerical model and the experimental behavior of short tie-columns. This study resulted in an improvement in the compressive strength, in the degree of confinement of the concrete, and in the efficiency of tie-columns with strapping spiral ties. In addition, an increase in the stiffness at the unloading stage was also obtained.

Keywords: spiral ties, strapping ties, short tie-columns, compressive strength

RESUMEN

Algunas de las viviendas en el mundo se construyen con muros confinados de mampostería. El confinamiento se logra mediante castillos y dalas de concreto reforzado. Estos castillos se refuerzan tradicionalmente mediante el uso de estribos tradicionales cerrados. En este trabajo se presenta un nuevo tipo de estribos para castillos: *estribos flejados y en espiral*. Estos estribos flejados se comparan con los estribos tradicionales mediante un modelo micro numérico tridimensional y el comportamiento experimental de castillos cortos. Este estudio resultó en una mejora en la resistencia a la compresión, en el grado de confinamiento del concreto y en la eficiencia de los castillos con estribos en espiral. Además, también se obtuvo un aumento de la rigidez en la etapa de descarga.

Palabras clave: estribos en espiral, estribos flejados, castillos cortos, resistencia a la compresión

Received: July 16th, 2021
Accepted: September 8th, 2022

Introduction

Masonry walls are of widespread use due to the availability of the materials needed to build them, along with their quick and cost-effective construction. Particularly in Mexico, 87% of the dwellings are built using masonry walls (INEGI, n.d.), wherein many cases are confined masonry walls. These types of walls are built using unreinforced masonry and reinforced concrete (RC), *i.e.*, tie-columns and bond-beams. Tie-columns and bond-beams provide confinement on the plane of the wall panels and reduce the out-of-plane bending effects. Furthermore, unreinforced masonry is constructed out of different masonry units, such as hollow clay/concrete and solid clay/concrete units. In order to provide confinement to the masonry units, the spacing of the tie-columns must be less than 4 m or 1,5 times the wall height, and their thickness must be more than 100 mm and not less than the width of the masonry unit (Rodríguez, 2009).

Previous research has focused on the effect of ties and stirrups on the behavior of columns and beams as isolated structural elements (Gribniak *et al.*, 2017; Hong *et al.*, 2006; Salah-Eldin *et al.*, 2019; Tan *et al.*, 2018). In this line

[1] Civil engineer from Instituto Superior Politécnico José Antonio Echeverría (CUJAE), CUBA. PhD from the Central University of Las Villas (UCLV), Cuba. Affiliation: Full-time professor at Universidad Autónoma de Nuevo León (UANL), México. Email: jose.alvarezpr@uanl.edu.mx

[2] Civil engineer from Instituto Superior Politécnico José Antonio Echeverría (CUJAE), CUBA. PhD from the Central University of Las Villas (UCLV), Cuba. Affiliation: Professor at Universidad Autónoma de Nuevo León (UANL), México. Email: mmesal@uanl.edu.mx

[3] Civil engineer from Universidad Autónoma de Nuevo León (UANL), PhD from Illinois Institute of Technology: Chicago, IL, US. Affiliation: Full-time professor at Universidad Autónoma de Nuevo León (UANL), México. Email: jorge.chavezgm@uanl.edu.mx

[4] Civil engineer from Instituto Tecnológico de Ciudad Victoria, Mexico. PhD from Illinois Institute of Technology: Chicago, IL, US. Affiliation: Full-time professor at Universidad Autónoma de Nuevo León (UANL), México. Email: bernardo.terantrr@uanl.edu.mx

[5] Civil engineer from Universidad Autónoma de Ciudad Juárez (UACJ), PhD from Universidad Autónoma de Nuevo León (UANL), México. Affiliation: Full-time professor at Universidad Autónoma de Nuevo León (UANL), México. Email: roman.hermosillomn@uanl.edu.mx

[6] Civil engineer from Universidad Autónoma de Nuevo León (UANL), México. MSc in Structural Engineering from Universidad Autónoma de Nuevo León (UANL), Mexico. Affiliation: Full-time Associate Professor at Universidad Autónoma de Nuevo León (UANL), México. Email: diego.cavazosd@uanl.edu.mx

How to cite: Álvarez-Pérez, J., Mesa-Lavista, M., Chávez-Gómez, J.H., Terán-Torres, B.T., Hermosillo-Mendoza R., and Cavazos-de-Lira, D. (2023). Strapping spiral ties for short tie-columns in confined masonry walls using a micro-numerical model. *Ingeniería e Investigación, 43*(2), e97253. https://doi.org/10.15446/ing.investig.97253

of research, unconventional geometries of ties and stirrups for these structural elements have been studied mainly on beams (Lima de Resende *et al.*, 2016; Pérez-Caldentey *et al.*, 2013). In the study conducted by de Corte and Boel (2013), spiral shear reinforcement was used on the beams. Colajanni *et al.*, 2014 also employed stirrups with different inclinations. Other authors have focused on the behavior of beams without stirrups (Arslan, 2012; Azam *et al.*, 2016; Ridha *et al.*, 2018). Other studies (Du *et al.*, 2017; Grgić *et al.*, 2017; Li *et al.*, 2018; L. Sun and Li, 2019) were conducted for ties in columns. Dong *et al.* (2018) proposed an innovative winding glass fiber-reinforced polymer tie (closed loop type). However, none of these studies have focused on the behavior of stirrups for tie-columns or bond-beams.

In this article, a new type of tie, denoted as a *strapping spiral tie* (SST), is studied. A company located in Monterrey, Mexico (Aceros-Titán-Company, 2016), patented the manufacturing process to produce this type of tie. The main advantages of using it are the reduction of labor cost and the increase in the speed of reinforcement placement (de Corte and Boel, 2013). SSTs can be produced with different spacings (Figure 1). The steel strips are produced using a cold formed method, which changes their mechanical properties (Yun and Gardner, 2017).

The aim of this research was to evaluate the behavior of SSTs in short tie-columns, along with their confinement capacity, and to provide a comparison between SSTs and traditional ties. This was achieved by means of experimental tests and a micro-numerical model. In order to achieve these goals, the next section describes the experimental design, materials, and tests along with the numerical model employed. Later, results and discussions are presented with regard to (1) the validation procedure, (2) the compressive strength comparison between traditional ties and SSTs, and (3) the behavior of SSTs. Finally, conclusions are drawn.

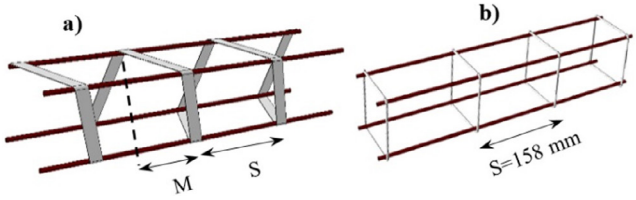

Figure 1. a) Strapping spiral ties (SST), b) traditional ties (pattern)
Source: Authors

Materials and methods

Experimental design for the specimens

For this study, 12 specimens of short tie-columns were fabricated. These specimens have ties with different spacings, which are specified in Table 1. According to the standards (ACI International, 2013; NTCM, 2017), tie spacing must be less than 200 mm or 1,5 times the thickness of the masonry unit. Three different values of spacing were considered (Table 1): (1) 200 mm, *i.e.,* the maximum spacing allowed; (2) 120 mm as the minimum, considering a minimum brick thickness of 80 mm; and (3) a spacing of 158 mm. The latter is the most widely used spacing by bricklayers in the region. From this point forward, the tie spacing will be identified through the machine spacing M, *i.e.*, the configuration on the machine that makes the straps (Figure 1). That is to say, 3, 3,95, and 5 cm long (Table 1).

Table 1. Experimental design for specimens

Tie	Specimens for testing	Configuration of the machine spacing (M) (cm)	Tie spacing (S) (mm)
Strapping spiral tie	3	3,00	120
	3	3,95	158
	3	5,00	200
Traditional tie	3	3,95	158

Source: Authors

Table 1 presents the number of specimens for each spacing and type of tie tested. Two types of ties were studied: traditional and SST. To characterize the specimens and validate their numerical models, three samples were tested for each type and spacing. Figure 6 shows their geometry.

Material tests

The characterization of the mechanical properties of the reinforcement steel were determined through uniaxial tensile tests, in accordance with ASTM standards (ASTM International, 2009, 2019). In addition, compression tests were conducted on concrete specimens (ASTM International, 2015, 2018). For the reinforcing steel, eight samples of the traditional ties and longitudinal bars (Figure 2a) and seven samples of the steel strapping strips with a characteristic length of 10 cm (Figure 2b) were tested in order to obtain their stress-strain curves. The elastic modulus was obtained by applying Equation (1), according to ASTM-A370 (ASTM International, 2019). Table 2 shows the average values of the elastoplastic parameters obtained for the longitudinal bars, traditional ties, and steel strapping strips. The stress-strain curves obtained are presented in Figure 3.

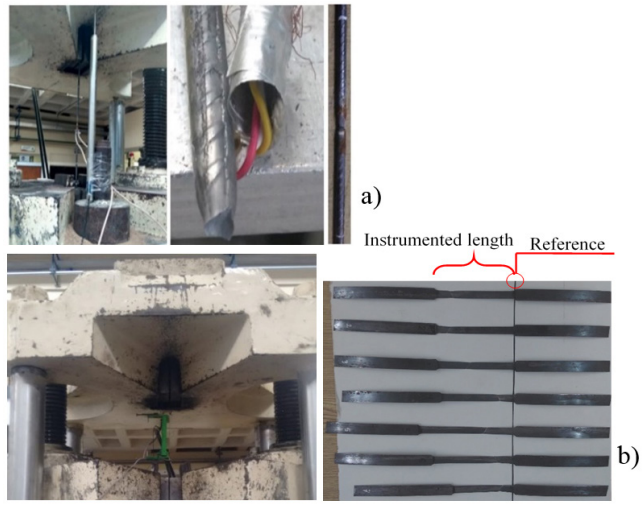

Figure 2. (a) Steel bars testing; (b) strapping strip test, using an electric displacement transducer and SST after testing
Source: Authors

Table 2. Material characteristics

Longitudinal bars (Ø = 6,0 mm)					
Parameters	**Yield stress (MPa)**	**Maximum stress (MPa)**	**Rupture stress (MPa)**	**Elongation at 10∅ (%)**	**Elastic modulus (MPa)**
Mean	528	656	473	10,36	145 938
Parameters	**Strain at the yield point**	**Strain at maximum stress**	**Rupture strain**	**Density (kg/m³)**	**μ Poisson ratio**
Mean	0,0056	0,16	0,21	7 850	0,30
Traditional ties (pattern) (Ø = 4,11 mm)					
Parameters	**Yield stress (MPa)**	**Maximum stress (MPa)**	**Rupture stress (MPa)**	**Elongation at 10∅ (%)**	**Elastic modulus (MPa)**
Mean	333	584	399	6	72 426
Parameters	**Strain at the yield point**	**Strain at maximum stress**	**Rupture strain**	**Density (kg/m³)**	**μ Poisson ratio**
Mean	0.0066	0.073	0,073	7 850	0,30
Steel strapping strips (rectangular section of 19 mm x 0,7 mm)					
Parameters	**Yield stress (MPa)**	**Maximum stress (MPa)**	**Rupture stress (MPa)**	**Elongation at instrumented length (%)**	**Elastic modulus (MPa)**
Mean	489	652	598	13	257 583
Parameters	**Strain at the yield point**	**Strain at maximum stress**	**Rupture strain**	**Density (kg/m³)**	**μ Poisson ratio**
Mean	0,0039	0,13	0,13	7 850	0,30

Source: Authors

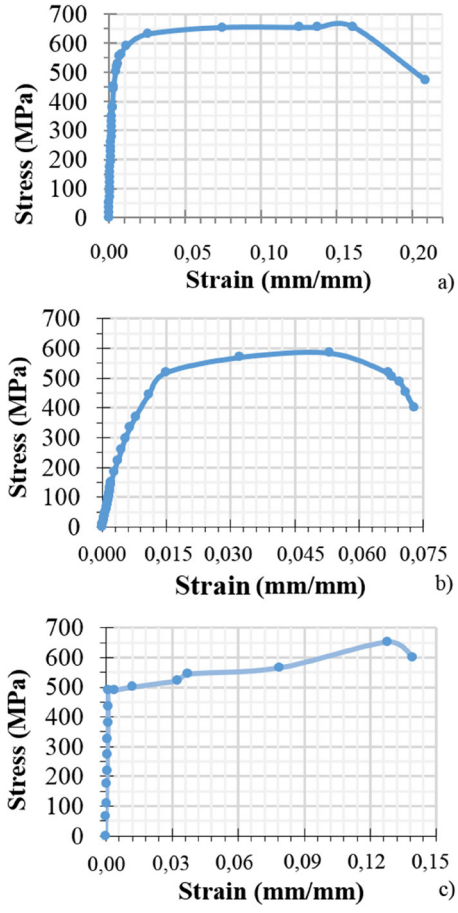

Figure 3. Stress-strain averaged curves for: a) longitudinal bars, b) traditional ties, c) strapping strips
Source: Authors

$$E = \frac{\acute{o}_f}{\left(\mathring{a}_f - 0,002\right)} \quad (1)$$

where E → Elastic modulus; σ_f → Yield stress; and ε_f → Yield strain.

To characterize the mechanical properties of the concrete, axial compression tests of 27 samples were carried out (Figure 4a) at 28 days. An average strength of $\bar{\sigma} = 15$ MPa was attained, with a coefficient of variation of δ = 0,0845. The cement used was CPC (Composite Portland Cement), with a maximum coarse aggregate size of 1/2 in (12,7 mm). Strain gauges were used to obtain the loading branch, while multiple linear variable differential transformers (LVDTs) were used to capture the unloading branch. Figure 4b shows the experimental results that will be introduced in the numerical model.

Specimen testing

The structural response of reinforced concrete specimens is conditioned by the mechanical properties of their constituent components: steel and concrete. To characterize their behavior, strain gauges and LVDTs were used (Figure 5). The dimensions of the short specimens were selected to avoid lateral instability problems and were 500 x 150 x 150 mm (length x height x thickness). All the SST specimens had ties with a cross-sectional area equal to the traditional tie area (Figure 6).

The specimens were tested using an electro-hydraulic press (Tinius Olsen brand). These tests were performed with

displacement speed control (0,005 mm/s) in order to obtain their post-peak behavior. In order to achieve a uniform load distribution on the top and bottom faces, 25 mm thick steel plates were placed (Figure 5d).

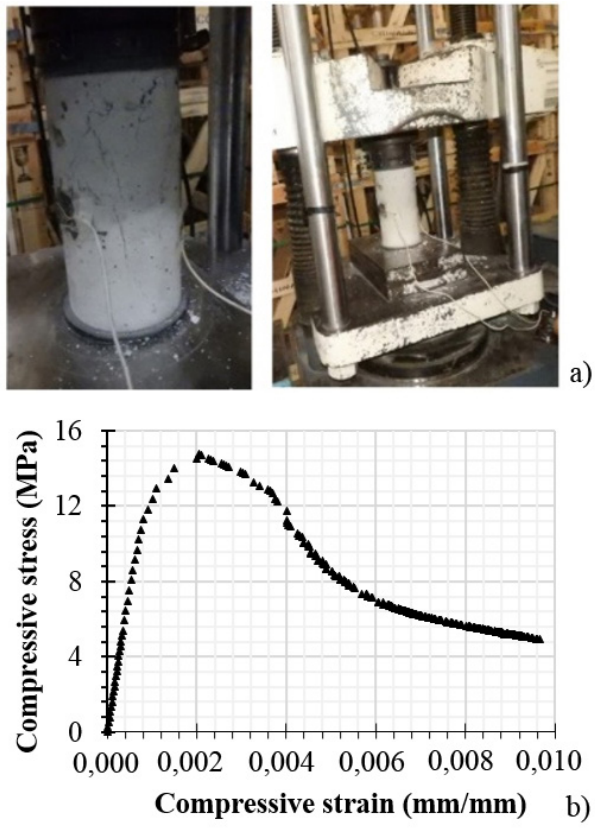

Figure 4. (a) Axial compression test for concrete, (b) concrete stress-strain relationships
Source: Authors

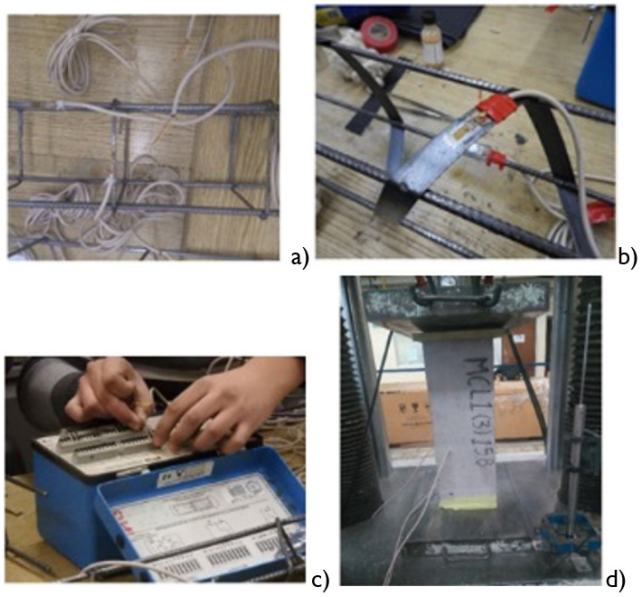

Figure 5. Instrumentation with strain gauges: a) longitudinal bars and traditional tie instrumentation, b) SST instrumentation, c) data acquisition device, d) specimen ready to be tested
Source: Authors

Sliding of concrete was the observed mode of failure (Figure 7a), along with buckling of the longitudinal bars (Figure 7c). For structural columns (ACI International, 2014), this implies structural collapse. However, for tie-columns, the wall would be able to stay up. This mode of failure is attributed to the use of a minimum transversal reinforcement area in the specimen. In addition, Figure 7b shows the averaged load-displacement's experimental results for the specimens. Furthermore, volumetric steel-concrete ratios for all the tested specimens, along with the percentage of reduction of the steel ratio for each set of SSTs, are presented in Table 3. It is noteworthy that, for a SST spacing of 5 cm, a significant reduction of 14,08% is observed.

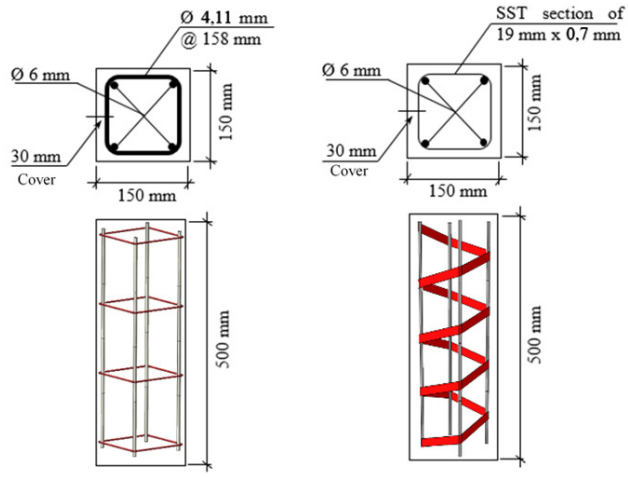

$$\underbrace{A=\frac{\pi D^2}{4}}_{\text{Circular section}}=13,27\,\text{mm}^2 \Rightarrow D=4,11\,\text{mm}$$

$$\underbrace{b*d}_{\text{Rectangular section}}=19\,\text{mm}*0,7\,\text{mm}=13,27\,\text{mm}^2$$

Figure 6. Specimen dimensions
Source: Authors

Numerical simulation

To obtain a higher level of computational precision, the three-dimensional micro-modeling technique was employed for the structural analysis of the four types of short tie-columns (Table 1 and Figure 8). The geometry of the steel bars and strips was modeled independently of the concrete matrix, with their corresponding constitutive laws (stress-strain curves). The ABAQUS/Explicit environment (Abaqus, 2016) was employed to carry out the simulations. The required integrations were performed by the well-known central difference integration scheme. Details of the mathematical modeling are provided in the following sections.

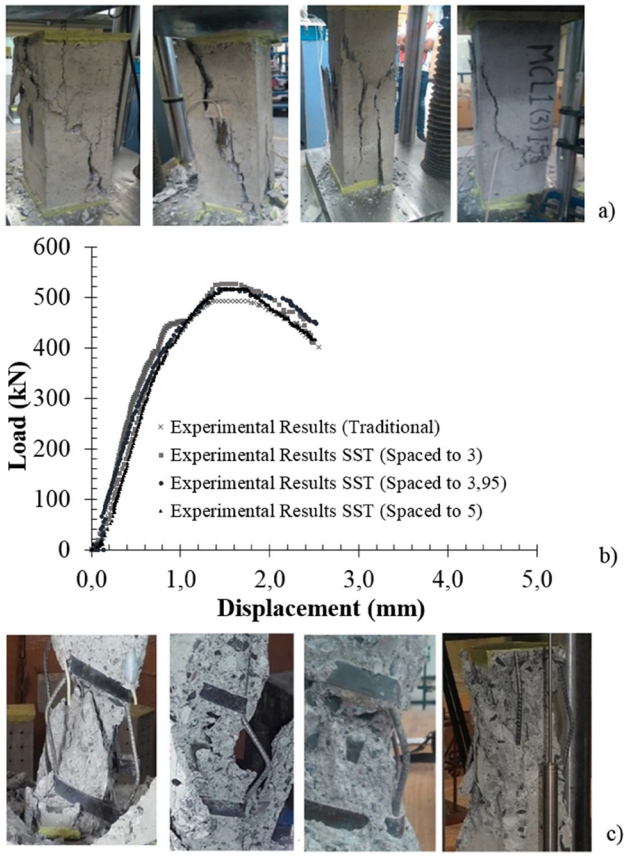

Figure 7. (a) Failure mode of the specimens, (b) averaged load-displacement experimental results, (c) loss of stability of the longitudinal bars
Source: Authors

Geometry, element types, and mesh

For the mathematical calibration, a finite element (FE) formulation, appropriate mesh size, and shape were considered (Mesa and Álvarez, 2011). Three-dimensional hexahedral elements C3D8R (eight contact nodes, reduced integration, and Hourglass control) were used for modeling the concrete matrix. For the longitudinal bars and traditional ties (Figure 8a), three-dimensional tetrahedral elements C3D10 (10 quadratic contact nodes) were employed. The SSTs (Figure 8b) were modeled with three-dimensional hexahedral elements C3D20R (20 quadratic nodes and reduced integration). The concrete and steel bonding zones were modeled using a contact surface. Table 4 shows the meshing used for the four three-dimensional models.

Boundary and loading conditions

The boundary conditions defined for the mathematical model are consistent with the support conditions of the experimental physical model. In other words, a uniform displacement of the top face is allowed only in the loading direction, and, at the bottom face, the movement is restricted for all the degrees of freedom. In addition, the mathematical model was subjected to a quasi-static load model by considering a displacement control of the top face, which was implemented by means of an explicit step function with soft amplitude. As a convergence criterion, a limit value of 5% was adopted for the ratio of kinetic energy and total internal energy (Fei *et al.*, 2017).

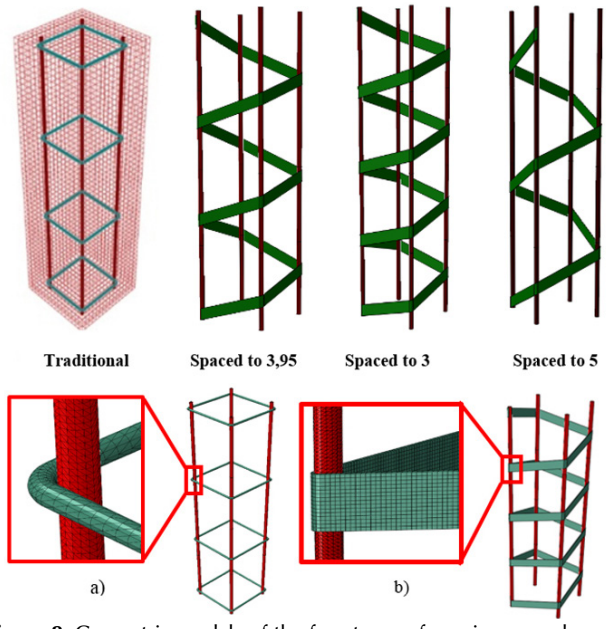

Figure 8. Geometric models of the four types of specimens and zoom of the mesh for: a) traditional ties, b) SST
Source: Authors

Table 3. Volumetric ratios between steel and concrete for the specimens

Configuration of the machine spacing of ties (cm)	Volume of steel $(V_a)(cm^3)$	Net volume of concrete $(V_a)(cm^3)$	Ratio $\left(\frac{V_a}{V_c}\right)(\%)$	Relative difference (%)
Traditional	79	11 171	0,71	Pattern
SST spacing of 3	77	11 173	0,69	2,82
SST spacing of 3,95	72	11 178	0,64	9,86
SST spacing of 5	68	11 182	0,61	14,08

Source: Authors

Table 4. Mesh description in geometric models

Configuration of the machine spacing of ties (cm)	Number of nodes	Number of elements	C3D8R	C3D10	C3D20R
Traditional	435 943	276 464	12 800	263 664	-
SST spacing to 3	520 721	263 860	12 800	231 860	19 200
SST spacing to 3,95	489 235	259 645	12 800	231 860	14 985
SST spacing to 5	465 997	256 270	12 800	231 860	11 610

Source: Authors

Constitutive laws

A concrete damaged plasticity model (CDPM) was used to define the nonlinear behavior of the concrete. A CDPM can simulate a quasi-brittle material behavior for both concrete and masonry, as well as the two main failure mechanisms of concrete: tensile cracking and compressive crushing. It is based on the basic models proposed by Lubliner *et al.* (1989) and improved by Lee and Gregory (1998) by considering the separation of damaged plasticity and the behavior of concrete under uniaxial tensile and compressive stresses.

The stress-strain relationship, under tensile stress, is linear-elastic up to the point where the peak tensile stress is reached. After that, the softening tensile behavior is modeled by stress-cracking strain or by considering fracture strain energy. Table 5 shows the cracking displacement when the complete loss of strength is attained (C. T. Sun and Jin, 2012; Telford, 2010). In this table, G_f is the fracture energy that represents the strain energy required to open a unit area crack, and f_c describes the tensile peak stress, as expressed in Equation (2).

$$G_f = G_{F0}\left(\frac{fc}{10MPa}\right)^{0,7};$$
$$G_{F0} = 0,030\frac{Nmm}{mm^2}; \quad (2)$$
$$f_c = 10\% f'c; \quad w_u = \frac{2G_f}{fc}$$

Where: G_f → Fracture energy, f_c → tensile peak stress, and w_u → crack opening at which concrete cannot resist larger stresses.

Table 5. Concrete model by the fracture energy criteria

Fracture energy of concrete GF $\left(\frac{N}{mm}\right)$	tensile peak stress f_c (MPa)	Crack opening at which concrete cannot resist a larger stress wu (mm)
0,039	1,47	0,053

Source: Authors

The following inelastic parameters were defined in order to determine the yield surface shape and the flow potential surface (Druker-Prager hyperbolic function): (1) a dilation angle; (2) flow potential eccentricity; (3) (f_{bo}/f_{co}), which represents the equi-biaxial/uniaxial compressive yield stress ratios; (4) K_c, the second stress invariant on tensile meridian *vs.* compressive meridian ratio; and (5) viscosity. The K_c value has influence on the yield surface shape (Sümer and Aktas, 2015).

Table 6 shows the values employed for these five parameters. The viscosity provides a quick convergence, as it allows a way to overcome the yielding zone as per the CDPM parameters. The viscosity value is fitted by trial and error. The Hill elastic plastic model (Caminero and Montans, 2010) was employed for a longitudinal and transversal steel constitutive ratio, with nonlinearity and hardening isotropy. The elastic parameters of concrete are defined in Table 7 (Telford, 2010).

Table 6. Parameters adopted for nonlinear analysis

Dilation angle	Eccentricity	Fb0/fc0	k	Viscosity parameter
31	0,1	1,16	0,66	0,005

Source: Authors

Table 7. Elastic parameters of concrete

μ (Poisson)	E (Elastic modulus) (MPa)	Limit of elastic strain	Limit of elastic stress (0,4 f'c) (MPa)	Density (kg/m3)
0,18	18 130	0,000325	5,88	2 000

Source: Authors

Results and discussion

Validation procedure

The experimental results of each specimen were obtained from the displacement-controlled test. Moreover, their corresponding load-displacement curves (LDC) were obtained from the numerical simulations. To validate the numerical model, the experimental results were compared to LDC. Figure 9 illustrates the averaged experimental results obtained from the specimens, along with the curves obtained from the numerical models (*i.e.*, LDC). The four models show a satisfactory fit. Table 8 shows a small relative difference (less than 5%) at maximum load.

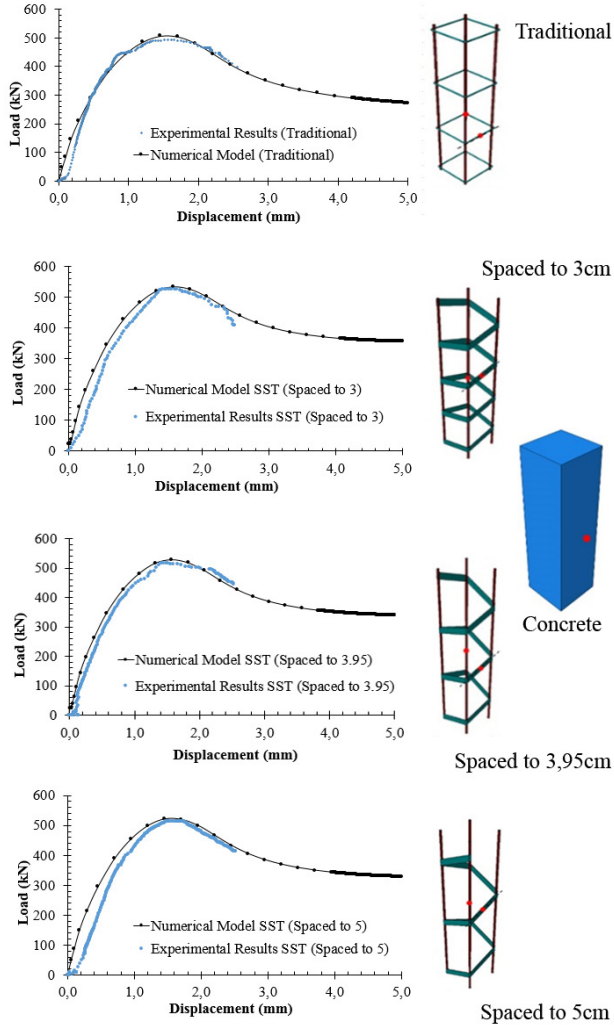

Figure 9. Load-displacement curves comparison between experimental results, and numerical models with location points where the strain gauges were placed in longitudinal steel, traditional ties, SST, and concrete
Source: Authors

Table 8. Maximum load comparison between averaged-experimental and FEM models

Configutarion of the machine spacing of ties (cm)	FEM (kN)	Experimental average (kN)	Relative difference
Traditional	507	492	3,1%
SST spacing to 3	535	528	1,4%
SST spacing to 3,95	529	517	2,3%
SST spacing to 5	522	516	1,1%

Source: Authors

During the validation process, strains measured by strain gauges in longitudinal bars, traditional ties, SST, and concrete (Figure 9) were compared to the strains from the numerical simulations (Table 9). The relative differences between these values were less than 13%. Thus, the numerical model is suitable to analyze SST, taking the different spacings into account.

Load-displacement curves comparison

It is well known that the longitudinal steel ratio is more meaningful than the transversal steel ratio on the compressive axial behavior of reinforced concrete. When using SSTs, a slight increment is observed in the compressive strength of the elements, in conjunction with a reduction in steel volume regarding the experimental results and FE models. This, despite the lower steel ratio in specimens with respect to traditional ties (Figure 10a and Table 10). On the other hand, Tables 10 and 11 imply that the rupture failure of the steel did not take place in the longitudinal bars, nor in the transversal steel. The variation of the von Mises stress in longitudinal bars is not significant, while the stress distribution in ties shows a relative difference of 88% when the maximum load is reached (Table 11), and 40% when the maximum displacement is reached (Table 12).

Table 9. Strain results comparison between numerical models and experimental specimens

Configuration of machine spacing of ties (cm)	Closed tie		Relative difference
	Exp	*FEM*	
Traditional	0,0109	0,0119	9%
SST spacing to 3	0,0101	0,0108	7%
SST spacing to 3,95	0,0098	0,0105	7%
SST spacing to 5	0,0073	0,007	4%
	Longitudinal steel		**Relative difference**
	Exp	*FEM*	
Traditional	0,0144	0,0162	13%
SST spacing to 3	0,0152	0,0163	7%
SST spacing to 3,95	0,0172	0,0165	4%
SST spacing to 5	0,0138	0,0143	4%
	Superficial concrete		**Relative difference**
	Exp	*FEM*	
Traditional	0,0161	0,0158	2%
SST spacing to 3	0,0152	0,015	1%
SST spacing to 3,95	0,0128	0,0137	7%
SST spacing to 5	0,0148	0,0143	3%

Source: Authors

Table 10. Maximum load from load displacement curves in FE model

Configuration of machine spacing of ties (cm)	Maximum load (kN) (FEM)	Relative difference	Absolute difference (kN)
Traditional	507	Pattern	Pattern
SST spacing to 3	535	5%	27,75
SST spacing to 3,95	528	4%	21,35
SST spacing to 5	521	3%	14,37

Source: Authors

Table 11. Von Mises criteria for longitudinal steel and ties when maximum load is reached

Configuration of machine spacing of ties (cm)	Maximum value for longitudinal steel (MPa)	Relative difference	Maximum value for tie steel (MPa)	Relative difference
Traditional	552	Pattern	322	Pattern
SST spacing to 3	552	0,15%	597	85,28%
SST spacing to 3,95	551	0,15%	597	85,31%
SST spacing to 5	564	2,34%	605	87,83%

Source: Authors

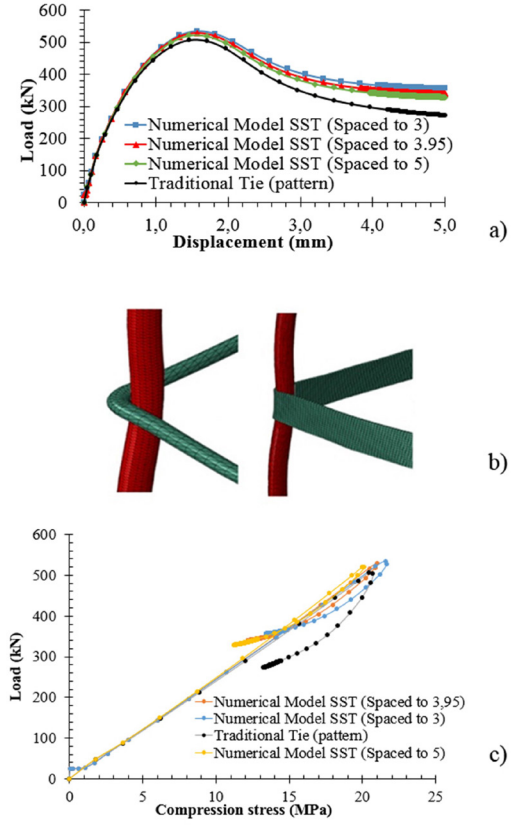

Figure 10. (a) Load displacement curves for ties (FEM model), (b) detail of the deformed union between ties and longitudinal steel, and (c) load branch *vs.* compressive stress at the center of mass node
Source: Authors

SST behavior

SST provides a greater confinement to the concrete specimens when compared to traditional ties, given the larger contact area against concrete (Figure 10b). The degree

of confinement was obtained by measuring the compressive stress at the center of mass of each model. Figure 10c shows that, at unloading, the compressive stress decreases more rapidly with traditional ties than with SST. This leads to better behavior and stability of the SST. This means that the traditional tie has more softening than the other ties in the center of mass of the concrete in the post-peak stage, which in turn implies a decrease in its confinement capacity in comparison with the other models. By comparing the last point in the curve of Figure 10c, the next ordered pairs are obtained (load, compressive stress): Traditional (277 kN, 13,2 MPa); SST spacing 3 (357 kN, 13,3 MPa); SST spacing 3,95 (344 kN, 12,2 MPa); and SST spacing 5 (335 kN, 11,70 MPa). This indicates a relative difference of -29% for SST spacing set to 3 cm, -24% with SST spacing set at 3,95 cm, and 21% when a SST spacing of 5 cm is employed. These results imply a better confinement for concrete in all scenarios. In this computation, the control value corresponds to the traditional ties. Additionally, the compressive stress levels in the central mass of the concrete have the following relative differences: 11,4, 7,6, and -0,8% for 5, 3,95, and 3 SST spacings, respectively.

Table 12. Von Mises criteria for longitudinal steel and ties when maximum displacement is reached

Configuration of machine spacing of ties (cm)	Maximum value for longitudinal steel (MPa)	Relative difference	Maximum value for tie steel (MPa)	Relative difference
Traditional	624	Pattern	475	Pattern
SST spacing to 3	631	1,04%	64	35,44%
SST spacing to 3,95	630	0,83%	645	35,65%
SST spacing to 5	626	0,30%	666*	40,17%

*The stress recorded is 2,15% larger than the maximum stress of the experimental results at Table 3

Source: Authors

When the maximum compressive strength is achieved, the yielding of steel is in its initial stage in the longitudinal bars, as well as in the SST (Table 2 and Figure 11). However, in traditional ties, yielding has not started yet (Table 2 and Figure 12). At this stage, concrete is in its softening zone (Table 13), *i.e.*, the post-peak stage. Traditional ties have already attained yielding when the maximum displacement is reached (Figure 13), and concrete has already exceeded the plastic strain (Table 14).

Table 13. Maximum plastic equivalent strain (PEEQ) when the model reaches maximum load

Configuration of machine spacing of ties (cm)	PEEQ (MPa)	Relative difference
Traditional	0,00290	Pattern
SST spacing to 3	0,00319	10,0%
SST spacing to 3,95	0,00316	9,0%
SST spacing to 5	0,0057	96,6%
Concrete parameters		
Inelastic strain corresponding to f'c		0,001727
f'c (MPa)		14,71

Source: Authors

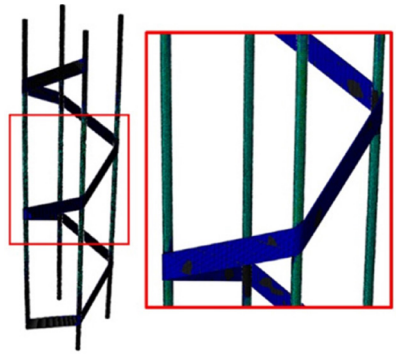

Figure 11. Yielding of the SST spacing of 5 when maximum load is attained. Black represents the yielded zone.
Source: Authors

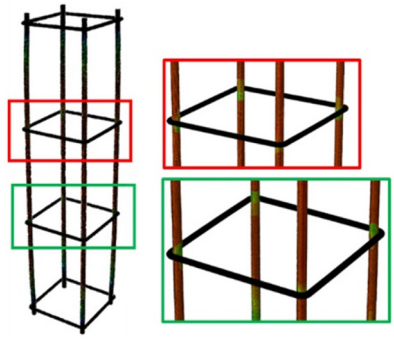

Figure 12. Yielding of the traditional ties (pattern) when maximum load is reached. Black represents the non-yielded zone. In this case, none of the ties reaches yielding.
Source: Authors

Table 14. Maximum plastic equivalent strain (PEEQ) when the model reaches maximum displacement

Configuration of machine spacing of ties (cm)	PEEQ (MPa)	Relative difference
Traditional	0,017	Pattern
SST spacing to 3	0,01787	5,12%
SST spacing to 3,95	0,01773	4,29%
SST spacing to 5	0,01791	5,35%
Concrete parameters		
Maximum inelastic strain in compression		0,014675
Rupture stress in compression		0,7203

Source: Authors

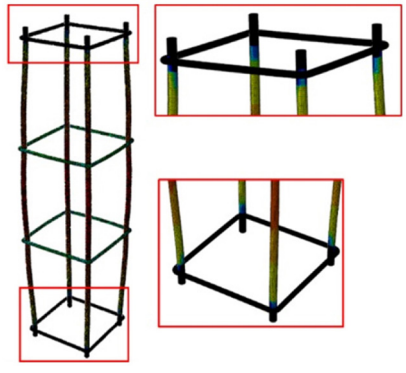

Figure 13. Yielding of traditional ties (pattern) when maximum displacement is reached. Black represents non-yielded zones. In this case, the tie middle reaches yielding, while ties at the end do not yield.
Source: Authors

Conclusions

In this paper, three-dimensional micro-numerical models were developed to analyze the behavior of RC short tie-columns. At the same time, FE models were calibrated and validated. Quadratic elements C3D20R and C3D10 were employed for steel modeling with circular cross-sections and strapping steel, respectively. Moreover, linear elements C3D8R were used to model concrete. At this stage, the following conclusions can be drawn when comparing SSTs and traditional ties:

An increase of 21% in the concrete confinement was attained in the unloading curve inside the elements (Figure 10c). This is due to a larger exposed contact area between steel and concrete. Once the maximum compressive strength of short tie-columns is reached, the loss of stiffness is lower in comparison with traditional ties.

The volume of steel is reduced. Table 3 shows a 14% of relative volume difference when the SST spacing is 5 cm, against traditional ties. This provides a significant reduction in the cost of raw materials for manufacturing these ties. Furthermore, the manufacturing time is also significantly reduced.

The SSTs with the spacings of 3, 3,95, and 5 cm offered a slight increase in compressive strength for short tie-columns when compared to traditional ties. However, due to large confinement and the reduction of labor costs, along with the speed of the reinforcement placing, this makes it a better option for reinforcement.

For future research, we recommend the inclusion of different steel ratios in flexural elements and larger tie-columns, as well as masonry walls.

Acknowledgement

We gratefully acknowledge Aceros Titán Company, as well as the Structural Engineering Department of Universidad Autónoma de Nuevo León for making this research possible. Project ID: PIEP-L-04-18-116/043-SC.

CRediT author statement

All authors: Conceptualization, methodology, validation, formal analysis, investigation, writing (original draft preparation, review, and editing), data curation, supervision, project administration, resources, and funding acquisition.

References

Abaqus (2016). *Analysis user's manual. Documentation*. Dassault Systemes Simulia Corporation.

Aceros Titán Company (2016). *Manufacture and distribution of steel products for the metal-mechanical and construction industries*. https://www.acerostitan.com/certifications

ACI International (2013). ACI-530. Building code requirements and specification for masonry structures and companion commentaries *TMS 602-13/4CI 530.1-13/ASCE 6-13* (pp. S-1-S-85). https://www.concrete.org/store/productdetail.aspx?ItemID=53013&Language=English&Units=US_Units

ACI International (2014). *ACI-318. Building code requirements for structural concrete*. https://civilshare.files.wordpress.com/2016/07/aci_318s_14_en_espanol.pdf

Arslan, G. (2012). Diagonal tension failure of rc beams without stirrups. *Journal of Civil Engineering and Management, 18*(2), 217-226. https://10.3846/13923730.2012.671264

ASTM International (2009). *ASTM-E8/E8M-09. Standard test methods for tension testing of metallic materials*. https://cypma.mx/mecanicas/astm-e8/ .

ASTM International (2015). *ASTM-C617/C617M-15. Standard practice for capping cylindrical concrete specimens*. https://www.astm.org/c0617_c0617m-15.html

ASTM International (2018). *ASTM-C39/C39M-18. Test method for compressive strength of cylindrical concrete specimens*. https://www.astm.org/c0039_c0039m-18.html

ASTM International (2019). *ASTM-A370. Standard test methods and definitions for mechanical testing of steel products*. https://www.astm.org/a0370-21.html

Azam, R., El-Sayed, A. K., and Soudki, K. (2016). Behaviour of reinforced concrete beams without stirrups subjected to steel reinforcement corrosion. *Journal of Civil Engineering and Management, 22*(2), 146-153. https://10.3846/13923730.2014.897979

Caminero, M. A., and Montans, F. J. (2010). *Anisotropic elasto-plasticity model based on the Hill yield criterion with mixed hardening: Implicit stress integration algorithm and consistent tangent modulus* [Conference paper]. XVIII National Congress of Mechanical Engineering, Ciudad Real, Spain. http://toc.proceedings.com/11510webtoc.pdf

Colajanni, P., La Mendola, L., Mancini, G., Recupero, A., and Spinella, N. (2014). Shear capacity in concrete beams reinforced by stirrups with two different inclinations. *Engineering Structures, 81*, 444-453. https://doi.org/10.1016/j.engstruct.2014.10.011

De Corte, W., and Boel, V. (2013). Effectiveness of spirally shaped stirrups in reinforced concrete beams. *Engineering Structures, 52*, 667-675. https://doi.org/10.1016/j.engstruct.2013.03.032

Dong, H.-L., Wang, D., Wang, Z., and Sun, Y. (2018). Axial compressive behavior of square concrete columns reinforced with innovative closed-type winding GFRP stirrups. *Composite Structures, 192*, 115-125. https://doi.org/10.1016/j.compstruct.2018.02.092

Du, M., Jin, L., Du, X., and Li, D. (2017). Size effect tests of stocky reinforced concrete columns confined by stirrups. *Structural Concrete, 18*(3), 454-465. https://doi.org/10.1002/suco.201600074

Fei, Z., Qiang, Z., Fenglai, W., and Xu, Y. (2017). Spatial variability and sensitivity analysis on the compressive strength of holow concrete block masonry wallettes. *Construction and Building Materials, 140*(129-138), 129-138. http://dx.doi.org/10.1016/j.conbuildmat.2017.02.099

Grgić, N., Radnić, J., Matešan, D., and Banović, I. (2017). Stirrups effect on the behavior of concrete columns during an earthquake. *Materialwissenschaft und Werkstofftechnik, 48*(5), 406-419. https://doi.org/10.1002/mawe.201700014

Gribniak, V., Rimkus, A., Torres, L., and Jakstaite, R. (2017). Deformation analysis of reinforced concrete ties: Representative geometry. *Structural Concrete, 18*(4), 634-647. https://doi.org/10.1002/suco.201600105

Hong, K.-N., Han, S.-H., and Yi, S.-T. (2006). High-strength concrete columns confined by low-volumetric-ratio lateral ties. *Engineering Structures, 28*(9), 1346-1353. https://doi.org/10.1016/j.engstruct.2006.01.010

INEGI (n.d.). *National Institute of Statistics and Geography*. https://www.inegi.org.mx/default.html

Lee, J., and Gregory, L. F. (1998). Plastic-Damage Model for Cyclic Loading of Concrete Structures. *Journal of Engineering Mechanics,, 124*(8), 892-900. http://doi:10.1061/(asce)0733-9399(1998)124:8(892)

Li, W., Sun, L., Zhao, J., Lu, P., and Yang, F. (2018). Seismic performance of reinforced concrete columns confined with two layers of stirrups. *The Structural Design of Tall and Special Buildings, 27*(12), e1484. https://doi.org/10.1002/tal.1484

Lima de Resende, T., da Conceição Domingues Shehata, L., and Abd El Malik Shehata, I. (2016). Shear strength of self-compacting concrete beams with small stirrups ratios. *Structural Concrete, 17*(1), 3-10. https://doi.org/10.1002/suco.201400084

Lubliner, J., Oliver, J., Oller, S., and Oñate, E. (1989). A plastic-damage model for concrete. *International Journal of Solids and Structures, 25*(3), 299-326. https://doi.org/10.1016/0020-7683(89)90050-4

Mesa, M., and Álvarez, J. (2011). Calibración numérica de un problema de ingeniería vial. *Revista de la construcción, 10*(3), 52-63. http://dx.doi.org/10.4067/S0718-915X2011000300006

NTCM (2017). *Normas técnicas complementarias para el diseño y construcción de estructuras de mampostería*. NTCM.

Pérez-Caldentey, A., Corres Peiretti, H., Peset Iribarren, J., and Giraldo-Soto, A. (2013). Cracking of RC members revisited: Influence of cover, $\phi/_{\rho s,ef}$ and stirrup spacing – An experimental and theoretical study. *Structural Concrete, 14*(1), 69-78. https://doi.org/10.1002/suco.201200016

Ridha, M. M. S., Al-Shaarbaf, I. A. S., and Sarsam, K. F. (2018). Experimental study on shear resistance of reactive powder concrete beams without stirrups. *Mechanics of Advanced Materials and Structures*, *27*(12), 1006-1018. https://doi.org/10.1080/15376494.2018.1504258

Rodríguez, M. (2009). *Confined masonry constructions*. https://www.world-housing.net/wp-content/uploads/2011/05/Confined-Masonry_Rodriguez.pdf. -

Salah-Eldin, A., Mohamed, H. M., and Benmokrane, B. (2019). Structural performance of high-strength-concrete columns reinforced with GFRP bars and ties subjected to eccentric loads. *Engineering Structures, 185*, 286-300. https://doi.org/10.1016/j.engstruct.2019.01.143

Sümer, Y., and Aktas, M. (2015). Defining parameters for concrete damage plasticity model. *Challenge Journal of Structural Mechanics, 1*(3), 149-155. https://doi.org/10.20528/cjsmec.2015.07.023

Sun, C. T., and Jin, Z. H. (2012). *Fracture mechanics*. Academic Press.

Sun, L., and Li, W. (2019). Cyclic behavior of reinforced concrete columns confined with two layers of stirrups. *Structural Concrete, 20*(4), 1279-1291. https://doi.org/10.1002/suco.201800229

Tan, R., Eileraas, K., Opkvitne, O., Žirgulis, G., Hendriks, M. A. N., Geiker, M., Brekke, D.-E., and Kanstad, T. (2018). Experimental and theoretical investigation of crack width calculation methods for RC ties. *Structural Concrete, 19*(5), 1436-1447. https://doi.org/10.1002/suco.201700237

Telford, T. (2010). *CEB-FIP, Model Code*. International Federation for Structural Concrete.

Yun, X., and Gardner, L. (2017). Stress-strain curves for hot-rolled steels. *Journal of Constructional Steel Research, 133*, 36-46. https://doi.org/10.1016/j.jcsr.2017.01.024

Research Article/Civil and Sanitary Engineering https://doi.org/10.15446/ing.investig.99197

Soil Conditions and Shield Tunneling Viability for Bogotá Metro Line 1

Análisis de las Condiciones del Suelo y Viabilidad para la Línea 1 del Metro de Bogotá con Tuneladora

Diana M. Matta-Diaz[1], Sebastián Rivera-Pardo[2], Xian Liu[3], and Yun Bai[4]

ABSTRACT

Bogotá, the capital city of Colombia, has experienced a critical situation regarding its public transport and road network condition. Unfortunately, the city has lacked an analytical long-term evaluation with regard to transport planning and infrastructure that is able to meet the growing demand. The metro system has been planned for more than half a century, and the existing soil investigations have not been fully used to evaluate the feasibility of building a metro in Bogotá's subsoil. In order to estimate the construction viability of an underground system in the city, the authors studied the ground conditions along the alignment of Metro Line 1, as proposed in 2014. This research brought forward the stratigraphic profile of the first 6,6 km of the alignment. The ground displacements induced by tunneling were estimated by means of a finite element analysis, and the results are presented in this paper along with their significance. The results forecast surface settlements lower than 10 mm, showing that the condition and strength of the soil are suitable for underground metro construction. However, soil consolidation and appropriate monitoring during and after tunneling should be taken under consideration for the sake of the project's success.

Keywords: congestion cost, lacustrine deposits, Bogotá subsoil, tunneling

RESUMEN

Bogotá, la capital de Colombia, se ha caracterizado por su situación crítica en temas de transporte público y condiciones de conexión vial. Desafortunadamente, la ciudad ha carecido de una evaluación analítica a largo plazo con respecto a la planeación del transporte, así como de una infraestructura que sea capaz de satisfacer la creciente demanda. El sistema metro ha sido planeado por más de medio siglo, y los estudios de suelos existentes no han sido aprovechados en su totalidad para evaluar la viabilidad de construir un metro en el subsuelo de Bogotá. Para estimar la viabilidad de construir un sistema subterráneo en la ciudad, los autores estudiaron las condiciones del suelo a lo largo del trazado de la Línea de Metro 1, tal y como se propuso en 2014. Esta investigación puso de manifiesto la columna estratigráfica de los primeros 6,6 km del trazado. Los desplazamientos del suelo inducidos por la construcción de túneles se estimaron mediante un análisis de elementos finitos, y los resultados se presentan en este artículo en conjunto con su significancia. Los resultados pronostican asentamientos menores a 10 mm, indicando que las condiciones y la resistencia del terreno son aptas para la construcción de un metro subterráneo. Sin embargo, la consolidación del suelo y un monitoreo adecuado durante y después de la construcción de los túneles deben ser consideradas en pro del éxito del proyecto.

Palabras clave: costo del congestionamiento vial, depósitos lacustres, subsuelo de Bogotá, construcción de túneles

Received: October 25th, 2021
Accepted: August 25th, 2022

Introduction

Bogotá is the fourth most populated and largest capital city in South America, with an urban population of 7,8 million (as of 2021) (DANE, 2020) and a great infrastructure demand. In the last five years, the city administration prioritized two projects to improve mobility and provide a solid transport system: i) the integration of the bus rapid transit (BRT) system with public buses, and ii) the construction of the first metro line (hereinafter referred to as BML1). Despite the economic and social costs of traffic congestion and more than US$45 million spent in the last eight contracts on the analysis of an urban mass transit system, Bogotá still lacks a reliable transit service. According to a study on the future impacts of traffic jams due to time lost, Bogotá ranked first in the Top 5 of global congestion impact ranking in 2018 (Read and Kidd, 2019), which is shown in Table 1.

[1] PhD Candidate, Tongji University, China. MScs in CEng, Department of Geotechnical Engineering, College of Civil Engineering, Tongji University, China. Email: diana@tongji.edu.cn

[2] MScs in Earth Science, Universidad Santo Tomas, Colombia. Email: sebastianriverapardo@gmail.com

[3] PhD, Professor, Tongji University, China. Professor, Department of Geotechnical Engineering, College of Civil Engineering, Tongji University, China. Email: xian.liu@tongji.edu.cn

[4] PhD, Professor, Tongji University, China. FICE, CEng, Professor, Department of Geotechnical Engineering, College of Civil Engineering, Tongji University, China. Email: baiyun1958@tongji.edu.cn

How to cite: Matta-Diaz, D. M., Rivera-Pardo, S., Liu, X., and Bai, Y. (2023). Soil Conditions and Shield Tunneling Viability for Bogotá Metro Line 1. *Ingeniería e Investigación, 43*(2), e99197. https://doi.org/10.15446/ing.investig.99197

Table 1. Top 5 most congested cities in the global congestion impact ranking

Impact Rank	City	Hour Lost	Last Mile Speed (MPH)
1	Bogotá	133	11
2	New York City	100	12
3	Moscow	100	15
4	Philadelphia	94	12
5	Paris	88	13

Source: Read and Kidd (2019)

Fenalco (2014) studied the cumulative cost of traffic congestion for Colombia in the 2013-2030 period, for which they estimate gridlock costs of US$3,9 billion. They classified congestion costs into direct costs, such as the value of fuel and the time spent in traffic and not at work; and indirect costs, where higher freighting and business fees from company vehicles idling in traffic are passed on as additional costs to household bills (Cebr, 2014). In addition to these already occurring congestion costs, future congestion costs resulting from the current BRT system must be considered. The capacity of the BRT system used in Bogotá is 45 000 passengers per hour per direction (pphpd), whereas the capacity of a metro system falls in the range of 60 000-80 000. In order for the BRT system to match the efficiency of a metro system, the city would need to invest in additional BRT lanes. The problem with adding more BRT lanes is that there is not enough space in the city to accommodate them without affecting the traffic of privately-owned cars, which results in an increase in the cumulative cost of traffic congestion.

This research aims to develop a model that is able to predict ground settlements caused by shield tunneling in Bogotá for future metro lines. Major advances have been made in shield tunneling, particularly with the introduction of the pressurized face type, which allows tunnels to be built in all types of soils. This includes recent advances on EPB (earth pressure balance) and BSS (bentonite slurry shield) operation and control, particularly under difficult ground conditions. Developments related to shield tunneling technology have been reviewed by Clough (1993), Fujita (1989), and Béjui and Guilloux (1989).

The model was built based on information and data from the BML1, including a precise analysis of ground conditions (soil parameters and water presence), location, and other aspects of construction (tunnel diameter and depth). Unlike a regular analysis, where a deterministic simulation based on known inputs is first used and a probabilistic study is then applied to provide realistic estimates and confirm the validity of the outputs, this study proposes building a statistical model that aims to provide the best inferences needed as inputs for the deterministic analysis.

Overview of metro plans

Cities like London, Madrid, Shanghai, México DF, and Bogotá share a common feature: a soft soil medium beneath their ground (Sainea-Vargas *et al*., 2020; Melis-Maynar, 1998; Ding and Xu, 2017). Bogotá's metro has been planned for over 70 years, but political issues and funding are the main reasons why citizens are still waiting to ride the first metro line (Figure 1). Table 2 lists some features of the four main studies that have been conducted for the BML1. Although these four proposals had different alignments, the proposed average length is 23,44 km. The estimated costs differ on the length and construction method; the lowest cost was US$1,96 billion of at-grade and cut-cover stations, and the highest cost was the earliest, proposed in 1981 with a combination of elevated, at-grade, and underground stations.

Table 2. Main BML1 construction proposal

Year	Alignment	Length [km]/ stations	Design capacity per hour	Construction method	Cost (billion USD)
1987	Ciudad Bolívar –C. Histórico & admo.	23/10	Unknown	TBM, at grade rail, bridge structure	7,97
2008-2010	San Victorino – Calle 170	19,7/19	29 300	Cut-cover, at-grade rail	1,96
2013-2015	Ptal. Américas, Av. Villao – Calle 127	27/27	48 000	TBM	7,55
2016	Ptl Americas-Calle 72	24/16	60 000	Bridge structure	3,48

Source: Contraloría de Bogotá (2019)

The feasibility study conducted between 2013 and 2015 for an underground metro line was significantly more detailed than the former. The detail-design phase reached 80% completion, whereas the others only reached the conceptual design phase. The estimated cost was 9,42% higher than the budget approved by both local and national governments, and therefore the project was never executed.

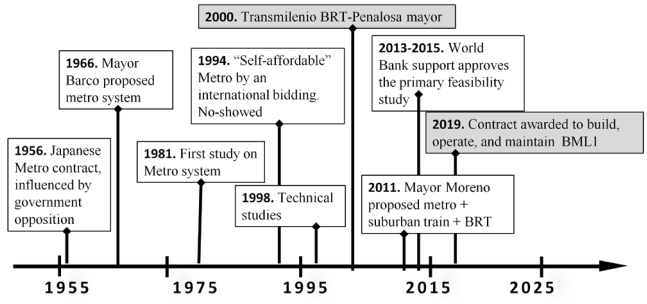

Figure 1. Timeline of Bogotá Metro Line 1
Source : Authors

In 2016, the city administration carried out a comparative study between the different construction alternatives in order to quantify and assess costs (Contraloría de Bogotá, 2019). The results suggested building an elevated metro line due to the decrement of initial costs compared to the underground

option proposed in 2014. Although this cost estimation was based only on conceptual designs, the international bidding to design, build, operate, and maintain the future metro line 1 was awarded for a US$5,16 billion contract.

Normally, the cost ratio for elevated *vs.* underground systems is approximately 1/2,5 (ITA-WG13, 2004). In the case of the BML1, the cost ratio of these two alternatives differs in the number of stations and trains, the length, BRT additions, and the design stage. However, from the overall cost of the two proposals, the cost ratio for elevated *vs.* underground systems can be calculated as 1/2,3. As shown in Figure 2, the proposal for an elevated line included 15 stations with a total length of 24 km, compared to an underground option of 27 stations within 27 km. The estimated construction cost of all 27 underground stations was US$2,14 billion, whereas the cost of the elevated stations was US$0,41 billion (Contraloría de Bogotá, 2019). Thus, the cost ratio of elevated *vs.* underground stations is approximately 1/2,8.

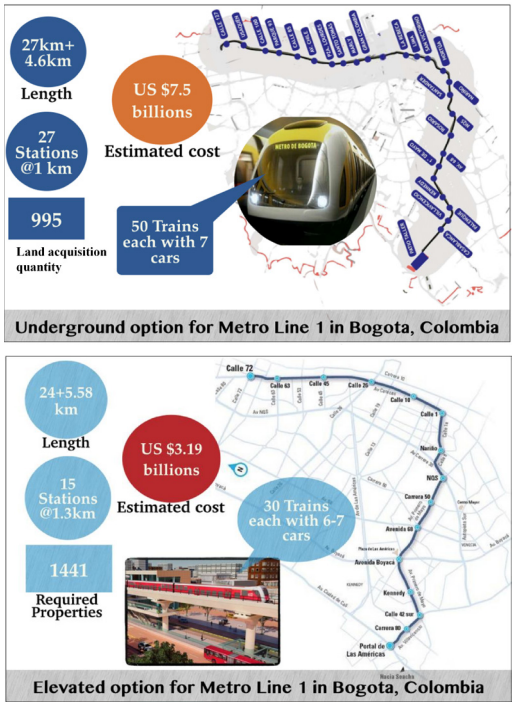

Figure 2. Key features of the BML1: a) underground metro line and b) elevated metro line
Source: Adapted from Contraloría de Bogotá (2019)

Methodology

The computational model is briefly divided into three stages: (1) the definition of stratigraphic soil profiles along the alignment of the BML1 via a statistical analysis of geotechnical data; (2) an approach to an optimal tunnel system suitable for Bogotá; (3) the collection of computational results by means of a numerical model which can approximate the real conditions to the model parameters with the aim of estimating the ground movements induced by shield tunneling. The software RStudio was used to analyze the data obtained from geotechnical investigations of each section of the alignment. The deterministic model was built using PLAXIS2D, a two-dimensional finite element code.

Statistical analysis

Geological, geotechnical, and hydrogeological investigations are the backbone of a baseline geological report. Previous experience in metro projects has shown that having a substantial amount of geotechnical investigation and using adequate methods with scientific accuracy can reduce construction costs and lower the risks. Therefore, laboratory and field testing (CPTu, SDMT, PMT, and geophysics) were performed on the BML1's alignment from 2013 to 2015 (Figure 3). The geotechnical data were collected within 0 to 50 m in depth and uploaded to an online open-access platform (IDU, 2013). Unfortunately, there were no stratigraphic profiles developed along the alignment, and the extensive laboratory data was not organized or verified. In order to get the stratigraphic profiles needed to conduct this study, a statistical analysis was carried out. This process is shown in Figure 4.

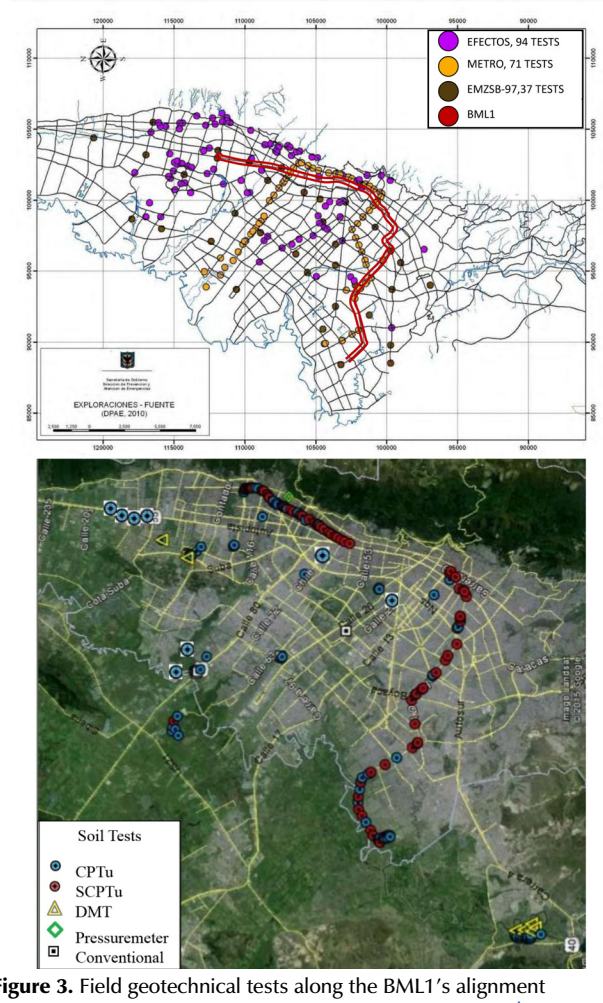

Figure 3. Field geotechnical tests along the BML1's alignment
Source: Adapted from Consorcio L1 (2015) and Alcaldía Mayor de Bogotá (2010)

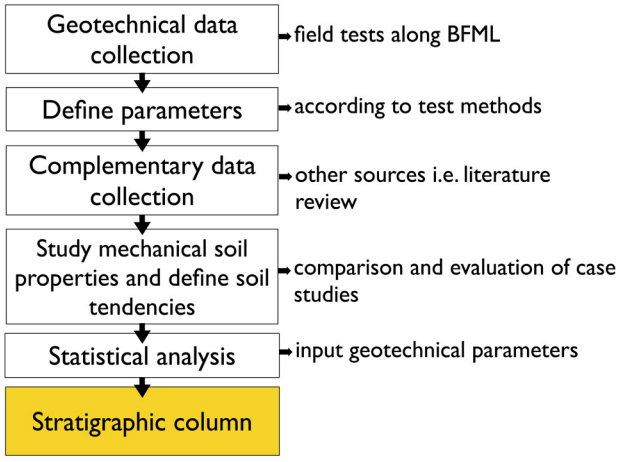

Figure 4. Statistical analysis process
Source: Authors

A statistical hypothesis is an assumption about a population parameter, which may or may not be true. Hypothesis testing is used to accept or reject a sample based on its consistency. There are two types of statistical hypotheses (null hypothesis H_o and alternative hypothesis H_1), as well as a region of acceptance α. For example, the hypothesis formulation used to analyze the values of the friction angle is described using the expression in Equation (1). Where μ can be equal to 35°, 32,5°, 30°, 25,5°, 24,5°, 23,5°, 22,5°, 17°, 16°, 15°, or 10° depending on the soil type to be tested, within a region of acceptance of 0,5°. The statistic used is described using Equation (2).

$$H\_o: \mu\_part = \mu \qquad H\_1: \mu\_part \neq \mu \tag{1}$$

$$\frac{\bar{X} - \mu}{s/\sqrt{\eta}} \sim N(0,1) \tag{2}$$

To analyze the laboratory data obtained from each section of the alignment, a statistical model was built by means of confidence intervals and t-test hypotheses via the RStudio software. The essential soil parameters that describe the deformation characteristics, strength, initial state, plastic, and elastic behavior of soils were studied, *i.e.*, friction angle, Poisson ratio, cohesion, modulus of deformation, and unit weight of the soil. The total length of the first metro line was divided into four sections (Table 3). This study presents the results obtained for Section I after analyzing the data obtained from 81 boring tests and 67 piezocone penetrations.

Proposed tunnel design

An optimal design for a subway tunnel satisfies the construction safety, operation, and maintenance requirements with a cost-benefit analysis. A diameter of 6,5 m was used in this study, referencing Shanghai's subway tunnels. However, the final values shall be decided by the owner of the project. The authors proposed two single parallel tubes for the Bogotá subway system. The clearance distance between them is discussed below.

Groundwater levels: The average water level value was defined from data analysis of in situ measurements, and it was also verified with values found in the literature review (Consorcio L1, 2015). The groundwater table for Section I is shown in Figure 5.

Table 3. Proposed stations and sections along BML1's alignment.

Section	Station$_{i,f}$	Crossing road	K$_{i,f}$	Length (km)
I	Portal de las Américas – Avenida 68	Av. Villavicencio, Av. 1 mayo, Av. 68	0+000 ~ 6+667	6,667
II	Avenida 68 – San Victorino	Av. 68, 1 mayo, NQS, de la Hurta, Av. Caracas, Cra. 10	6+667 ~ 13+996	7,329
III	San Victorino – Lourdes station	Cra 10, Plaza la Rebeca, Cra.13 Plaza Lourdes, Cra.11	13+996 ~ 20+162	6,166
IV	Lourdes station – Calle 127	Cra. 11, Cra 9, Calle 127	20+162 ~ 27+064	6,902

Source: Consorcio L1 (2015)

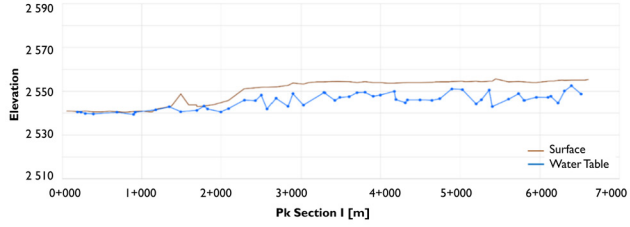

Figure 5. Water table for Section I
Source: Adapted from Consorcio L1 (2015)

Overburden: the ideal condition is to excavate throughout the most favorable strata. According to tunnel design guidelines (ITA, 1988), the overburden of shield tunnels shall be greater than 1,5-2 times the diameter of the shield machine. Two scenarios were modeled in order to compare the feasibility of subway construction based on studies about the prediction of surface settlements and parallel tunnels interaction (Hossaini *et al.*, 2012) (Table 4). This method can be used if i) the depth and tunnel diameter ratio is greater than 1,5, and ii) the distance between one tunnel center and the other is equal or greater to 1,3 D. The factors considered in each modeling scenario are the ratio of tunnel depth (z) and diameter (D), the clearance between parallel tunnels (center-center) d/D, and the water level.

Table 4. Description of scenarios used on the deterministic analysis

Section	Z_{crown} (m)	Z_{crown}/D	d (m)	d/D	Water level (m)
Scenario 1	16,25	2,5	22,80	3,5	-3
Scenario 2	13	2	16,22	2,5	-3

Source: Authors

Numerical analysis

Nowadays, almost every tunneling project requires numerical modeling in order to predict ground movement and behavior at ground surface in response to tunneling. PLAXIS 2D is one of the finite element programs that are commonly used in geotechnical applications to calculate deformations and stability. It considers both, construction and ground conditions (geometry, initial stresses, ground behavior, excavation stages, *etc.*). This software was available to compute the estimated ground response to tunnel excavation during this research. Both, settlement curves after excavation and the consolidation phenomenon were analyzed.

According to the conditions described below, the elastic-plastic MC model was used as a primary approach to calculate the settlements induced by tunneling for Section I. When soil parameters meet a sufficient condition, the results from the deterministic analysis are viable in terms of the inputs, which are good enough to make the outputs reliable. The excavation of two parallel shallow tunnels for the BML1 is expected from *Portal de las Américas* to *Primera de Mayo* (*Section 1*). It includes six stations with a total length of 6 667 m, mainly passing through stiff clay.

Lining inputs were selected according to the assumed tunnel diameter of 6,5 m. Six-plate elements of 0,35 m in thickness were connected to simulate one ring. Table 5 shows the properties of the segmental lining used for this model. The simulation in PLAXIS2D also allows for a staged construction mode by defining different calculation phases. In addition, time-dependent deformations can be calculated during consolidation. The calculation phases for this study were:

- *Phase 0*. Initial phase
- *Phase 1*. Excavation of the first tunnel (left side, referred to as LT) and lining installation.
- *Phase 2*. Excavation of the second tunnel (right side, referred to as RT) and lining installation.
- *Phase 3*. Consolidation analysis up to 365 days.

Table 5. Properties of tunnel lining

Property	Value	Unit
Thickness	0,35	m
Weight	8,40	kN/m/m
Flexural rigidity	1,43E5	kNm²/m
Normal stiffness	1,4E7	kN/m
Poisson ratio	0,15	-

Source: Authors

Results and discussion

Data obtained from the statistical analysis

The results obtained are of great value, not only for this research, but also for future studies on the behavior of Bogotá's soil. The values obtained to build the stratigraphic column of Section 1 (Table 6) were compared with data gathered from other projects in order to verify their reliability. These values were used as soil layer inputs of the numerical model (Figure 6).

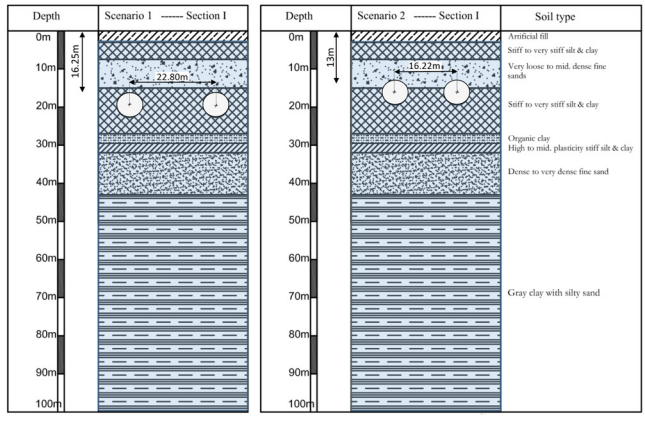

Figure 6. Illustration of modeling condition for Scenarios 1 and 2
Source: Authors.

Table 6. Soil parameters along Section I of the alignment

No.	Name of soil	Thickness [m]	Unit weight [kN/m3]	Modulus of deformation	μ Poisson ratio	Cohesion [kPa]	Angle of internal friction [º]
1	*Artificial fill*	3	17,64	18,24	0,1	0	25,00
2	*Stiff to very stiff silts and clays*	4,5	20,18	33,05	0,4	2	20,25
3	*Very loose to mid. dense fine sands*	7,5	18,14	52,26	0,3	0	33,00
4	*Stiff to very stiff silts and clays*	12	20,18	33,05	0,4	2	20,25
5	*Organic silt clay*	2,5	14,01	6,85	0,4	7	10,00
6	*High to mid. plasticity stiff silts and clays*	2,5	18,63	0,83	0,4	15	0,59
7	*Dense to very dense find sands*	11	19,5	97,27	0,3	0	33,47
8	*Grey clay with silty sands*	7,5	20,18	82,24	0,4	6	16,11

Source: Authors.

Numerical analysis

The soil values obtained were entered in the model, and the geometry of the mesh was built. The water table remains at -3 m (being the surface at 0 m) in both scenarios for Section I of the alignment. The geometry of the mesh also remains the same; only the position of the tunnel in the x- and y-directions changes for each scenario (Figure 7).

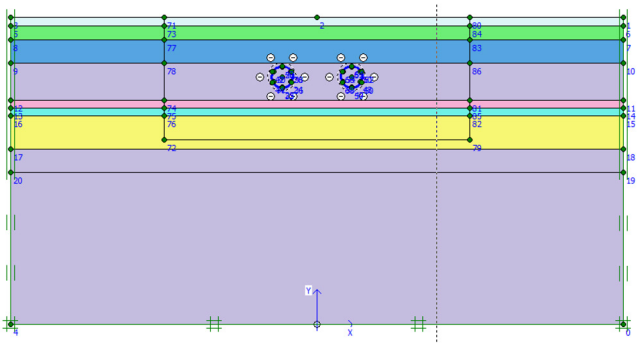

Figure 7. Mesh geometry and boundary conditions (Scenario 1)
Source: Authors

Vertical displacements: In the first scenario, the maximum surface settlement induced by the excavation of the two parallel tunnels is 8,96 mm. The excavation of the RT is expected to start once the construction of the LT has finished. Therefore, the immediate displacements will have already occurred, and they will have no influence on the excavation of the RT. The cumulative surface settlements induced by the excavation of both tunnels for Scenario 1 is estimated to be 8,96 mm. The heave of the surface is estimated to happen with a maximum value of 0,29 mm in a range of 40-50 m away from the tunnel axis in the x-direction (Figures 8 and 9).

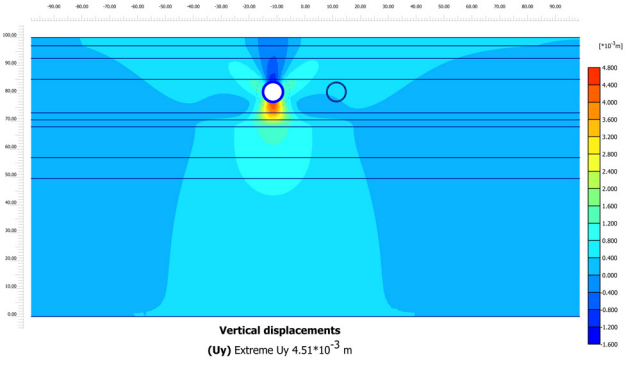

Figure 8. Vertical displacements induced by tunneling (Scenario 1 – Phase 1)
Source: Authors

The same procedure and assumptions were applied for Scenario 2. The maximum surface settlement estimated by the excavation of the two tunnels was 7,87 mm. The heave of the surface is a common phenomenon during tunneling, which is due to the stresses released from excavation. In this scenario, the maximum heave is greater than the one in Scenario 1, with a value of 0,53 mm. The soil moves upwards in a range of 0-40 m from side to side from the middle point of each tunnel, which, in the model, corresponds to the coordinates (x=0, y=100) (Figures 10 and 11).

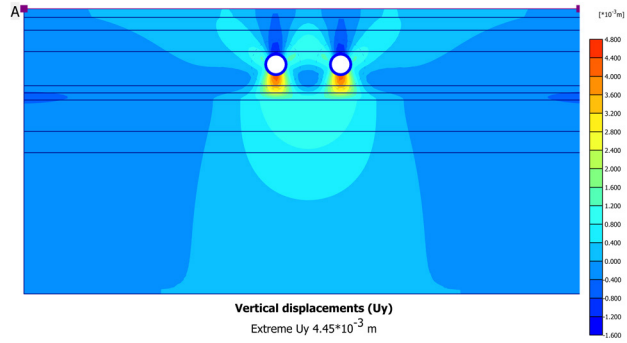

Figure 9. Vertical displacements induced by tunneling (Scenario 1 – Phase 2)
Source: Authors

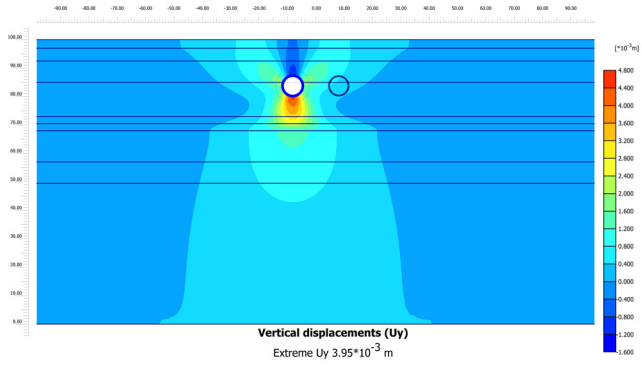

Figure 10. Vertical displacements induced by tunneling (Scenario 2 – Phase 1)
Source: Authors

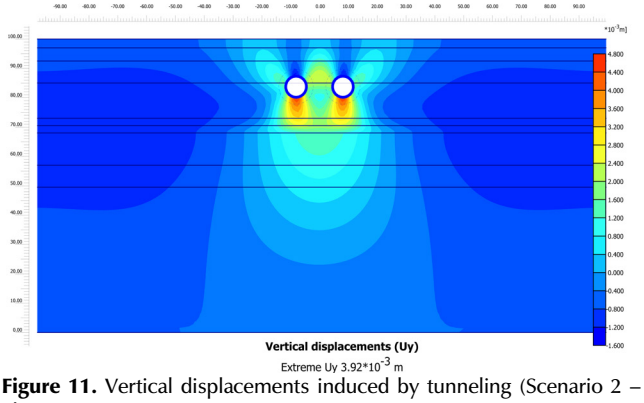

Figure 11. Vertical displacements induced by tunneling (Scenario 2 – Phase 2)
Source: Authors

Consolidation analysis: A consolidation analysis was performed (Phase 3) to evaluate the development or dissipation of pore pressures as a time function. This elastoplastic consolidation analysis was made possible by the features of PLAXIS2D. The maximum vertical displacement for Scenario 1 was 3,16 mm whereas the maximum value for Scenario 2 was 172,68 mm (Figure 12b).

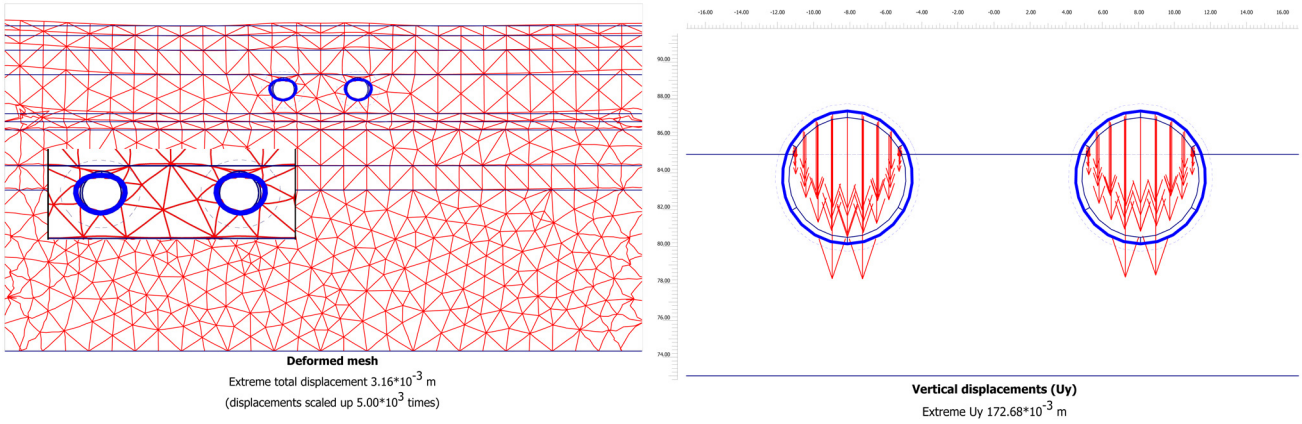

Figure 12. Consolidation analysis: a) deformed mesh for Scenario 1, and b) vertical displacements for Scenario 2
Source: Authors

Discussion

Surface settlements: The results show that the excavation depth of tunnels affects the deformation of the soil (Table 7). The heterogeneity of the subsurface plays a key role in the primary and secondary consolidation, so the behaviour of soils shall be carefully studied to choose an appropriate excavation depth. For example, in Scenario 1, the immediate settlements are slightly higher than those of Scenario 2, but the estimated secondary consolidation is significantly smaller than that of Scenario 2. This could be explained by the characteristics of the crossing layers: soft soils have low hydraulic conductivity, which means that consolidation processes in sands happen much faster than in clays.

Table 7. Surface settlements induced by excavation of metro tunnels for the BML1.

Scenario	Phase 1	Phase 2	Phase 3
1 (at -16,25 m)	4,51 mm	4,45 mm	3,16 mm
Cumulative settlements	4,51 mm	8,96 mm	***12,12 mm***
2 (at -13 m)	3,95 mm	3,92 mm	172,68 mm
Cumulative settlements	3,95 mm	7, 87 mm	***180,55 mm***

Source: Authors

Secondary consolidation: Although the consolidation values for Scenario 1 are lower, it is important to acknowledge that consolidation in clays will continue to happen over a long period. Secondary consolidation would mainly affect the settlement of the tunnel structure. Liao *et al*. (2011) and Cui *et al*. (2015) studied the cumulative settlement of Shanghai's Metro Line 1 during the 1995-2009 period. The maximum and minimum cumulative settlements were 287,8 mm and 5,8 mm, respectively, according to *in-situ* monitoring data of the Metro Line 1 in Shanghai (Cui *et al*., 2015). It is worth mentioning that the maximum allowed settlement value for construction of underground metro lines in Shanghai is 20 mm. There, the subsoil can also be characterized as low strength soft soil with friction angles in the range of 8,5-16,9°. Numerical analysis showed cumulative settlements lower than 10 mm induced by the excavation of two parallel tunnels at different depths and tunnel clearance. Thus, shield tunneling in Bogotá soil is viable.

Grant and Taylor (2000), Wilson *et al*. (2011), and Sahoo and Bibhash (2019) numerically and experimentally studied the support pressure of circular tunnels in cohesive soils and the effect of an overlying sand layers on the stability of tunnel excavation in the lower clay layer, as it is the case of the BML1. These studies can be used to decide the thickness and stiffness of the lining required to support the surrounding soil for the BML1.

Forces acting on the lining: The performance of the lining is considered as a whole system, whose ultimate goal is to provide an overall stability of the opening. As for the tunnels excavated in soft ground by shield machines, segmental lining should maintain the structural integrity of the excavation opening as the shield moves forward and minimize the immediate movement of the surrounding ground. Larger forces are expected to act on the lining for Scenario 1 because the overburden pressure is higher. These values can be considered for reference by engineers in order to determine the future design of the segmental lining of Bogotá's metro (Figures 13, 14, and 15).

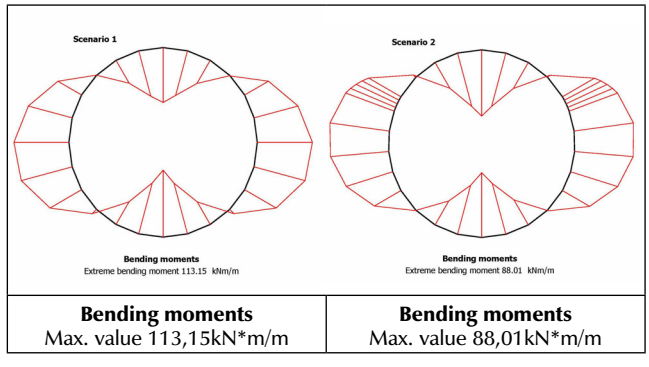

Figure 13. Lining bending moments for Scenarios 1 and 2
Source: Authors

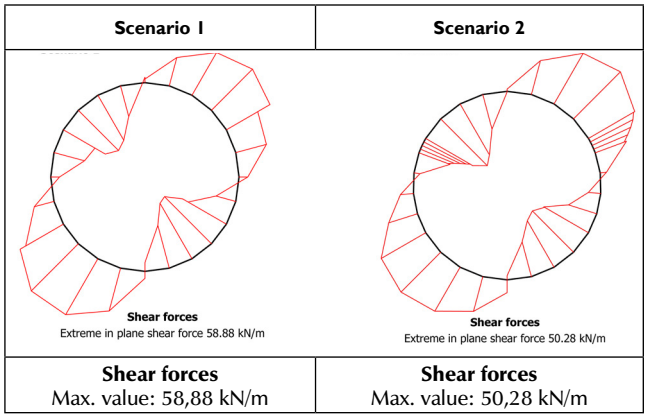

Figure 14. Lining shear forces for Scenarios 1 and 2
Source: Authors

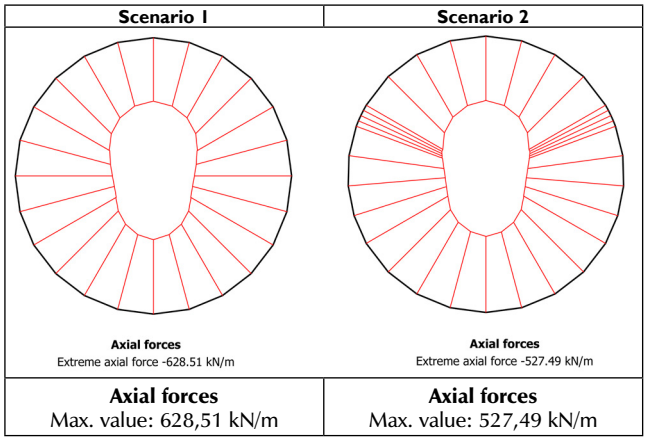

Figure 15. Axial forces acting on the lining for Scenarios 1 and 2
Source: Authors

Conclusions

The application of statistical analysis to define the soil characteristics of Bogotá's subsoil gave green light for the numerical analysis to estimate settlements induced by tunneling. An extensive analysis was performed to make use of the laboratory and *in situ* test results obtained in 2014, which resulted in the stratigraphic profile of the BML1's first 6,6 km. The numerical analysis showed cumulative settlements lower than 10 mm induced by the excavation of two parallel tunnels at different depths and tunnel clearance. Thus, shield tunneling in Bogotá soil is viable. As in Shanghai, the consolidation phenomenon shall be considered by the contractors of future metro tunnels in Bogotá, with sufficient long-term monitoring of settlements. Throughout the course of this research, the authors found valuable technical facts that can be used for future metro projects in Bogotá, Colombia.

Acknowledgements

The authors are grateful to the Statistics and the Civil Engineering Department of USTA University (Colombia) and the Tongji University's College of Civil Engineering for their financial support on the software needed to conduct this analysis. Thanks are owed to Germán Pardo for providing information, to Steven Zhou for proofreading this paper, and to the Colombian Institute of Urban Development (IDU) and Empresa Metro de Bogotá for making the data available for public use.

CRediT author statement

All authors: Conceptualization, methodology, validation, formal analysis, investigation, writing (original draft preparation, review, and editing), data curation, supervision, project administration, resources, and funding acquisition.

References

Alcaldía Mayor de Bogotá (2010). *Zonificación de la respuesta sísmica de Bogotá para el diseño sismo resistente de edificaciones*. https://www.idiger.gov.co/documents/20182/112614/Zonificacion_Respuesta_Sismica-FOPAE-2010.pdf

Béjui, H., and Guilloux, H. (1989). Recent soft ground tunneling techniques. Ecole Nationale des Ponts et Chaussées (Eds.), *Proceedings of the International Conference on Tunnels and micro-tunnels in Soft Ground: From field to theory* (pp. 475-502). Ecole Nationale des Ponts et Chaussées.

Cebr (2014). *50% rise in gridlock costs by 2030*. https://cebr.com/reports/the-future-economic-and-environmental-costs-of-gridlock/

Clough, G. W., and Leca, E. (1993). EPB shield tunneling in mixed face conditions. *ASCE Journal of Geotechnical Engineering, 119*(10), 1640-1656. https://doi.org/10.1061/(ASCE)0733-9410(1993)119:10(1640)

Consorcio L1 (2015). *Producto 2 – Estudio geotécnico base: diseño para la primera línea de metro en el marco del sistema integrado de transporte publico –SITP– para la ciudad de Bogotá*. Metro de Bogotá. https://www.metrodebogota.gov.co/sites/default/files/documentos/Resumen%20Ejecutivo%20Primera%20L%23U00ednea%20Metro%20de%20Bogot%23U00e1.pdf

Contraloría de Bogotá (2019). *Primera línea de metro para Bogotá –PLMB– efectos en las finanzas del Distrito Capital* (PAE 2019). Dirección de estudios de Economía y Política Pública.

Cui, ZD., Tan, J. (2015). Analysis of long-term settlements of Shanghai Subway Line 1 based on the in-situ monitoring data. Nat Hazards 75, 465–472. https://doi.org/10.1007/s11069-014-1331-0

DANE (2020). *La información del DANE en la toma de decisiones de las ciudades capitales, Feb. 2020*. https://www.dane.gov.co/files/investigaciones/planes-departamentos-ciudades/210203-InfoDane-Bogota.pdf

Ding, L. Y., and Xu, J. (2017). A review of metro construction in China: Organization, market, cost, safety and schedule. *Frontiers of Engineering Management, 4(1), 4-19*. https://doi.org/10.15302/J-FEM-2017015

Fenalco (2014). *Bitácora económica*. http://www.fenalco.com.co/node/1347

Fujita, K. (1989). Underground construction, tunnel, underground transportation. *Proceedings of the 12th International Conference on Soil Mechanics and Foundation Engineering, 4*, 2159-2176. https://www.issmge.org/uploads/publications/1/33/1989_04_0002.pdf

Grant, R. J., and Taylor, R. N. (2000, November 19-24). *Stability of tunnels in clay with over- lying layers of coarse-grained soil* [Conference presentation]. ISRM International Symposium Lancaster, PA, USA. https://onepetro.org/ISRMIS/proceedings/IS00/All-IS00/ISRM-IS-2000-581/50627

IDU (2013). *Instituto de desarrollo urbano, transparencia, informacion de interés, datos abiertos*. http://opendata.idu.gov.co

ITA Working Group 13 (ITA-WG13) (2004). Underground or aboveground? Making the choice for urban mass transit systems. 'Direct and indirect advantages of underground structures'. *Tunneling and Underground Space Technology, 19*(1), 3-28. https://doi.org/10.1016/S0886-7798(03)00104-4

ITA (1988). Guidelines for the design of tunnels. *Tunneling and Underground Space Technology, 3*(3), 237-249. https://tunnel.ita-aites.org/media/k2/attachments/public/Tust_Vol_3_3_237-249.pdf

Melis-Maynar, M. (1998). Construcción de los túneles del FFCC del metro de Madrid en suelos blandos. *Ferroviaria '98: Congreso nacional de ingeniería ferroviaria, 1998*, 217-248. https://ruc.udc.es/dspace/bitstream/handle/2183/10634/CC%2041%20art%2022.pdf?sequence=1&isAllowed=y

Read T. and Kidd J. (2019). *INRIX 2018 Global Traffic Scorecard*. INRIX. https://inrix.com/scorecard/index.php/estadisticas-por-tema/demografia-y-poblacion/proyecciones-de-poblacion

Sahoo, J. P., and B. Kumar. (2019). Stability of circular tunnels in clay with an overlay of sands. *International Journal of Geomechanics, 2019, 19*(3), 06018039. https://doi.org/10.1061/(ASCE)GM.1943-5622.0001360

Sainea-Vargas, C. J., and Torres-Suárez, M.C. (2020). Assessing and updating damage probabilities for a deep excavation in Mexico City soft soils. *Indian Geotechnical Journal, 50,* 671-688). https://doi.org/10.1007/s40098-019-00405-2

S. M. F., Hossaini, M. Shaban, and A. Talebinejad. (2012). Relationship between twin tunnels distance and surface distance subsidence in soft ground of Tabriz-Metro Iran. In University of Wollongong (Eds.), *12th Coal operators' Conference* (pp. 163-168). University of Wollongong, Australasian Institute of Mining and Metallurgy. https://ro.uow.edu.au/cgi/viewcontent.cgi?article=2064&context=coal&httpsredir=1&referer=

Liao, S. M., Shen, M. l., Zhou, L., Shao W. (2011, March 13-16). *In-situ experimental study on SDC grouting in Shanghai saturated soft clay* [Conference presentation]. Geo-Frontiers 2011, Dallas TX, USA. https://ascelibrary.org/doi/10.1061/41165%28397%29256

Wilson, D. W., Abbo, A. J., Sloan, S. W., and Lyamin, A. V. (2011). Undrained stability of a circular tunnel where the shear strength increases linearly with depth. *Canadian Geotechnical Journal, 48*(9), 1328-1342. https://doi.org/10.1139/t11-041

Research Article/Civil and Sanitary Engineering https://doi.org/10.15446/ing.investig.91603

Urban Road Network Serviceability Analysis Using Traffic Flow Profiles

Análisis de la capacidad de servicio de la red de carreteras urbanas mediante perfiles de flujo de tráfico

Sasmita Mallick[1] and Gopikrishnan T.[2]

ABSTRACT

Urban road networks are lifelines for cities in fulfilling the transportation needs of their inhabitants. The Patna Urban Agglomeration Area (PUAA) lacks properly planned roads; many of them have varying widths, with encroachments that reduce effective road width. A serviceability analysis is required through a traffic survey in order to create a traffic flow profile. This profile aids in performing time-based path, elevation, and serviceability analyses. In this study, traffic data were collected using cameras at vital road junctions and signals. A manual traffic survey was conducted at locations where active traffic was observed during peak hours. The road network of the study area was created using Google Maps, digitizing roads as lines and utilities as points. The traffic survey data, the road network, and the utilities were analyzed in the Network Analyst tool of the ArcGIS software. The analyses revealed suitable routing at underpass and overpass, as well as feasible paths during peak hours and locations with poor utility access. The analysis focused on the low-income group of people who depend on public transport and utilities and are the driving force of a developing economy. Suitable solutions are suggested to improve the existing road network.

Keywords: road network, utilities, path analysis, serviceability analysis

RESUMEN

Las redes de carreteras urbanas son líneas vitales en las ciudades para satisfacer las necesidades de transporte de sus habitantes. El Área de Aglomeración Urbana de Patna (PUAA) carece de carreteras debidamente planificadas; muchas tienen anchos variables con invasiones que reducen el ancho efectivo del camino. Se requiere un análisis de capacidad de servicio a través de una encuesta de tráfico para crear un perfil de flujo de tráfico. Este perfil ayuda a realizar análisis de ruta, elevación y capacidad de servicio en función del tiempo. En este estudio, los datos de tráfico se recolectaron usando una cámara en cruces de carreteras y señales vitales. Se llevó a cabo un estudio de tráfico manual en lugares donde solo se observó tráfico activo en horas pico. La red de carreteras del área de estudio se creó usando Google Maps, digitalizando las carreteras como líneas y los servicios públicos como puntos. Los datos de la encuesta de tráfico, la red de carreteras y los servicios públicos se analizaron con la herramienta Network Analyst del software ArcGIS. Los resultados revelaron rutas adecuadas en el paso subterráneo y elevado, así como rutas factibles durante horas pico y las ubicaciones con acceso deficiente a los servicios públicos. El análisis se centra en el grupo de personas de bajos ingresos que dependen del transporte y los servicios públicos y son la fuerza que impulsa una economía en desarrollo. Se sugieren soluciones adecuadas para mejorar la red vial existente.

Palabras clave: red de carreteras, servicios públicos, análisis de ruta, análisis de capacidad de servicio

Received: November 17th, 2020
Accepted: November 22th, 2022

Introduction

A road connects a minimum of two places on land. It allows people to travel from one location to another and aids in the transportation of commodities. A road network is a system of interconnected paths that facilitate the movement of vehicles or pedestrians from one location to another (Olawale and Adesina, 2013). The road network through transportation impacts the socioeconomic value of a country (Blackwall, 1906). The road network in a city connects all of the utilities in it. A utility is a service area that provides benefits to people (Li and Lai, 2019). It could be an educational institution, a bank, an ATM, a hotel, a restaurant, a police station, *etc*. The people in the city use the road network to reach their utilities (Ayo-Odifiri *et al*. 2017).

According to the literature, the public transport system of the bus network in Ho Chi Minh City was analyzed using topological and temporal analysis, indicating that the latter better addressed the heterogeneity of public transport issues

[1] MTech Transportation Engineering, Department of Civil Engineering, National Institute of Technology Patna, Patna – 800005, Bihar, India. Email: sasmita.tina.23@gmail.com

[2] PhD in GIS and Remote Sensing, Anna University, India. Affiliation: Assistant Professor, Department of Civil Engineering, National Institute of Technology Patna, Patna – 800005, Bihar, India * Corresponding author: Gopikrishnan T, gktphd@gmail.com

How to cite: Mallick, S., and Gopikrishnan, T. (2023). Urban Road Network Serviceability Analysis Using Traffic Flow Profiles. *Ingeniería e Investigación, 43*(2), e91603. https://doi.org/10.15446/ing.investig.91603

than topological network analysis (Huynh and Barthelemy, 2021). The Analytic Hierarchy Process (AHP) method was used to analyze the transport mode selection in the city of Vienna, for which the students of Vienna University (Economics and Business specialization) were used as the target audience. The collected data were processed to identify preference rates based on subjective factors that fulfill objective ones. The results proved useful for planning the city's transport network (Šinko *et al*., 2021). General Transit Feed Specification data was used for a comparative analysis of the para-transit transport service network between seven African cities. A network analysis of the nearest para- and public transit was carried out regarding accessibility, frequency, and network coverage. The study also revealed the transport inequality and segregation of urban areas, and it indicated the need to understand the transport differences and dynamics in a developing country (Falchetta *et al*., 2021). Rapid urbanization in developing nations results in inadvertent and perplexing scenarios where urban works are not controlled by master plans. The road network is directly correlated with population growth, and population density is correlated with road and area density. The results highlighted the insufficiency of current systems, highlighting the need for the proposal of a hybrid transit system (Maity *et al*., 2021).

In this study, the network analysis tool of ArcGIS is used to determine the serviceability of utilities, perform elevation analysis, and establish the shortest and quickest paths. The traffic survey data used for the analysis of this study were collected from the people living in the study area (*i.e.*, the Patna Urban Agglomeration Area), as well as from daily commuters. The advantage of these data is that they can be used for immediate transport planning and in the near future. Thus, traffic and transport projections will be more reliable than conventional data sources for the study area (Khahro *et al*., 2019).

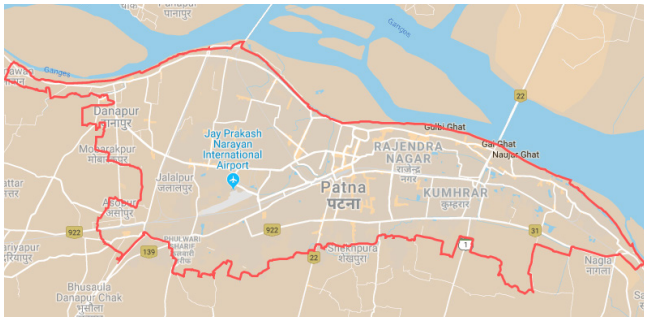

Figure 1. Study area: Patna Urban Agglomeration Area, Bihar, India
Source: Authors, base image from Google maps

The study area corresponds to the Patna Urban Agglomeration Area (PUAA), which comprises the Patna Municipality Corporation (PMC), Danapur, Khagaul, and Phulwari Sharif. Patna is one of the most populated cities in the Indian state of Bihar. Most of the uncontrolled and unplanned urban development takes place in the PUAA, which also direly needs road network and utility analysis. This study area is shown in Figure 1, with a red boundary line. The state of Bihar is lagging behind other states in India with regard to urban planning. The capital city of Patna is facing intense uncontrolled and unplanned urban growth, where the master plan of the city has no effect. The urbanization rate increased from 9,59% in 1981 to 11,29% in 2011. This, in comparison with 22,89 and 31,16% for the entire nation during the same years. Urbanization has had a delayed effect in the state of Bihar. The developments are out of schedule, according to the Patna master plan. Urban transport is negligible in the state and serves only up to 22% of the population. Patna has the lowest public transport accessibility index among the 30 traffic survey cities. About 11% of the population lives in slums, where roads, sanitation facilities, and infrastructure such as the electricity and water supply are poor or even absent. There are 259 places that are recorded as slums, and there are several places that remain unrecorded. Rural poverty has declined, and urban poverty has increased due to the migration of the population towards urban centers. The lag of urban planning further deteriorated the urban settlements' infrastructure (Pandey 2021).

The state of Bihar failed to develop after India's independence from the British in 1947. The causes for this are multitudes of issues. A few noteworthy issues are political instability because of the coalition government and schismatic politics relying on ethnic, caste, and class divisions (Rasul and Sharma, 2014). The majority of the people migrating to Patna come from agrarian societies with low literacy rates. These people serve as the service industry labor force and are classified as low-income groups. Blue-collar workers such as share autorickshaw drivers, bike taxi drivers, delivery boys for couriers, online sellers, plumbers, electricians, air conditioner mechanics, and carpenters are included in this low-income group.

In light of the above, road network analysis will aid in the development of the low-income group and, indirectly, in the country's economic development. The inducing factors for migration into the study area are the need for education, exam coaching, and medical facilities, as well as a lack of jobs in other districts of Bihar. There is a population outburst in the study area because of this. The infrastructure (*i.e.*, roads, water supply, electricity, and sewage networks) has become meagre to support the growing population, which directly impacts the traffic conditions of the study area (Papageorgiou *et al*., 2003). The roads are becoming narrower every day because of the many roadside shops. The roads are clogged with vehicles during peak hours (Al-Mamun and Paul, 2018), and the number of traffic miscreants is perpetually increasing. The increasing number of auto rickshaws and e-rickshaws adds ardent to the traffic turmoil. The vigilant traffic police officers scuffle to maintain traffic discipline. Therefore, in this study, an analysis of the study area is carried out. The major problems of said area are identified, and amicable solutions to these problems are provided. All roads in the study area, as well as crucial utilities, are taken into consideration. As a contribution, people will be able to make more informed decisions if

they are aware of the locations of critical utilities (Emerink *et al.*, 1995). These decisions will enable people to reach their destination on time (Boyce, 1988), thus spending less time and money on visiting their destinations (Kumar *et al.*, 2005). This road network analysis will allow low-income group workers to select the optimal path to carry out their services to society, and it will aid in the socioeconomic development of the study area. Google Maps was used to collect data for the study area's road network and utilities, which was then cross-checked with real-world entities. The data were processed in the Network Analyst tool of the ArcGIS software.

Methodology

The study area was selected based on the existing traffic issues. The data for the study area were collected and processed through digitization. The adopted methodology is presented in this section and depicted in Figure 2. The digitized lines and points were used to create a road network dataset. This dataset was used to determine the shortest and quickest paths, to conduct an elevation analysis, and to assess the serviceability of utilities.

Road network preparation: Road network and utility maps were created using Google maps. The roads were digitized as lines on Google maps (the roads were absent in a few locations). These locations were circumspectly analyzed for ground truth verification (Hai et al., 1993). The digitized road network and utilities are shown in Figure 3. Routine and crucial utilities such as educational institutions, government offices, hospitals, banks, ATMs, petrol pumps, market areas, police stations, hotels, and restaurants were digitized as points.

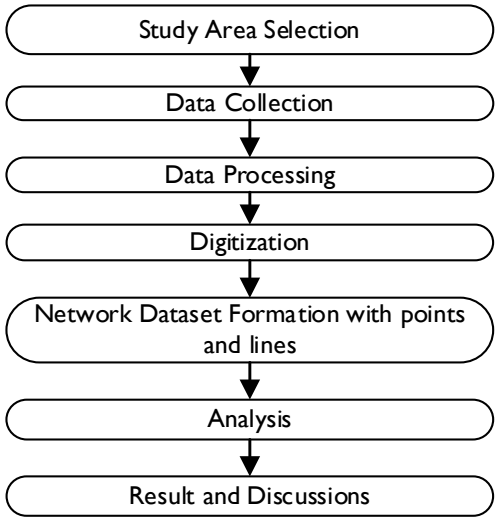

Figure 2. Flow diagram of the adopted methodology
Source: Authors

A new map was created for the study area, which included roads and utility points. The digitized data were in the KML format. The KML file was converted into a layer format file in ArcGIS. The data processing procedure is presented below.

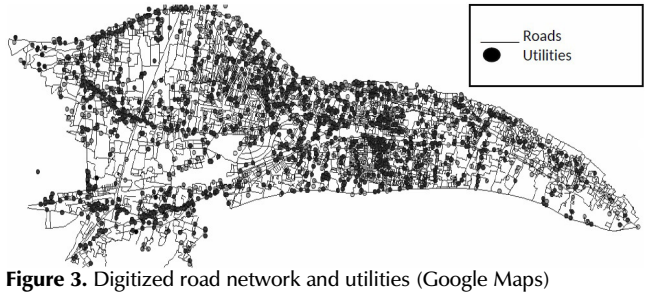

Figure 3. Digitized road network and utilities (Google Maps)
Source: Authors

Network dataset: Network datasets are fundamental need for modelling transport network analysis. The network datasets are formed using features like points, lines and turns. The turns are entities that store turning restrictions in a network junctions. The network analysis will be executed in the network dataset in ArcGIS. The network datasets manages the network analysis by abiding the network rules such as one-way, overpasses or tunnels, turns and restrictions. The relationship between the intersections, junctions, nodes, point and lines in a network are stored as network policies. Through the network policies the network analysis in a network dataset can be executed. Therefore, the road network, utilities, turns, intersections, junctions, overpasses and tunnels or underpasses details in the study area are created in the network dataset and used for road network analysis. This step is explained in the Figure 2.

Road network data processing: All analyses were carried out using the network dataset. A new database was created with lines and points that were converted via ArcGIS, where a new network dataset was created. The modifications considered while building the dataset are presented below:

1) All roads were given names based on their geographical location. These roads were classified into three categories based on the importance of the roads: primary roads, secondary roads, and tertiary roads. All national highways (NH), state highways (SH), and major roads were added to the primary road category. Other district roads and important roads were considered secondary, and the remaining streets and lanes were classified as tertiary roads.

2) The roads were assigned a specific speed limit based on their classification. These speed limits were tested during the traffic survey. The drive time was calculated for each road between one junction and another. The speed factor (*i.e.*, the relative speed of a vehicle when compared to its actual observed speed) was calculated based on the observations made during traffic surveys. The actual observed speed is the free flow speed, and it must not exceed the predefined speed limit of the roads. This factor was crucial in identifying vehicle speed with respect to time; as the time of day varies, so does the traffic speed with respect to traffic volume (Falcocchio *et al.*, 2015). Figure 4 shows a graph of the time of day *vs.* the speed factor.

3) In the study area, one-way and two-way roads were digitized and processed for road network analysis.

4) Turn features were added to the city's major intersections. This facilitates the movement of traffic with a cost impedance (*i.e.*, time). When a person is willing to travel across a major junction, the impedance of time will be applied to the person's travel time. Travelling via junctions will cost comparatively more time than other routes. This intersection optimization was discussed by Zhang (2019).

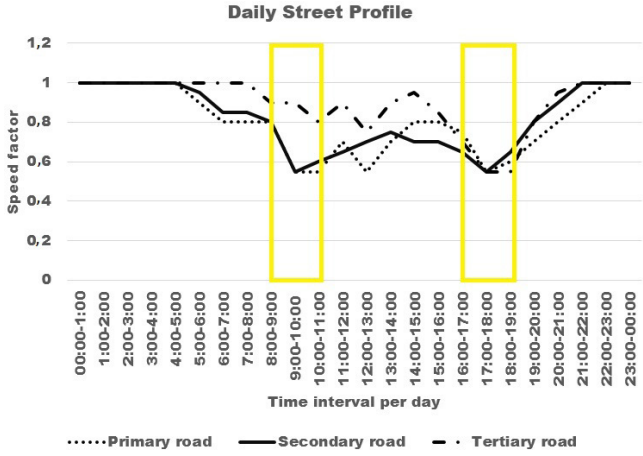

Figure 4. Time of day *vs.* speed factor
Source: Authors

Figure 4 shows how the low-speed factor changes with respect to the time of day. In this Figure, the y-axis represents the speed factor, and the x-axis represents 1 h intervals of the day. The primary, secondary, and tertiary roads are plotted in this graph. The traffic survey data were collected through cameras fitted at the road junctions and traffic signals. The data for secondary and tertiary roads were collected through field surveys at peak hours. The traffic peak hours in the morning of the study area were 8:00 am to 11:00 am and 4:00 pm to 7:00 pm. The peak hour time slots are highlighted in yellow in Figure 4. This time is suitable to collect traffic because the traffic volume remains challenging for traffic management. Peak hour traffic tends to increase in a developing nation with respect to its development and population migration (Droj *et al.*, 2021).

5) There are overpasses and underpasses in the study area. The road network is created in such a way that the overpasses and underpasses connect to the road network at the proper elevation. To restrict movement from two different elevations, overpass and underpass data were processed to represent elevation differences.

6) Two tables were created, namely daily_profile and street_daily_profile. The first table shows the drive time for all roads with an hourly value, and the second table presents the traffic profile for different days of the week. The street_daily_profile was used as a historical traffic database for carrying out road network analysis. Profiling took place for seven days a week, with profiles 1 and 7 representing the weekend. The aforesaid data and tables were used in the creation of a road network dataset, which is described below.

Road network and utility analysis

All analyses, which focused on the paths and serviceability of utilities, were carried out using an extension called *Network Analyst* in ArcGIS.

Path and elevation analysis

The path analysis aimed to determine the shortest and quickest paths, providing the travel directions, distance, and time (Weiping and Chi, 1999). The study area has traffic profiles for weekdays and weekends, which may change according to the time of day. Traffic profiles, associated with the speed factor, influence the travel time. If the time of day for travelling changes, the quickest path is also subject to change, but the shortest path remains the same for all traffic profiles. Note that this shortest path may be suitable for pedestrian travel. The quickest path tool finds a route based on travel time, which is calculated from the point of origin to the destination based on the traffic profiles (Zhang and Yi, 2012). Therefore, the quickest distance is not always the shortest distance. Figure 5 shows the routes calculated for the shortest (red) and the quickest path (black). Note that the latter must follow the overpass and underpass elevations of the road network. The overpasses in the study area are the flyovers that go over the road networks and railway lines. There are underpasses in the study area that go below the flyovers, where height restrictions are also imposed. The effectiveness of route guidance is briefly described by Bonsall (1992).

Figure 5. Shortest and quickest path analysis
Source: Authors

The variations in elevation for overpasses and the height restrictions in underpasses were marked and analyzed using the aforementioned extension of ArcGIS, and the performance of the road network dataset was analyzed regarding the serviceability areas of the utilities in the study area.

Serviceability of the study area

The *serviceable area* is the area that can be serviced by a utility within a specific time or distance. The total area of Patna is 136 km^2, which comprises the municipal area (around 99 km^2) and the suburban area (36 km^2). Most utilities are situated in the urban area, which implies more access for the inhabitants of urban areas. Consequently, people in suburban areas must travel a greater distance to access utilities (Talpur *et al.*, 2014).

The aforementioned serviceability analysis was carried out to show the accessibility efficiency of utilities to people in the study area. In the elaborated maps, the outputs showing points are utilities, and lines represent roads. The light grey color hatchings represent areas that can be reached in less time, and dark grey shows areas that require comparatively more time. Figure 6 shows the results of the bus stop serviceability analysis of the study area regarding the pedestrian travel mode. In this Figure, points show the geographical location of bus stops, and the lines show roads. Grey hatchings show areas within 10 minutes of walking time, and grey shade hatchings show areas within 15 minutes. From the results, it is clear that the city's bus stop distribution is not even, and it lacks connectivity through public transport services. Therefore, people use shared e-rickshaws, autorickshaws, and rickshaws for transportation, thereby increasing the traffic load on the road network. The low-income group uses public transportation more than the high- and middle-income groups combined. Market places are important for low-income people's daily work (AlKheder *et al*., 2022). The marketplace is not evenly distributed across the study area either; there are places without markets to promote economic activity (Talpur *et al*., 2016). Figure 7 shows the results obtained through the market-place pedestrian serviceability analysis.

Figure 8 shows the results of the police station pedestrian serviceability analysis. People in the low-income group are more vulnerable to crimes, which commonly include roadside robbery and petty crimes. Access to police stations for low-income groups is vital because they are active contributors to the developing economy. The results show that there are locations in the study area that lack quick access to these utilities. In light of the above, the police should provide frequent patrolling services in low-access areas, which involves setting up police booths, checkpoints, and virtual patrol webcams. Low-income workers play an essential role in a booming economy, because they spend more money than people in the high- and middle-income groups. The needs of low-income people are not fulfilled, and they will grow from one level of necessity to the next. When these workers have money, they will spend more on consumption. If the need for food is met, low-income people spend their money on clothes, travel, rent, and education. In a developing economy, spending on education is very high compared to any other expense. Therefore, spending by low-income groups will indirectly boost economic growth. This part of the population requires immediate access to utilities because they are major players in the service industry, given that, due to the global pandemic, high- and middle-income groups now prefer to shop online for

Figure 6. Pedestrian serviceability for bus stops
Source: Authors

Figure 7. Pedestrian serviceability for marketplaces
Source: Authors

Figure 8. Pedestrian serviceability for police stations
Source: Authors

groceries, medicines, and almost all other purchases. The need for the transport-based service industry is booming, as online selling giants are buying warehouses throughout their business venues.

Results and discussion

In this study, ArcGIS was used to analyze and solve traffic net-work-based transportation problems. The road network and utilities of the study area were digitized in Google Maps. These data were transferred to ArcGIS to create a road network dataset for carrying out road network analysis. This analysis was able to provide various routes based on traffic profiles obtained through a traffic survey of vehicles that travelled through the road network for a week. For the road network analysis, a suitable traffic profile was selected for the study area. Path and elevation analyses were carried out based on these traffic profiles. A serviceability analysis was also conducted to find easily accessible routes of utility that may benefit the low-income groups' economic growth. The study showed that geographical information systems (GIS) is a reliable tool in solving transportation network issues. Network analysis using ArcGIS was able to aid people by recommending the best route for travelling. This route-based knowledge will assist them in saving time and money. Moreover, ArcGIS showed the effective serviceability of different utilities in the study area, identifying zones with poor access to particular utilities. Based on this result, effective future utility planning can be carried out.

Conclusions

Developing nations struggle to cope with new requirements via old infrastructures. Urban road networks are one such example, and it affects the majority of the population. Traffic volume changes and population migration towards urban spaces cannot be limited, but abrupt changes in the traffic volume will be difficult to manage, resulting in accidents and traffic regulation issues. The employment of urban road network analysis using GIS eased the road traffic decision-making process. The elevation analysis identified the time-based traffic volume through the over- and underpass locations, which is essential for managing and diverting traffic in times of emergency, *e.g.*, rerouting services during accidents, road damage repair, and following security protocols in the study area. The path analysis provided the shortest and quickest routes, which is essential for emergency services such as ambulances and the time-based product delivery of perishable goods in the study area. The serviceability analysis indicated locations in the study area with poor access to utilities. The locations with poor access to infrastructure are mostly inhabited by low-income groups. Infrastructure planning, the provision of new amenities, increased patrolling, and the distribution of utilities can be easily carried out with the aid of this type of analysis. This study explored the possibilities and optimal solutions that may be implemented in the study area without causing major urban road network infrastructure changes (García-Luna-Aceves *et al.*, 1999). Furthermore, the study provided essential insights into the existing urban road network serviceability of utilities. Feasible suggestions are provided to improve these aspects with regard to low-income living areas. The adapted method proposed in this study provided amicable results for planning and managing urban traffic within the existing road infrastructure. The study of future urban space expansion will aid in the sustainable transport development of the study area.

Acknowledgements

The data for this study were obtained from the comprehensive mobility plan (CMP) for Patna. The project is funded by the state government of Bihar. The faculties of the National Institute of Technology Patna who took part in the project are Principal Investigator Prof. (Dr.) Sanjeev Sinha, Co-Principal Investigator Dr. Ranja Bandyopadhyaya, GIS Expert Dr. Gopkrishnan T., Planning Expert Dr. Subhajit Sadhukhan, and the CMP Team.

Author contributions

Gopikrishnan T. conceived the idea and conducted the background research. *Sasmita Mallick* collected the data, developed the workflow, and performed the assessment. *Gopikrishnan T.* supervised the research and provided critical feedback. *Sasmita Mallick* led the manuscript's writing process and wrote its main part, to which the other author contributed.

Conflicts of interest

The authors declare no conflict of interest.

Data availability

The data may be provided via email by the corresponding author for educational purposes, only with an authorization by the Principal Investigator of the project.

References

AlKheder, S., Abdullah, W., and Al Sayegh, H. (2022). GIS-based employment availabilities by mode of transport in Kuwait. *Applied Geomatics*, *14*(1), 1-15. https://doi.org/10.1007/s12518-021-00406-y

Al-Mamun, A., and Paul, S. K. (2018). Rural road network planning approaches in India: review of earlier works. *International Journal for Research in Applied Science and Engineering Technology, 6*(3), 1379-1387. https://doi.org/10.22214/ijraset.2018.3211

Ayo-Odifiri, O. S., Fasakin, J. O., and Henshaw, F. O. (2017). Road connectivity approach to eased traffic congestion on market roads in Benin metropolis, Nigeria. *American Journal of Engineering Research* (*AJER*), *6*(6), 41-48. https://www.ajer.org/papers/v6(06)/G06064148.pdf

Blackwall, J. (1906). Country roads for modern traffic. *Minutes of the Proceedings of the Institution of Civil Engineers*, *165*(1906), 8-14. https://www.amazon.in/Minutes-Proceedings-Institution-Civil-Engineers/dp/1273857585

Bonsall, P. (1992). The influence of route guidance advice on route choice in urban networks. *Transportation, 19*(1), 1-23. https://doi.org/10.1007/BF01130771

Boyce, D. E. (1988). Route guidance systems for improving urban travel and location choices. *Transportation Research Part A: General, 22*(4), 275-281. https://doi.org/10.1016/0191-2607(88)90005-2

Droj, G., Droj, L., and Badea, A. C. (2021). GIS-Based survey over the public transport strategy: An instrument for economic and sustainable urban traffic planning. *ISPRS International Journal of Geo-Information, 11*(1), 16. https://doi.org/10.3390/ijgi11010016

Emmerink, R. H., Axhausen, K. W., Nijkamp, P., and Rietveld, P. (1995). Effects of information in road transport networks with recurrent congestion. *Transportation*, 22(1), 21-53. http://worldcat.org/isbn/1840645555

Falchetta, G., Noussan, M., and Hammad, A. T. (2021). Comparing paratransit in seven major African cities: An accessibility and network analysis. *Journal of Transport Geography, 94*, 103131. https://doi.org/10.1016/j.jtrangeo.2021.103131

Falcocchio, J. C., and Levinson, H. S. (2015). *Road traffic congestion: a concise guide* (vol. 7). Springer. https://doi.org/10.1007/978-3-319-15165-6

García-Luna-Aceves, J. J., Vutukury, S., and Zaumen, W. T. (1999, June). A practical approach to minimizing delays in internet routing. *1999 IEEE International Conference on Communications*, *1*, 479-483). https://doi.org/10.1109/ICC.1999.767986

Hai, Y., Ryuichi, K., Paul P. J., Kenneth M. V., Mohamed A. A. (1993). Exploration of route choice behavior with advanced traveler information using neural network concepts, *Transportation*, 20, 2,199-223. http://worldcat.org/issn/00494488

Huynh, N., and Barthelemy, J. (2022). A comparative study of topological analysis and temporal network analysis of a public transport system. *International Journal of Transportation Science and Technology, 11*(2), 392-405. https://doi.org/10.1016/j.ijtst.2021.05.003

Khahro, S. H., Chandio, I. A., and Talpur, M. A. H. (2019). Data Preparation for GIS based Land Suitability Modelling: A Stepped Approach. *E3S Web of Conferences*, *101*, 02001. https://doi.org/10.1051/e3sconf/201910102001

Kumar, P., Singh, V., and Reddy, D. (2005). Advanced traveler information system for Hyderabad City. *IEEE Transactions on Intelligent Transportation Systems, 6*(1), 26-37. https://doi.org/10.1109/TITS.2004.838179

Li, J., and Lai, X. (2019). Modelling travellers' route choice behaviours with the concept of equivalent impedance. *Transportation, 46*(1), 233-262. https://doi.org/10.1007/s11116-017-9799-6

Maity, B., Mallick, S. K., and Rudra, S. (2021). Integration of urban expansion with hybrid road transport network development within Haldia Municipality, West Bengal. *The Egyptian Journal of Remote Sensing and Space Science, 24*(3), 471-483. https://doi.org/10.1016/j.ejrs.2020.10.005

Olawale, T. N., and Adesina, K. I. (2013). An assessment of the relationship between road network connectivity and tourists' patronage in Lokoja Metropolis, Kogi State. *Journal of Natural Sciences Research, 3*(9), 1-11. https://www.iiste.org/Journals/index.php/JNSR/article/view/7403

Pandey, M. K. (2021). *Bihar, in a State of Messy Urbanization-Way Forward*. https://iglus.org/bihar-in-a-state-of-messy-urbanization-way-forward/

Papageorgiou, M., Diakaki, C., Dinopoulou, V., Kotsialos, A., and Wang, Y. (2003). Review of road traffic control strategies. *Proceedings of the IEEE, 91*(12), 2043-2067. https://doi.org/10.1109/JPROC.2003.819610

Rasul, G., and Sharma, E. (2014). Understanding the poor economic performance of Bihar and Uttar Pradesh, India: A macro-perspective. *Regional Studies, Regional Science, 1*(1), 221-239. https://doi.org/10.1080/21681376.2014.943804

Šinko, S., Rupnik, B., Prah, K., and Kramberger, T. (2021). Spatial modelling of the transport mode choice: application on the Vienna transport network. *Transport, 36*(5), 386-394. https://doi.org/10.3846/transport.2021.16128

Talpur, M. A. H., Madzlan, N., Irfan, A., Chandio, I. A., and Hussain, S. (2014). Time-space geography: A creditable transport accessibility measure for rural dwellers. *Applied Mechanics and Materials, 567*, 763-768. https://doi.org/10.4028/www.scientific.net/AMM.567.763

Talpur, M. A. H., Chandio, I. A., Memon, I. A., Napiah, M., and Jafri, K. H. (2016). A brief review on the role of regional transport accessibility in the development process of distant sub-regions. *Indian Journal of Science and Technology, 9*(13), 1-9. https://doi.org/10.17485/ijst/2016/v9i13/62116

Weiping, H., and Chi, W. (1999). *Urban road network accessibility evaluation method based on GIS spatial analysis techniques*, [Joint International Conference on Theory, Data Handling and Modelling in GeoSpatial Information Science] ISPRS Archives – Volume XXXVIII - Part 2, 2010, Hong Kong. https://www.isprs.org/proceedings/xxxviii/part2

Zhang, H. (2019). Traffic organization optimization of urban road combined intersections. *Journal of Transportation Technologies, 9*(3), 325-330. https://doi.org/10.4236/jtts.2019.93020

Zhang, L., and Yi, J. (2012). Study the method of the optimum path based on GIS features. In Y. Wu (Eds.), *Software Engineering and Knowledge Engineering: Theory and Practice* (pp. 995-1001). Springer. https://doi.org/10.1007/978-3-642-03718-4

Research Article/Electrical,Electronic and Telecommunications Engineering https://doi.org/10.15446/ing.investig.102038

Comparison of Aluminum and Copper Winding Materials for Switched Reluctance Machines with Finite Element Analysis

Comparación de materiales de bobinado de aluminio y cobre para máquinas de reluctancia conmutada con análisis de elementos finitos

Cihan Sahin[1]

ABSTRACT

Today, with the decrease in fossil fuel reserves, interest in electric vehicles has grown. Undoubtedly, electric machines are one of the most important parts of electric vehicles. Studies on electrical machines directly affect vehicle performance. Since the electrical machine used is mounted on the vehicle, reducing the total weight without changing the output power will positively affect the overall performance of the vehicle. The windings used to create the magnetic field in electrical machines are made of copper. Electrical machinery manufacturers try to use completely different materials instead of copper or partially reduce its use. At this point, aluminum emerges as an attractive material for various manufacturers. This study analyzed the winding structure of a switched reluctance machine (SRM) proposed for an electric vehicle by using copper and aluminum at an equivalent resistance value, the results of which were compared. As a result of a 2D finite element analysis, it was observed that the machine's output performance is largely kept when aluminum is used instead of copper for the winding. It was also observed that the aluminum total winding weight decreased by 43,40% compared to that of copper.

Keywords: copper, aluminum, alloys, electrical resistivity

RESUMEN

Hoy, con la disminución de las reservas de combustibles fósiles, ha aumentado el interés por los vehículos eléctricos. Sin duda, las máquinas eléctricas son una de las partes más importantes de los vehículos eléctricos. Los estudios sobre máquinas eléctricas afectan directamente el rendimiento del vehículo. Dado que la máquina eléctrica utilizada está montada en el vehículo, la reducción del peso total sin cambiar la potencia de salida afecta positivamente el rendimiento general del vehículo. Los devanados utilizados para crear el campo magnético en las máquinas eléctricas están hechos de cobre. Los fabricantes de maquinaria eléctrica intentan utilizar materiales completamente diferentes en lugar del cobre o reducir su uso parcialmente. En este punto, el aluminio emerge como un material atractivo para varios fabricantes. En este estudio se analizó la estructura de bobinado de una máquina de reluctancia conmutada (SRM) propuesta para un vehículo eléctrico, utilizando cobre y aluminio con un valor de resistencia equivalente, cuyos resultados se compararon. Como resultado de un análisis de elementos finitos 2D, se observó que el rendimiento de salida de la máquina se mantiene en gran medida cuando se utiliza aluminio para bobinado en lugar de cobre. Se observó que el peso total del devanado de aluminio disminuyó en un 43,40 % en comparación con el de cobre.

Palabras clave: cobre, aluminio, aleaciones, resistividad eléctrica

Received: Abril 07th, 2022
Accepted: February 07th, 2023

Introduction

Developing technologies, increasing population, and growing industrialization have increased energy consumption and the amount of required energy (Ayaz *et al*., 2020). In addition, due to the gradual decrease in the use of fossil fuels and the damage they do to the environment, environmentally friendly practices have taken an important place in our lives. CO_2 emissions are regarded as the source of the most serious damages caused by fossil fuels to the environment. According to the reference values of 1990 under the Kyoto Protocol, the European Union (EU) aims to reduce its greenhouse gases (GHG) emissions by 80-95% as of 2050. Similarly, road, rail, sea, and air transport should contribute to this aim by reducing the 1990 emission levels by 60% as of 2050 (de Gennaro *et al*., 2019). In this context, electric vehicles (EV) are an effective solution to reduce CO_2 emissions (Cai and Zhao, 2021).

EVs, which constitute the best alternative for an environmentally friendly transportation vehicle, are also an ideal solution to the problems experienced regarding urban air quality (Hooftman *et al*., 2016). Especially in recent years, the production and development of electric or hybrid vehicles has been increasing due to energy and environmental issues (Jang *et al*., 2015). By using electric vehicles (EVs) or hybrid electric vehicles (HEVs) instead of conventional fuel vehicles, substantial reductions in

[1] Technical Sciences Vocational School, Manisa Celal Bayar University. Affiliation: Assistant professor, Manisa Celal Bayar University. E-mail: cihan.sahin@cbu.edu.tr

How to cite: Sahin, C. (2023). Comparison of aluminum and copper winding materials for switched reluctance machines with finite element análisis. *Ingeniería e Investigación, 43*(2), e102038. https://doi.org/10.15446/ing.investig.102038

carbon emissions will occur, and improvements in urban air quality will be achieved. This is also very important for reducing cases of respiratory diseases (de Gennaro *et al*., 2019).

Today, EVs, which have significant positive effects on the quality of life, consist of various parts, namely the electric machine, the battery group, the on-board charger, and the electric power control unit. Research and development (R&D) studies continue for all these parts in parallel with developing technologies. EV-related technologies such as electric motor drive design and selection, power converter topologies and control algorithms, and power supply and system configuration are under extensive development (Cai and Zhao, 2021). One of the common target points of these studies is minimal energy consumption. Within this framework, electrical machines are of great importance for EVs. There are many different studies in the literature in the field of electrical machines for EVs.

Electrical machines are also widely used in industrial applications (Jang *et al*., 2015). The use of copper (Cu) in windings, which are an important part of electrical machines, is common since this element is a good conductor (Ayaz *et al*., 2020). Cu is widely used, especially in the windings of high-performance electrical machines. This is due to a high electrical conductivity, enabling high current density machine designs that minimize DC winding losses (Widmer *et al*., 2016). In addition, the high strength and increased electrical conductivity of Cu alloys are highly desirable for many wire and cable applications (Islamgaliev *et al*., 2014).

Sullivan, in his study in 2007, stated that the prices of Cu would be both high and variable in the future, and, therefore, products with a large amount of Cu, such as power electronics and transformers, should be reassessed in terms of cost. He also indicated that it is not a preferred method to reduce the efficiency of the machine in order to increase the amount of Cu, and Cu windings can be completely removed by using Al windings (Sullivan, 2007). In this context, in recent years, Al materials have been used as an alternative for copper windings in transformers and electrical machines.

The most important reason for this is that Al materials have good conductivity and are abundant and cheap around the world (Hergul *et al*., 2020). In addition, the cost of an Al conductor of the same resistance and length is significantly lower than the cost of a Cu conductor. Al has a cost approximately 30% of copper per unit mass, or 10% per unit volume (Sullivan, 2007; Widmer *et al*., 2014, 2016). Furthermore, recycling is very important nowadays: while Al can be recycled with steel, Cu is a major pollutant in the steel recycling process (Widmer *et al*., 2014, 2016). This is one of the disadvantages of using Cu.

The weight of electrical machines is of great importance according to their use areas. A low mass is particularly important in the design of 'mobile' electric motors used in applications ranging from electric vehicles to electric aircraft (Widmer *et al*., 2014). At this point, Al is one step ahead of copper. Al has a mass density of 30% that of Cu. Therefore, it is an attractive conductor in applications where low mass is important (Widmer *et al*., 2014, 2016). The most important feature to be considered at this point is that the cross-sectional area of an Al conductor is 56% larger than that of Cu for the same current carrying capacity (Pryor *et al*., 2008). Therefore, the material cross-section conditions must be taken into account when selecting the material.

In this study, the winding structure of a SRM, which is one of the electrical machines that is preferred for EVs and will have an even more important place in the future, as it does not contain rare-earth magnets in its structure, was defined as Al and Cu, and transient analyses were carried out. As a result of the analysis, the performance of the machine and the weight of the winding were compared.

Switched reluctance machines (SRMs)

Conventional SRMs have one of the simplest structural configurations among electrical machines (Gupta *et al*., 2021). SRMs that do not have windings or magnets in the rotor have only stator windings. Rotor rotation and energy conversion take place according to the principle of minimum reluctance (Sahin *et al*., 2012; Sun *et al*., 2021). In other words, SRMs convert electrical energy into mechanical energy with reluctance force (Omaç *et al*., 2018).

SRMs are strong candidates for EV and HEV applications due to their simple structure, low cost, flexible control, strong environmental sustainability, high fault tolerance capability, and high starting torque (Cai and Zhao, 2021; Haque *et al*., 2021; Li *et al*., 2015; Wang and Li, 2020). In particular, their high fault tolerance capability enables SRMs to work reliably and efficiently in harsh environments, such as automotive and aviation applications (Haque *et al*., 2021). Compared to permanent magnet (PM) machines, SRMs are in a more advantageous position to be used in EVs due to these features (Li *et al*., 2015). PM machines are widely used for wind energy generation due to their high efficiency and high power density (Jiang *et al*., 2021).

Additionally, since SRMs use iron cores in magnetically fully saturated regions, they have a much higher power density when compared to other machines such as induction motors and brushless DC machines. Therefore, the machine size is much smaller than that of other machines (Yoon, 2020). This feature constitutes an advantage for the aviation and automotive sectors. In addition to all these advantages regarding SRMs, these electric machines have the ability to work for a long time under high temperature and high speed conditions (Gan *et al*., 2021). Figure 1a presents the sample model of a 6/4-pole SRM, and Figure 1b shows the machine phase windings.

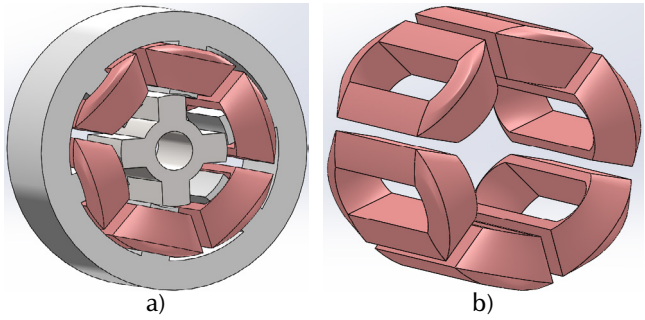

a) b)

Figure 1. a) Model of a 6/4 pole SRM; b) machine phase windings
Source: Authors

High-speed SRMs that face increasing power density requirements in diverse applications such as EV and HEV have a limited area to improve torque and power. The performance improvement of high speed SRMs is basically divided into two stages: the first is to increase the motor torque and the other is to improve the loss distribution. The most direct method of increasing the torque is to improve the winding structure and current density, given that, in high speed SRMs, only stator windings are energized. Therefore, windings are very important in SRMs.

Nowadays, flat copper wire, hairpin windings, and similar improved winding structures are used in various machine types (Chai *et al*., 2020). According to the winding structure to be applied to the machine, the selection of the material to be used is also important, as it directly affects machine losses. In addition, one of the important points to be considered in loss distributions is the control parameters of the machine. Control parameters directly affect the iron and Cu (winding) losses of the machine and therefore affect its efficiency (Yan *et al*., 2020).

Materials and method

The design of electrical machines is particularly challenging for electric or hybrid vehicle applications. In the design process, an optimization based on the evaluation of the different losses that occur in the machine is required for each operating point (Boumesbah *et al*., 2021). A high-performance SRM design, on the other hand, is usually handled in a two-step process. In the first stage, preliminary design analyses are carried out. At this stage, various options, such as stator/rotor pole combinations, inner and outer rotor topologies, winding configurations, and different materials, among others, are examined via finite element analysis (FEA). Thus, the proposed design options are compared to obtain a start-up design. In the second and final stage, optimization techniques such as a heuristic approach or a genetic algorithm are used (Rocca *et al*., 2020). This study involves the first stage of machine design. The winding configurations of the proposed SRM model were evaluated (Cu and Al) at equivalent resistance values, and FEA analyses were performed. The results obtained were compared, and a start-up model was proposed for the phase winding material. Coils for electrical machines are traditionally handmade components and are a limiting factor for machine operation. Studies on issues such as the fabrication and modulation of the coils are also an important step in production (Silbernagel *et al*., 2019).

Comparison of Al and Cu winding materials

One of the important components of an electrical machine is its windings, which consist of coils. Coils consist of wires made of conductive material surrounded by resistive insulating material. A conductive core is desired to have a low electrical resistance and minimize the Joule losses. These materials are generally copper, silver, gold, and aluminum. Table 1 presents the electrical resistance and density of metals and alloys commonly used in electricity at room temperature (Silbernagel *et al*., 2018).

Table 1. Metals and alloys commonly used in electrical applications

Main element	Electrical resistivity (μΩ-cm)	Density (g/cm^3)
Pure copper (Cu)	1,7241	8,94
Pure aluminum (Al)	2,6548	2,688
Aluminum 1350 (1350 Al, electrical alloy)	2,82	2,705
Pure silver (Ag)	1,586	10,492
Pure gold (Au)	2,192	19,37

Source: Silbernagel *et al.* (2018)

Among the elements and alloys given in Table 1, Cu and Al are the two most commonly used materials for conductors and bus bars in electrical equipment. The Cu used in electrical equipment has a pure 98% conductivity, according to the International Annealed Copper Standard (IACS) (Pryor *et al*., 2008). Pure Al, on the other hand, has good conductivity, but it is too soft to be processed for the manufacture of electrical wires (Pryor *et al*., 2008; Silbernagel *et al*., 2018). For this reason, 1350 Aluminum (1350 Al) alloy was developed for electrical purposes. The 1350 Al alloy is categorized as EC (Electrical Conductor) class aluminum, with 99,50% Al content. Although 1350 Al was developed for electrical purposes and has 61,2% the conductivity of Cu, it is still soft when compared to Cu in terms of mechanical properties (Pryor *et al*., 2008; Silbernagel *et al*., 2018).

In addition, in recent years, both automotive and electrotechnical applications require innovative materials that can be used to replace expensive and heavy Cu conductors. Therefore, there are transitions to complex, gradient, multiphase, and composite materials with tailored microstructures and properties for specific functionalities (Kunčická *et al*., 2022).

Metallic clad composites (MCCs), which typically consist of two or more separate components with different physical or chemical properties, show superior behavior and properties than the components used, given the combination of the components used. In the literature, there are various MCCs (*e.g.*, Al/Mg, Al/Ni, Al/Sn, Cu/Ni, Cu/Ti, Cu/Zr, Al/Cu/Mg,

Al/Cu/Sn, Al/Cu/Zn, Al/Cu/steel, Al/Ti/Mg, Al/Ti/Al, Cu/Al/Cu, *etc*.). However, the Al/Cu system is among the most popular, as it is very promising for both automotive and electrotechnical applications (Kunčická *et al*., 2022).

Since the electrical conductivity of Al windings is lower compared to those of Cu, the resistance value per unit winding length is higher, as shown in Equation (1) (Widmer *et al*., 2014, 2016).

$$\partial_R = \frac{R_{Al}}{R_{cu}} = \frac{\sigma_{Cu} S_{FF}^{Cu}}{\sigma_{Al} S_{FF}^{Al}} \cong 1,64 \frac{S_{FF}^{Cu}}{S_{FF}^{Al}} \quad (1)$$

where R is the resistance, σ is the electrical conductivity of the winding material, and S_{FF} is the slot fill factor. The electrical conductivities of Al and Cu at 20 °C are $\sigma_{Cu} = 58,0x10^6\ S/m$ and $\sigma_{Al} = 35,4x10^6\ S/m$ (Widmer *et al*., 2014, 2016).

Cu losses in a fixed area are calculated using the Ohmic DC (direct current) resistance (R_{DC}) and current (I), as given in Equation (2) (Schenk and de Doncker, 2013).

$$P_{DC} = R_{DC} * I^2 \quad (2)$$

In general, the total losses are calculated with the specific resistance (ρ) and the current density (j) as given in Equation (3) (Schenk and de Doncker, 2013).

$$P_{AC} = \iiint \rho J^2 dV \quad (3)$$

Additionally, Equation (3) can be rewritten as given in Equation (4) with an equivalent AC (alternating current) resistor (R_{AC}) according to Equation (2) (Schenk and de Doncker, 2013).

$$P_{AC} = R_{AC} * I^2 \quad (4)$$

As seen in Table 1, the electrical resistances and densities of Cu and Al are different. In order for their resistances to be equal, the expression in Equation (5) must be fulfilled.

$$\rho_{Cu} \frac{l_{cu}}{S_{cu}} = \rho_{Al} \frac{l_{Al}}{S_{Al}} \quad (5)$$

In Equation (5), ρ is the specific resistance (Ωm), l is the winding length (m), and S is the winding cross-section (m^2).

When the lengths, cross-section diameter, and specific weights of the conductors used in both winding models are substituted into Equation (6), the weight of the winding used for a pole is found. In Equation (6), d is the density (kg/dm^3), m is the weight (kg), and v is the volume (dm^3).

$$d = \frac{m}{v} \quad (6)$$

In addition to all these, when compared to Au and Ag, Cu is widely used in electrical components, given its low electrical resistance and average price balance (Silbernagel *et al*., 2019). However, Al is less costly than cu. Thus, it can carry more current per kilogram or dollar. With this feature, it provides great advantages in automotive and aviation applications, among others where weight and cost are important (Silbernagel *et al*., 2018). When the prices per kg of Al and Cu are compared, it is observed that, while aluminum was $2,35/kg in 2021, Cu was $9,04/kg (London Metal Exchange, n.d.).

The thermal conductivities of Al and Cu are $387,7 Wm^{-1}K^{-1}$ and $230 Wm^{-1}K^{-1}$, respectively. The ratio for their thermal conductivities is given in Equation (7) (Widmer *et al*., 2016).

$$\partial_k = \frac{\lambda_{Al}}{\lambda_{cu}} \cong 0,593 \quad (7)$$

They Al and Cu both oxide when exposed to the atmosphere. Al oxidizes easily when exposed to air, and a strongly bonded, hard outer layer of electrically insulating oxide quickly forms around the metal. Cu also oxidizes when exposed to air, but the oxide formed is relatively soft and conductive, although not as conductive as the base metal (R. F. Frank and Morton, 2005, 2007).

Aluminum and copper windings for SRMs

A SRM is a rotating electrical machine with nonlinear materials (Boumesbah *et al*., 2021). It also has a non-linear electromagnetic structure that is highly dependent on changes in phase current and rotor positions (Alharkan *et al*., 2021). Because of these features, when creating a SRM model, it must include the non-linear behavior of the machine and the rotation features, as this affects its behavior. Within this context, the use of the Finite Element Method (FEM) provides a high precision (Boumesbah *et al*., 2021). In addition, when the results obtained from numerical methods are compared to those from analytical methods, they can be seen to have a higher accuracy. Therefore, numerical methods are preferred by users, among which finite element analysis is one of the most widely used (Alipour-Sarabi *et al*., 2020). Due to all these advantages, the proposed SRM model was analyzed using 2D modeling. To this effect, the Cu winding was first assigned, and then the Al winding. Afterwards, transient analyses were carried out using the FEA. The general parameters and geometric dimensions of the proposed SRM model are given in Table 2.

Table 2. General parameters and geometric dimensions of the proposed SRM

General dimensions of stator		General dimensions of rotor		General electrical parameters	
Outer diameter	100 mm	Outer diameter	40 mm	Rated speed	1 750 rpm
Inner diameter	41 mm	Inner diameter	14 mm	Rated voltage	50 V
Number of the poles	6	Number of the poles	4	Rated output power	1 000 W
Yoke thickness	10,6 mm	Yoke thickness	5 mm	Operating temperature	75 cel

Source: Authors

Finite element analysis

Finite element analysis (FEA) is a computer simulation technique used for analysis in engineering. In this technique, a numerical strategy called the *Finite Element Method* (FEM) is used (Kumar and Isha, 2008). By using the FEM, approximate solutions of partial differential equations (PDE) such as electrical, magnetic, or temperature distribution equations are found (Son-In and Amornsawatwattana, 2022). FEA is generally divided into three stages. The first one is *pre-processing*, in which the FEM and the environmental factors to be applied to it are defined. The second is the *analysis solver* stage, where the solution of the finite element model is carried out, and the last stage is the *post-processing of results*, where visualization tools are used (Kumar and Isha, 2008).

FEM analysis is essential because of the double salient structure of SRMs and the intense saturation effects that occur at partially aligned stator-rotor poles (Kumar and Isha, 2008). In this study, 2D FEM analysis was performed via the Ansys/Maxwell software. For the analysis, the modeling and assignment of material properties, the determination of boundaries, the definition of excitations, the creation of the mesh structure, and the assignment of setup properties are first performed. At this point, one of the important issues to be considered is the mesh structure. The quality of the FEM analysis results depends on the density within the global mesh structure. In high-precision studies, a denser mesh structure can be used at the points where high reliability is desired (ManâaBarhoumi *et al*., 2015). In the analysis of this study, the Backward Euler method was selected among the time integration methods. The basic governing equations used for simulation were Maxwell's equations. In FEA, profiles such as torque, magnetizing, self-inductance, and mutual inductance, required in the analysis and modeling of SRMs, are obtained depending on the change of phase current and rotor position via Maxwell's equations. They can be calculated from the flux density B (Tesla or Wb/m^2) and the field intensity H (Nguyen and Ta, 2011).

The differential form of Maxwell's equations, which can be written in differential and integral forms, is given in Equations (8)-(11), as Faraday's law of induction, Gauss's law for magnetism, Ampere's law, and Gauss's law for electricity, respectively (Ansoft, n.d.).

$$\nabla \times E = -\frac{\partial B}{\partial t} \tag{8}$$

$$\nabla \bullet B = 0 \tag{9}$$

$$\nabla \times H = J + \frac{\partial D}{\partial t} \tag{10}$$

$$\nabla \bullet D = \rho \tag{11}$$

In Equations (8)-(11), E is the electric field intensity (V/m), B is the magnetic flux density (Tesla or Wb/m^2), H is the magnetic field strength (A/m), D is electric flux density (C/m^2), t is time (s), ρ represents the electrical charge density (C/m^3), and J represents the current density (A/m^2).

For SRMs, the magnetic potential vector equations in each direction are used to calculate electromagnetic issues, as shown in Equation (12) (Son-In and Amornsawatwattana, 2022; Torkaman and Afjei, 2009).

$$\frac{\partial}{\partial x}\left(\gamma \frac{\partial A}{\partial x}\right)+\frac{\partial}{\partial y}\left(\gamma \frac{\partial A}{\partial y}\right)+\frac{\partial}{\partial z}\left(\gamma \frac{\partial A}{\partial z}\right)+J=0 \tag{12}$$

where A represents the magnetic vector potential (Wb/m) and γ represents magnetic reluctivity. The relationship between magnetic reluctivity γ and magnetic permeabilitiy μ (H/m) is expressed in Equation (13). In addition, $\mu = \mu_0 x \mu_r$ (Son-In and Amornsawatwattana, 2022).

$$\gamma = \frac{1}{\mu} \tag{13}$$

Considering appropriate boundary conditions, Equation (12) is solved to obtain the magnetic vector potential A. Moreover, the magnetic flux density B can be expressed in terms of A, as given in Equation (14) (Torkaman and Afjei, 2009).

$$B = \nabla \times A \tag{14}$$

The relationship between the magnetic field strength H and the magnetic flux density B can be expressed as shown in Equation (15) (Kim and Doh, 2016).

$$H = \gamma . B \tag{15}$$

Results and discussion

All other analysis conditions were kept the same, except for the winding material type of both models, whose transient

analysis was performed using FEA. Here, the effects of many factors such as air gap width, pole head, and yoke properties on motor output performance can be examined. However, since the main point of the study was the effect of the winding material on the output performance, all other geometric and material properties were kept the same. The induced voltage, torque, flux, and loss graphs obtained from the analyses are given in Figures 2-5.

Figure 2 presents the induced voltage graphics of the Cu- and Al-wound SRM model, Figure 3 presents the torque curves of the two models, Figure 4 shows their magnetic flux lines, and Figure 5 presents their loss curves.

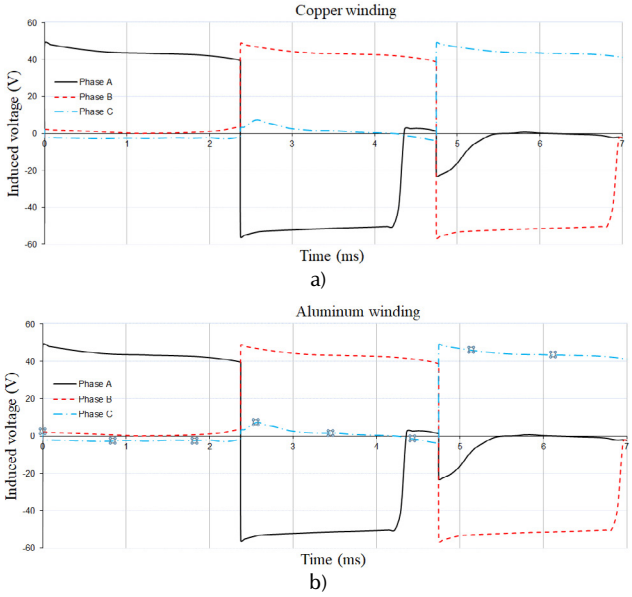

Figure 2. Induced voltage curve: a) Cu winding; b) Al winding
Source: Authors

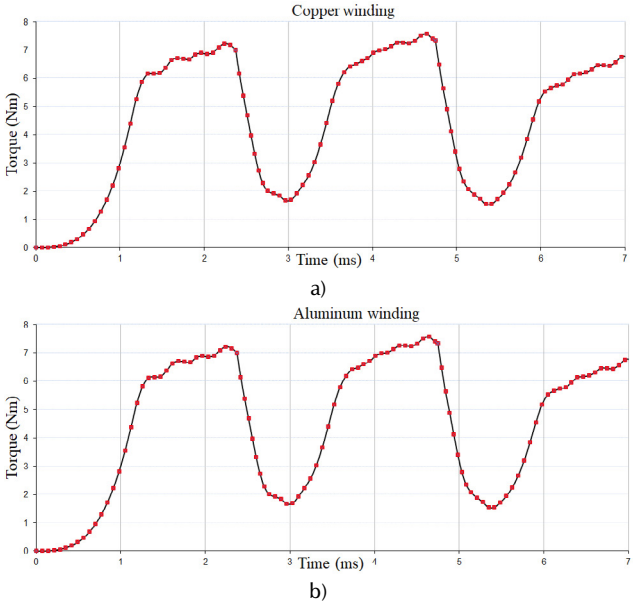

Figure 3. Torque curve: a) Cu winding; b) Al winding
Source: Authors

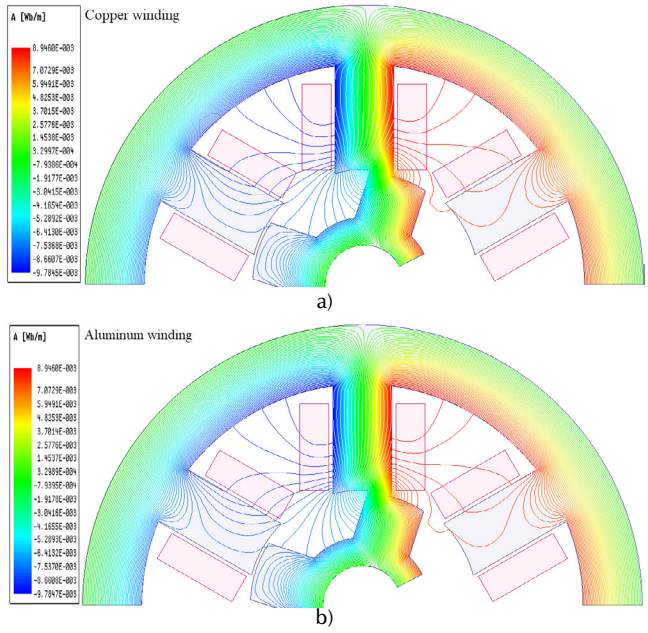

Figure 4. Flux lines: a) Cu winding; b) Al winding
Source: Authors

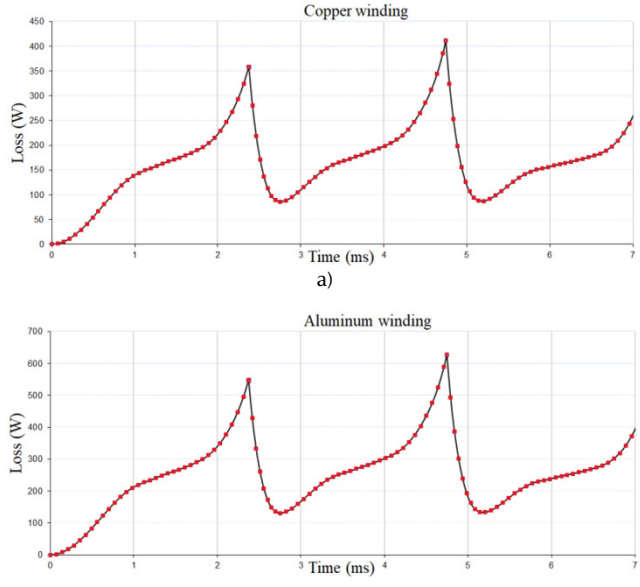

Figure 5. Loss curve: a) Cu winding; b) Al winding
Source: Authors

As can be seen in Figures 2-4, both models were induced with the same voltage, and similar flux distributions and similar torque plots were obtained. However, the important point to be considered here is the losses in the windings. As it can be seen in Table 1, since the electrical resistivity values of Cu and Al used in the windings are different, the losses in the windings are accordingly different. The loss curves of both models are shown in Figure 5. The losses in both models are similar in characteristics but different due to the winding resistance. When the average losses in the Cu and Al winding models were calculated by taking the average of the graphs given in Figure 5, they were obtained

as $P_{loss-cop} = 167,2W$ and $P_{loss-alu} = 255,1W$. In order to calculate the output power of both models, the power-torque relationship given in Equation (16) was used.

$$P = T\omega_r = \frac{T2\pi n_r}{60} \tag{16}$$

where P is the motor power, T is the torque, ω_r is the angular velocity, and n_r is the rotor rotation speed in rpm. In both models, $n_r = 2100\,rpm$ was analyzed. The average output torque of both models was obtained as 4,6 Nm by taking the average of the graph given in Figure 3. By writing the average torque and rotational speed into Equation (16), the average output power of both models was obtained (1 011,08 Watts). However, since the losses are different in both models, the input power is also different. Therefore, their efficiency is accordingly different. The efficiency of both models can be calculated via the expression given in Equation (17).

$$\eta = \frac{P_{out}}{P_{in}\left(P_{out} + P_{loss}\right)} \tag{17}$$

where η represents the efficiency, P_{out} represents the output power, and P_{in} represents the input power ($P_{out} + P_{loss}$). When Cu winding was used in both models with the same output power, P_{in} = 1 178,28 W was obtained, and it was obtained as P_{in} = 1 266,71W when Al winding was used. Therefore, the efficiency was obtained as $\eta_{cop} = 85,81\%$ for the Cu winding model, and as $\eta_{alu} = 79,86\%$ for the Al winding model. However, the important point to be noted here is that the improvement or protection of the motor performance is essential in the studies carried out in electric motors. In addition, both models must have the same efficiency, and therefore the same losses, in order for them to be compared. The absolute condition for this is that the winding losses in both structures must be the same. In other words, the winding resistance of both proposed models should be the same.

As seen in Equations (2)-(4), the main element in the losses occurring in the machine windings is the winding resistance. Therefore, in order for the windings made of different materials (such as Cu and Al) not to have a negative or different effect on the machine output performance, the resistance values must be equal.

When Cu winding was used for the proposed SRM model in this study, Cu wire with a length of approximately 26 m and a wire diameter of 0,5 mm was used for one pole. In this case, the resistance of one pole copper winding was calculated as 2,36 Ω. In this case, the pole winding resistance of the second proposed model with Al winding should be 2,36 Ω. To this effect, considering the motor depth and the winding filling factor, the length of the Al conductor was kept constant, and the cross-sectional area was increased. When the necessary expressions in Equation (5) are replaced, the diameter of the Al conductor wire to be used is approximately 0,63 mm.

By replacing the necessary expressions in Equation (6), it can be stated that 45,87 g of Cu should be used for a pole in the Cu-wound SRM, while 21,96 g of Al should be used for a pole in the Al-wound SRM. In this case, a 43,40% reduction in winding weight occurs, with the same performance. Although there are changes in the geometrical properties of the SRM, such as diameter and depth, among others, when the Al winding is used, there is a significant decrease in the weight of the winding. Therefore, the Al-wound machine will be lighter than the Cu-wound one. This will provide a significant advantage in mobile robots used in EVs, and especially in the aviation industry.

Conclusions

In this study, copper and aluminum materials were compared in terms of the winding structure of SRMs, which are widely used in electric land and air vehicles. One of the most important parameters of electrical machines is their windings. In recent years, fluctuations in Cu prices have adversely affected electrical machinery manufacturers, as well as end users. Therefore, Al has been widely used due to its features and price-benefit balance. In this study, the winding structures of the proposed SRM model were examined with both Cu and Al, and transient analyses were carried out. It was seen that the obtained torque and flux results were quite close. In order for the results obtained in the comparison to be realized in practice, the losses in the winding, and thus the winding resistances, must be equal. Considering the winding filling factor, the sections were changed while keeping the same winding length. Winding weights were calculated after obtaining the winding cross-section and length with equal resistance. When Cu winding is used, 45,87 g of copper should be used for one pole, while, in the case of Al, the pole winding weight should be 21,96 g. As a result, it has been calculated that Al implies 43,40% lighter windings with equal resistance. Thus, it is concluded that aluminum is a conductor that could be easily preferred as a winding material in applications where the total mass of the machine is important.

As a continuation of this study, the thermal behavior of the Al and Cu winding structures of the SRM applied in this study could be examined. In addition, the aging of the windings could be evaluated by observing the effects of the phase currents on the winding when the power switches used in the driver circuit operate at different frequencies (such as 5, 10, and 15 Khz).

CRediT author statement

All authors contributed equally to the research.

References

Alharkan, H., Saadatmand, S., Ferdowsi, M., and Shamsi, P. (2021). Optimal tracking current control of switched reluctance motor drives using reinforcement Q-learning scheduling. *IEEE Access, 9*, 9926-9936. https://doi.org/10.1109/ACCESS.2021.3050167

Alipour-Sarabi, R., Nasiri-Gheidari, Z., and Oraee, H. (2020). Development of a three-dimensional magnetic equivalent circuit model for axial flux machines. *IEEE Transactions on Industrial Electronics, 67*(7), 5758-5767. https://doi.org/10.1109/TIE.2019.2934065

Ansoft (n.d.). Maxwell 2D v12. User's Guide, http://ansoft-maxwell.narod.ru/english.html

Ayaz, M., Tasdemirci, E., Yuce, M., Mese, E., and Hergul, A. S. (2020). Comparative study on winding materials for wind turbine alternators. *Emerging Materials Research, 9*(2), 360-365. https://doi.org/10.1680/jemmr.19.00029

Boumesbah, A. E., Martin, F., Krebs, G., Belahcen, A., and Marchand, C. (2021). Comparison of model order reduction methods for a switched reluctance machine characterization. *IEEE Transactions on Magnetics, 57*(4), 1-6. https://doi.org/10.1109/TMAG.2021.3059969

Cai, J., and Zhao, X. (2021). An on-board charger integrated power converter for EV switched reluctance motor drives. *IEEE Transactions on Industrial Electronics, 68*(5), 3683-3692. https://doi.org/10.1109/TIE.2020.2982112

Chai, F., Li, Z., Ou, J., and Yu, Y. (2020). *Torque analysis of high-speed switched reluctance motor with amorphous alloy core* [Conference presentation]. 2020 International Conference on Electrical Machines (ICEM), Gothenburg, Sweden. https://doi.org/10.1109/ICEM49940.2020.9270715

De Gennaro, M., Jürgens, J., Zanon, A., Gragger, J., Schlemmer, E., Fricassè, A., Marengo, L., Ponick, B., Trancho-Olabarri, E., Kinder, J., Cavallini, A., Mancinelli, P., Hernández, M., and Messagie, M. (2019). Designing, prototyping and testing of a ferrite orrosión magnet assisted synchronous reluctance machine for hybrid and electric vehicles applications. *Sustainable Energy Technologies and Assessments, 31*, 86-101. https://doi.org/10.1016/j.seta.2018.12.002

Frank, R., and Morton, C. (2005). *Comparative corrosion and current burst testing of copper and aluminum electrical power connectors* [Conference presentation]. 14th IAS Annual Meeting, Conference Record of the 2005 Industry Applications Conference, Hong Kong, China. https://doi.org/10.1109/IAS.2005.1518345

Frank, R. F., and Morton, C. P. (2007). Comparative corrosion and current burst testing of copper and aluminum electrical power connectors. *IEEE Transactions on Industry Applications, 43*(2), 462-468. https://doi.org/10.1109/TIA.2006.889973

Gan, C., Chen, Y., Sun, Q., Si, J., Wu, J., and Hu, Y. (2021). A Position sensorless torque control strategy for switched reluctance machines with fewer current sensors. *IEEE/ASME Transactions on Mechatronics, 26*(2), 1118-1128. https://doi.org/10.1109/TMECH.2020.3017864

Gupta, T. D., Chaudhary, K., Elavarasan, R. M., Saket, R., Khan, I., and Hossain, E. (2021). Design modification in single-tooth winding double-stator switched reluctance motor for torque ripple mitigation. *IEEE Access, 9*, 19078-19096. https://doi.org/10.1109/ACCESS.2021.3052828

Haque, M. E., Chowdhury, A., Chowdhury, S. M., Harasis, S., Das, S., Sozer, Y., Gundogmus, O., Vadamodala, L., Venegas, F., Colavincenzo, D., Geither, J. (2021). DC-Link current ripple reduction in switched reluctance machine drives. *IEEE Transactions on Industry Applications, 57*(2), 1429-1439. https://doi.org/10.1109/TIA.2021.3053222

Hergul, A. S., Yuce, M., Ayaz, M., and Mese, E. (2020). Investigation on aluminum alloys as winding materials for alternators in wind turbines. *Emerging Materials Research, 9*(3), 789-795. https://doi.org/10.1680/jemmr.20.00096

Hooftman, N., Oliveira, L., Messagie, M., Coosemans, T., and Van Mierlo, J. (2016). Environmental analysis of petrol, diesel and electric passenger cars in a Belgian urban setting. *Energies, 9*(2), 84. https://doi.org/10.3390/en9020084

Islamgaliev, R., Nesterov, K., Champion, Y., and Valiev, R. (2014). Enhanced strength and electrical conductivity in ultrafine-grained Cu-Cr alloy processed by severe plastic deformation. *IOP Conference Series: Materials Science and Engineering, 63*, 012118. https://doi.org/10.1088/1757-899X/63/1/012118

Jang, J.-H., Chiu, H.-C., Yan, W.-M., Tsai, M., and Wang, P.-Y. (2015). Numerical study on electromagnetics and thermal cooling of a switched reluctance motor. *Case Studies in Thermal Engineering, 6*, 16-27. https://doi.org/10.1016/j.csite.2015.05.001

Jiang, J., Zhang, X., Zhao, X., and Niu, S. (2021). A novel winding switching control strategy for AC/DC hybrid-excited wind power generator. *IEEE Transactions on Magnetics, 57*(6), 1-4. https://doi.org/10.1109/TMAG.2021.3074926

Kim, J., and Doh, W. (2016). *Electromagnetic torque calculation of 12/10 outer rotor type switched reluctance motor using finite element method* [Conference presentation]. 2016 3rd International Conference on Systems and Informatics (ICSAI), Shanghai, China. https://doi.org/10.1109/ICSAI.2016.7810946

Kumar, P. N., and Isha, T. (2008). *Inductance calculation of 8/6 switched reluctance motor* [Conference presentation]. 2008 Joint International Conference on Power System Technology and IEEE Power India Conference, New Delhi, India. https://doi.org/10.1109/ICPST.2008.4745325

Kunčická, L., Kocich, R., and Jambor, M. (2022). Shear strain induced recrystallization/recovery phenomena within rotary swaged Al/Cu composite conductors. *Materials Characterization, 194*, 112399. https://doi.org/10.1016/j.matchar.2022.112399

London Metal Exchange (n.d.) *LME*. https://www.lme.com/

Li, L., Li, S., Li, G., Li, D., and Lu, Z. (2015). Design and performance prediction of switched reluctance motor with amorphous cores. *Materials Research Innovations, 19*(3), 28-32. https://doi.org/10.1179/1432891715Z.0000000001421

ManâaBarhoumi, E., Wurtz, F., Chillet, C., and Salah, B. B. (2015). *Reluctance network model for linear switched reluctance motor* [Conference presentation]. 2015 IEEE 12th International Multi-Conference on Systems, Signals & Devices (SSD15), Mahdia, Tunisia. https://doi.org/10.1109/SSD.2015.7348156https://doi.org/10.1109/SSD.2015.7348156

Nguyen, B.-H., and Ta, C.-M. (2011). *Finite element analysis, modeling and torque distribution control for switched reluctance motors with high non-linear inductance characteristics* [Conference presentation]. 2011 IEEE International Electric Machines & Drives Conference (IEMDC), Niagara Falls, ON, Canada. https://doi.org/10.1109/IEMDC.2011.5994895

Omaç, Z., Polat, M., Öksüztepe, E., Yıldırım, M., Yakut, O., Eren, H., kaya, M., and Kürüm, H. (2018). Design, analysis, and control of in-wheel switched reluctance motor for electric vehicles. *Electrical Engineering, 100*(2), 865-876. https://doi.org/10.1007/s00202-017-0541-3

Pryor, L., Schlobohm, R., and Brownell, B. (2008). *A comparison of aluminum vs. copper as used in electrical equipment*. *https://library.industrialsolutions.abb.com/publibrary/checkout/Alum-Copper?TNR=White%20Papers%7CAlum-Copper%7Cgeneric#:~:text=The%20copper%20used%20in%20electrical,thus%20alloyed%20with%20other%20materials*.

Rocca, R., Capponi, F. G., De Donato, G., Papadopoulos, S., Caricchi, F., Rashed, M., and Galea, M. (2020). Actual design space methodology for preliminary design analysis of switched reluctance machines. *IEEE Transactions on Industry Applications, 57*(1), 397-408. https://doi.org/10.1109/TIA.2020.3038352

Sahin, C., Amac, A. E., Karacor, M., and Emadi, A. (2012). Reducing torque ripple of switched reluctance machines by relocation of rotor moulding clinches. *IET Electric Power Applications, 6*(9), 753. https://doi.org/10.1049/iet-epa.2011.0397

Schenk, M., and de Doncker, R. W. (2013). *Automated copper loss calculation for switched reluctance machines* [Conference presentation]. 2013 15th European Conference on Power Electronics and Applications (EPE), Lille, Farnce. https://doi.org/10.1109/EPE.2013.6631886

Silbernagel, C., Ashcroft, I., Dickens, P., and Galea, M. (2018). Electrical resistivity of additively manufactured AlSi10Mg for use in electric motors. *Additive Manufacturing, 21*, 395-403. https://doi.org/10.1016/j.addma.2018.03.027.

Silbernagel, C., Gargalis, L., Ashcroft, I., Hague, R., Galea, M., and Dickens, P. (2019). Electrical resistivity of pure copper processed by medium-powered laser powder bed fusion additive manufacturing for use in electromagnetic applications. *Additive Manufacturing, 29*, 100831. https://doi.org/10.1016/j.addma.2019.100831

Son-In, S., and Amornsawatwattana, I. (2022). *3-D finite element method based analyzing of torque ripple in 6/4 and 8/6 switched reluctance motor* [Conference presentation. 2022 International Electrical Engineering Congress (IEECON), Khon Kaen, Thailand. https://doi.org/10.1109/iEECON53204.2022.9741653

Sullivan, C. R. (2007). *Aluminum windings and other strategies for high-frequency magnetics design in an era of high copper and energy costs* [Conference presentation]. 22nd Annual IEEE Applied Power Electronics Conference and Exposition, Anaheim, CA, USA. https://doi.org/10.1109/APEX.2007.357498

Sun, C., Li, J., Ding, H., Yang, H., Han, S., and Han, N. (2021). Characteristic Analysis of a New Double Stator Bearingless Switched Reluctance Motor. *IEEE Access, 9*, 38626-38635. https://doi.org/10.1109/ACCESS.2021.3064017

Torkaman, H., and Afjei, E. (2009). Comprehensive magnetic field-based study on effects of static rotor eccentricity in switched reluctance motor parameters utilizing three-dimensional finite element. *Electromagnetics, 29*(5), 421-433. https://doi.org/10.1080/02726340902953354

Wang, H., and Li, F. (2020). Design consideration and characteristic investigation of modular permanent magnet bearingless switched reluctance motor. *IEEE Transactions on Industrial Electronics, 67*(6), 4326-4337. https://doi.org/10.1109/TIE.2019.2931218

Widmer, J. D., Martin, R., and Mecrow, B. C. (2016). Precompressed and stranded aluminum motor windings for traction motors. *IEEE Transactions on Industry Applications, 52*(3), 2215-2223. https://doi.org/10.1109/TIA.2016.2528226

Widmer, J. D., Spargo, C. M., Atkinson, G. J., and Mecrow, B. C. (2014). Solar plane propulsion motors with precompressed aluminum stator windings. *IEEE Transactions on Energy Conversion, 29*(3), 681-688. https://doi.org/10.1109/TEC.2014.2313642

Yan, W., Chen, H., Liu, Y., and Chan, C. (2020). Iron loss and temperature analysis of switched reluctance motor for electric vehicles. *IET Electric Power Applications, 14*(11), 2119-2127. https://doi.org/10.1049/iet-epa.2020.0166

Yoon, Y.-H. (2020). Performance of proposed resonant c-dump converter in switched reluctance motor drive. *Journal of Electrical Engineering & Technology, 15*(4), 1911-1919. https://doi.org/10.1007/s42835-020-00467-w

Research Article/Electrical, Electronic, and Telecommunications Engineering https://doi.org/10.15446/ing.investig.98975

Multi-Tone Optical Source Generation for Applications in Next-Generation Passive Optical Networks using Photonic Structures

Generación de fuentes ópticas multitono para aplicaciones en redes ópticas pasivas de próxima generación usando estructuras fotónicas

Andrés F. Calvo-Salcedo[1], Neil Guerrero-González[2], and José A. Jaramillo-Villegas[3]

ABSTRACT

This study presents the design and simulation of an integrated multi-carrier optical source with a 227 GHz bandwidth for passive optical network (PON) applications. The optical comb generation attained using a photonic structure known as a micro-ring resonator fabricated in silicon nitride (Si3N4) facilitates cost reduction when produced on a large scale. Additionally, the generated optical comb accomplishes non-uniform tones in terms of the optical signal-to-noise ratio (OSNR), which allows for the dynamic assignment of carriers to retainable customers as a function of the data rate and transmission distance requirements. The design and simulation demonstrate the generation of frequency combs with optical carriers in a range of 5-40 tones, an OSNR range of 20-80 dB, and a free spectral range (FSR) of 50-3 610 GHz. To achieve these features, a geometric design of the device is proposed, and its response to variations of input laser parameters is described. In summary, the device uses two optical micro-resonators with radii of 100 and 450 µm and controls the power and the tuning of laser parameters. The proposed method allows generating a deterministic and reliable path to the frequency combs. Finally, the characteristics of the obtained combs are tested to determine their potential use in PON transmissions.

Keywords: next-generation PON, micro-ring resonator, frequency combs, optical communications

RESUMEN

Este trabajo presenta el diseño y simulación de una fuente óptica multiportadora integrada con un ancho de banda de 227 GHz para aplicaciones en redes ópticas pasivas (PON). La generación de peine óptico, que se logra utilizando una estructura fotónica conocida como microresonador óptico fabricada en nitruro de silicio (Si3N4), facilita la reducción de costos cuando se produce a gran escala. Además, el peine óptico generado logra tonos no uniformes en términos de la relación señal óptica a ruido (OSNR), lo que permite la asignación dinámica de portadoras a clientes retenibles en función de los requisitos de velocidad de datos y distancia de transmisión. El diseño y la simulación demuestran la generación de peines de frecuencia con portadoras ópticas con un rango de 5-40 tonos, un rango OSNR de 20-80 dB y un rango espectral libre (FSR) de 50-3 610 GHz. Para lograr estas características, se propone el diseño geométrico del dispositivo y se caracteriza su respuesta ante la variación de los parámetros del láser de entrada. En resumen, el dispositivo utiliza dos microresonadores ópticos con radios de 100 y 450 µm y controla la potencia y la sintonización del láser. El método propuesto permite obtener una ruta determinista y confiable a los peines de frecuencia. Finalmente, se evalúan las características de los peines obtenidos para determinar su potencial uso en las transmisiones con PONs.

Palabras clave: PON de próxima generación, microresonador, peines de frecuencia, comunicaciones ópticas

Received: October 11th, 2021
Accepted: January 19th, 2023

Introduction

A passive optical network (PON) is a fiber network that does not require amplification and power elements to transmit information. This network uses a point-to-multipoint topology and optical splitters to transmit data from a single point to multiple endpoints. In comparison with an active optical network, power is required only at the sending and receiving ends, so this network offers efficiency and low implementation costs (Van Veen, 2020). The growing demand for retainable customers has allowed for the evolution of PONs in recent decades. The advanced modulation formats involved in the process and the use of coherent optical technologies have enabled spectrum optimization and

[1] MSc, Universidad Tecnológica de Pereira, Pereira, Risaralda, Colombia. Affiliation: Professor at Universidad Tecnológica de Pereira, Pereira, Risaralda, Colombia. E-mail: afcalvo@utp.edu.co

[2] PhD, Technical University of Denmark, Lyngby, Denmark. Affiliation: Professor at Universidad Nacional de Colombia, Manizales, Caldas, Colombia. Email: nguerrerog@unal.edu.co

[3] PhD, Purdue University, West Lafayette, IN, USA. Affiliation: Professor at Universidad Tecnológica de Pereira, Pereira, Risaralda, Colombia. E-mail: jjv@utp.edu.co

How to cite: Calvo-Salcedo, A. F., Guerrero-González, N., and Jaramillo-Villegas, J. A. (2023). Multi-Tone Optical Source Generation for Applications in Next-Generation Passive Optical Networks using Photonic Structures. *Ingeniería e Investigación, 43*(2), e98975. https://doi.org/10.15446/ing.investig.98975

increased network speeds (Van Veen, 2020; Serpa *et al*., 2021). Thus, many possibilities for new technology have opened to develop optimization tasks without involving rising costs. Significant advances in photonic devices have enabled the development of integrated circuits for optical digital processing. An example of this is the generation of multi-carrier optical sources, filtering, amplification, and other tasks. These devices help to reduce implementation costs and concurrently optimize the required space, thereby increasing the efficiency of several activities (Van Veen, 2020; Komagata *et al*., 2021). One of the challenges of these networks is the design and implementation of optical sources that allow for the generation of multi-carriers without raising the cost of implementation. One can take advantage of the benefits of transmission methods focusing on wavelength multiplexing transmission by exploring a new issue in parallel transmission and implementing a flexible network (Van Veen, 2020; Serpa *et al*., 2021). This study presents the design and simulation of an optical source based on optical micro-resonators made of silicon nitride. The design of this source offers an approach to a deterministic generation and control of the combs based on the features of geometric rings and power and the tuning of laser parameters. Furthermore, this study presents a strategy to implement a network that allows for spectrum optimization according to distance requirements and the bandwidth of customers, paving the way for the possible creation of next-generation PONs.

The Evolution of PONs

In the 1980s, PONs were identified as an economical and practical method to guarantee broadband to last-mile clients (Serpa *et al*., 2021). In 1995, the full-service access network (FSAN) group formalized a time-division multiplexed passive optical network (TDM-PON) standard. Then, the International Telecommunication Union (ITU-T) standardized two normalized generations of PONs: the asynchronous transfer mode passive optical network (APON) and the broadband passive optical network (BPON). Thus, owing to the importance of the Ethernet protocol, BPONs were modified to allow for frame exchange. Therefore, the Ethernet PON (EPON) standard was created, and a symmetric bit rate was used to upload and download data (FSAN, 2020; Thangappan *et al*., 2020). Subsequently, a standard focused on PON systems of 10 GB, called *XG-PON* (G.987), and EPONs of 10G were introduced. The FSAN group researched 40 Gbit/s PON systems. These systems focused on communication protocols that improved spectral efficiency by highlighting multi-wavelength. This research helped to develop the standard as wavelength-division multiplexing PON (NG-PON2/TWDM-PON – G.989). Although these solutions help with bandwidth implementation, high costs are thereby incurred (Ghoniemy, 2018). The ITU started a process in 2020, attempting to standardize a descending 50 Gbit/s time-division multiplexing-passive optical network (TDM-PON) named *G.hsp*. Recent commercial applications and emergent services such as 5G mobile transport could require symmetric and asymmetric bandwidth in FTTH (Fiber to the Home) applications (IEEE, 2018; Houtsma *et al*., 2021). Currently, the industry is targeting optical access networks focused on wireless traffic, an effort that requires considerable investments in fiber and optic components (Houtsma *et al*., 2021).

Challenges of next-generation PONs

There are multiple challenges in improving bandwidth while reducing costs in optical networks. Factors such as equalization, error correction, energy optimization, flexible design, and low-cost source design should be considered. Next-generation PONs should flexibly connect to networks. In addition, the characteristics of point-to-multipoint communications established in standardized PONs demonstrate the advantage of a flexible line rate. This flexibility enables wideband reconfiguration, transmission speed, and cost based on customer demand. Because of this, it is necessary to develop new approaches capable of optimizing network flexibility by taking advantage of optical comb generation, power supply, and the separation of end users (Houtsma *et al*., 2021; Shbair *et al*., 2021; Rodríguez-García *et al*., 2021). Electronic and photonic integration will be an issue of next-generation PON design.

Reducing costs in multitone generation is a significant issue. The incorporation of a wavelength involves the addition of a laser, which increases the investment costs. However, this device constrains the number of tones for transmission and reception. Increasing the number of wavelengths or reducing the required lasers can make this technology more attractive to last-mile customers. Hence, implementing these methods could increase the speed of transmission. Consequently, the photonic approach becomes a focus for improving the design of PONs. This approach makes it possible to create portable devices that generate multitone while using only one laser. These devices are known as *micro-ring resonators* and enable the application of this technology due to the generation of frequency combs (Lundberg *et al*., 2020). Frequency combs refer to a set of evenly spaced spectral lines that are well-defined in the frequency spectrum. This concept allows using every tone to generate PON transmission in an ascending or descending manner (Lundberg *et al*., 2020).

Frequency comb generation: applicability in photonic integration

Recent studies have accomplished frequency combs for coherent optical communication systems. Transmission speeds –including 1,44Tbit/s– have been attained in distances close to 80km using up to 25 tones. Although these methods generate a multitone source to be applied in advanced modulation techniques, they are made with electro-optical elements, ignoring the features of frequency combs manufactured with photonic integrated optical micro-resonators. A frequency comb generates numerous wavelengths with equally separated frequency and phase synchronization. Its generation depends on a double balance between loss and input power, as well as on nonlinearity and Kerr's dispersion (Kippenberg *et al*., 2020). In addition,

different techniques have been implemented for generating frequency combs, which enables the appearance of multiple frequency components in the generated signal.

A common technique is a cascade of optical modulators, which harnesses the benefit of the spread spectrum via phase and amplitude modulation to make new tones in the spectrum from a nonlinear process. Although this technique generates frequency combs, it usually has a high insertion loss (6dB). It also requires large dimensions to reach integration (centimeter scale), which is a disadvantage for implementing this technique in optical networks. The typical component used in this application is lithium niobate ($LiNbO_3$). Other methods use modulators with indium phosphide (InP) semiconductors, where the dimension reduction is considerable and the insertion loss is still high (5dB) (Komagata *et al.*, 2021). Applying recirculating ring modulators is another technique used for optical combs generation. This method uses the recirculation of the wavelength through a phase modulator supplied by a radio-frequency oscillator. Thus, sidebands around the leading tone are generated. Moreover, when the output recirculation is executed, new sidebands are generated around the others, developing a frequency comb. Although this technique manages to yield a spread bandwidth (1THz), it requires a large dimension (meters) to configure the recirculating structure (Mittal *et al.*, 2021).

A different approach involves using a continuous wave laser and modifying its power, detuning in a resonance frequency and thus generating an optical frequency comb (Kippenberg *et al.*, 2020; Mittal *et al.*, 2021). This technique has advantages in frequency comb stability and the noise made. On the other hand, its integration is reached in lithography by using materials such as SI_3N_4 and SiO_2, and it does not require large dimensions (Kippenberg *et al.*, 2020). Although using a pulsed laser has advantages on frequency combs generation, it requires modifying input parameters for laser power and frequency detuning. Depending on the input conditions, it is possible to attain different performance behaviors on the cavity.

These behaviors generate different spectral response patterns, such as stable cavity solitons (SCS), unstable cavity solitons (UCS), and stable modulation instability (SMI-Turing rolls) (Kippenberg *et al.*, 2020; Komagata *et al.*, 2021; Jaramillo-Villegas *et al.*, 2015; Qi *et al.*, 2019). In the spectral domain, these patterns generate optical frequency combs with multitone. Turing rolls are one of the most interesting patterns for generating optical sources (Qi *et al.*, 2019). This approach involves several oscillating pulses throughout the azimuthal direction in the disc and generates an optical frequency comb in its spectrum, with stabilization of the free spectral range (FSR). This comb is considered to aid optical communications because it is more effective against noise. Moreover, it provides consistency within individual comb lines and brings more stability to maintain the pattern over time (Qi *et al.*, 2019). One key to this frequency combs generation is avoiding the chaotic region. Turing rolls provide a solution because they generate combs to keep the power laser constant by applying the linearly swept frequency theory. Other patterns such as SCS or UCS require specific controllers to achieve exponential functions in laser power variation. This increases implementation costs and prevents the use of SCS and UCS combs (Mittal *et al.*, 2021). Many researchers support using compound-ring resonators and thermal control to easily modify the device dynamics and access regions in the parametric space (Ma *et al.*, 2021; Jaramillo-Villegas *et al.*, 2015; Chaitanya *et al.*, 2016; Xiaobao *et al.*, 2021). Although these techniques enable the study of SCS and UCS regions, the generation of frequency combs depends on complex controls involving nonlinear pathways.

Other approaches use optical micro-resonators and Mach-Zehnder modulators, which allow generating a flat comb with numerous wavelengths. Although researchers have achieved high-speed transmissions, these approaches increase the economic costs of implementation by requiring additional processing and not using the optical comb generated by the micro-resonator alone (Das, 2020; Dutta, 2022). Recently, it was possible to demonstrate a transmission of 1,84 Pbit/s over a 37-core, 7,9 km-long fiber via 223 wavelength channels using optical micro-resonators. Although this approach showed the potential for this type of application, its goal was communication with a single receiving transmitter and the maximization of the speed that can be achieved, meaning that a PON scenario was not considered (Jørgensen, 2022). This research proposes a novel approach for generating frequency combs in PON optical communications through the use of micro-resonators as multi-tone sources. A reliable route has been developed based on the intrinsic parameters of the micro-resonator structure, demonstrating the feasibility of this technique for frequency combs generation in PONs.

Methodology for optical frequency combs generation

This research adopts a three-stage methodology (Figure 1) in a PON to generate a comb. First, the design of an optical micro-resonator structure that aims to define an adjusted geometry to a dynamic response or resonator is considered. Second, the parametric space is characterized as $(\Delta, |S|^2)$ in order to understand how these parameters are involved in comb generation. Thereupon, these different approaches enabling frequency combs generation on Turing rolls and USC regions are suggested (Qi *et al.*, 2019). Lastly, the generated comb is tested to verify whether it meets the spectral features to function as a multitone generation source.

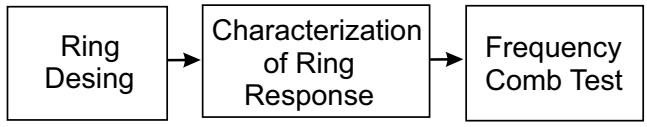

Figure 1. Methodology diagram
Source: Authors

To design a photonic device for multi-carrier generation, a proposed MRR is presented in Figure 2. The selected waveguide and cladding materials are Si_3N_4 and SiO_2, respectively. This structure exhibits an anomalous dispersion with a quality factor $Q = 1,67\times10^6$ and photon lifetime $t_{ph} = t_R/(2\alpha) = 1,37\,\text{ns}$. It is necessary to differentiate the FSR from frequency combs, so this study recommends using two different radius values (100 and 450μm). These values generate FSR 227 and 50GHz. Hence, two different FSR are considered to fulfill different customer bandwidth requirements. This physical configuration is selected because large dimensions (μm) are not required, and those FSR values allow for bandwidths suitable for communications applications. The Lugiato-Lefever Equation (LLE) is used to simulate the optical combs generation process in the micro-resonator structure, as well as split-step Fourier as a solution method (Jaramillo-Villegas *et al.*, 2015). This approach allows verifying the dynamic response of the ring and its spectrum when different variations of input laser parameters are generated. The following simulation parameters are used in the first ring: $t_R = 1/226\,\text{GHz}$, $\beta_2 = -4,7\times10^{-26}\,\text{s}^2\text{m}^{-1}$, $\alpha = 0,00161$, $\gamma = 1,09\,\text{W}^{-1}\text{m}^{-1}$, $L = 2\pi\times100\,\mu\text{m}$, and $\theta = 0,00064$ (Chaitanya *et al.*, 2016; Xiaobao *et al.*, 2021). The following simulation parameters are used in the second ring: $t_R = 1/50\,\text{GHz}$, $\beta_2 = -4.7\times10^{-26}\,\text{s}^2\text{m}^{-1}$, $\alpha = 0,00161$, $\gamma = 1,09\,\text{W}^{-1}\text{m}^{-1}$, $L = 2\pi\times450\,\mu\text{m}$, and $\theta = 0,00064$ (Chaitanya *et al.*, 2016; Xiaobao *et al.*, 2021).

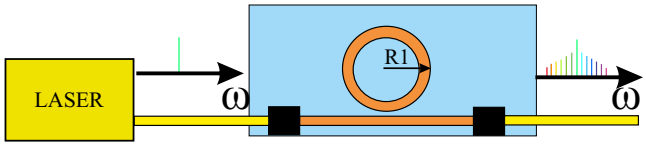

Figure 2. Micro-ring resonator structure for frequency combs generation
Source: Authors

Anomalous dispersion is used in the simulation. Moreover, simulations are performed to initialize the intra-cavity field in the frequency domain E(ω) with a circularly symmetric complex Gaussian noise field with a standard deviation $10^{-9} = 10^{-9}$ [$P = |E|^2$]. In addition, the normalization $P = |E|^2$ is equivalent to a mean power of -150 dBm per cavity mode and a random uniform phase that aims to create a realistic condition. To obtain the parametric space $(\Delta, |S|^2)$, the power and the detuning of input laser are swept. First, indicating the starting point $(\Delta_1, |S_1|^2)$, a path with a linear sweep to a final point is generated $(\Delta_2, |S_2|^2)$. The next step is counting the number of pulses produced in a round-trip, and each region is characterized depending on the number of peaks (Jaramillo-Villegas *et al.*, 2015). These results are shown in Figures 3b and 3e. If the signal behavior shows fewer peaks, its FSR will be smaller. By contrast, if the signal behavior has more peaks, its FSR increases. In Figures 3b and 3e, parametric spaces for the suggested method are shown. In Figure 3c, SCS and USC regions appear in the upper right corner of the graph. These regions cannot be attained with a constant power parameter. Hence, this generation is difficult due to the exponential power variation required to avoid the chaotic region. However, Figure 3c shows that the SMI-Turing rolls region is on the left side of the graph, making it accessible to create a path with power constantly avoiding the chaotic region and enabling combs generation (Figures 3b and 3e). The magenta hexagon indicates the initial point where characterization and simulation start. This point is chosen due to its stability and low-intensity noise. However, the Turing rolls achieve phase-locked states that are independent of the initial conditions (Jaramillo-Villegas *et al.*, 2015).

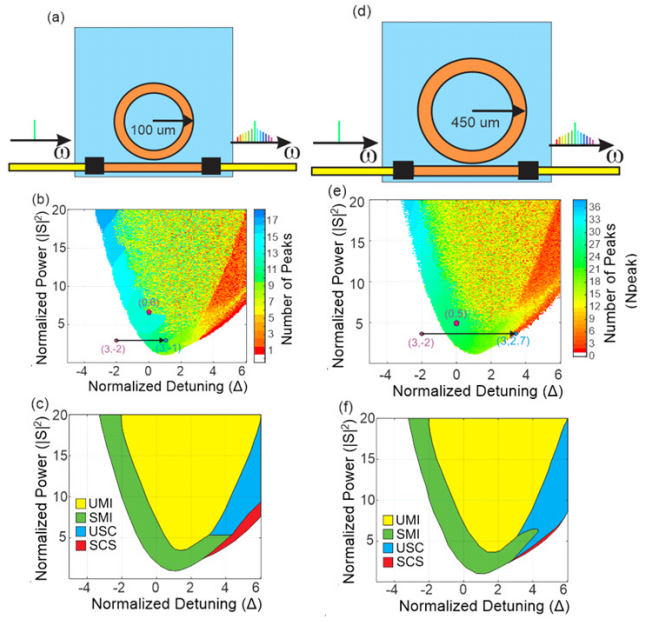

Figure 3. a) Basic structure of an MRR with an FSR of 226 GHZ . **b)** Parametric spacing as a function of the number of peaks $(\Delta, |S|^2)$ with respect to the MRR with an FSR of 226 GHZ. **c)** Characterization of regions according to variation $(\Delta, |S|^2)$ regarding the MRR with an FSR of 226 GHZ. **d)** Basic structure of an MRR with an FSR of 50 GHZ. **e)** Parametric space as a function of peak numbers $(\Delta, |S|^2)$regarding the MRR with an FSR of 50 GHZ. **f)** Characterization of regions according to variation $(\Delta, |S|^2)$regarding the MRR with an FSR of 50 GHZ.
Source: Authors

The optical frequency combs can be generated by decreasing the optical frequency of the pump laser towards the resonance, which makes this pattern a good choice for the initial point. To demonstrate the combs generation, several paths to the SMI region are proposed.

This region was selected because optical frequency combs of the Turing rolls type are robust to noise and exhibit high coherence among the individual comb lines. At the same time, it is possible to ensure a trajectory with constant power to control input variables. This simplifies the generation process by creating a path that only requires linear variation of the frequency.

A path with a constant power that has been normalized is defined. Subsequently, a linear tuning sweep that has also been normalized is performed along this path. An adiabatic process is considered for manipulating the laser input parameters because the variation must be slow. This, in order to ensure processing in the computational systems. Accordingly, the total simulation time is 1 ms.

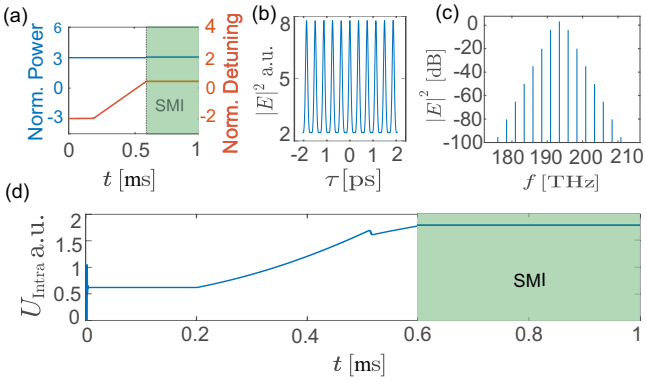

Figure 4. a) Power pump (blue) and detuning (red) in a slow time (t). **b)** Intensity value. **c)** Spectrum. **d)** Intracavity energy against time (t) to reach the point of Figure 5a.
Source: Authors

Figures 4 and 5 show the suggested paths to frequency combs generation based on the characterization shown in Figures 3b and 3e.

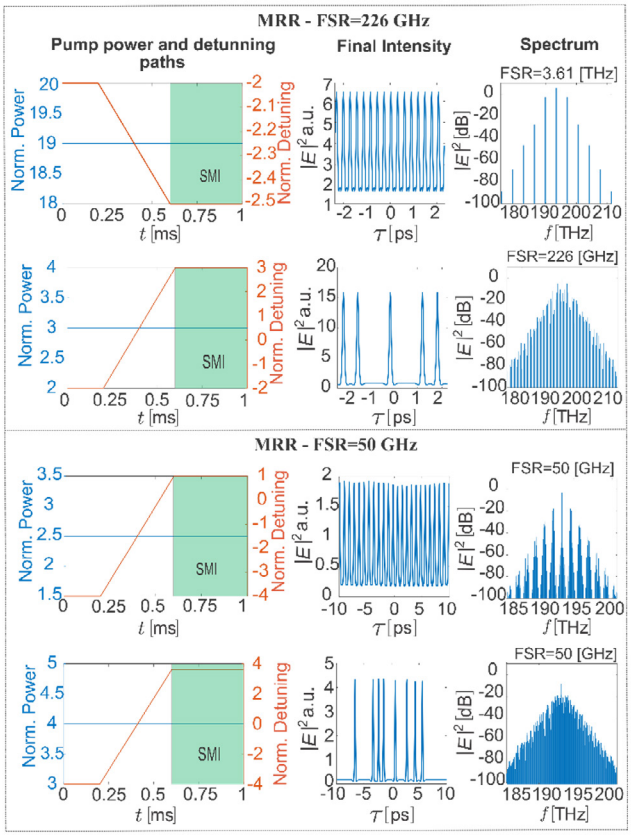

Figure 5. Results of the simulation regarding frequency combs generation
Source: Authors

According to Figure 5, different frequency combs are ensured depending on the power and tuning values. In contrast, peak numbers are lower where the FSR decreases in the intensity graph. Hence, it is important to highlight the line separation change depending on the ring ratio, as well as the result with 36 peaks for the structure with a radius of $450\,\mu m$, achieving an FSR smaller than a comb of $100\,\mu m$ peaks with a $100\,\mu m$ ratio. The combs obtained in this work do not have noise because they are the results of a simulation. This factor is important because the wavelengths of the comb have higher ONSR than those generated in a real device. To avoid this problem, the spectral power of each wavelength is reduced, since this would be the effect that produces noise in the photonic structure.

It is important to emphasize that each ring has different features depending on its geometry, and it attains different FSR and different bandwidths. The frequency comb test calculates the behavior of the total intracavity power for a comb of 16 peaks. This parameter is used because it is proportional to the integral result of intensity during a round trip, enabling the generation of an idea of comb stability. In Figure 5d, the micro-resonator exhibits stable generation as it does not generate oscillatory behaviors when located within the SMI region. This observation underscores the robustness and reliability of the micro-resonator in generating stable signals. This behavior allows deducing permanence, one of the main features of using it as an optical source.

Application of frequency combs to next-generation PONs

The application of optical frequency combs focuses on long-distance communication networks with a fixed transmission distance. This implies that device design methods attempt to achieve many spectral lines with the minimum possible power, generating a spectrum with uniform carriers. Some optical processing activities that spend more energy must be executed in order to fulfill this task. Furthermore, wavelengths are discarded because they do not perform the activities with the required power levels. Hence, limiting the carrier numbers and spending significant resources on other scenarios must be considered (Van Veen, 2020; ITU, 2021). However, the PON scenario is different because its approach is multi-point. These networks focus on the last-mile customer, and the distances change from the central node –distances close to 80 km are also considered. Consequently, a frequency comb with different energy levels is desirable as a multi-carrier source.

This has two significant advantages. First, optical micro-resonators are used because they generate a comb with carriers and different energy values. Second, any activity that attempts uniformity in a comb is avoided, decreasing the implementation costs of the network. There is another issue for consideration in this case: the optical signal-to-noise ratio (OSRN) directly combines two essential features of the network. First, when the OSNR increases, the transmission distance becomes larger since the information is acquired quickly. Second, when the OSNR increases, it is possible to increase the modulation order, optimizing the spectral efficiency. The algorithm must assign spectral lines suitable for bandwidth and distance demand. Wavelength numbers and energy values specific to the frequency comb must be established. Furthermore, this approach must create a modulation format that sends information via wavelength-division multiplexing (WDM) according to the OSNR features.

Figures 6a and 6b illustrate the significance of increasing the OSNR as the transmission distance growing. Therefore, the farthest customers use the blue carriers. Orange-colored customers use spectral lines with less energy than blue ones. Finally, green customers use tones with less energy, allowing them to assign spectral lines according to distance requirements. In Figure 6, a graph presents two scenarios with PONs. The first scenario shows a network with three customers located at different distances. In Figure 6d and 6e, one customer requires significant bandwidth. The second scenario adds different bandwidths in the same network.

These scenarios show how to use frequency combs according to OSNR, distance, and bandwidth. Hence, when multiple carriers are implemented, communication protocols can be applied for multi-wavelengths to take advantage of the spectrum. In contrast, the green customer requires a BW2 bandwidth, implying fewer spectral wavelengths. In this case, lines with more energy are assigned according to the customer's distance. The scenarios in Figure 6 help to verify the number of carriers of frequency combs to optimize the current spectral resources. This aids in cost reduction and optimizes the optical source. These traits allow this method to set these types of sources in next-generation PON design.

To verify the use of optical combs, a test is proposed in which different request scenarios are simulated in an optical network. The network consists of multiple users and an optical micro-resonator source. This network uses wavelength multiplexing and transmits the signals using 16 QAM modulation, with a BER = 0,7 x 10^{-9} and an attenuation for the waveguides of 0,2 dB km^{-1}.

The ONSR of each wavelength is also decreased by 50 dB to simulate the noise conditions of a real device. A wavelength allocation algorithm was designed with this scenario, based on the abovementioned rules. This algorithm uses information from the frequency comb, such as the number of carriers, the OSNR, and the modulation format, in order to calculate the transmission distances that each carrier can guarantee without compromising the quality of service (QoS).

Our assignment algorithm searches for available wavelengths in the optical source and computes the maximum transmission distance of each wavelength for the 16 QAM modulation format. Subsequently, calculating the required number of carriers for each request, the wavelengths are assigned, ensuring that they have a greater distance than what is requested by the customers' location. This algorithm prioritizes requests with greater distance due to the physical shape of the comb.

Otherwise, the wavelength with the longest transmission distance could be assigned to a request very close to the central office, thus wasting resources. Therefore, the requests are organized from longest to shortest distance, and from highest to lowest bandwidth. The allocation algorithm is presented in Figure 7.

Initially, the allocation process is visualized, proposing an optical frequency comb with 11 lines and an FSR of 50 GHz. In parallel, a scenario with four clients with different bandwidths is offered, and the allocation process involving the proposed algorithm is observed. Here, the first user requests 400 Gbit/s at 25 km, the second user requests 100 Gbit/s at 70 km, the third user requests 300 Gbit/s at 40 km, and the fourth user requests 70 Gbit/s at 40 km.

Figure 8 shows the 11 lines of the optical comb, their kilometer capacity, and the spectrum allocation result for the four requests. Note that our method assigns the request of the second customer to the wavelength with the highest distance capacity, and it assigns the other requests according

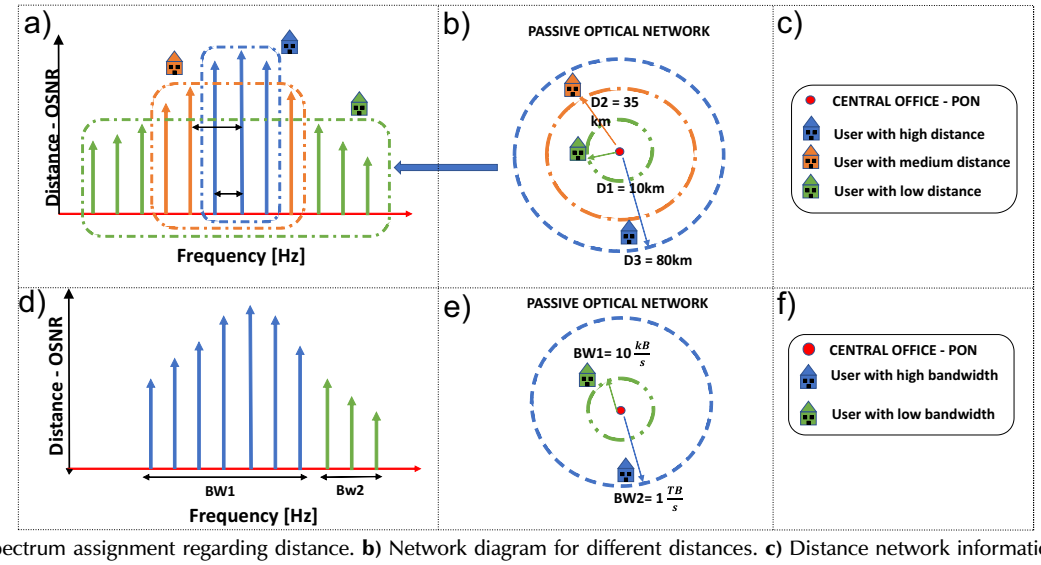

Figure 6. a) Spectrum assignment regarding distance. **b)** Network diagram for different distances. **c)** Distance network information. **d)** Spectrum assignment regarding bandwidth. **e)** Network diagram for different bandwidths. **f)** Bandwidth network information.
Source: Authors

to the distance required by each demand. Also note how the requests with bandwidths of 400 and 300 Gbit/s use super-channels to support the modulation. The above allows verifying that the algorithm responds to the ideas put forward for the allocation.

```
input:
atf     % Fiber attenuation dB/km
BER     % BER of communication
FSR     % Free spectral range
Bd[j]   % Bandwidth of the jth client
Dd[j]   % Distance of the jth client
P44     % Comb spectrum dB
EbEN0   % OSNR for BER and 16QAM modulation
tamd    % Requests size
tams    % Slot size
Ouput:
VA      % Accepted assignment array
RE      % Rejected requests array
%% Computation of bandwidth for 16 QAM modulation and
wavelengths
for j=1:length(dd)
 bw_mod[j]=compute_BW(Bd[j],'16QAM');
 num_WL[j]= number_wavelengths(FSR,bw_mod[j]);
end
dist=(fre_comb-EbEN0)./atf;
% Calculate requests by distance and bandwidth
VP=0.2*Bd+0.8*dd;
% Sort by bandwidth and distance based on VP [bd1,dd1, num_
WL1]=sort(VP,Bd,Dd);
D2=dist;
%% Allocation process
VA=zeros(1,tams);
for i=1:length(bd1)
  r=D2>=dd1[i];
  if sum(r)>= num_WL1[i]
   % Find the consecutive wavelengths
   cell=separate_consecutive(r);
   % Compute group sizes
   tcel=length(cell)
   for j=1:tcel
   CE=cell{j};
   % Select candidate group
   if length(CE)>= num_WL1[i]
    jj=jj+1;
    for K=1:num_WL1[i]
    % Index VA with the request identifier
    VA[CE[K]]=ibd[i];
    % Fill in the assigned wavelengths with zeros
    D2[CE(K)]=0;
    end
% Stop iteration when ibd[i] is allocated
    break
   end
  end
 end
 if jj==0
   % Store rejected demand with ibd[i] value
   con=con+1;
   RE[con]=ibd[i];
 end
end
```

Figure 7. Allocation algorithm
Source: Authors

Initially, the allocation process is visualized, proposing an optical frequency comb with 11 lines and an FSR of 50 GHz. In parallel, a scenario with four clients with different bandwidths is offered, and the allocation process involving the proposed algorithm is observed. Here, the first user requests 400 Gbit/s at 25 km, the second user requests 100 Gbit/s at 70 km, the third user requests 300 Gbit/s at 40 km, and the fourth user requests 70 Gbit/s at 40 km.

Figure 8 shows the 11 lines of the optical comb, their kilometer capacity, and the spectrum allocation result for the four requests. Note that our method assigns the request of the second customer to the wavelength with the highest distance capacity, and it assigns the other requests according to the distance required by each demand. Also note how the requests with bandwidths of 400 and 300 Gbit/s use super-channels to support the modulation. The above allows verifying that the algorithm responds to the ideas put forward for the allocation.

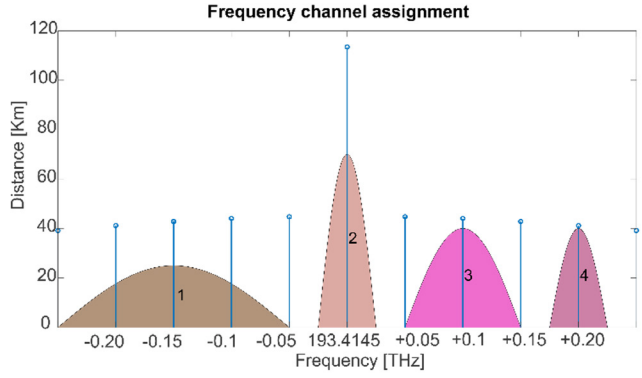

Figure 8. Spectrum allocation
Source: Authors

Next, a network scenario is created in which different request configurations are proposed and the allocation algorithm is computed to verify the network bandwidth blocking ratio in 200 scenarios. To simulate each scenario, our experiment models the number of users, their bandwidth, and their distances to the central office as discrete random variables.

This ensures that each request has the same probability of appearing. The range of users varies between [1 100] users, the bandwidth varies between [1 100] Gbit/s, and the distances are between [0 and 80] km.

Figure 9 shows the algorithm responsible for the 200 scenarios. For each of these, the bandwidth blocking ratio is computed $\left(BBR=\frac{\sum_{i=1}^{n} BWR_i}{\sum_{i=1}^{n} BWS_i}\right)$ because it allows quantifying how much bandwidth can be allocated in a set of requests. Note that our proposal obtains 99 requests with zero blocking probability (Figure 10). This is because our method uses wavelengths that were discarded for having low spectral power in other approaches.

The results above show the potential of the proposal; note that, when the bandwidth and the number of customers grow to high values, the comb cannot support the requests

(Figure 9). This implies that optical combs must be generated with as many lines as possible in order to extend the capacity of the proposal.

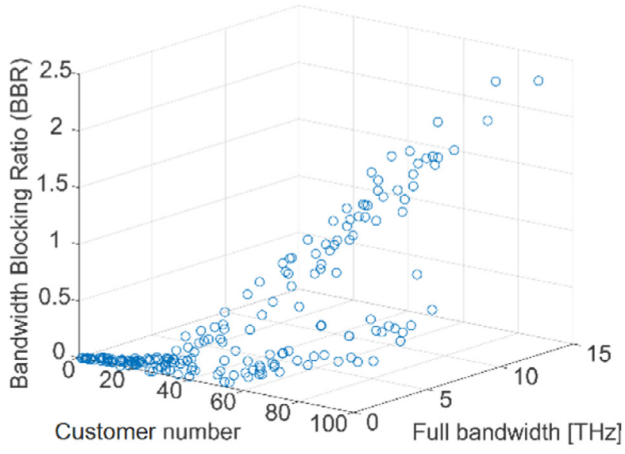

Figure 9. Customer number and full bandwidth *vs.* bandwidth
Source: Authors

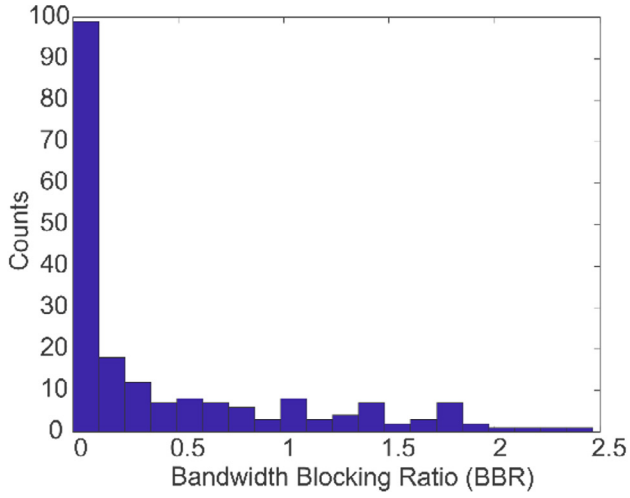

Figure 10. BBR histogram for 200 repetitions
Source: Authors

Conclusions

This paper presents a significant vision for the development of next-generation passive optical networks (PONs). First, it discusses the concept of flexibility, in which an optical network generates adaptive solutions while considering the fluctuation of bandwidth demand and its increasing trend. The method provides multiple carriers with a different signal-to-noise ratio (SNR), which allows assigning wavelengths according to the distance requirements of the customers' geographic locations. This solution optimizes the energy consumption of network resources. To accomplish these goals, modulation formats with high spectral efficiency must be used, which requires using coherent technology to perform phase and amplitude modulation, including multiplexing approaches such as wavelength-division multiplexing (WDM), which allow for the parallel transmission of multiple wavelengths and facilitate the transmission of information. Thus, an optical source is designed to generate multiple wavelengths while using only one laser. This optimizes the implementation costs because it avoids buying numerous sources. To this effect, optical micro-ring resonators are used. These rings should be designed in silicon nitride (Si_3N_4) to take advantage of its photonic integration. Their design must be replicated in an optical chip that requires little space, allowing to replicate it on a large scale and reduce energy consumption. Hence, by applying this technology, costs are reduced. To obtain a robust optical source that guarantees transmission, the laser parameters are controlled to achieve a frequency comb in the Turing rolls and SCS regions. These regions are selected because they feature spectral sources that are constant without considering wastage issues and waveguide dispersion. Moreover, the control algorithm is easily replicated with current network devices. This is because it does not require varying the laser power, and frequency tuning is performed with a linear sweep. The reliability of this approach allows differentiating the FSR of the comb, achieving the different bandwidths used in the flexible scenario. A physical device could be designed in future works which enables the generation of multiple carriers, digital processing techniques, and machine learning, allowing for the dynamic assignation of wavelengths according to the customer's bandwidth requirements and distance. To this effect, two criteria must be applied. The first one depends on the optical SNR of carriers with the distances of the end users; when the SNR increases, it should attain more distance. The second criterion is the bandwidth requirement, as a high number of carriers will be assigned, or the spectral distance will be modified to increase or decrease the bandwidth. This will enable the development of new future telecommunication services that help society in terms of production, economics, and the development of new technologies. This, including the least developed countries, where the development of telecommunications is essential.

Acknowledgements

The authors would like to thank Universidad Tecnológica de Pereira and their support from the program titled *Reconstrucción del tejido social en zonas de posconflicto en Colombia*, part of the Project *Modelo ecosistémico de mejoramiento rural y construcción de paz*, funded by Fondo Nacional de Financiamiento para la Ciencia, la Tecnología y la Innovación, Fondo Francisco José de Caldas (contract no. 213-2018, code 58960).

CRediT author statement

All authors: Conceptualization, methodology, validation, formal analysis, investigation, writing (original draft preparation, review, and editing), data curation, supervision, project administration, resources, and funding acquisition.

References

Chaitanya, J., Jae K. J., Luke, Kevin., Xingchen J. I., Miller, S. A., Klenner, Alexander., Okawachi, Y., Lipson, M., and Gaeta, A. L. (2016). Thermally controlled comb generation and soliton modelocking in microresonators. *Optics Letters, 41*(11), 2565-2568. https://doi.org/10.1364/OL.41.002565

Das, B., Mallick, K., Mandal, P., Dutta, B., Barman, C., and Patra, A. S. (2020). Flat optical frequency comb generation employing cascaded dual-drive mach-zehnder modulators. *Results in Physics, 17*, 103152. http://doi.org/10.1016/j.rinp.2020.103152

Dutta, B., Sarkar, N., Atta, R., Kuiri, B., Santra, S., and Patra, A. S. (2022). 640 Gbps FSO data transmission system based on orbital angular momentum beam multiplexing employing optical frequency comb. *Optical and Quantum Electronics, 54*, 132. http://doi.org/10.1007/s11082-021-03509-3

FSAN (2020). *Full-Service Access Network*. https://www.fsan.org/

Ghoniemy, S. (2018). *Enhanced time and wavelength division multiplexed passive optical network* (*TWDM-PON*) *for triple-play broadband service delivery in FTTx Networks* [Conference presentation]. 2018 International Conference on Computer and Applications (ICCA), Sydney, Australia.

Houtsma, V., Mahadevan, A., Kaneda, N. and Veen, D-V. (2021). Transceiver technologies for passive optical networks: Past, present, and future [Invited Tutorial]. *IEEE/OSA Journal of Optical Communications and Networking 13*(1), A44-A55. https://doi.org/10.1364/JOCN.403500

IEEE (2018). *IEEE Standard for Ethernet 802.3-2018* (*Revision of IEEE Std 802.3-2015*). https://doi.org/10.1109/IEESTD.2018.8457469

Jaramillo-Villegas J. A., Xue. X., Wang, P. H., Leaird, D. E., and Weiner, A. M. (2015). Deterministic single soliton generation and compression in microring resonators avoiding the chaotic region. *Optics Express 23*(8), 9618-9626. https://doi.org/10.1364/OE.23.009618

Jørgensen, A. A., Kong, D., Henriksen, M. R., Klejs, F., Ye, Z., Helgason, Ò. B., Hansen, H. E., Hu, H., Yankov, M., Forchhammer, S., Andrekson, P., Larsson, A., Karlsson, M., Schröder, J., Sasaki, Y., Aikawa, K., Thomsen, J. W., Morioka, T., Galili, M., Torres-Company, V., and Oxenløwe, L. K. (2022). Petabit-per-second data transmission using a chip-scale microcomb ring resonator source. *Nature Photonics, 16*(11), 798-802. http://doi.org/10.1038/s41566-022-01082-z

Komagata, K., Tusnin, A., Riemensberger, J., Churaev, M., Guo, H., Tikan, A., and Kippenberg, T. H. (2021). Dissipative Kerr solitons in a photonic dimer on both sides of exceptional point. *Communications Physics, 4*, 159. https://doi.org/10.1038/s42005-021-00661-w

Kippenberg, T. J., Gaeta, A. L., Lipson, M., and Gorodetsky, M. L. (2018). Dissipative Kerr solitons in optical microresonator. *Science, 361*(6402), 361-567. https://doi.org/10.1126/science.aan8083

Lundberg, L., Mazur, M., Mirani, A., Foo, B., Schröder, J., Torres-Company, V., Karlsson, M., and Andrekson, P. A. (2020). Phase-coherent lightwave communications with frequency combs. *Nature Comunications, 11*, 201. https://doi.org/org/10.1038/s41467-019-14010-7

Ma, W., Liu, Z., Kudyshev, Z. A., Boltasseva, A., Cai, W., and Liu, Y. (2021). Deep learning for the design of photonic structures. *Nature Photonics, 15*, 77-90. https://doi.org/10.1038/s41566-020-0685-y

Mittal, S., Moille, G., Srinivasan, K., Chembo Y. K., and Hafezi, M. (2021). Topological frequency combs and nested temporal solitons. *Nature Physics, 17*, 1169-1176. https://doi.org/10.1038/s41567-021-01302-3

Qi. Z., Wang, S., Jaramillo-Villegas J. A., Qi. M., Weiner, A. M., D'Aguanno G., Carruthers T. F., and Menyuk, C-R. (2019). Dissipative cnoidal waves (Turing rolls) and the soliton limit in microring resonators. *OSA Journal, 6*(9), 1220-1232. https://doi.org/10.1364/OPTICA.6.001220

Rodríguez-García, A. B., Ramírez-López, L., and Travieso-Torres, J. C. (2015). New heuristic algorithm for dynamic traffic in WDM optical networks. *Ingeniería e Investigación, 35*(3), 100-106. https://doi.org/10.15446/ing.investig.v35n3.51676

Serpa-Imbett, C. M., Gómez-Cardona N. D., Borrero. A., and González, N. (2009). Design and construction of a fiber optic network for analysis of topologies and transmission Design in devices for WDM-PON networks. *TecnoLógicas, 23*, 55-64. https://doi.org/10.22430/22565337.236

Shbair, W. W., El-Nahal, F. I. (2021). Coherent passive optical network for 5G and beyond transport. *Optoelectronics Letters, 17*, 546-551. https://doi.org/10.1007/s11801-021-0178-3

Thangappan, T., Therese, B., Suvarnamma, A., and Swapna, G. S. (2020). Review on dynamic bandwidth allocation of GPON and EPON. *Journal of Electronic Science and Technology, 18*(4), 100044. https://doi.org/10.1016/j.jnlest.2020.100044

Van Veen, D. (2020). *Transceiver technologies for next-generation PON* (*Tutorial*) [Conference presentation]. Optical Fiber Communication Conference and Exhibition (OFC), San Diego, CA, USA.

Xiaobao, Z., Hui, L., Wei, X., Xinlin. C., Xiang. H., and Guangzong, X. (2021). *Numerical study of dissipative Kerr soliton generation in a microcavity processed by sol-gel method* [Conference presentation]. First Optics Frontier Conference, Hangzhou, China.

Ingeniería e Investigación vol. 43 No. 2, August - 2023 (e100218)
Research Article/Education in Engineering
https://doi.org/10.15446/ing.investig.100218

Curricular Experiences Leading to the ABET Accreditation in the Electrical and Electronics Engineering Programs

Experiencias curriculares para lograr la acreditación ABET en los programas de Ingeniería Eléctrica y Electrónica

Luis E. Gallego[1], Diego Tibaduiza[2], Jhon J. Ramírez-Echeverry[3], and Hernando Díaz[4]

ABSTRACT

Accreditation processes not only recognize the high quality of curricular programs; they also guarantee their continuous self-improvement. This paper aims to socialize the curricular experiences in the Electrical and Electronics Engineering programs of Universidad Nacional de Colombia (Bogotá Campus) within the framework of the decade-long efforts made to achieve the international ABET accreditation in 2021. This work thoroughly describes the implementation of the CDIO curriculum design methodology and its subsequent transition towards a curricular assessment based on learning outcomes. The results of some qualitative studies regarding the perceptions of faculty and alumni are presented, as well as a detailed proposal of the skills to be developed in each year of the syllabus, establishing their level of implementation. Moreover, a detailed description is provided regarding the methodology adopted for measuring performance indices during four semesters, as well as the main results of the assessment of each learning outcome. Finally, the main curricular challenges to be addressed over the following years within the Electrical and Electronics Engineering programs are described.

Keywords: engineering education, learning outcomes, self-assessment, ABET, CDIO, curricular design, curricular improvement

RESUMEN

Los procesos de acreditación no solo reconocen la alta calidad de los programas curriculares; también garantizan el mejoramiento continuo de los mismos. Este artículo pretende socializar las experiencias curriculares de los programas de Ingeniería Eléctrica e Ingeniería Electrónica de la Universidad Nacional de Colombia (Sede Bogotá), en el marco de los esfuerzos de más de una década para lograr la acreditación internacional ABET en el año 2021. Este trabajo describe detalladamente la implementación de la metodología de diseño curricular CDIO y su posterior transición hacia una evaluación curricular por objetivos de aprendizaje. Se presentan los resultados de algunos estudios cualitativos sobre las percepciones de profesores y egresados, así como la propuesta detallada de las habilidades a desarrollar en cada año del plan de estudios, distinguiendo su nivel de implementación. A su vez, se detalla la metodología de medición adoptada para los indicadores de desempeño durante cuatro semestres, así como los principales resultados de la evaluación (*assessment*) para cada meta de aprendizaje. Finalmente, se describen los principales desafíos curriculares a enfrentar en los próximos años en los programas de Ingeniería Eléctrica y Electrónica.

Palabras clave: educación en ingeniería, resultados de aprendizaje, autoevaluación, ABET, CDIO, diseño curricular, mejoramiento curricular

Received: December 21st 2021
Accepted: March 14th 2023

Introduction

The year 2021 brings to the School of Engineering of the Universidad Nacional de Colombia — Bogotá Campus — the commemoration of its 160 years and, therefore, the authors, on behalf of the Curricular Area of Electrical and Electronics Engineering, join this celebration. It should be noted that only after a century of founding our School, as if the age of majority was reached at 100 years, the emerging specializations in different disciplinary fields gave rise to the conception of new curricula beyond Civil Engineering. Consequently, after its creation, on May 22, 1961, 60 years of the Electrical Engineering degree was celebrated in 2021. Therefore, this occasion constitutes a double dose of celebration for our academic community.

On the other hand, wonderful cabals are woven around the number 60 since Agreement 60 of 1961 of the Academic Council formally originated the Electrical Engineering career. Even beyond his 60 years, our founder, the German engineer Martín Lutz, deployed his best efforts between 65 and 76 years to consolidate this dream (Mejía, 2011). Additionally, at 60 and 24 years for the Electrical and

[1] Electrical engineer, Universidad Nacional de Colombia. Master's degree in High Voltage, Universidad Nacional de Colombia. PhD in Engineering with an emphasis in Electrical Engineering, Universidad Nacional de Colombia. Affiliation: Full professor at the Department of Electrical and Electronics Engineering, Faculty of Engineering, Universidad Nacional de Colombia, Bogotá Campus. Email: lgallegov@unal.edu.co
[2] Electronics engineer, Universidad Industrial de Santander, Colombia. Master's degree in Engineering, Electronics area, Universidad Industrial de Santander. PhD in Seismic Engineering and Structural Dynamics, Universidad Politécnica de Cataluña, Spain. Affiliation: Full professor at the Department of Electrical and Electronics Engineering, Faculty of Engineering, Universidad Nacional de Colombia, Bogotá Campus. Email: datibaduizab@unal.edu.co
[3] Specialist in Telecommunications, Universidad de Manizales, Colombia. Master's degree in Telecommunications Engineering, Universidad Nacional de Colombia. PhD in Projects and Systems Engineering, Universidad Politécnica de Cataluña, Spain. Affiliation: Associate professor at the Department of Electrical and Electronics Engineering, Faculty of Engineering, Universidad Nacional de Colombia, Bogotá Campus. Email: jjramireze@unal.edu.co
[4] Electrical engineer, Universidad Nacional de Colombia. Master's degree in Power Systems, Universidad Nacional de Colombia. PhD in Electrical Engineering, Rensselaer Polytechnic Institute, NY, USA. Affiliation: Full professor at the Department of Electrical and Electronics Engineering, Faculty of Engineering, Universidad Nacional de Colombia, Bogotá Campus. Email: hdiazmo@unal.edu.co

Electronics Engineering plans, respectively, we can celebrate a relevant academic milestone: the international ABET accreditation, recently obtained in August 2021. Giving some context, ABET - *Accreditation Board for Engineering and Technology* - is the most prestigious accrediting agency for programs in applied and natural sciences, computer science, engineering, and engineering technology, whose mission is to ensure that an academic program meets the international quality standards of the profession for which its graduates are prepared (ABET, 2021).

This article describes the experiences achieved during the ABET accreditation process that began in 2008 and 12 years later crystallized in this recognition. The experiences will be organized into four large parts as follows:

1. The CDIO Initiative (Conceive, Design, Implement and Operate); (2008-2012).
2. The consolidation of the Educational Project of the Program - PEP (2012-2016).
3. The ABET approach.
4. Future curricular challenges.

The CDIO initiative (2008-2012)

Generalities

As mentioned, the Electrical Engineering and Electronics Engineering programs have been very active in the curricular revision processes, particularly since 2008 due to the last Academic Reform (CSU, 2007). Strictly speaking, this reform raised some fundamental principles such as (i) comprehensive training, (ii) flexibility, (iii) contextualization, (iv) internationalization, and (v) interdisciplinarity. Accordingly, the relevant question at the time inquired about which strategies should be used to apply the previous principles to the design of the programs' curricula. As a possible response to such a challenge, the ongoing direction of the curricular area explored some educational approaches for implementing these principles in the study plans. That is how the programs adopted the CDIO initiative (Crawley *et al.*, 2006).

In general terms, CDIO "provides an educational framework for developing the fundamentals of engineering in the context of **C**onceive, **D**esign, **I**mplement and **O**perate * real-world systems or products." (Crawley *et al.*, 2006). In particular, this framework is represented by an explicit set of hierarchical skills (4 sublevels) whose development is desirable throughout the curriculum in three different levels of training known as "Introduction (I)", "Exposure (E)" and "Use by the student (U)".

Among other desirable features, this initiative addresses aspects of engineering education that conformed to the new principles proposed in the 2007 Academic Reform where, beyond the purely disciplinary or technical programmatic contents, the development of some fundamental competencies such as oral and written communication and teamwork was demanded by the students (Tadmor, 2006; Kennedy, 2006; Wulf, 1998; Boeing, 1996).

One of the first tasks to advance this initiative consisted in establishing the desirable and necessary competencies for an engineer and the desired level of performance for each one. Today, there is a consensus about the skills engineers must have to compete in a globalized world. Both, graduate engineers and professors from many regions agree that it is necessary to (i) identify the skills and other required competencies, (ii) make explicit the training objectives in all areas, and (iii) establish the appropriate mechanisms to achieve these objectives (Crawley *et al.*, 2006; NAE, 2005; Diamond, 2008; Vest, 2006).

Consequently, one of the fundamental stages of this curricular reform consisted of establishing how to answer the following fundamental questions (Diamond, 2008):

- What are the knowledge, skills, and aptitudes (competencies) must graduates of our engineering programs possess? Furthermore, what is the desired level of sufficiency in each of those aspects?
- How can we support students to acquire or foster these skills before graduating?

To establish the set of required competencies and the desired level of proficiency, it was necessary to collect the opinion of the programs' main stakeholders (Students, Industry (employers), and Professors) about the pertinence of the acquired competencies during their university education.

CDIO — the point of view of Graduates

The opinion of the graduates of both programs in 2008 (115 and 54 graduates of Electrical and Electronics Engineering, respectively) was estimated through the application of a survey, following a methodology similar to that carried out by the World Chemical Engineering Council (WCEC), whose results are reported in Díaz (2008). This survey asked to rate the importance of some relevant competencies for the practice of the profession, according to the scale shown in Table 1.

Table 1. Scale of levels of importance in each skill or competence. CDIO Graduates Survey.

Value	Rating
1	Nothing important
2	Less important
3	Moderately important
4	Considerably important
5	Very important

Source: Authors

The results for both programs are presented in Table 2, illustrating the order of importance given by the graduates of each program to each of the competencies investigated.

How to cite: Gallego L. E., Tibaduiza D., Ramírez-Echeverry J. J. and Díaz H. (2023). Curricular Experiences Leading to the ABET Accreditation in the Electrical and Electronics Engineering Programs. *Ingeniería e Investigación*, *43*(2), e100218. https://doi.org/10.15446/ing.investig.100218

*Hence the acronym CDIO.

Table 2. CDIO Graduates survey. Skill's priority reported by graduates about the most required competencies in the workplace.

Priority	Electronics Engineering	Electrical Engineering
1	Information gathering	Information gathering
2	Problem-solving	Teamwork
3	Information Analysis	Leadership
4	Self-learning	Communication
5	Communication	Information gathering
6	Teamwork	Problem-solving
7	Long-term learning	Broadview perspectives
8	Foreign language	Long-term learning
9	IT proficiency	Foreign language
10	Leadership	Work Ethics

Source: Authors

Table 3. CDIO Faculty's Survey. Expected proficiency levels in the development of CDIO skills.

Value	Rating
1	Have seen it or witness its use
2	Being able to participate in the process of using it
3	Being able to understand it and explain it
4	Have experienced its application or implementation
5	Being able to conduct it, improve it or innovate it

Source: Authors

CDIO - Faculty's point of view

The perception of the professors was also estimated through a survey at the same year as the applied to the graduates (2008). The scale of the level of proficiency expected in the students is shown in Table 3. The survey was answered by 28 professors from the program, mostly full-time. The survey results for each level 2 CDIO skill are shown in Table 4.

CDIO - Gap analysis

Once the opinion of Graduates and Professors was collected, the study's primary purpose was to evaluate the most remarkable differences between the competencies required for the job and those that the University emphasizes during the degree. Therefore, for each competency analyzed, the gap was estimated as the difference between the average values of the importance rating given by teachers and graduates. Consequently, the gap will be (i) *positive* if the University offers tools to achieve more competence than what is required for professional life or (ii) *negative* if the needs of professional life exceed what is acquired in university education. The results for this gap analysis are shown in Figures 1 and 2 for Electrical and Electronics Engineering, respectively.

The only areas for which the gap was *positive* were the competencies related to applying physics, mathematics, and chemistry knowledge. On the other hand, for the areas of "Application of engineering concepts" and "Research capacity", the gap is very close to zero, which implies that what is learned during university education is very close to what is necessary.

Table 4. Faculty's CDIO Survey. Resulting scores for the expected proficiency to be developed by the students in any CDIO skill (Level 2).

ID	CDIO Skill (Level 2)	Score
1	Designing	4,15
2	Engineering reasoning and problem solving	4,12
3	Personal skills and attitudes	4,12
4	Professional skills and attitudes	4,08
5	Communication	3,96
6	Teamwork	3,73
7	Experimentation and knowledge discovery	3,62
8	System thinking	3,62
9	Conceiving engineering systems	3,62
10	Communication in foreign languages	3,56
11	Implementing	3,44
12	Enterprise and business context	3,31
13	Operating	3,12
14	External and societal context	3,08

Source: Authors

Table 5. Most deficitary skills

Orden	Competence/skill
1	Management skills
2	Quality control and management
3	Business approach
4	Marketing
5	Project management
6	Financial analysis principles
7	Foreign language
8	Sustainable development
9	Leadership capability
10	Team work
11	Ethical responsibility
12	Multi-disciplinary focus

Source: Authors

On the other hand, the skills for which the gap was mostly deficient (*negative*) are shown in Table 5.

Although Figures 1 and 2 illustrated a situation that could be considered dramatic, it is necessary to mention that this situation was highly consistent with the results obtained in different studies from different countries and with the results from the study of chemical engineers from 63 countries, see DeChema (2004), pages 41-57. In almost all cases, the only skills with a positive gap were those related to purely technical knowledge. Of course, although in 2008 it was a global trend, it was no less problematic.

Similarly, the common characteristic of all these deficient competencies was closely related to the principles of the 2007 Academic Reform, whose spirit went beyond the strictly technical. In this sense, the CDIO initiative was very appropriate to address, in a structured and systematic way, the problem of a curricular design in both programs that could strengthen these competencies.

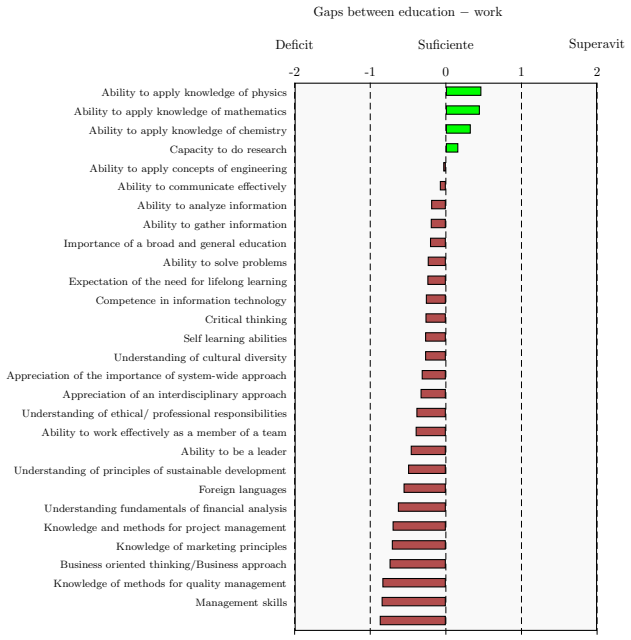

Figure 1. Electrical Engineering: The gaps between what the University provides and what is required on the job, ordered from largest to smallest. Positive values (green bars) mean excess, while negative values (red bars) imply a deficit between what the University provides and what is required at work.

Source: Authors

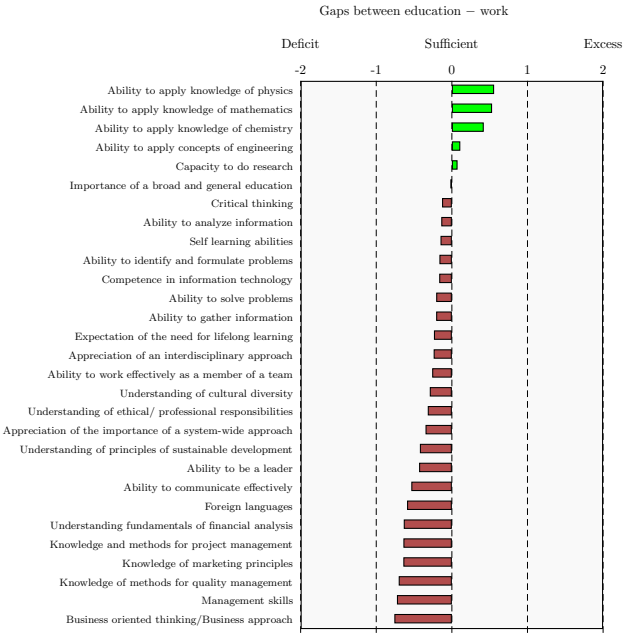

Figure 2. Electronics Engineering: The gaps between what the University provides and what is required on the job, ordered from largest to smallest. Positive values (green bars) mean excess, while negative values (red bars) imply a deficit between what the University provides and what is required at work.

Source: Authors

CDIO - Implementation in the curriculum

As a result of the gap analysis, CDIO skills up to level 3 were selected to be developed along the curriculum. This selection was based on (i) the scores given by the teachers to the level 2 CDIO skills (Table 4) and (ii) the most deficient skills revealed by the graduates (Table 5). On the other hand, the selection of the CDIO skills at level 3 was based on the scores obtained for each skill, so only the skills above the average scores were selected. This selection helped to limit the set of CDIO skills to level 3 so that the levels desired by the teachers matched the most deficient skills expressed by the graduates.

Once the skills up to level 3 were selected, the new challenge consisted of making an adequate distribution of them throughout the study plan. Two variables were considered in this distribution as follows:

1. Temporality: Determining at what point certain skills should be developed. It was decided to divide the academic trajectory into five periods, each of one year.
2. Depth: Knowing how deep a particular skill must be developed. In this regard, the previously mentioned levels of Introduction (I - skills developed in a very introductory way and almost at an informative level), Exposure (E - skills formally exposed to the student for future use), and Use (U - the student must use the exposed skills within the activities planned in the subjects).

Similarly, the distribution of these skills was only carried out within the groupings of disciplinary courses in the study plan. This strategy made it possible to define teams per grouping, leading to effective communication among professors of the same work area. The subject groupings for both programs are shown in Table 6.

Table 6. Subject groupings in Electrical and Electronics Engineering

Grouping	ID
Circuits and fields	1
Signals – Systems and control	2
Electrotechnics (Conversion, Installations, etc)	3
Digital and analog electronics	4
Power systems – Communications and applications	5
Context (Introduction to engineering + Workshops)	6

Source: Authors

Now, based on the identification (ID) presented in Table 6 for each grouping, Table 7 shows its location along the years of the academic trajectory (Temporality).

Likewise, skills at level 2 were coded according to the ID number shown in Table 4. Subsequently, the level 2 skills were distributed in each group of subjects, indicating temporality and depth. This distribution was made for each grouping in Table 6. A sample of this distribution is shown in Table 8 for the Analog and Digital Electronics grouping, where I, E, and U correspond to the Introduction, Exposure, and Use levels, respectively. Accordingly, numbers shown in Table 8 refer to the ID number shown in Table 4. For further details on implementing the CDIO strategy, see Gallego (2011).

Table 7. Temporalidad de las agrupaciones por año

Year	Grouping
1	6
2	2,1,4
3	6,1,3,4,2
4	2,4,5
5	5,6

Source: Authors

Table 8. Distribution of level 2 CDIO skills in the Digital + Analog Electronics grouping

	Level 2 CDIO skills (ID)													
Yr	**1**	**2**	**3**	**4**	**5**	**6**	**7**	**8**	**9**	**10**	**11**	**12**	**13**	**14**
1	x	x	x	x	x	x	x	x	x	x	x	x	x	x
2	E	I	x	x	EU	U	E	x	x	EU	I	x	x	x
3	E	E	x	x	EU	EU	E	x	x	U	I	x	x	x
4	E	EU	U	EU	EU	U	U	E	IE	U	IE	x	x	x
5	x	x	x	x	x	x	x	x	x	x	x	x	x	x

Source: Authors

Based on the distribution of CDIO skills at level 2, the professors of each subject received their corresponding matrices (similar to the one shown in Table 8) as input to determine not only what skills but also how deep these skills may be developed. In summary, the implementation in each course was carried out based on the following steps:

1. Reconsider subject contents, strictly in what has to do with the CDIO level 1 skill on technical knowledge and reasoning, that is, the contents related to:
   (a) Basic science knowledge.
   (b) Basic engineering knowledge and methods.
   (c) Knowledge and methods of Electrical Engineering and Electronics Engineering.
2. Document any contents and methodological modifications as a result of the academic reform implementation.
3. Select the skills at level 3 with their respective depth levels (I, E or U).
4. Formulate the learning objectives based on the level 3 skills intended to be developed. For this formulation of objectives, Bloom's Taxonomy (Anderson, Krathwohl, 2001) was used to select a series of verbs closely related to the depth level. Likewise, these objectives were written in such a way as to specify what the student should be able to do once the course is finished.
5. Formulate the methodology to follow by describing the activities to be developed during the course along with the objectives and skills that are intended to be developed. It is intended to make a conceptual map between each activity and the skills that are intended to be developed.

The COMFIE Accompaniment Program for students

Parallel to the curricular design process, it was necessary to implement a strategy that would accompany students during their adaptation to university life once they enter the programs. Therefore, an interdisciplinary team was defined between the School of Engineering, the Department of Psychology, and the Student Health division from the Welfare Directorate - (Bogotá Campus), which formulated the project called *COMFIE - A Study in Promotion of Health from the Academic Practice in Engineering. Phases I - IV*. With the support of some professors from the Departments of Electrical Engineering and Electronics Engineering and Chemical and Environmental Engineering and with the leadership of the psychologist Nohora Acuña, this project developed a longitudinal study with four cohorts of admitted students achieving, among others, the following results:

1. Implementation of disciplinary content articulated methodology, along with the development of teaching strategies to support the student's formative process. For this, the subject *Introduction to Engineering* was selected as the axis of the implementation with the purpose that accompanying actions were duly articulated to the academic process developed *in-classroom*. These reflections even gave rise to a greater intensity of work in this subject and therefore, from the logic of the curricular design, it was decided that this course would have the highest number of credits in the student's first semester for both programs.
2. Beyond the disciplinary learning objectives of the subject, the development of transversal competencies such as (i) teamwork or (ii) oral and written communication, formally became learning outcomes of the course. Since these skills were considered essential, teaching accompaniment around was implemented around specific activities during the course with their corresponding evaluation criteria.
3. Early self-assessment of the students allowed honing in the skills to be worked on. Entering students were evaluated using two instruments that were designed by the teaching team. They are called "First Semester Student Questionnaire" and "Coping Styles Questionnaire". Thus, the competencies to be developed were selected based on both, the needs indicated by the students and those chosen by the research team.

Once the implementation of COMFIE was completed, the dropout rates of the intervened groups (cohorts 2008-II, 2009-I, and 2009-II) were compared with the control groups (cohorts 2006-II, 2007-I, and 2007-II), observing a decreasing trend in the dropout rates in the intervened group, which showed that the strategy was successful in its purpose of student accompaniment in a training process beyond disciplinary contents, that is, of comprehensive training. Furthermore, this strategy impacted the culture of the School of Engineering and the Bogotá Campus since this strategy was later implemented in the six remaining programs of the School and more than 30 programs at the Bogotá Campus. More details on implementing the COMFIE strategy can be found at Acuña *et al*. (2011).

In conclusion, from 2008 to 2012, the CDIO initiative was the educational approach adopted to address deficient skills regarding our graduates in line with the new challenges imposed by the principles promulgated by the Academic Reform of 2007. Through a structured and systematic framework, this initiative served us to identify the skills students needed to foster throughout the curriculum. In other words, the CDIO initiative helped us to identify the "*What?*" and "*Where?*" of the curriculum design strategy while arousing curiosity to start addressing the "*How?*" of the *teaching strategies* and the *assessment* of these skills, steps that would be addressed in later years.

Consolidation of the Educational Project of the Program - PEP (2012-2016)

During 2012-2016, the consolidation of the CDIO initiative and the COMFIE program continued, which impacted the educational objectives of both programs. The declaration of educational objectives in the context of the CDIO initiative is evidenced in the objectives declared in the agreements of the year 2008, where the words "Conceive, Design, Implement, and Operate" were an explicit part of the objectives for both programs (Acuerdo 223, 2008; Acuerdo 248, 2008).

Additionally, in 2012, an institutional initiative was promoted by the National Directorate of Undergraduate Curricular Programs, whose purpose was to formalize the educational projects of all the curricular programs of the Universidad Nacional de Colombia (DIRNALPRE, 2012). In general, the Program Educational Project (PEP) is a document that contains the guidelines, policies, and principles that guide the development of the program. Likewise, it becomes an instrument of reference and navigation within an academic and argumentative exercise of "wanting to be." In this sense, this document must specify the educational objectives of the curricular program and its articulation with the courses included in the study plan so that both the development of these objectives and their evaluation are made evident. (DIRNALPRE, 2012).

Derived from the nature and purposes of this document, it was necessary to carry out a review and formalization of the ongoing initiatives in which the mapping of educational objectives and CDIO skills to the different subjects of the curricular plan was made explicit. These mappings can be consulted in PEP Electrónica (2013) and PEP Electrónica (2013).

Once the Educational Project for both programs was consolidated and, recognizing that the curricular design process followed guidelines that met some international standards, the programs began to analyze whether it was possible to achieve recognition of their curricular dynamics. The recognition exercises at the national level were already carried out, given that High-Quality accreditation had been achieved for both programs before the National Accreditation Council - (CNA). In fact, there was a certain dichotomy in carrying out these recognition processes since the national accreditation models were not adequate to think about a curricular design for educational objectives, and therefore, the reflections on the academic improvement of the programs resulting from these processes were not necessarily so governable and not so academic. Consequently, in 2016, after eight years of implementation of the CDIO initiative, the possibility of achieving an international accreditation that was more in tune with the curricular dynamics of our programs began to be evaluated, and, therefore, the ABET accreditation seemed to be a good alternative.

The ABET approach (2016-2020)

After 8 years of reflections on the CDIO initiative and the consolidation of the Educational Project of the Program, some valuable agreements seemed to have been reached on (i) which skills to develop and (ii) where to develop them throughout the curriculum. However, there were still some challenges in terms of how to assess these skills, which includes some reflections on (i) the development of course activities aimed at developing and measuring these skills, (ii) possible assessment tools, (iii) the frequency of measurement and (iv) a clear feedback and improvement scheme, among others.

At the same time, some professors of the Department had the opportunity to attend some preparatory courses for a possible application to the international ABET accreditation, which was financed by initiatives of the Faculty of Engineering - (Bogotá Campus), the Academic Directorate - (Bogotá Campus), and the National Directorate of Undergraduate Curricular Programs. In contrast to the High-Quality National Accreditation - (CNA), our programs were convinced that the ABET accreditation approach based on educational objectives, provided not only better strategies to be implemented in our teaching-learning activities but also a systematic framework of characterization and feedback to the academic processes that ensured their improvement.

In general terms, the evaluation process within the ABET model can be summarized in two large cycles corresponding to (i) the continuous review of educational objectives and (ii) the implementation and evaluation of learning outcomes throughout the curriculum. Figure 3 illustrates the two workflow cycles mentioned, which will be developed in the following sections.

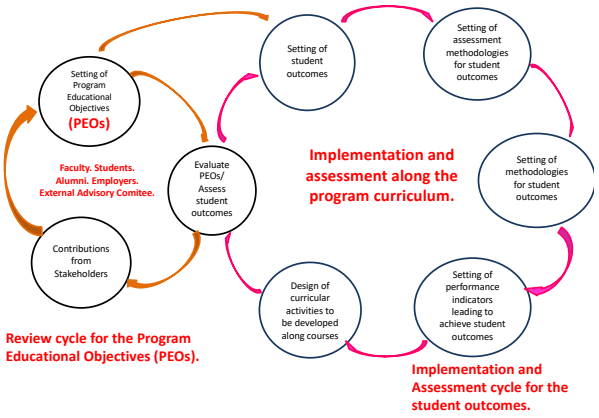

Figure 3. Workflow cycles involved in the ABET Accreditation model.

Source: Authors

[†]Adapted from https://www.abet.org/wp-content/uploads/2015/04/IDEAL-Presentation-Slides.pdf

Table 9. Adopted student outcomes for the ABET accreditation in Electrical and Electronics Engineering.

Id	Student outcome
1	An ability to identify, formulate, and solve complex engineering problems by applying principles of engineering, science, and mathematics.
2	An ability to apply engineering design to produce solutions that meet specified needs with consideration of public health, safety, and wellness, as well as global, cultural, social, environmental, and economic factors.
3	An ability to communicate effectively with a range of audiences.
4	An ability to recognize ethical and professional responsibilities in engineering situations and make informed judgments, which must consider the impact of engineering solutions in a global, economic, environmental, and social context.
5	An ability to function effectively on a team whose members together provide leadership, create a collaborative and inclusive environment, establish goals, plan tasks, and meet objectives.
6	An ability to develop and conduct appropriate experimentation, analyze and interpret data, and use engineering judgment to draw conclusions.
7	An ability to acquire and apply new knowledge as needed, using appropriate learning strategies.

Source: Authors

From the CDIO Syllabus to learning outcomes

One of the first tasks carried out consisted of finding a mapping between the CDIO level 2 skills and the learning outcomes, according to ABET (student outcomes). Regarding the learning goals, it is important to take into account that this equivalence began with a model called A-K (a set of 11 goals or outcomes numbered from literal A. to K.), which became a set of seven learning outcomes in the new ABET accreditation model. In general, this mapping was possible since there was a high degree of correspondence between what the CDIO initiative proposed and the ABET model.

Another important task consisted in determining how the level of achievement of these goals was going to be characterized. To this end, a set of performance indicators was determined through the joint agreement of the teachers of both programs. This step was quite significant since it required recognizing what was considered important in each skill and thereafter, what was *teachable* in our courses. Consequently, these indicators required the design of specific activities to be carried out in each course. The set of outcomes in the model from 1 to 7 is shown in Table 9.

On the Program Educational Objectives (PEOs)

According to the workflow cycle of the ABET model, programs must have a continuous review of their educational objectives. This review is carried out jointly with the so-called "stakeholders" which, in the case of both programs, were made up of (i) students, (ii) professors, (iii) graduates, (iv) employers, and (v) external advisory committee. In this regard, the external advisory committee represented one of the main innovations in the process, since it required the creation of a collegiate body made up of associations of graduates, employers, and graduates to provide feedback on the objectives and curricular dynamics of the programs.

Table 10. Relationship between educational objectives and ABET student outcomes.

Program Educational Objectives (PEO's)	Student outcomes
Graduates from the Electrical Engineering program are expected to attain or achieve the following Program Educational Objectives within a few years of graduation:	
I. Will apply science, technology, and management knowledge in conceiving, designing, and implementing solutions to Electronics Engineering problems considering social and environmental sustainability criteria.	1, 2 and 6.
II. Will contribute to comprehensive solutions to engineering problems by virtue of leadership and effective communication in multidisciplinary teams.	3 and 5.
III. Will apply long-term learning skills in defiance of social, economical, and technological challenges recognizing the ethical responsibilities involved in its professional practice.	4 and 7.

Source: Authors

This new milestone led both programs to review the program's objectives that began in October 2019 through a workshop with graduates and employers where some observations were received on the needs of the external sector that were not explicitly covered in the study plans, among which were notable (i) the development of design skills that include not only technical or economic restrictions but social and environmental ones, (ii) the preparation of transversal skills to function in work environments, and (iii) the importance of ethics in engineering and the ability to resolve conflicts in organizational contexts.

At the same time, a process of reflection was carried out by the faculty on the objectives of the program in light of the learning outcomes that had begun to be formally characterized and evaluated since 2018 in both programs. In this sense, when comparing the objectives of the Educational Project of the Program with the ABET approach, there was not necessarily an adequate academic alignment. For this reason, at the beginning of 2020, an adjustment was made to the objectives of the program in such a way that they were better aligned with the learning goals of the ABET model (Acuerdo 181, 2020; Acuerdo 182, 2020). These new educational objectives and their correspondence with the learning goals are illustrated in Table 10, in which it is worth noting that, for the first time in history, they are exactly the same for both programs, which constitutes a common agreement on what our students, regardless of the program they are in, should achieve.

Assessment of student outcomes

One of the main challenges in implementing this new approach was the characterization of performance indicators for each learning goal. This implied a discussion about the evaluation tools and the proposed methodology for the assessment of each one of the outcomes. In general, the evaluation was developed in two modalities as follows:

1. An internal evaluation, made up of the characterizations carried out in the courses through the use of rubrics, agreeing on the use of a single rubric that would include all the outcomes and their respective performance indicators. In particular, 4 performance

levels were established for each indicator called "Bad", "Fair", "Good" and "Excellent".

2. An external evaluation comprised the co-advisor's evaluations in student internships or internships and the results of the SABER Pro tests, which were mapped to each of the proposed performance indicators.

Once the learning goals and corresponding performance indicators were established, a pilot attempt began in 2017 in 15 courses with 49 indicators. Several instances of the process were reformulated from this initial exercise to make this process sustainable, leading to the assessment during four semesters (years 2018 and 2019) with only 24 indicators.

Other criteria to adopt consisted of the level of "attainment" for which both programs considered that the objectives were achieved. In this sense, it was established that 70% of the students should reach the "Good" or "Excellent" levels for these skills to be considered as "satisfactorily achieved" within the process.

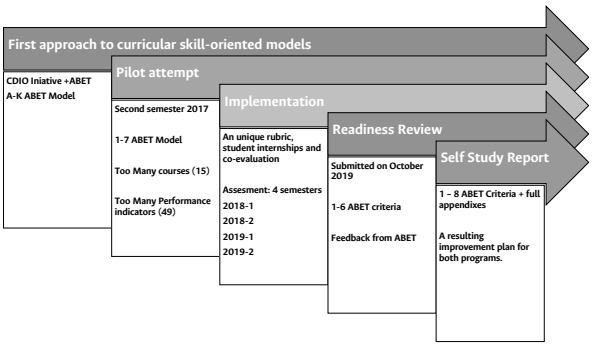

Figure 4. Timeline for the ABET Accreditation in Electrical and Electronics Engineering.

Source: Authors

The details of the subjects, the proposed curricular activities, and the evaluation tools used for each performance indicator can be consulted at ABET Electrónica (2020) and ABET Electrónica (2020).

Likewise, the detail of the rubrics used, as well as the results for each performance indicator and the mapping with the SABER Pro exam, can be consulted at ABET Electrónica (2020) y ABET Electrónica (2020).

Results of the ABET self-assessment

After the characterization was carried out for a period of four semesters, we proceeded to the analysis of each performance indicator and its corresponding assessment. Table 11 shows the main results for each learning goal (outcome). Some of these strengths and challenges will be discussed in the next section. However, beyond the results themselves, it is worth highlighting their particular nature. Unlike other accreditation models, including Colombia's national (CNA) accreditation, the tenor of the challenges earned is completely governable and deeply academic. These characteristics, which can be considered minor, are especially significant in our case. Consequently, the proposals for improvement plans emerging from this evaluation are, for the most part, developed by teachers in the curricular activities during their courses. These features facilitate the mitigation of the detected academic weaknesses since their improvement depends entirely on our intra-classroom academic work at the expense of other initiatives that are not necessarily governable. Details of the proposed action plans can be found in ABET Electrónica (2020) and ABET Electrónica (2020).

Table 11. Improvement opportunities per student outcome detected during the ABET assessment.

Outcome	Most relevant improvement opportunities
1	- Attainment level (70%) reached in internal assessment. - Need for improvement of modeling skills by considering uncertainty and incomplete information. - Based on Saber Pro tests, it was evident a low performance in interpreting information to tackle problems and formulating strategic solutions. - Engineering problems must consider a certain degree of multidimensionality in the solutions proposed by the students.
2	- Attainment level (70%) reached, except for the internal assessment of performance indicators PI-1 and PI2 in 2019. - Need to reinforce the ability to (i) formulate alternative solutions, (ii) identify constraints, (iii) assess design requirements compliance by considering societal, environmental, and economic aspects in the Colombian context. - Saber Pro test results show an attainment level lower than expected. (60%)
3	- Attainment level (70%) reached, except for the internal assessment of performance indicators related to oral communication in English. - Based on Saber Pro test results, a high proficiency level is observed in English written communication (B1 and B2). - Saber Pro test results show the need to reinforce argumentation capabilities, in non-technical documents in Spanish.
4	- Attainment level (70%) reached in internal assessment. - Based on both, Saber Pro test and results from the student internships, is important to work on ethical responsibilities recognition, which was previously suggested by alumni and employers. - Some improvement opportunities were detected such as (i) examining performance indicators that directly assess ethical issues and (ii) re-evaluating the courses where this kind of assessment is more suitable.
5	- Attainment level (70%) reached in internal assessment with outstanding results. - This performance is a mid-term result of the implementation of the COMFIE strategy, which included some related activities along the curriculum. - Actions must be taken to maintain good performances including not only co-evaluation but also hetero-evaluation during the assessment.
6	- Attainment level (70%) reached in internal assessment. However, Saber Pro test results show a lower attainment level than expected, so that, improvement is needed in the skills related to proposing models for forecasting purposes. - There is still a gap between (i) knowing and (ii) applying experimentation methods. This gap may be covered by including formal experimentation design theory in early lab courses and practices.
7	- Attainment level (70%) reached in internal assessment in 2018. - In 2019, some attainment levels were not reached. Consequently, some self-learning skills must be reinforced, in particular those related to (i) time management, (ii) study methods and (iii) learning goals planning. - Skills related to using reliable and pertinent information sources must be improved.

Source: Authors

ABET visit Experiences

A timeline of the processes carried out within the ABET accreditation in Electrical and Electronics Engineering is shown in Figure 4. As can be seen, the application for ABET accreditation begins with a step called *Readiness Review*, which took place in October 2019 and aims to determine if the programs are accreditable before the ABET accreditation agency.

Once this preliminary evaluation —where both programs were evaluated as *accreditable*— was passed, the self-assessment report for accreditation purposes was sent in June 2020. Subsequently, the visit took place on November 17-19, 2020, in virtual modality due to the COVID-19 pandemic. For this visit, the ABET agency appointed three peers, one of them as coordinator of the visit (Chairman) and a pair in charge of reviewing each program, all of them with excellent academic track records at top-level American universities and with extensive experience as peer reviewers in ABET accreditations.

Some of the most relevant experiences during this visit are the following:

- The visit began a month before the scheduled date. In this accreditation model, the review of the material by the peer reviewers begins one month before the formal date since early contact is established with the coordinating team by the Universidad Nacional de Colombia. During this period, the peer reviewers' concerns about the self-assessment reports sent were cleared up. It is understood that the formal visit constitutes the final part of this process, where interaction with other actors other than the coordinating team is achieved. This process ensured detailed knowledge by the peer reviewers of the self-assessment reports and, therefore, a very objective and rigorous evaluation of the curricular program.

- Due to the virtual modality, creating an adequately organized repository with evidence of achieving the learning goals was necessary. This evidence is made up of samples of work carried out by the students and their corresponding evaluation rubrics so that the evaluating peers can verify if the learning goals are being met. This exhaustive review of the evidence constitutes a differentiating element compared to national accreditation.

- It was necessary to "virtualize" numerous infrastructure spaces that the curricular programs have. More than 20 videos showed the curricular programs' teaching spaces, laboratories, and other academic spaces (Espacios-Físicos, 2020) have.

- Although the model was being implemented and most of the professors were already familiar with the process, the preparation for the visit among the teachers was very rigorous. To this end, numerous preparatory meetings were held to ensure that teachers fully knew the accreditation model as well as the processes of characterization of learning goals and their corresponding evaluation. Several virtual evaluation instruments were even developed to achieve adequate preparation.

- Aspects related to industrial safety in laboratories and, in general, in all academic spaces constituted a challenge for the program. Within this accreditation model, security in the facilities is as important as the learning goals, which constitutes a differentiating element concerning national accreditation models. To this end, several implementations were carried out regarding safety guides, signaling, and provision of equipment for the mitigation of occupational risks, fire, and, in particular, electrical risks in laboratory spaces.

- The evaluation and feedback times on the program are precise and mandatory. Once the visit is over, specific observations are provided on the weaknesses found in the program. It is noted that the program will have 30 days to demonstrate early improvement actions that reflect the program's commitment to their mitigation. These times are fully met and allow the program to keep real traceability of its continuous improvement process. Once these 30 days have elapsed, the program must have delivered the details of the actions undertaken for improvement. Six months later, the final decision on the accreditation of the curricular programs is received. In our case, at the beginning of August 2021, ABET officially decided that both programs were accredited from 2018 to 2023 in the case of Electronics Engineering and 2025 in the case of Electrical Engineering. In the case of Electronics Engineering, the accreditation was extended until 2025 after requested additional evidence was presented to the agency.

Future curricular challenges

Without a doubt, this international accreditation is the reward for a process that began more than ten years ago in a genuine effort to achieve curricular improvements in both programs. Several improvements have been achieved (See Table 11), and other improvement opportunities have been identified, highlighted in these final paragraphs.

One of the great strengths identified by the peer reviewers was being able to address the aspect of "Complex Problems in Engineering adequately". This aspect is formally defined in the ABET model, whose characteristics mainly involve interdisciplinary approaches to engineering problems. In this sense, the course Interdisciplinary Projects Workshop - TPI, whose implementation originates as a response to the principle of interdisciplinarity proposed during the 2007 Academic Reform, was recognized as the main strength of our curricular programs. This commitment to address real problems in our communities with widely multidisciplinary engineering approaches represents the right path toward comprehensive and socially relevant training.

On the other hand, one of the main challenges is formalizing the development of engineering design skills throughout the curriculum. Although there is a final design experience in both programs, there is still a need to develop additional work on developing design skills, not only in the last semesters but also throughout the curriculum in existing subjects, as is the case of the Engineering Workshops.

Another improvement opportunity consists of incorporating the aspect of *multidimensionality* in the engineering

problems addressed during the curriculum. For example, although the Interdisciplinary Projects Workshop already exists, only some of the problems addressed in this course are directly related to Electrical Engineering and Electronics Engineering. For this reason, it would be convenient to include this multidimensional approach where environmental, social, and cultural contexts are addressed in some of the typical disciplinary problems in the curriculum.

One of the improvement opportunities detected is related to the formal inclusion of *uncertainty* or missing *data* in formulating problems within our programmatic contents. In the case of Electrical Engineering, one of the requirements that must be worked on consists of the formalization of Probability and Statistics applications to purely disciplinary problems, which constitutes a unique opportunity to address the elements related to the concept of uncertainty.

Likewise, another of the opportunities for improvement is related to the formalization of concepts related to the theory of *Design of Experiments* and *Data Analysis*, which can be part of the thematic offer offered in some courses related to laboratory practices or free experimentation, as is the case of engineering workshops.

Finally, the curricular experiences described in this work are part of the collective effort of a group of professors concerned about curricular design and evaluation. A sample of this genuine interest represents the obtaining of the international ABET accreditation, for which scholarly and rigorous work of more than a decade was necessary for which there was never any obligation in response to an interest of the university government; on the contrary, the primary motivation consisted of an own initiative for the continuous improvement of our academic processes. For this reason, the authors of this article expressly thank all the Department of Electrical and Electronics Engineering faculty for this collective effort in commemorating its 60 years of existence. In the same manner, students, businessmen, graduates, and in general, the entire academic and administrative community that supported the different stages of this path.

CRediT author statement

All authors: Conceptualization, methodology, validation, formal analysis, investigation, writing (original draft preparation, review, and editing), data curation, supervision, project administration, resources, and funding acquisition.

References

ABET - Accreditation Board for Engineering and Technology (2021) *Setting The Standard Worldwide*, https://www.abet.org/accreditation/

Acuña, N., Díaz H., Ramírez-Echeverry, J.J. (2011). Integrating competence development into the curriculum - Engineering first year diagnostic and experience *IEEE EDUCON Education Engineering 2011*. Amman, Jordan. Apr. 4-6, 2011

Anderson, L. W. and Krathwohl, D. R. (Eds.). (2001). *A taxonomy for learning, teaching and assessing:* A revision of Bloom's Taxonomy of educational objectives: Complete edition, New York: Longman.

Area Curricular de Ingeniería Eléctrica y Electrónica (2013). PEP- Proyecto Educativo del Programa Ingeniería Eléctrica - Sede Bogotá *Dirección Nacional de Programas de Pregrado*. http://www.pregrado.unal.edu.co/docs/pep/pep_2_15.pdf

Area Curricular de Ingeniería Eléctrica y Electrónica (2013). PEP- Proyecto Educativo del Programa Ingeniería Electrónica - Sede Bogotá *Dirección Nacional de Programas de Pregrado*. http://www.pregrado.unal.edu.co/docs/pep/pep_2_45.pdf

Área Curricular de Ingeniería Eléctrica e Ingeniería Electrónica. Espacios físicos de los Programas de Ingeniería Eléctrica e Ingeniería Electrónica de la Universidad Nacional de Colombia - Sede Bogotá, 2020, https://ingenieria.bogota.unal.edu.co/es/formacion/pregrado/ingenieria-electronica.html#info-espacios

Consejo Académico (2008). Acuerdo 223 de 2008 *Por el cual se modifica la estructura del plan de estudios del programa curricular de Ingeniería Electrónica de la Facultad de Ingeniería de la Sede Bogotá de la Universidad Nacional de Colombia, para ajustarse al Acuerdo 033 de 2007 del Consejo Superior Universitario*. Noviembre de 2008. http://www.legal.unal.edu.co/rlunal/home/doc.jsp?d_i=34432

Consejo Académico (2008). Acuerdo 248 de 2008 *Por el cual se modifica la estructura del plan de estudios del programa curricular de Ingeniería Eléctrica de la Facultad de Ingeniería de la Sede Bogotá de la Universidad Nacional de Colombia, para ajustarse al Acuerdo 033 de 2007 del Consejo Superior Universitario*. Noviembre de 2008. http://www.legal.unal.edu.co/rlunal/home/doc.jsp?d_i=34469

Consejo Académico (2020). Acuerdo 181 de 2020 *Por el cual se modifican los objetivos educativos del programa curricular de Ingeniería Eléctrica de la Facultad de Ingeniería de la Universidad Nacional de Colombia, Sede Bogotá*. Mayo de 2020. http://www.legal.unal.edu.co/rlunal/home/doc.jsp?d_i=95468

Consejo Académico (2020). Acuerdo 182 de 2020 *Por el cual se modifican los objetivos educativos del programa curricular de Ingeniería Electrónica de la Facultad de Ingeniería de la Universidad Nacional de Colombia, Sede Bogotá*. Mayo de 2020. http://www.legal.unal.edu.co/rlunal/home/doc.jsp?d_i=95469

Crawley, E.F., Malmqvist, J., Ostlund, S., Brodeur, D.R., Edstrom, K. 2006. *Rethinking Engineering Education. The CDIO Approach*. ISBN-13: 978-1441942609. Springer. First Edition.

CSU - Consejo Superior Universitario (2007). *Acuerdo 033 de 2007*. http://www.legal.unal.edu.co/rlunal/home/doc.jsp?d_i=34245.

Diamond, Robert M. (2005). Designing and Assessing Courses and Curricula: A Practical Guide. *Jossey-Bass*

Díaz, Hernando. (2008). ¿Cuáles competencias requieren los Ingenieros?. ¿Cuáles enfatiza la Universidad?. *Departamento de Ingeniería Eléctrica y Electrónica*, 2008.

DIRNALPRE - Dirección Nacional de Programas de Pregrado de la Universidad Nacional de Colombia. (2012). Guía para consolidar el Proyecto Educativo de Programa - PEP. http://www.pregrado.unal.edu.co/docs/acreditacion/general/Guia_PEP_2012.pdf.

Electrical and Electronics Engineering Department (2020). *ABET Self-study report for the Electrical Engineering Program*. June 2020. School of Engineering. Bogotá Campus. Universidad Nacional de Colombia

Electrical and Electronics Engineering Department (2020). *ABET Self-study report for the Electronics Engineering Program*. June 2020. School of Engineering. Bogotá Campus. Universidad Nacional de Colombia

Gallego, Luis. (2011). The CDIO Approach: Implementation in Electrical and Electronics Engineering Curricula. *The North American CDIO International Meeting - Innovations in Engineering Education Pedagogy*. Naval Postgraduate School Stanford University Oct. 17-19, 2011

Kennedy, Theodore (2006). The "Value-Added" Approach to Engineering Education: An Industry Perspective *The Bridge- National Academy of Engineering*, Vol 36, pp 14-16.

Mejía Umaña, A. (2011). *Ingeniería Eléctrica en la Ciudad Universitaria. Cincuenta Años Realizando Sueños* (Primera Edición). pág 7. https://ingenieria.bogota.unal.edu.co/images/userupload/640/50AC3B1os_realizando_sueC3B1os_fe38f.pdf

National Academy of Engineering. (2005). Educating the Engineer of 2020: Adapting Engineering Education to the New Century. *NAE - National Academy of Engineering*, National Academies Press

Tadmor, Zehev (2006). Redefining Engineering Disciplines for the Twenty-First Century. *The Bridge-Washington-National Academy of Engineering*, Vol 36(2), 33-37.

The Boeing Company (1996) Desired Attributes of an Engineer: Participation with Universities. *Available at http://www.boeing.com/companyoffices/pwu/attributes/attributes.html*

Vest, Charles. (2006). Educating Engineers for 2020 and Beyond. *The Bridge - National Academy of Engineering*, Vol 36 , pp 38-47.

Vicerrectoría Académica (2012). Guía para consolidar el Proyecto Educativo del Programa - PEP *Dirección Nacional de Programas Curriculares de Pregrado*. Septiembre de 2012. http://www.pregrado.unal.edu.co/docs/acreditacion/general/Guia_PEP_2012.pdf

World Chemical Engineering Council - WCEC. Secretariat c/o DECHEMA e.V. (2004). Survey of experienced and newly employed chemical engineers. *How does chemical engineering education meet the requirements of employment ?*, Technical report, September 2004.

Wulf, W.A. (1998). The Urgency of Engineering Education Reform. *The Bridge - National Academy of Engineering*, Vol 28., pp 48.

https://doi.org/10.15446/ing.investig.101200

Women at the Faculty of Engineering of Universidad Nacional de Colombia, Bogotá Campus: History, Present, and Future

Las mujeres de la Facultad de Ingeniería de la Universidad Nacional de Colombia, sede Bogotá: historia, actualidad y futuro

María Alejandra Guzmán-Pardo[1] and Liz Karen Herrera-Quintero[2]

ABSTRACT

The Faculty of Engineering of Universidad Nacional de Colombia (UNAL) has a rich and complex history, which is inexorably linked to the convulsed history of Colombia. This article seeks to give visibility to the participation and historical contributions of women in the growth and development of the Department of Engineering throughout its 161 years of existence, as well as to recognize their contributions with the names of their protagonists, in order to honor their struggles and achievements in favor of women's rights in the country. This article also shows data and testimonials that reflect the significant gender gaps that still persist in the Faculty, it characterizes the women who are part of the academic community in their roles as students, professors, researchers, and directors, it lists the actions undertaken as institutional policies for closing gender gaps, and it proposes future measures to be implemented.

Keywords: women in engineering, history of the School, gender gap

RESUMEN

La Facultad de Ingeniería de la Universidad Nacional de Colombia (UNAL) cuenta con una rica y compleja historia, unida inexorablemente a la convulsionada historia de Colombia. Este artículo busca visibilizar la participación y las contribuciones históricas de las mujeres en el crecimiento y desarrollo de la Facultad de Ingeniería en sus 161 años de existencia, así como reconocer sus aportes con el nombre de sus protagonistas, en aras de honrar sus luchas y conquistas en favor los derechos de las mujeres en el país. El artículo también muestra cifras y testimonios que reflejan las significativas brechas de género que aún persisten en la Facultad, hace una caracterización de las mujeres que hacen parte de la comunidad académica en sus roles de estudiantes, profesoras, investigadoras y directivas, enumera las acciones emprendidas como política institucional para cerrar las brechas de género y propone acciones futuras a implementar.

Palabras clave: mujeres en ingeniería, historia de la facultad, brecha de género

Received: February 22th, 2022
Accepted: March 4th, 2023

Introduction

The Faculty of Engineering of Universidad Nacional de Colombia (UNAL) has a profound and complex history, which is inexorably linked to the last two centuries of Colombia's convulsed history. The origins of the Faculty date back to 1848, with the creation of the Military College, sponsored by General Tomás Cipriano de Mosquera. The political pugnacity that characterized this time had a great impact on the Military College's fate, which was closed in 1854 and thus remained until General Mosquera, once again in power, issued a decree on August 24, 1861, which restored the College and founded the Polytechnic School. This date is recognized by historians as the creation of the Faculty of Engineering, only four decades after the Republic of Colombia gained independence from the rule of the Spanish empire. Therefore, the foundation of the Faculty is considered to be one of the first successful projects of the fledgling Republic to change the state of affairs inherited from colonial times.

Nowadays, the Faculty offers nine undergraduate programs, four specializations, 16 Master's programs, and eight doctoral programs. Thus, it harbors more than 7 5000 students, 278 full professors, 92 administrative employees, and invaluable collaborators. It is thanks to all members of this community that, as of 2023, this is still the most important and representative Faculty of Engineering in Colombia, given its tradition, its prestige, its public nature, the quality of education offered, and the human and professional quality of more than 40 0000 men and women engineers who call themselves *alumni*.

During the Faculty's first 80 years, sociocultural conditions radically hindered access by both young and adult women as students or professors, so, until the 1930s, this was an all-male Faculty. The story of women in the Faculty

[1]Mechanical engineer, Universidad Nacional de Colombia, Colombia. PhD Mechanical engineer, Universidade de Sao Paulo, Brasil. Affiliation: Dean Faculty of Engineering, Universidad Nacional de Colombia, Colombia. E-mail: maguzmanp@unal.edu.co
[2]Materials engineering, Universidad de Antioquia, Colombia. MSc Engineering, Universidad de Antioquia, Colombia. PhD Materials Science, Universidad de Sevilla, España Affiliation: Associate Professsor, Universidad Nacional de Colombia, Colombia. E-mail: lkherreraq@unal.edu.co

How to cite: Guzmán M.A., Herrera L.K. (2023). Women at the Faculty of Engineering of Universidad Nacional de Colombia, Bogotá Campus: History, Present, and Future. *Ingeniería e Investigación*, *43*(2), e101200. https://doi.org/10.15446/ing.investig.101200

only began in 1943, with the admission of the first two women students. Throughout the following eight decades, women have been gaining terrain as students, professors, researchers, and executives. Despite this, the Faculty is still the most masculinized in UNAL (Quintero, 2016).

Several studies have concluded that the absence of women role models is one of the reasons why girls and female teenagers do not choose careers in engineering as life options (Oliveros *et al.*, 2016; Bello, 2020; Olmedo-Torre *et al.*, 2018; Dulce-Salcedo *et al.*, 2022). Thereupon, this article seeks to provide visibility to the historical participation and contribution of women to the Faculty of Engineering's growth and development, acknowledging their contributions by name in order to honor their struggles and victories in support of women's rights in the country.

In recognition of the women that make up the Faculty's current community, this article presents a characterization of the women students, professors, and researchers of the last 10 years, with the aim to evince the immense gender gaps that still remain. Likewise, this work aims to highlight the actions undertaken by the Faculty as policies to foster gender equality.

The objective of this paper is to provide visibility to the drive, leadership, and contributions of women, who have managed to become role models for our academic community and our country, in the construction and development of UNAL's Faculty of Engineering. To this effect, this article is organized as follows. In the section pertaining to students, a brief review is made regarding the history of the presence of women as students in the Faculty; by means of testimonials and statistical figures, historical gender gaps are evidenced, and data types are shown, disaggregated by sex, which are provided by institutional information systems, thus allowing to characterize the current students. In the section dedicated to teachers, a historical review is included which highlights the first women teachers in each Faculty department, showing the figures that evidence the gender gaps in academia, and characterizing the current teachers based on institutional data. The section pertaining to women executives highlights the women who have held leadership and directorship positions in the Faculty. This section shows the figures that evidence the contribution of women teachers as leaders in research and extension projects. The section addressing the gender gaps in the Faculty allows identifying, with the help of figures, the issues that still remain in the Faculty. The last section highlights the measures taken during the last 10 years in the Faculty of Engineering which have been aimed at mitigating the existing gender gaps and proposing future actions. Finally, conclusions are presented.

With this general view of the history of women's participation in the strengthening of the mission functions of the Faculty, we seek to provide visibility, by means of data, to the female population's own nature, showing the role of women in engineering programs and contributing to a documented gender perspective in order to draw lines of future action in the Faculty.

The students

The record regarding the first two women admitted as students in the Faculty dates back to 1943. Their names are Guillermina Uribe Bone and Rosalba Pachón Gómez. Eng. Uribe received her degree as a Civil Engineer on December 18, 1948, being the Faculty's first female graduate (Mayor Mora, 2011).

With the creation of new academic programs, other young women were motivated to attend engineering programs. Some of these programs' women alumni were María Stella Miranda González, civil engineer, 1967; Alicia Salazar Jaramillo, electrical engineer, 1970; Carmen Aminta Moreno, chemical engineer, 1971; Blanca Cecilia López Rico, electrical engineer, 1973; Fanny Villamizar Copete, agricultural engineer, 1975; María Rozo Méndez, agricultural engineer, 1976; Leticia del Carmen Gil Caraballo, mechanical engineer, 1979; María Constanza Parra Bohorquez, mechanical engineer, 1983; Elvira Elena Polo de la Barrera, systems engineer, 1985; Diana María Rojas Ordus, electronics engineer, 2003; Nohora Rodríguez, industrial engineer, 2006; and Jennifer Paola Corredor Gómez, mechatronics engineer, 2008.

The path paved by these valuable pioneers was not without obstacles. The almost absolute masculinization of the Faculty, in addition to the traditional exclusion of women in these areas (Quintero, 2016) caused situations of discrimination to be normalized for decades. These include those mentioned by engineers Guillermina Uribe Bone during an interview (Mayor Mora, 2011) and Alicia Salazar Jaramillo and Victoria Beatriz Durán in the discussions held with the first women alumni, within the framework of the celebration of the Faculty of Engineering's 160th anniversary (FI-UNAL, 2021a).

According to Guillermina Uribe Bone's testimonial (Mayor Mora, 2011, p. 203), "she found most of her teachers very kind and fiendly, but socially distant, as they made her feel that engineering was not for women".

Eng. Salazar (FI-UNAL, 2021a) said: "when the program's actual subjects began, I always found myself alone. I had teachers who found it funny that a woman was studying the program. I also had teachers who told me... The Electrical Machines professor - I won't forget - told me one day that he did not understand why women meddled in the field of men, and I answered: 'because you're a rebel when you're young, and the program doesn't belong to you; it belongs to science'. Of course, I failed Machines. Twice."

On her part, Eng. Durán recounts (FI-UNAL, 2021b): "I always chose the Faculty of Sciences or the Faculty of Engineering to have a cup of coffee because there were women's bathrooms. Meanwhile, in Engineering, they were notoriously absent. (...) It was terrible because there were men's bathrooms, but it seemed as though women didn't need any bathrooms". This situation continued for decades, as recounted by systems engineer Liz Jeannete Cubillos (2022, personal communication, January 26, 2022): "in the early 80s, in the facilities of the Faculty of Engineering, there were no women's bathrooms. We usually had to go to the Architecture Building. Of course, from Engineering's Old Building, it was wasy to get there, but it was a long way off from the New One. So, given the need, we made groups with the girls at that time, the largest groups were composed of the students of systems and chemical engineering (we were upt to ten per semester), and we talked and said that we needed a bathroom, and that one of the two bathrooms next to the A, B, and C auditoriums of Building 453 should

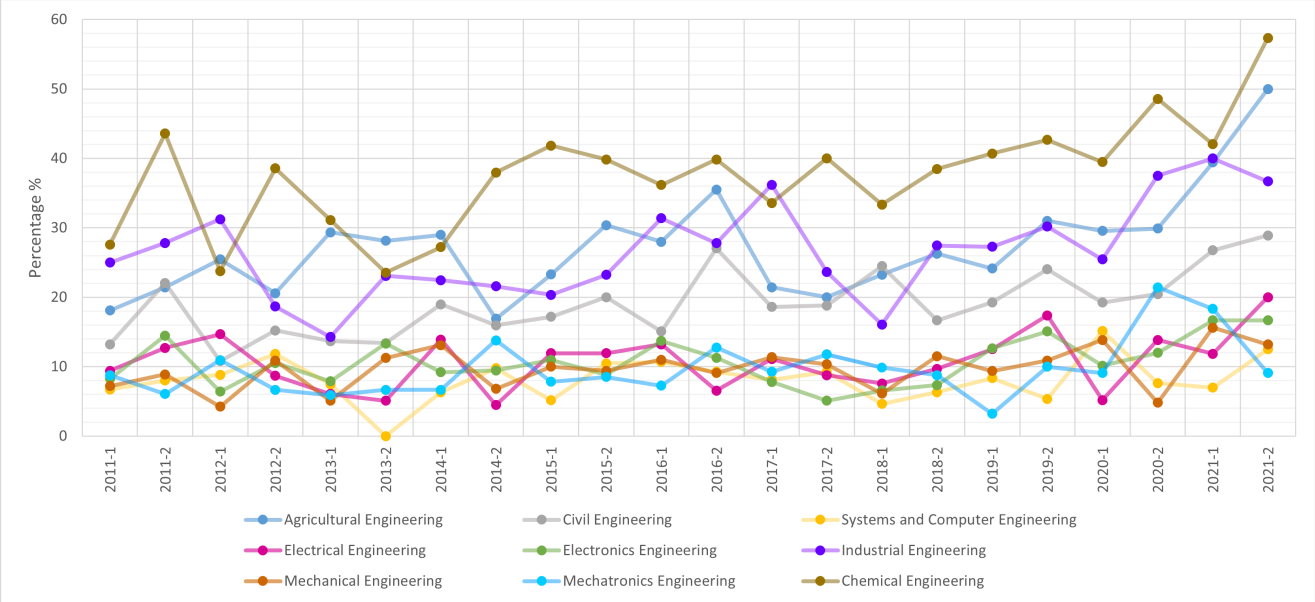

Figure 1. Percentage of women admitted to Faculty programs between 2011-1 and 2021-2
Source: Authors, based on the information recorded in the DNINFOA (2021) reports

be ours. Then, we decided to *seize* the bathroom. That meant painting the door pink and hanging signs saying it was a women's bathroom. And we started to go into this bathrooms and tell the cleaning ladies that it was ours. We went to the bathroom in groups after we got out of class, and, if we found a man there, we whistled at him and got him out. So, we started telling all the girls that we should use the bathroom, that it was ours and that we had the right, and so we made it. Within a semester, we managed to appropriate the bathroom, and it became a fact that that bathroom belonged to us women."

As another act of discrimination that has been normalized and therefore socially accepted, until the 1970s, the Faculty of Engineering granted its women graduates the title of *ingeniero* (engineer, with a masculine ending in Spanish). It was thanks to the lonely battle waged by student Blanca Cecilia López Rico that the title of *ingeniera* was first granted in 1973. In her case, it was *ingeniera electricista* (electrical engineer).

Countless battles and conquests such as these are part of the Faculty's history, and it is thanks to these struggles for women's rights that the Faculty of Engineering today holds a place of honor in the history of education and the practice of engineering in Colombia.

As of 2023, the participation gap between men and women in the Faculty is still significant. According to the information provided by the Planning Directorate of UNAL's Bogotá Campus (UNAL, 2021a), the Faculty has 1 482 women and 5 612 men as active undergraduate students, and 169 women and 472 men as active graduate students. These figures evince participation gap between men and women as students of the Faculty. In the undergraduate programs, only 20,89% of the students are women, and in the graduate programs, this percentage goes down to 26,3% (UNAL, 2021a).

Figure 1 shows the percentage of female students admitted to the programs of the Faculty between the 2011-01 and 2021-02 semesters. In turn, Figure 2 presents the amount of men and women graduated from the Faculty between 2012-1 and 2021-2. Table 1 shows the average percentage of men and women graduates per program within the analyzed time interval.

Figure 1 identifies two program groups as a function of the percentage of admitted women. With figures higher than 11% are the Civil, Agricultural, Industrial, and Chemical Engineering programs. With percentages lower than 11% are the Electrical, Electronics, Mechanical, Mechatronics, and Systems and Computer Engineering programs.

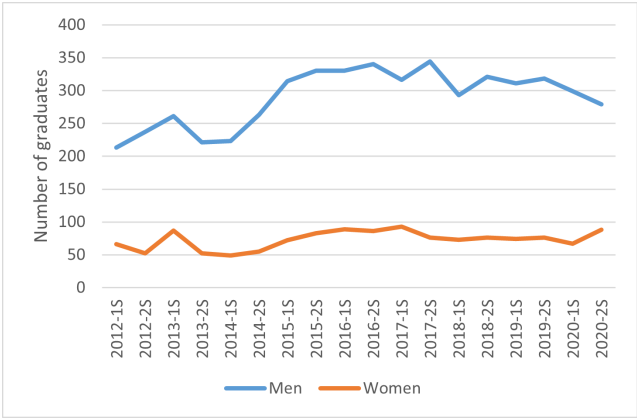

Figure 2. Number of graduates by gender between 2012-1 and 2020-2
Source: Authors, based on the information recorded in the reports provided by DNINFOA (2021)

In Figure 2, it can be seen that the number of women graduates is proportional to the percentage of admitted women. On average, during the analyzed time window, 20% of the undergraduate curricular programs' alumni were women.

Table 1 shows the marked difference between the percentages of men and women graduates. The programs

Table 1: Average percentage between men and women graduated from each program of the Faculty of Engineer between 2012-1 and 2021-2

Program	Women [%]	Men [%]
Agricultural Engineering	37	63
Civil Engineering	21	79
Systems and Computer Engineering	8	92
Electrical Engineering	12	88
Electronics Engineering	12	88
Industrial Engineering	27	73
Mechanical Engineering	7	93
Mechatronics Engineering	8	92
Chemical Engineering	41	59

Source: Authors, based on the information recorded in the reports provided by DNINFOA (2021)

closer to parity are Chemical Engineering and Agricultural Engineering. The greatest inequality is found in the Mechanical, Mechatronics, and Systems and Computer Engineering programs. This behavior follows a similar trend to that of Figure 1, which shows the percentage of admitted women per program.

Producing relevant information and statistical data disaggregated by sex is fundamental and essential to analyzing the causes of gender inequality (PNUD *et al.*, 2017). As stated by Navi Pillay,a United Nations High Commissioner for Human Rights (2008-2014) (PNUD *et al.*, 2017, p. 19) "more than treasuring what we measure, it is necessary to measure what we measure", which is why this paper highlights the advances made by UNAL in this regard, and it shows some of the statistical data disaggregated by sex that are available in the institutional information systems.

Some average socioeconomic and academic characteristics of the students who have successfully completed their studies are shown in Figures 3a, 3b, 4a, 4b, and 4c.

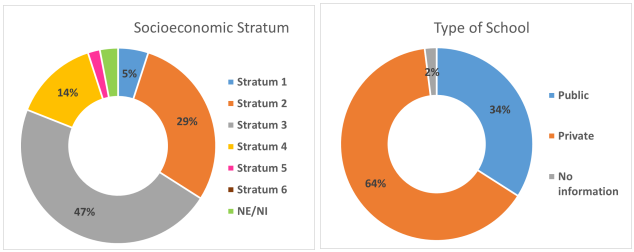

(a) Socioeconomic status **(b)** School type

Figure 3. Characterization of women alumni between 2012-1 and 2021-2 by (socioeconomic) stratum and school type
Source: Authors, based on the information recorded in the reports provided by DNINFOA (2021)

Figures 3a and 3b show that, in the analyzed time window, most Faculty alumni belonged to socioeconomic strata 2 and 3 and came from private schools.

Figure 4 shows that most students graduated between 23 and 24 years old. Figures 4b and 4c show that only 8% of the alumni attended the study plan in the expected time (ten semesters), and most students attended their corresponding program in 11-13 semesters and obtained academic averages between 3,8 and 4,1.

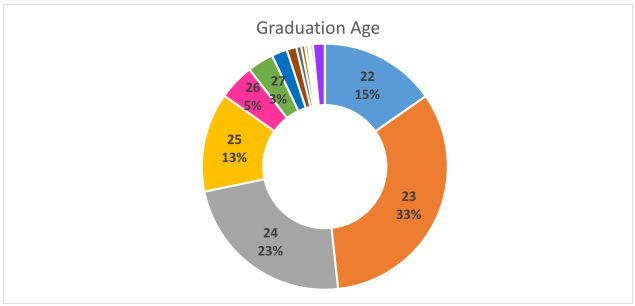

(a) Graduation Age

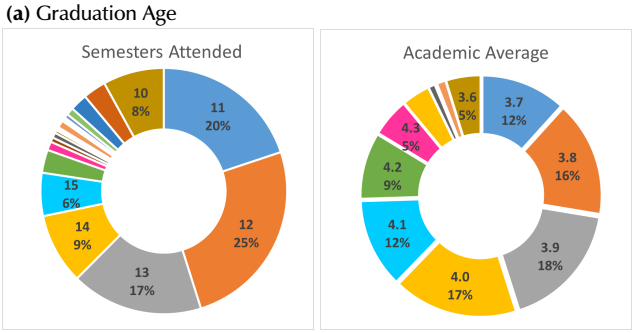

(b) Semesters attended **(c)** Academic average obtained

Figure 4. Characterization of women alumni between 2012-1 and 2021-2 by age, semesters attended, and academic average
Source: Authors, based on the information recorded in the reports provided by DNINFOA (2021)

The professors

The incursion of women as teachers of the Faculty of Engineering started at the end of the 60s, with the employment of chemical engineer Elena Pineda Gutiérrez (1969). As the program offering grew in the Faculty, and with different dynamivs in each department, the employment of women teachers increased. Some of the first teachers attached to the different departments and programs were Fanny Villamizar, who joined the Agricultural Engineering program in 1977; Estrella Esperanza Parra López, linked to the Electrical Engineering program since 1980; Victoria Beatriz Durán (1975) and Luz Amanda Salazar (1979), linked to the Civil Engineering program; Dolly Santos Barbosa and Angela Quintero, linked to the Chemical Engineering program since 1990; and María Alejandra Guzmán Pardo, linked to the Mechanical Engineering program since 1997.

The total number of professors attached to the Faculty has remained constant in the last decade. Currently, outr of the 278 full-professors, 35 are women. Figure 5 shows the amount of women teachers attached to the Faculty, disaggregated by category, between 2012 and 2020. Even though the data show a moderate increase in the percentage of Faculty women teachers, going from 8,9 to 12,5%, the employment gap between men and women is still very wide.

As for the schooling level, according to the information provided by the Bogotá Campus Planning Directorate of UNAL (2021a), 77,1% of the Faculty's women professors have a PhD degree - the average percentage of Bogotá Campus teachers with a PhD is 52,15%, and that of the Faculty of Engineering is 57,64%.

Women executives

Women teachers have contributed to the planning, development, and governance of the University and the Faculty, serving as executives in academic-administrative positions.

Table 2: Women teachers of the Faculty in academic-administrative positions between 2012-1 and 2021-2

Name	Position	Start - End
Claudia Patricia Pérez Rodríguez	* National Research and Laboratories Director	10/05/2018 8/02/2019
	* Research and Extension Vice-Dean	5/09/2012 9/05/2018
María Alejandra Guzmán Pardo	* Director of the Mechanical and Mechatronics Curricular Area	11/08/2011 19/07/2012
	* Academic Vice-Dean	21/07/2016 14/06/2018
	* Dean of the Faculty of Engineering	01/09/2018 Present
Dolly Santos Barbosa	*Faculty Director of Welfare	21/06/2012 20/07/2016
Carol Andrea Murillo Feo	* Director of the Department of Civil and Agricultural Engineering	2/07/2010 14/06/2012
	* Director of the Department of Civil and Agricultural Engineering	1/07/2016 12/06/2018
Sandra Liliana Rojas Martínez	* Director of the Department of Systems and Industrial Engineering	22/11/2016 12/06/2018
	* Faculty Director of Welfare	3/07/2018 4/07/2019
Ruth Janneth Lancheros Salas	* Director of Department of Chemical and Environmental Engineering	3/07/2018 30/10/2022
Caori Patricia Takeuchi Tam	*Director of the Department of Civil and Agricultural Engineering	19/06/2018 14/07/2019
Carolina María Sánchez Sáenz	*Director of the Civil and Agricultural Engineering Curricular Area	14/01/2021 5/09/2022
Jenny Marcela Sánchez Torres	* Director of the Systems and Industrial Engineering Curricular Area	3/07/2018 1/02/2022
	* National Research and Laboratories Director	3/03/2022 Present
Gloria Margarita Varón Durán	*Director of the Electrical and Electronics Engineering Curricular Area	3/07/2012 20/07/2016
Sonia Esperanza Monroy Varela	*Director of the Extension and Research Institute (IEI)	21/01/2015 19/06/2018
Angela Celmira Barrera Puerto	*Advisor to the Bogotá Campus Vice-Principal	2/08/2021 Present
Gloria Inés Beltrán Calvo	* Faculty Director of Welfare	4/07/2019 5/10/2020
Liz Karen Herrera Quintero	* Coordinator of the University's National Laboratories Division (UNALab)	01/11/2019 Present
	* Coordinator of the Permanent Faculty Seminar	01/08/2018 Present
Libia Denise Cangrejo Aljure	Director of the Department of Systems and Industrial Engineering	01/12/2022 Present

Source: Authors, based on the information of DNINFOA (2022a)

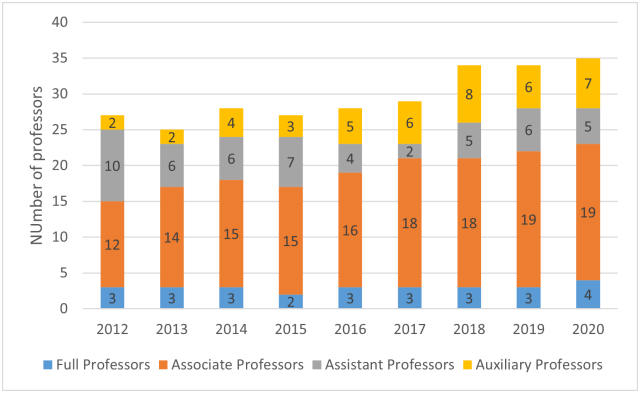

Figure 5. Amount of Faculty women teachers (2012-2020)
Source: DNINFOA (2022a)

In its 161 years of history, three women have occupied the Dean's office, the highest management position of the Faculty. They are:

- Victoria Beatriz Durán Betancourt, civil engineer, who graduated in 1975 from UNAL's Faculty of Mines, Medellín Campus. Her term as dean started in 1990 and ended in 1994.
- Luz Amanda Salazar Hurtado, civil engineer, who graduated in 1972 from UNAL's Faculty of Engineering and Architecture, Manizales campus. Her term as dean started in 2000 and ended in 2002.
- María Alejandra Guzmán Pardo, mechanical engineer, who graduated in 1996 from UNAL's Faculty of Engineering, Bogotá Campus. Her term as dean started in 2018, and she is still in office.

Other women professors who have stood out in management positions in the last ten years are shown in Table 2.

As seen in Table 2, in the last ten years, 15 women professors have occupied management positions in the Faculty and the University, *i.e.*, 42,85% of women professors have participated in the construction and execution of the Faculty's action plans, as well as in its governance, assuming leadership roles.

Women leaders in research and extension projects

Next, this section analyzes women participation in research and extension by women in the Faculty of Engineering during the last ten years.

As for research work in the Faculty of Engineering, there is progress in the number of female professors leading projects between 2005 and 2020, with a significant increase specifically during 2019-2020 (Figure 6).

Figure 7 shows a classification of female professors of the Faculty according to the last three Minciencias calls. A rise in rank is observed for female professors (from associate researcher to senior researcher), which is an indicator of the increased academic and research productivity of women in the Faculty of Engineering.

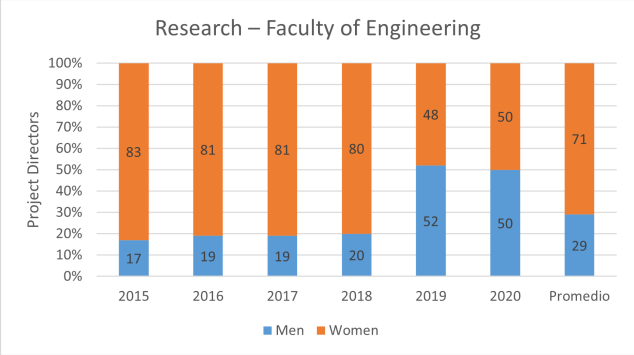

Figure 6. Research project directors, 2005-2020
Source: Authors, based on the information of the HORUS system (UNAL, 2021b)

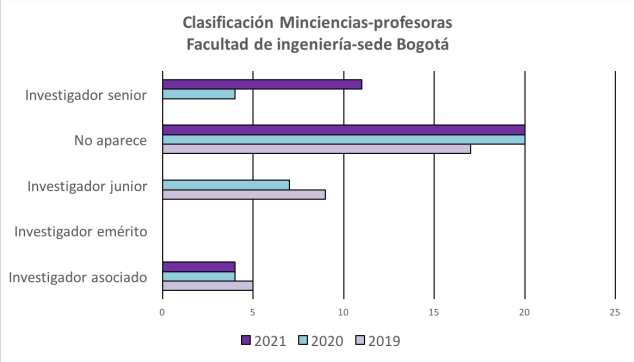

Figure 7. Female researcher classification for UNAL's Faculty of Engineering
Source: Authors, based on the information of the Research and Extension Vice-Principalship of UNAL's Faculty of Engineering

As for the participation of female professors in extension, Figure 8 shows the percentage of professors who led or took part in teams developing extension projects. A very low participation by female professors in this regard is evidences.

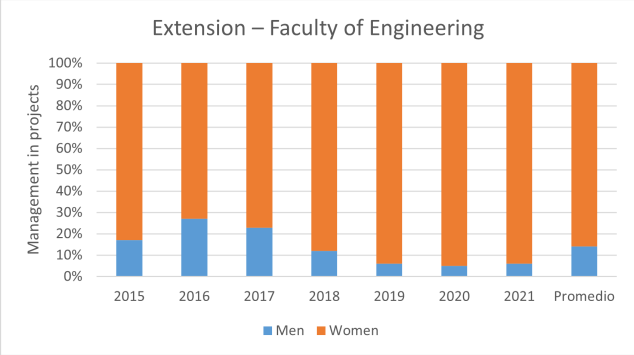

Figure 8. Extension project directors of the Faculty of Engineering, Bogotá Campus
Source: Authors, based on the information of the HORUS system (UNAL, 2021b)

Gender gaps in the Faculty of Engineering

A gender gap is a measurement of the distance between men and women with regard to an indicator. In the previous sections, it has been evinced that the number of male students in the Faculty is four times higher than that of women. Female professors represent only 12,5% of the Faculty's full-professors. Similar percentages are found when analyzing the participation of women as directors of research and extension projects, as well as in high administrative offices. All of the above demonstrate the existence of gender gaps in the Faculty of Engineering..

This situation is far from being exclusive to UNAL's Faculty of Engineering. Around the world, the gaps in the STEM areas (science, technology, engineering, and mathematics) are remarkable. According to UNESCO (2019), during the 2014-2016 period, at a global level, the average participation of men, specifically in fields such as information and communication technologies and engineering, manufacturing, and construction, significantly surpasses that of women (Figure 9).

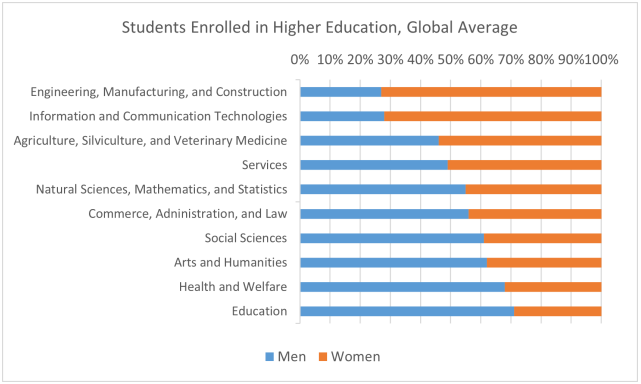

Figure 9. World average of student participation in higher education by sex and field
Source: Authors, based on data from UNESCO (2019)

Figure 9 shows that, in the fields of engineering, technology, and construction, 27% of students are women; in the case of information and communication technologies, 28% are women. According to the data published by UNESCO's Statistics Institute (Bello, 2020), as of 2019, the percentage of women researchers was 29,3%, and only 3% of the Science Nobel Prizes had been awarded to women.

In light of a situation taking place all around the world, why should the gender gaps in the field of engineering and in UNAL's Faculty of Engineering be addressed?

As stated by María Noel Vaeza (UNESCO, 2019, p. 7),

"It is often said that professional careers in STEM are the jobs of the future, in order to foster sustainable development; these are not only useful to boost innovation, but also social welfare and inclusive growth. According to data of UNESCO's Statistics Institute, a person working in STEM earns two thirds more than people employed in other fields. Despite their relevance, women have been persistently under-represented in several STEM fields.

Providing women with equal opportunities to develop and thrive in STEM careers helps to reduce the gender wage gap, improves women's economic safety, guarantees a diverse and talented workforce, and prevents biases in these fields and in the products and services elaborated within them."

In our country, despite the advances made in recent decades, closing the gender gaps in engineering faculties is still not regarded as a priority, as shown by the results of the

Colombian Engineering Departments Association's Survey on the Perception of Services (ACOFI, 2021), where 120 deans and 29 officers of Colombian Faculties of Engineering took part. According to this survey, promoting women's access to engineering programs ranks seventh in the list of priorities, below issues such as curriculum and pedagogy analysis, the use of digital technologies, teaching staff qualification, access by vulnerable populations, and student mobility.

What has been done in the Faculty?

Although there have been important sociocultural changes in Colombia and the world since 1943, when the first two women were admitted as students of the Faculty, there is still much to be done. The Faculty is still deeply masculinized, and it is still a long way off from parity.

Gender equality as an institutional concern from the Faculty's management was evidenced in professor José Ismael Peña's deanship (2012-2018). During the three terms of his administration, the Academic Vice-Deanship, the Research and Extension Vice-Deanship, the management of the Extension and Research Institute, the Welfare Directorate, and the management of the Department of Civil and Agricultural Engineering were led by women in different terms, all of them representing leader female voices and with a capability to make decisions in the Faculty Council. Another initiative was the creation of the video series *Andrea y la ingeniería* (Andrea and Engineering), which are available on Youtube and are aimed at Colombian girls and female teenagers, in order for them to recognize engineering careers as an opportunity for professional and personal development (FI-UNAL, 2015). On the other hand, the radio show *Ingeniería y nación* (Engineering and Nation) was created, which is transmitted weekly via UN Radio and has dedicated many broadcasts to providing visibility to the women in the Faculty.

Starting in 2018, closing the gender gaps has been a priority for the Faculty's management. For the first time since it was created, the management of the Department of Chemical and Environmental Engineering would be led by a woman, professor Ruth Janeth Lancheros Salas. Profs. Sandra Liliana Rojas Martínez and Gloria Inés Beltrán Calvo have been Directors of Welfate in the Faculty, and professors Carolina María Sánchez and Marcela Sánchez Torres have been at the forefront of the Civil and Agricultural Engineering and the Systems and Industrial Engineering Curricular Areas, respectively. Prof. Liz Karen Herrera is the coordinator of the Permanent Faculty Seminar, and professor Libia Denis Cangrejo is the director of the Department of Systems and Industrial Engineering.

During 2019, with the collaboration of female experts in gender issues attached to the WICA organization (Women in Concrete), workshops were conducted with Faculty professors on gender equality, while also aiming to disseminate the *Protocolo para la prevención y atención de casos de violencias basadas en género y violencias sexuales* (Protocol for the prevention and attention of cases involving gender and sexual violence) (UNAL, 2017), with the participation of 110 professors.

Between 2018 and 2020, and up until there were face-to-face classes on the campus, which were interrupted by the COVID-19 pandemic, in the digital billboards distributed in Faculty spaces, campaigns were permanently disseminated which were related with gender equality and non-violence against women.

In 2020, in collaboration with executives, men and women professors, and students of UNAL's Faculty of Engineering, Faculty of Mines, and Tumaco Campus, and with the support of the Research and Extension Vice-Principalship, the Thinktank for the Strengthening of Leadership and Empowerment of Colombian Women in STEM Areas (CPMC), managed by the Dean of the Faculty of Engineering.

Figure 10 summarizes some of the actions undertaken by the Thinktank, which has managed to visibilize and implement actions with a gender focus in the Bogotá Campus, the Medellín Campus, and the Tumaco Campus. UNAL's thinktanks are associations of researchers from diverse areas of knowledge and social actors, who, via research, academic debate, the production of documents, and the interaction with strategic sectors and problems of the national reality, define and influence, upon the basis of their networking, the evaluation and formulation of public policies (UNAL, 2022b). The objective of this Thinktank is to strengthen leadership and empower Colombian women in the areas of science, technology, engineering, and mathematics, by means of spaces for discussion and research aimed at designing roadmaps that allow to articulate initiatives and develop public policies at the regional and national levels, empowering women in education and science.

In 2019, as an initiative of the Faculty of Engineering, which was led by professor Elizabeth León Guzmán, the Prototype Business Intelligence System for Monitoring the Scientific and Technological Capabilities of Universidad Nacional de Colombia (HORUS) (UNAL, 2021b). The objective of the HORUS system is to integrate and visualize the information on scientific and technological productivity generated by the teachers of UNAL's Faculty of Engineering, contributing to an improved national and international visibility, which allows generating strategic alliances and supporting decision-making. HORUS allows obtaining information disaggregated by sex, providing data that support the measurement of indicators with a gender focus. This prototype of the Faculty has been endorsed for an institution-wide scaling.

Starting in November 2021, as part of the action plan outlined by the Faculty's Welfare Directorate, a professional psychologist with experience in gender issues was added to the team, in order for her to support the elaboration of a strategy for fostering equity, gender equality, and women empowerment, as well as the promotion of new masculinities in the Faculty's community.

From the management of the Faculty of Engineering, with the accompaniment provided by a female professional expert in gender issues, the main axes of the strategy *Equidad con ingenio* (Equity with wit) have been designed. This strategy will be implemented during 2022-2023 and will set the foundations of what will be applied until 2025. The axes of this strategy are: violence and equity, women empowerment in STEM, and research on gender-based partner violence. This strategy includes workshops and awareness and alphabetization campaigns, as well as addressing issues such as new masculinities, the prevention

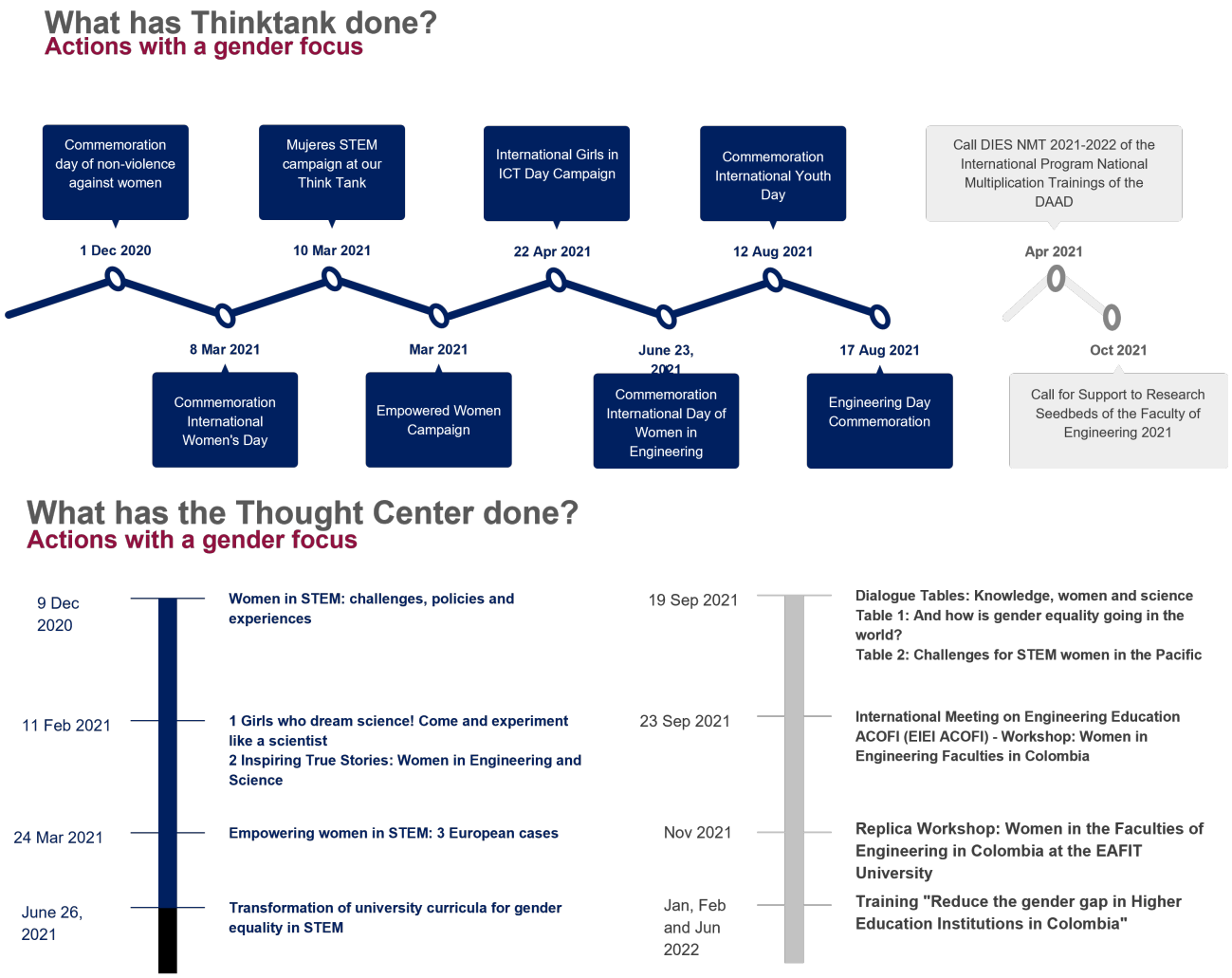

Figure 10. Activities of the Thinktank for the Strengthening of Leadership and Empowerment of Colombian Women in STEM Areas
Source: Authors, based on the information of the CPMC

of gender violence, and the promotion of active femininities, among others.

Measuring and visibilizing to advance

We evidenced a need to continue working on gender equality policies in UNAL anf the Faculty. The general behavior of the Faculty indicates a low proportion of women at each level, which does not exceed a 21% participation.

This analysis provides visibility to the data in order to identify gender gaps, and, as a function of the results, it indicates the need to favor effective equality in the Faculty of Engineering, by means of gender strategies implemented by the Research and Extension and Academic Vice-Principalships, as well as by the Faculty's Welfare Directorate, which allow acting and making progress in contributing to equality policies for higher education institutions in Colombia.

In general terms, gender data collection must be strengthened in the Faculty and the University. Statistics show a gradual increase in women participation as teachers in the Faculty of Engineering, going from 8,9 to 12,7%. As for research work in the Faculty of Engineering, there is progress in the presence of female project directors, with a quite significant increase specifically for 2019, 2020, and 2021. The presence of women in extension projects should continue to be strengthened, as a low participation is evidenced regarding female project leaders or women in the teacher teams of extension projects. The data show that, at a general level, in the last three Minciencias calls, there is a significant number of female professors from the Faculty who are not classified as researchers, which is why the participation of women teachers-researchers in these calls must be encouraged. On the other hand, it is evidenced that associate researchers have been promoted to senior researchers, which implies an increase in academic and research productivity by the women at the Faculty of Engineering.

Challenges, actions, and recommendations

As a function of the data reported in this paper, strategies must be proposed in order to encourage the participation of more female teachers in research and extension. It is also important to highlight that, in recent years, there has been an improvement in the presence of women in management roles at the Faculty. On the other hand, the Faculty of Engineering has proposed some recommendations and

actions, such as generating internal policies to strengthen the Faculty's gender perspective, to encourage academic networks led by graduate and undergraduate students with equal involvement, to encourage gender-focused research and extension projects within the Faculty, to continue fostering the participation of Faculty female teachers in management-level positions, and to continue participating in STEM networks in higher education institutions and government and private entities, with the aim to promote the strengthening of women in Colombia.

Conclusions

Women's participation in the construction and development of UNAL's Faculty of Engineering started with the admission of the first two female students in 1943. Since then, the contributions made by women to the growth and positioning of the Faculty have been conrinuous and significant. Giving visibility to the women at the Faculty is an important step to achieve the recognition they deserve.

As for the testimonials and statistical figures presented in this article, it can be inferred that it is necessary to visibilize the existence of gender gaps in engineering areas (particularly in the Faculty), as well as to raise the awareness many actors in all levels regarding what gender gaps are, why they must be tackled, and which actions contribute to closing them.

The under-representation of women in engineering areas around the world, in Colombia, and in the Faculty is an issue with a high social impact which must be acknowledged and addressed by the actors involved. Therefore, it is necessary to insist on the development of strategies allowing Colombian girls and female teenagers to see engineering as feasible options while choosing a professional career in which they can also achieve the personal and professional fulfillment that they desire.

As for women professors and researchers, we evidenced the need to permanently visibilize the work and contributions made by women in teaching and research processes. In this sense, it is important to advance initiatives such as the HORUS system, which, for the first time, has allowed collecting research and extension data discriminated by gender, employing a data analysis strategy that gives visibility to the work carried out by men and women teachers of the Faculty in a dynamical and continuous way.

With regard to leadership positions, the figures show a high interest by female professors at the Faculty in occupying academic administration positions with decision power. Visibilizing this fact not only acknowledges their commitment; it is also a motive for other female professors to engage in leadership roles.

Acknowledgements

The authors would like to thank the National Academic Information Directorate (DNINFOA) and the Academic Staff and Administrative Directorate of Universidad Nacional de Colombia.

CRedit author contributions

Guzmán, M. A.: Conceptualization-idea, formal analysis, and writing.

Herrera, L. K.: Conceptualization-idea, formal analysis, and writing.

References

Asociación Colombiana de Facultades de Ingeniería (ACOFI) (2021, septiembre 21-24). *Encuesta de percepción de actividades de ACOFI* [Presentación]. Encuentro Internacional de Educación en Ingeniería ACOFI 2021, Cartagena, Colombia.

Bello, A. (2020). *La mujeres en ciencias, tecnología, ingeniería y matemáticas en América Latina y el Caribe*. ONU Mujeres. https://lac.unwomen.org/sites/default/files/Field%20Office%20Americas/Documentos/Publicaciones/2020/09/Mujeres%20en%20STEM%20ONU%20Mujeres%20Unesco%20SP32922.pdf

Dulce-Salcedo, O., Maldonado, D., y Sánchez, F. (2022). Is the proportion of female STEM teachers in secondary education related to women's enrollment in tertiary education STEM programs?. *International Journal of Educational Development, 9*, 102591, https://doi.org/10.1016/j.ijedudev.2022.102591

Facultad de Ingeniería de la Universidad Nacional de Colombia (FI-UNAL) (2015). *Andrea y la ingeniería mecánica* [Video]. https://www.youtube.com/watch?v=nLKxRZg161w

Facultad de Ingeniería de la Universidad Nacional de Colombia (FI-UNAL) (2021a). *Conversatorio con nuestras primeras egresadas* [Video]. https://www.youtube.com/watch?v=3e0Z3SFkhwU

Facultad de Ingeniería de la Universidad Nacional de Colombia (FI-UNAL) (2021b). *Conversatorio con decanas de ingeniería* [Video]. https://www.youtube.com/watch?v=jxfTY8IEhRo

Mayor, A. (2011). *Innovación{ Excelencia{Tradición, Facultad de Ingeniería 1861-2011. Universidad Nacional de Colombia, Facultad de Ingeniería.*

Oliveros, M., Cabrera, E., and Velez, B. (2016). La motivación de las mujeres por las carreras de ingeniería y tecnología. *Entreciencias: Diálogos en la Sociedad del Conocimiento, 4*(9), 89-96.

Olmedo-Torre, N., Sánchez, F., Salán, M., López, D. , Perez-Poch, A., and López-Beltrán, M. (2018). Do female motives for enrolling vary according to STEM profile?. *IEEE Transactions on Education, 61*(4), 289-297. https://doi.org/10.1109/TE.2018.2820643

Programa de las Naciones Unidas para el Desarrollo (PNUD), Fondo de Población de las Naciones Unidas (UNFPA), ONU Mujeres, Comisión Económica para América Latina (CEPAL) (2017). *Brechas de género y desigualdad: de los Objetivos de Desarrollo del Milenio a los Objetivos de Desarrollo Sostenible*. https://colombia.unwomen.org/sites/default/files/Field%20Office%20Colombia/Documentos/Publicaciones/2017/09/PDF%20WEB%20BRECHAS%20DE%20GENERO%20Y%20DESIGUALDAD_final.pdf

Quintero, O. (2016). La creciente exclusión de las mujeres de la Universidad Nacional de Colombia. *Revista Nómadas, 44*, 123-145. https://www.redalyc.org/pdf/1051/105146818008.pdf

UNESCO (2019). *Descifrar el código: La educación de las niñas y las mujeres en ciencias, tecnología, ingeniería y matemáticas (STEM)*. https://unesdoc.unesco.org/ark:/48223/pf0000366649.

Universidad Nacional de Colombia (UNAL) (2017). *Protocolo para la prevención y atención de casos de violencias basadas en género y violencias sexuales en la Universidad Nacional de Colombia*. http://www.bienestar.unal.edu.co/fileadmin/user_upload/OAG/publicaciones-de-interes/Protocolo_Violencias_Genero.pdf

Universidad Nacional de Colombia (UNAL) (2021). *Dirección Nacional de Información Académica*. https://dninfoa.unal.edu.co/

Universidad Nacional de Colombia (UNAL) (2021a). *Caracterización de docentes Sede Bogotá Universidad Nacional de Colombia*. http://planeacion.bogota.unal.edu.co/sede_en_cifras/reportes_interactivos/docentes/

Universidad Nacional de Colombia (UNAL) (2021b). *Proyecto HORUS. Prototipo de Sistema de Inteligencia de negocio para la vigilancia de las capacidades cientfficas y de base tecnológica de la Universidad Nacional de Colombia*. https://horus.unal.edu.co/

Universidad Nacional de Colombia (UNAL) (2022a). *Dirección de personal académico y administrativo Sede Bogotá*. https://bogota.unal.edu.co/estructura/direccion-de-personal/

Universidad Nacional de Colombia (UNAL) (2022b). *Escuela Permanente de Pensamiento Universitario*. http://pensamiento.unal.edu.co/la-escuela/

Revista Ingeniería e Investigación
Continuous periodicity
https://revistas.unal.edu.co/index.php/ingeinv

Editorial Policy
Ingeniería e Investigación

Aim and scope

The *Ingeniería e Investigación* (I&I) journal is an open access digital scientific publication issued since 1981, with a continuous periodicity of three issues per year. Its main objective is to promote the dissemination of original and unpublished scientific research and technological developments in all disciplines related to engineering. Papers published in I&I invite discussion on current issues relevant to the academic community.

I&I is an international journal published in English which uses a double-blind peer review system to ensure the quality and originality of the published content. Editing of the journal is carried out with high standards of professional quality, via a completely autonomous editorial management platform that hosts the content in different formats, with the aim to adapt to current needs regarding visualization and digital preservation.

The journal **has no cost for readers or authors**, as it is funded by the Faculty of Engineering of Universidad Nacional de Colombia under the Diamond open access model.

I&I publishes scientific and technological research articles, review articles, and case reports in the following areas of engineering:

- Agricultural Engineering
- Biomedical Engineering
- Chemical, Environmental, and Food Engineering
- Civil and Sanitary Engineering
- Electrical, Electronics, and Telecommunications Engineering
- Industrial Engineering
- Mechanical, Mechatronics, and Materials Engineering
- Systems and Computer Engineering
- Engineering Education

Before submitting an article, please read the editorial and data policies of the I&I journal carefully.

Language of publication

English

Frequency of publication

The I&I journal has a continuous periodicity (three issues per year). Once the article has been accepted and the editing phase has been completed, it will be available online.

Open access policy

The *Ingeniería e Investigación* journal publishes its articles through the *Open Journal Systems* platform, as the editorial team firmly believes that allowing access to research results by the scientific community and the general public bolsters its quality and is a factor of equity. Likewise, due to its characteristics, the use of this tool allows for a better control of the editorial process, facilitating communication between its actors.

Article evaluation process

The process is described in the following Figure:

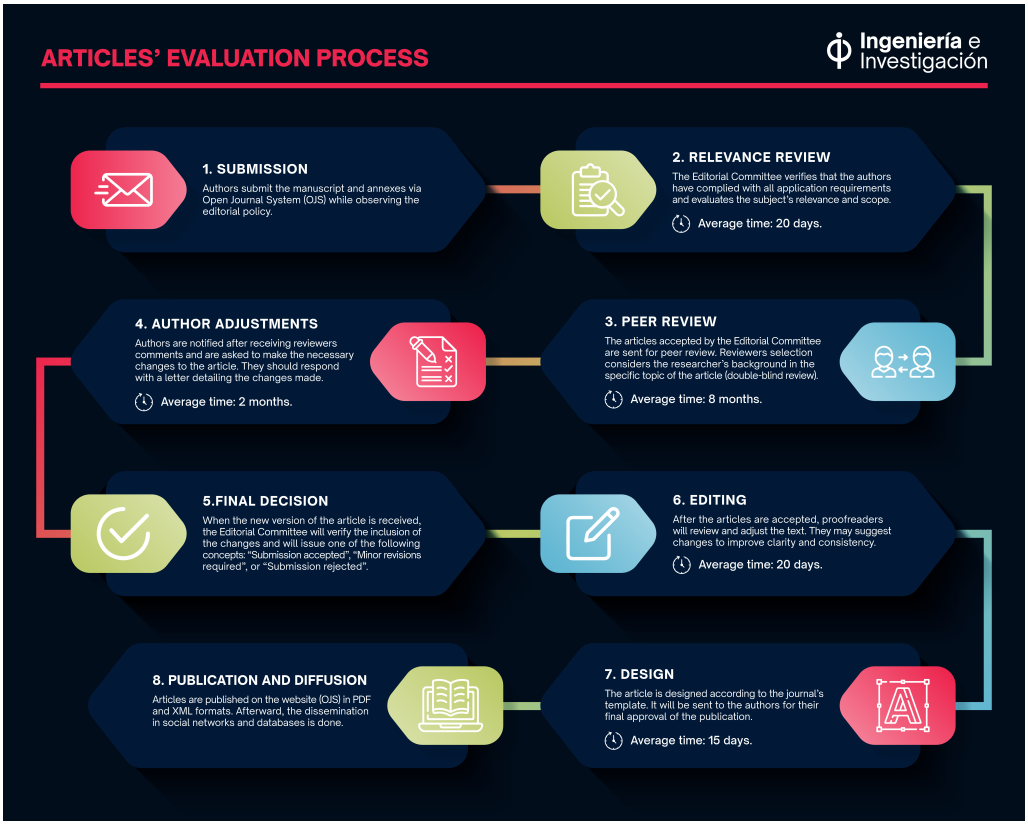

Note: the authors will receive notifications regarding new developments in each of the phases. It will also be possible to monitor any developments directly on the OJS.

Articles submitted to the I&I journal undergo an internal evaluation process by the Editorial Committee, in order to define, according to the subject of the article and the scope of the journal, whether the peer review process should begin.

Preliminary review (average time of 10 days): in this round of evaluation, the editorial team verifies whether the authors have complied with all application requirements, among them: format, license, and originality.

Relevance review by the Editorial Committee (average time of 30 days): this evaluation is carried out by the journal's editors, who assess the relevance and development of the topic.

Peer review (average time of 8 months): the articles accepted by the Editorial Committee are sent for peer review. Peer selection considers the trajectory of a researcher in the specific topic of the manuscript, upon the condition that the peer reviewer has *recent* publications in indexed journals, articles related to the topic of the manuscript to be evaluated, and an academic level corresponding to the highest degree of the authors (*peers with an H-index greater than 5 are considered*). The reviewers do not know the name of the authors and vice versa (double-blind review). The possible verdicts are:

1. Submission accepted
2. Revisions required (minor changes)
3. Resubmit for review
4. Resubmit elsewhere
5. Submission declined
6. See comments

Please keep in mind:

- In the event that the concepts of the two reviewers differ from each other, the Editorial Committee will appoint a third one.
- A maximum of **20 reviewers** will be assigned. If these requests are not accepted or completed, the Editorial Committee will inform the authors of the status of the process and will give them the option to continue with it.
- The journal does not accept new submissions of articles that were declined at this stage.

(academic peer assessment form).

Final decision by the Editorial Committee (average time of 30 days): once the evaluations of at least two peers have been received, they are consolidated, and a concept is sent to the authors, so that the necessary actions can be taken. The authors should send a response letter indicating all the changes made to the article.

When the new version of the article is received, the Editorial Committee will verify the inclusion of the peer reviewers' comments. Based on the initial verdict, the article may initiate a second round of peer review.

The possible outcomes of the evaluation are:

1. Submission accepted
2. Minor revisions are required
3. Submission declined

Only at the end of this stage can a letter of acceptance of the article be issued by the I&I journal.

Editing (average time 20 days): once the articles are accepted, proofreaders will check spelling, grammar, and punctuation, in addition to verifying consistency in the structure and style of the manuscript. They may also suggest changes to improve the clarity and coherence of the text.

Design (average time of 15 days): once the editing phase is completed, the design process begins, which is based on the journal's template and complies with all editorial normalization standards. The designed layout of the article will be sent to the authors for their final approval of the publication. At this stage, the authors may only correct minor typographical and layout errors.

Guidelines for peer reviewers

The objectives of the peer review process of the I&I journal are to verify the quality of the research before publication, to identify errors unnoticed by the authors, and to provide feedback to the authors for the improvement of their research processes.

As a reviewer, it is essential to maintain the confidentiality of the evaluated articles and not to share them with any third parties.

The reviewer will consider the following evaluation criteria and the scope of the journal.

Originality	The topic is sufficiently novel and interesting to warrant publication in the journal.
Relevance	The subject of the article corresponds to the scope of the journal, and the topics covered are important and contribute to the development of engineering.
Article structure	The structure of the article complies with the article submission guidelines established by the journal, namely: it contains introduction, methodology, results, discussion, and conclusions sections. The way these texts are written is clear and effectively communicates the process and findings of the research.
Title	The title adequately describes the content of the article.
Abstract	The abstract adequately describes the content of the article and presents, in a general way, the context of the research, its development, the objective, the methodology, the main results, and the general conclusion.
Introduction	The introduction contains the definition of the research problem, its development, and the hypothesis. To this effect, the authors may briefly present the context of the research, the results of other works, and the challenges to be addressed. The experiments/simulations performed should also be presented in a general way.
Methodology	The information provided by the authors is sufficient to replicate the research, clearly explains how the data were obtained, describes the equipment and materials in an adequate and technical manner, and presents the design of experiments/simulations and the way in which the statistical analysis of the data was performed.
Results	The authors present their research findings clearly and in logical sequence. Their explanation is reasonable and duly supported both scientifically and technically.
Discussion	The authors interpret and discuss the results of their study with regard to the existing literature and the broader context of their field of research. The authors discuss how their study contributes to the field of research and the possible theoretical, practical, or public policy implications of their findings. The limitations of the study are discussed, and possible sources of bias and error are mentioned.
Conclusions	The conclusions agree with the results and their analysis, and they are consistent with the objective of the research and the proposed hypotheses. The main points of the discussion are included.
Language	The authors make appropriate use of language to communicate the information contained in the article.
Tables and figures	The tables and figures are of high graphic quality, necessary, and duly used in the text.
References	The sources are relevant and current, and they are adequately cited and referenced within the text and at the end of the article.

Considering the evaluation criteria and the scope of the journal, the reviewer will report the result according to the following options:

1. Submission accepted. This option is selected if it is recommended that the submission be accepted as is.
2. Revisions required. This option is selected when the articles need small modifications.
3. Resubmit for review. This option is selected when the article needs substantial modifications and must undergo a second round of peer review.
4. Resubmit elsewhere. This option is selected when the article is declined for publication in I&I and it is recommended that it be submitted to another journal.
5. Submission declined. This option is selected when the article is declined for publication in I&I.
6. See comments. This option is selected if the reviewer does not agree with any of the previous options.

Copyright notice

The authors or copyright holders of each article grant the *Ingeniería e Investigación* journal of Universidad Nacional de Colombia a non-exclusive, limited, and free authorization on the article, which, once evaluated and approved, will be published. This authorization includes the following considerations:

1. The authors submit the corrected version in accordance with the reviewers' suggestions and clarify that the aforementioned article is an unpublished document for which they have the authorized rights.
2. The authors assume full responsibility for the content of their work before the *Ingeniería e Investigación* journal, before Universidad Nacional de Colombia, and before third parties.
3. The authorization granted will be effective from the date it is included in the corresponding volume and issue of the *Ingeniería e Investigación* journal, in the Open Journal Systems platform, and in the journal's home page (https://revistas.unal.edu.co/index.php/ingeinv), as well as in the different databases and indices hosting I&I.
4. The authors authorize the *Ingeniería e Investigación* journal of Universidad Nacional de Colombia to publish the document in the format required (print, digital, electronic, or any other known or unknown format), as well as to include the work in the indices and search engines deemed necessary to promote its dissemination.
5. The authors accept that this authorization is given free of charge. Therefore, they waive any right to receive any emolument for the publication, distribution, public communication, and any other use made under the terms of this authorization.
6. The authors are informed of and accept the publication in the *Ingeniería e Investigación* journal under a Creative Commons 4.0 license (CC-BY 4.01).

Sponsors

Universidad Nacional de Colombia (Bogotá Campus), Faculty of Engineering.

Ethics in scientific publishing

Ethics in scientific publishing is essential to ensure the integrity and reliability of research. The *Ingeniería e Investigación* journal is committed to implementing the best ethical practices in the publication of scientific articles and expects all authors, reviewers, and editors involved in the editorial process to follow the same ethical standards. This section presents the journal's ethical policies and guidelines to ensure transparency, honesty, and accountability in the publication of research.

In accordance with the policies for the publication of articles in *Ingeniería e Investigación*, it will be considered unethical for authors to submit articles for review which have been previously published, lack proper citation and referencing criteria, or have been simultaneously submitted for review in different publications. Moreover, considering that the evaluation process is *double-blind*, any attempt to contact the reviewers with the intention of coercing the outcome of the evaluation will be considered unethical.

When an author or group of authors incur in serious misconduct (as listed in the journal's ethics document), such as plagiarism, duplicate publication, scientific fraud, fragmentation, improper use of sources, and uninformed consent, the Editorial Committee of the Ingeniería e Investigación journal, for legal purposes, will take the necessary actions through the Legal Office of Universidad Nacional de Colombia.

General criteria

1. Articles published in I&I should contain sufficient details and references to replicate or refute the study.
2. Fraudulent or deliberately inaccurate statements constitute unethical behavior.
3. If a study includes chemicals, procedures, or equipment representing unusual hazards inherent to their use, the author should clearly identify them.
4. If the study involves animals or humans, the author should ensure that the article explicitly states that all procedures were performed in accordance with laws and institutional guidelines.
5. The privacy rights of human beings must be respected.

Authorship criteria

An author is a person who has made a significant intellectual contribution to the article. Therefore, all persons named as authors must meet the authorship requirements,

and all those who meet them must be explicitly mentioned. Three basic criteria must all be met to be recognized as an author:

a. Substantial contribution to the conception and design, data acquisition, and analysis and interpretation of the study.

b. Drafting or revision of the intellectual content.

c. Approval of the final version.

The I&I journal requests that the authors declare their specific contributions according to the CRediT taxonomy.

There are three types of authorship that are considered unacceptable: the ghost author, who contributes substantially but is not acknowledged; the guest author, who makes no discernible contribution, but is named to increase the chances of publication; and honorary authorships, which are based solely on a small affiliation with a study.

The I&I journal magazine makes the following recommendations:

1. Any individuals who participate in a study but do not meet the authorship criteria should be listed as collaborators in the acknowledgments section. The authorship order should be a joint decision of the authors.

2. Before starting a research, it is recommended to document the role and the way in which the authorship of each researcher will be acknowledged.

3. There must be no lies regarding a person's participation in the research or publication. If their contribution is deemed substantial, authorship is justified, be it as author or contributor.

4. Authorship should not be declared without the consent of the individual.

5. Some groups place authors in alphabetical order, sometimes with a note explaining that all authors made equal contributions to the study and publication.

The I&I journal will consider changes in authorship. This refers to the addition, deletion, or reorganization of the names of the authors of an accepted article.

Any requests to add or remove an author, or to rearrange the names of authors, should be sent by the corresponding author of the accepted article and should include the reason for the request. I&I requests that all authors confirm in writing (via e-mail) that they agree to the addition, deletion, or rearrangement of author names.

Conflict of interest

The *Ingeniería e Investigación* journal requires all authors, reviewers, and editors to disclose any potential conflicts of interest that may influence the content or review of a manuscript. A conflict of interest can be any financial, personal, professional, or institutional relationship that may influence the judgment or objectivity of the author, reviewer, or editor.

Potential conflicts of interest may include but are not limited to the following:

1. Participation in an organization that may have a financial interest in the results of the work presented.
2. Owning shares, patents, or copyright related to the subject of the manuscript.
3. Receiving funding from an organization that may have a financial interest in the outcome of the work presented.
4. Having personal or professional relationships with one or more of the authors of the manuscript.
5. Having some type of institutional conflict, i.e., employment, fees, consulting to sponsoring organizations, ownership of investment funds, paid expert testimony.

It is the responsibility of the authors, reviewers, and editors to disclose any possible conflicts of interest. If any such conflict is identified, the journal will take steps to ensure that the manuscript is reviewed and published in a fair and objective manner. If the conflict of interest is deemed incompatible with a fair and objective review or publication, the journal reserves the right to decline the manuscript or withdraw it from publication. In this regard, I&I makes the following recommendations:

1. Authors, reviewers, and editors must inform if they have any real or potential conflict of interest that inappropriately influences the findings or results of the work presented. This, within three (3) years of starting the work.
2. The role of the study's sponsor(s), if any, must be reported in any of the stages of the work.
3. The authors should not enter into any agreements that interfere with access to all data and the ability to independently analyze them, as well as to prepare and publish the manuscripts.
4. When submitting a document, a statement (titled *Funding*) should be made in a separate section of the text, which should be placed before the *References* section.
5. Examples of potential conflicts of interest that must be disclosed include: employment, consulting, stock ownership, fees, paid expert testimony, patent applications/registrations, grants, and other funding.
6. All sources of financial support for the project must be disclosed.
7. The sponsor's role in the study should be described.

Duplicate publication

Authors are required to ensure that their article is based on original research (which has never been published). Intentional submission or resubmission of their work for duplicate publication is considered a breach of editorial ethics. One of the main reasons why the duplicate publication of original research is considered unethical is because it may result in inappropriate weighting or the unintentional double counting of the results of a single study, thus distorting the available evidence.

Publication or distribution on the Internet may be regarded as prior publication and compromises the originality of the article. However, I&I will allow the publication of articles in non-commercial *preprint* repositories, subject to a prior evaluation by the Editorial Committee.

I&I considers that a duplicate or multiple publication occurs when two or more articles, without referring to each other, share essentially the same hypotheses, data, results or discussion points, and conclusions. This can occur to different extents: literal duplication, partial but substantial duplication, or even duplication by paraphrasing. In this regard, I&I states the following:

1. Articles submitted for publication in the *Ingeniería e Investigación* journal must be original and must not have been submitted to another publisher or scientific journal.
2. At the time of submission, authors should disclose the details of related articles (even if they are in another language), similar articles in press, and translations. This implies that, at the time of application, authors must notify I&I if their article has been previously published in a *preprint* repository and indicate a link to it.
3. It is recommended to avoid submitting articles describing essentially the same research to more than one journal. Even if a submitted article is being reviewed and the authors are uncertain about the process, they should wait for I&I to inform them of its status before submitting it to another journal or publisher.
4. It is recommended to always report any previous submissions (continuity of work) that could be a duplicate publication.
5. It is recommended not to write about one's own research in two or more articles from different perspectives or about different aspects of the research without mentioning the original article.
6. If an author wishes to submit an article to a journal that will be published in a different country or in a different language, they must inform I&I and the other journals involved.
7. At the time of submission, all details regarding related articles in a different language should be indicated, as well as existing translations.

Recognition of sources

Authors should cite the publications that have influenced their work. Any information obtained privately should be used only with the explicit written permission of the source.

The reuse of tables and figures must be authorized by their author and the editor, and this must be adequately mentioned in the corresponding legend.

Data fabrication and falsification

Data fabrication and falsification are practices of scientific fraud that correspond to presenting false data or conclusions that have not been generated through a rigorous research process. Both data fabrication and falsification are serious forms of misconduct, as they do not accurately reflect the results of a research work. I&I establishes the following types of fraud in the publication of research results:

a. *Data fabrication:* inventing data and results and then communicating them.

b. *Data falsification:* manipulating research materials, images, data, equipment, or processes. Falsification includes the modification or omission of data or results in such a way that the research is not accurately presented.

Authors should be aware of editorial policies and their research data. Before submitting an article to the I&I journal, please read the journal's editorial and data policies carefully. Moreover:

a. Never modify, change, or omit data in a deliberate way. This includes research materials, processes, equipment, tables, citations, and bibliographic references.

b. Properly manage the data supporting your research, taking special care in its collection, production, preservation, analysis, and communication.

c. Keep a thorough record of the raw data, which should be accessible if required by the editor, even after the article has been published.

Plagiarism

The I&I journal considers plagiarism to be a serious violation of academic and scientific integrity. Plagiarism is defined as the presentation of ideas, words, or graphic material by other authors without giving them the corresponding credit. Plagiarism includes but is not limited to directly copying a work without citing the source, using the structure and style of another work without proper attribution, inappropriate paraphrasing, and presenting previously published material as one's own.

Plagiarism has different levels of severity, according to the amount of someone else's work that was taken (several lines, paragraphs, pages, the whole document) and the nature of the text copied (results, methods, or introduction sections). However, I&I considers plagiarism in all its forms to be unethical conduct and unacceptable. Verbatim copying is only acceptable if the source is indicated and the copied text is enclosed in quotation marks, with its corresponding page number.

The I&I journal provides the following recommendations to prevent plagiarism:

a. Always remember that it is essential to acknowledge the work of others (including the work of your assistant or your own previous work) as part of the process.

b. Do not reproduce a work word for word, in whole, or in part without permission and acknowledgment of the original source.

c. Keep a record of the sources you use when conducting research and where you used them in your paper.

d. Be sure to fully acknowledge and properly cite the original source in your article (if it has a DOI, use it).

e. Refrain from using other people's work word for word, even when referencing the source, unless you do so in quotation marks (direct quotation).

f. Remember that paraphrasing is only acceptable if the source is correctly indicated and its meaning or intent is not changed.

g. Quote and cite all the content you have taken from a previously published source, even if you are saying it in your own words.

The I&I journal will conduct a thorough review of each manuscript to detect any form of plagiarism. If an author is found to have committed plagiarism, the journal will take appropriate action to address the unethical conduct, including the withdrawal of the article and the prohibition of any future publications. In addition, I&I will notify the author's institution and other allied journals if it is determined that plagiarism was deliberately or repeatedly committed.

Fragmentation

Fragmentation in scientific publishing refers to the publication of the same data in different articles, without a clear reference or mention of the other related works. This type of behavior is regarded as scientific fraud by I&I, as fragmentation can result in a distortion of the literature, misleading readers into believing that the data presented in each fragment (*i.e.*, journal article) are derived from a different sample of subjects. This not only biases the scientific database, but also involves a repetitive process that wastes the time of editors and reviewers, who must deal with each paper separately. In addition, the number of references where the author is cited is unreasonably inflated.

To prevent fragmentation in scientific publishing, the I&I journal establishes the following policies:

- Authors should clearly indicate whether their work is based on previously published data or results. If so, a complete and accurate reference to the original source must be provided.
- Authors should make sure that the data or results presented in their article are new and original and have not been published elsewhere.
- Authors should avoid publishing the same data or results in different articles without a clear reference or mention of the other related papers.
- The I&I journal reserves the right to decline papers that evince fragmentation or the unjustified duplication of previously published data or results.
- Authors should inform I&I of any other publication or submission of their work elsewhere, be it in whole or in part.

- Authors must follow I&I journal policies regarding authorship and the acknowledgement and citation of sources in the publication of their work.

Informed consent

The *Ingeniería e Investigación* journal believes that an informed consent policy is critical to ensuring the protection of the participants and the ethical integrity of a research work. In this regard, I&I establishes the following policies:

a. Informed consent is mandatory for all research participants, including human and animal subjects.

b. Informed consent should be obtained by researchers voluntarily and free of any pressure or coercion. Informed consent must be obtained in writing and signed by the participant or his/her legal representative before participating in a research work.

c. The content of the informed consent should be clear and understandable, and it should include information on the purpose of the research, the procedures the participant will undergo, the potential risks and benefits, and the option to withdraw participation at any time.

d. Participants should be informed of the possibility that the results of the research may be published, and their specific consent should be obtained for the publication of any information that identifies them.

e. The main researcher is responsible for ensuring that informed consent is appropriately obtained and for maintaining appropriate records.

f. In the case of research involving vulnerable participants, such as minors, persons with disabilities, or dependent persons, special procedures must be followed to ensure their protection and informed consent.

These policies are in line with the ethical and legal standards established in the field of science. In addition, I&I may require authors to provide evidence that informed consent has been obtained prior to the publication of an article that includes research data involving human or animal participants.

Correcting published articles

When an author discovers a significant error or inaccuracy in the published work, it is their obligation to immediately notify the journal and cooperate in the correction process.

When an author or group of authors commit a serious fault of scientific fraud as those listed herein, *i.e.*, plagiarism, duplicate publication, data fabrication and falsification, fragmentation, improper use of sources, and uninformed consent, the Editorial Committee of the *Ingeniería e Investigación* journal, for legal purposes, will take the necessary actions through the Legal Office of Universidad Nacional de Colombia.

Statement on Artificial Intelligence (AI)

AI and AI-assisted technologies should not be listed as authors or co-authors, nor cited as such. Authorship implies responsibilities and tasks that can only be attributed to and performed by human beings.

Authors should report the use of generative AI and AI-assisted technologies by adding a statement at the end of their manuscript, before the *References* list.

Example:

> During the elaboration of this work, the author(s) used [NAME OF TOOL/SERVICE] with the aim to [REASON]. After using this tool/service, the author(s) reviewed and edited the content as necessary and take full responsibility for the content of the publication.

Guidelines for authors

Only articles written in English with a maximum of 6000 words will be accepted. The word count includes the whole text and its references, figures, and tables (a higher word count will be evaluated by the Editorial Committee). All articles should be submitted in the journal template. The template can be downloaded at the following link: Word/LaTeX template.

The author must sign up in the system and submit their article in a five-step process. Once received, the corresponding author will be notified via e-mail or will be able to check the status of their article in the system.

If accepted, the author must make the corrections recommended by the reviewers and the Editorial Committee for the subsequent publication of the article.

Article types

The I&I journal considers the following types of articles for publication:

- **Research articles:** original articles presenting the results of an original research work conducted by the authors. These articles include an introduction that establishes the context and importance of the research, a methodology section that describes the procedures employed, a results section that presents the findings, and a discussion that interprets the results and relates them to the existing literature.
- **Review articles:** articles that summarize and critically evaluate the existing literature on a particular topic. These articles often include an introduction that outlines the context of the topic, a methodology section that describes the criteria used to select the studies reviewed, a results section that summarizes the findings of said studies, and a discussion that assesses the quality of the evidence and makes recommendations for future research.

- **Case studies:** detailed reports of one or more cases that illustrate a particular phenomenon or problem. Case studies may include an introduction that outlines the context of the problem, a methodology section that describes how the case was selected and how data were collected, a results section that presents the findings of the case, and a discussion that interprets the results and makes recommendations for future research.
- **Letters to the editor:** short articles that usually comment on an article previously published in the journal or on a relevant topic within the scope of the journal. Letters to the editor can also be used to correct errors or clarify misunderstandings in previously published articles.

Content

In order for any article to be considered by the Editorial Committee, and for its potential publication in the *Ingeniería e Investigación* journal, it must have at least the following sections:

- Title
- Abstract
- Keywords
- Introduction
- Methodology
- Results
- Discussion and conclusions
- References

Title

The title of the article should be brief and explanatory. It should answer the reader's question: Is this a relevant article for my research? To this effect, the title should be clear and concise, using keywords relevant to the subject of the article.

In addition, the title should be informative, reflect the content of the article accurately and clearly, and avoid the use of jargon or technical terms unfamiliar to most readers. It is important to be direct and avoid superfluous words. Consider using a short, effective phrase rather than a complete sentence. Check spelling and grammar to ensure that the title is easily understandable and contains no typographical errors.

Author information

All authors must register in the submission system, with their full name, e-mail address, country, ORCID, institutional affiliation, and a short biography indicating academic titles, current position, institution, and country.

Social media profiles

I&I asks authors to provide links to their professional or academic social networking profiles, if available. Social media profiles are a valuable tool to help readers learn more about the authors and their work. If you would like to share your social media profiles, please include the corresponding links in the online submission form. Make sure the links are active and accurate. Please note that providing your social media profiles is optional and will not affect the consideration of the article for publication in our journal.

Abstract

The abstract should briefly present the background, research objective, methodology, main results, and main conclusions. It should be clear and concise, using keywords and indexing terms relevant to the subject of the article. The abstract should be written in the past tense, contain no more than 250 words, and be informative enough for the reader to understand the nature and scope of the research without having to read the entire article.

Graphical abstract

A graphical abstract is a concise, visual representation of the article's content, designed to capture the attention of a broad readership. Although optional, its use is recommended, as it increases the online visibility of the article.

To submit a graphical abstract, please attach a separate file in the online submission system. Be sure to provide an image with a minimum size of 531 × 1328 pixels (height × width) or proportionally larger.

Practical application

This is an optional section of the article that seeks to achieve a wider dissemination of the results among professionals and the non-academic public. This section should be written in simple language, aimed at a broad audience, and should present the results, their significance, and the possible practical application of both the results and the methodology used. The authors may use examples of real cases to contextualize readers in the practical application of the research. This section should contain 150-200 words and should be placed after the abstract and before the keywords in the article file.

Keywords

Keywords are terms or phrases that describe the content of the article and relate it to the field of research. Keywords are important to help readers find the article in online databases and search engines. It is recommended that the author provide three to five relevant keywords. Keywords should be specific and reflect the content of the article. Words other than those used in the title and abstract should be used to optimize search engine processes and results. Avoid general terms and use keywords that are directly related to the subject of the article. Make sure that the keywords are not too long and are separated by commas. The keywords should be included after the abstract in the same document.

Note: the title, abstract, and keywords must be written in English and Spanish.

Highlights

Highlights are a brief list of the main points that summarize the most important and novel aspects of an article. Highlights should be concise and clearly and accurately explain the content and findings of your article. It is recommended that the author provide three to five highlights. Each point should be a short phrase and should not exceed 85 characters. The highlights should be included in the same document as the full article and should appear immediately after the abstract.

Introduction

The introduction is a crucial part of the article and should provide the reader with an overview of the subject, including the relevance of the topic, a literature review focused on establishing the background and state of the art of the problem under study and the research questions addressed. This section should also highlight the novelty of the work presented. It is important to clearly describe the studied problem and present the information in an organized and coherent manner, focusing on a logical structure and progressively presenting the information. It is recommended that it takes up the first two pages of the article and does not include specific details of the methodology or the results of the study, which should be addressed in the corresponding sections of the article.

Methodology

The methodology section is a fundamental part of the article and should describe the processes and tools used to address the problem and prove or disprove the hypothesis. The experimental and analytical procedures performed should be clearly and thoroughly presented, including the selection of samples and participants, the data collection instruments and techniques, the data analysis, and possible biases or limitations of the methodology used. It is important that the authors explain the reasons behind the selection of a particular methodology and how it addresses the research questions. Furthermore, sufficient details should be provided, so that other investigators can replicate the study. If new or innovative methodologies are used, their characteristics and advantages with regard to other conventional methodologies must be clearly explained.

Results

The results section presents the findings and conclusions derived from the study. In this section, the data and results obtained should be described clearly and concisely. It is advisable to use tables, figures, and graphs to help visualize and better understand the information. It is important to highlight the most relevant and significant results regarding the research questions. The authors should provide an adequate interpretation of the results, highlighting the implications and possible applications of the findings for solving the problem and for the subject of the study in general. In addition, the results should be compared with those of other previous studies, and possible limitations

and biases in the research should be analyzed. The results should answer the following questions: Why does this research offer a new solution? How can it be useful to others?

Tables, figures, images, and equations

When the paper is accepted, we might request the following files: *tables, high-resolution figures*, and *images*. All those files should be uploaded separately via our online submission system OJS according to:

1. **Tables:** Please submit tables in Word format at the end of the document. Tables should be created using the Microsoft Word table editor, preferably. Please save the files as Table. 1, Table. 2. . .
2. **Figures and Images:** all the figures and images should be upload separately, in one of these formats: **TIFF** or **EPS**. High-resolution with a minimum 300 dpi (ppp). Named the files as Fig. 1a, Fig. 1b, Fig. 2. . .
3. **Equations:** all the equations should be uploaded separately. The equations have to be edited in MathType. Please save the files as Eq1, Eq2. . .

Discussion

The discussion section should allow the authors to reflect and argue on the results presented, as well as to compare them with other relevant studies in the literature. It is important that the authors explain the importance and implications of their findings, as well as the way in which they can contribute to solving the studied problem. In addition, the authors should address any limitations that may have affected the research and how this could be improved in future studies. It is also important that the authors discuss the practical and theoretical implications of their results, as well as the way in which they can be applied in the real world.

Conclusions

This section should clearly explain what the research has achieved with respect to the problem formulated in the introduction. The conclusions should include a summary of the main results and their implications for the field of study. The benefits and limitations of the proposed solution should be indicated, and future lines of research should be suggested.

Acknowledgements

The acknowledgements section is a space to express gratitude to the people, institutions, and sources of support that contributed to the study. It may include acknowledgements to advisors, collaborators, participants, funding sources, institutions, technical collaborators, and administrative support. It is important to keep the section concise, as well as to get permission before mentioning names.

Author contributions

This section should mention the specific contribution of each author according to the CRediT taxonomy. This, with the purpose of recognizing the individual contributions of the authors, minimizing controversies with regard to authorship, and encouraging collaboration.

Example:

Author 1: conceptualization, methodology, software. Author 2: data curation, writing – elaboration of the original draft. Author 3: visualization, research. Author 4: supervision. Author 5: software, validation. All authors: writing – review and editing.

Access to research data

Research data are the result of observations or experiments that validate the conclusions of a research work. In order to promote data reproducibility and reusability, this journal encourages authors to share complete data, as well as software, codes, models, algorithms, protocols, methods, and other materials related to their project.

If you have deposited your research data in a repository, you can link your article directly to the dataset, allowing other researchers to access the data and promoting research transparency.

Conflict of interest

Authors should report any possible conflict of interest in the development of their research.

Appendices

Appendices should be added at the end of the document. These generally refer to mathematical demonstrations.

References

Bibliographic references should be recent, preferably from a period not exceeding five years. It is important to use up-to-date and relevant sources to support the arguments and assertions presented in the article. Keeping bibliographic references within a limited time horizon also reflects attention to current events, as well as to the advancement of scientific knowledge in a specific area.

Bibliographic references for all articles must be included at the end of the document and follow the most current version of the IEEE citation and reference standards.

Authors may use the following document as a reference: https://ieeeauthorcenter.ieee.org/wp-content/uploads/IEEE-Reference-Guide.pdf

Examples:

- Journal article
  - A. R. F. Pinto and M. S. Nagano, "An efficient algorithm applied to optimized billing sequencing," *Ing. Inv.*, vol. 42, no. 2, e83394. https://doi.org/10.15446/ing.investig.v42n2.83394
- Conference paper
  - R. M. Azuma, G. P. Coelho, and F. J. Von Zuben, "Evolutionary multi-objective optimization for the vendor-managed inventory routing problem," in *2011 IEEE Cong. Evol. Comp.*, 2011, pp. 1457-1464. https://doi.org/10.1109/CEC.2011.5949787
- Book
  - M. de la Arada Juárez, *Optimización de la cadena logística*, Madrid, España: Paraninfo, 2019.
- Edited book
  - L. Stein, "Random patterns," in *Computers and You*, J. S. Brake, Ed., New York, NY, USA: Wiley, 1994, pp. 55-70.
- Website
  - Chevalier, "El pedido de comida en línea en América Latina en 2021," Statista, 2021. [Online]. Available: https://es.statista.com/grafico/19027/ingresos-generados-en-pedidos-en-linea-de-comida-a-domicilio/
- Thesis
  - F. Jensen, "Electromagnetic near-field far-field correlations," Ph.D. dissertation, Dept. Elect. Eng., Tech. Univ. Denmark, Lyngby, Denmark, 1970. [Online]. Available: www.tud.ed/jensen/diss

For more details do not hesitate to contact us
Journal E-mail: revii_bog@unal.edu.co